CMB-S4 Science Book: Working Draft

CMB-S4 Collaboration

March 13, 2016

Contents

1

Exhortations

(send feedback on this chapter to jc@kicp.chicago.edu)

Fourteen billion years ago, in the first fraction of a second of our universe's existence, the most extreme high-energy physics experiment took place. Our ability to use the cosmic microwave background (CMB) to investigate this fantastic event, at energy scales a trillion times higher than can be obtained at the CERN, is at the very core of our quest to understand the fundamental nature of space and time and the physics that drive the evolution of the universe.

The CMB allows direct tests of models of the quantum mechanical origin of all we see in the universe. Subtle correlations in its anisotropy imparted by the interplay of gravitational and quantum physics at high energies contain information on the unification of gravity and quantum physics. Separately, correlations induced on the background at later times encode details about the distribution of all the mass, ordinary and dark, in the universe, as well as the properties of the neutrinos, including the number of neutrino species and types, and their still unknown masses.

Here we describe the scientific case for the next generation ground-based cosmic microwave background experiment, CMB-S4, consisting of dedicated telescopes at the South Pole, the high Chilean Atacama plateau and possibly a northern hemisphere site, all equipped with new superconducting cameras that will provide a dramatic leap forward in cosmological studies, crossing critical thresholds in testing inflation, the number and masses of the neutrinos or the existence of other 'dark radiation', providing precise constraints on the nature of dark energy, and testing general relativity on large scales.

Through the efforts of the CMB experimental groups over the last decade, the technologies needed for CMB-S4 are now in place. There are, however, considerable technical challenges presented by the required scaling up of the instrumentation as well as by the scope and complexity of the data analysis and interpretation. CMB-S4 will require: scaled up superconducting detector arrays with well understood and robust material properties and processing techniques; high throughput mm-wave telescopes and optics with unprecedented precision and rejection of systematic contamination; full characterization of astronomical foreground emission; large cosmological simulations and theoretical modeling with accuracies yet to be achieved; and computational methods for extracting minute correlations in massive, multi-frequency data sets contaminated by noise and a host of known and unknown signals.

The purpose of this document is to set the scientific goals for CMB-S4 and (eventually) the instrumental configuration required to achieve them. This is of course an iterative process, involving detailed simulations as well as cost considerations. So, at this time the Science Book is a working document with this first iteration focused primarily on defining the possible science reach in several areas, along with the simulations needed to refine science case and set the specifications of the needed measurements. This will set the stage for defining the instrument in the next iteration of the Science Book.

In this chapter we set out the overarching goals for CMB-S4, which are then refined in later chapters. We start with a brief history and the current status of CMB measurements.

1.1 Brief History and Current Status of CMB measurements

From its discovery 50 years ago, measurements of the cosmic microwave background (CMB) have led to spectacular scientific insights into the fundamental workings of space and time, from the quantum mechanical origin of the Universe at extremely high energies in the first moments of the Universe, through the growth of structure and the emergence of the dark energy that now dominates the energy density of the Universe. Studies of the CMB connect physics at the smallest scales and highest energies with the largest scales in the Universe, roughly 68 orders of magnitude in length scale. They connect physics at the earliest times to the structure that surrounds us now, over 52 magnitudes in time scale.

The deep connections of CMB studies and particle physics predate the discovery of the background, going back to the 1940s when Alpher and Gamow were considering a hot, dense, early Universe as a possible site for nucleosynthesis. To produce the amount of helium observed in the local Universe, they concluded there had to be about 10^{10} thermal photons for every nucleon. Alpher and Herman subsequently predicted that this background of photons would persist to the present day as a thermal bath at a few degrees Kelvin.

The continuing, remarkably successful, story of CMB studies is one driven by the close interplay of theory and phenomenology with increasingly sensitive and sophisticated experiments. The high degree of isotropy of the CMB across the sky, to a part of one in a hundred thousandth, led to the theory of inflation and cold dark matter in the 1980's. It was not until 1992 that COBE discovered the anisotropy, and pinned the level of anisotropy for the following higher angular resolution measurements to characterize. In 2006 the COBE measurements of the background anisotropy and its black-body spectrum were recognized with the second Nobel Prize in physics; the first was awarded in 1978 to Penzias and Wilson for the discovery of the CMB. In the decade after the COBE results, measurements with ground and balloon-based instruments revealed the acoustic peaks in the CMB angular power spectrum, which showed that the Universe was geometrically flat in accord with predictions of inflation and provided strong support for contemporary Type 1a SN based claims for an accelerating Universe, which were recognized with the 2011 Nobel Prize in physics. The early anisotropy measurements also provided an estimate of the universal baryon density and found it to be in excellent agreement with the level estimated at $t \sim 1$ second by BBN calculations constrained to match the observed elemental abundances. The CMB measurements also clearly showed that dark matter was non-baryonic. The polarization anisotropy was discovered ten years after COBE at the level predicted from temperature anisotropy measurements. The now standard ΛCDM cosmological model was firmly established.

Two CMB satellites have mapped the entire sky over the last 15 years, first WMAP with moderate angular resolution up to 12 arcminutes, followed by Planck with resolution up to 5 arcminutes. Higher resolution maps of smaller regions of the sky have been provided by ground-based experiments, most notably by the 10m South Pole Telescope (SPT) and the 6m Actacama Cosmology Telescope. The primary CMB temperature anisotropy is now well characterized through the damping tail, i.e., to multipoles $\ell \sim 3000$, and secondary anisotropies have been measured to multipoles up to $10,000$. The ΛCDM model continues to hold up stunningly well, even as the precision of the CMB determined parameters has increased substantially. Inflationary constraints include limits on curvature constrained to be less than 3% of the energy density, non-Gaussian fluctuations limited to $f_{NL} < 10$, and the predicted small departure from pure scale invariance of the primordial fluctuations detected at 5 sigma confidence. Also of interest to particle physics, the effective number of light relativistic species (i.e., neutrinos and any yet identified "dark radiation") is shown to be within one sigma of $N_{\rm eff} = 3.046$, the number predicted by BBN. The sum of the masses of the neutrinos is found to be less than 0.6 eV. Dark matter is shown to be non-baryonic matter at > 40 sigma. Early dark energy models are highly constrained as are models of decaying dark matter.

There remains much science to extract from the CMB, including: 1) using CMB B-mode polarization to search for primordial gravitational waves to constrain the energy scale of inflation and to test alternative

models, and to provide insights into quantum gravity; 2) obtaining sufficiently accurate and precise determinations of the effective number of light relativistic species (dark radiation) to allow independent and rigorous tests of BBN as well as our understanding of the evolution of the Universe at $t = 1$ sec; 3) a detection of the sum of the neutrino masses, even if at the minimum mass allowed by oscillation experiments and in the normal hierarchy; 4) using secondary CMB anisotropy measurements to provide precision tests of dark energy through its impact on the growth of structure; and 5) testing general relativity and constraining alternate theories of gravity on large scales.

Currently the best cosmological constraints come from analyzing the combination of primary and secondary CMB anisotropy measurements with other cosmological probes, such as baryon acoustic oscillations (BAO) and redshift distortions, weak lensing, galaxy and galaxy cluster surveys, Lyman-alpha forest, Hubble constant, Type 1a SN, and others. The CMB primary anisoptropy measurements provide highly complementary data for the combined analysis, in particular by providing a precision measurement of the Universe at $z = 1100$, which will provide a precise prediction for measurements of the late time Universe for any cosmological model and set of parameters – the Hubble constant, BAO scale, and the normalization of the present day matter fluctuation spectrum being excellent examples. Secondary CMB measurements provide late time probes directly from the CMB measurement, e.g., CMB lensing, the SZ effects and SZ cluster catalogs, which will provide critical constraints on the standard cosmological models and extensions to it. The cosmological reach of future cosmological surveys at all wavelengths will be greatly extended by their joint analyses with secondary CMB anisotropy measurements.

1.2 Science reach of CMB-S4

CMB-S4 should be the definitive ground-based CMB project. The key science it should cover, and cover well, are

1. Inflation: CMB-S4 should make the definitive B-mode measurements of the recombination bump at degree angular scales. This includes multiple bands to untangle the foregrounds and degree through arcminute angular scales to obtain the required CMB lensing and E-mode measurements for de-lensing inflationary gravitational wave B-modes. If it can be demonstrated that foregrounds and atmospheric noise can be mitigated at very low multipoles, CMB-S4 should also target the re-ionization bump. At the lowest multipoles, CMB-S4, balloon and satellite mission would be highly complementary.

   CMB-S4 should answer whether or not large scale slow-roll-single-field inflation models are viable ($r \gtrsim 0.01$) with high significance. If no detection at $r \gtrsim 0.01$, then CMB-S4 should be able to test the currently popular Starobinski model and others by achieving $\sigma(r) < 10^{-4}$ with an ultra deep survey.

   If r is detected before or by CMB-S4, then CMB-S4 should provide a robust cosmic variance limited measure of its value (requiring a large area survey), and set the best possible constraints on n_t (requiring an ultra deep survey).

   CMB-S4 should provide the polarization data to test predictions of models that attempt to explain the low-ell temperature power spectrum "anomalies", that may offer clues to inflation. It will be particularly important to achieve accurate $20 < \ell < 100$ E-mode measurements.

   CMB-S4 will also extend the leverage arm for n_s, particularly in the EE spectrum. It may be possible to extend the primary E-mode spectrum to multipoles exceeding 10,000 because of the very low level of polarized foregrounds at high ℓ.

   The CMB-S4 data set should be the definitive data set with which any model for the origin of the primordial fluctuations, be it inflationary or an alternative theory, must be consistent with to be viable.

2. Neutrinos and light relativistic species:

   There are two primary areas in which CMB-S4 will provide interesting neutrino constraints.

   a) The first is the effective number of light relativistic species, $N_{\rm eff}$. This is uniquely probed by the CMB and provides a critical constraint on any model for the neutrinos and their interactions. It is a highly complementary probe to BBN and to sterile neutrino models. Finding consistency with $N_{\rm eff} = 3.046$ at a precision of 0.020 would be an exciting and fundamental achievement linking particle physics and our understanding of the evolution of the first seconds of the Universe. Finding a departure from 3.046 would be even more exciting.

   b) The second is the constraint on the sum of the masses of the neutrinos, Σm_ν. Here CMB-S4 will achieve $\sigma(\Sigma m_\nu) = 16$ meV (with DESI BAO prior), with the CMB sensitivity coming primarily through CMB lensing. This will lead to a definite detection of neutrino mass, even at the minimum mass and the normal hierarchy. The sensitivity of cosmic probes to the sum of the masses is unique and complementary to terrestrial neutrino experiments.

3. Dark Energy and Gravity:

   The CMB can be used to investigate dark energy through growth of structure tests, i.e., CMB lensing and SZ clusters, and through testing Gravity on large scales, i.e., though exploiting the kinematic SZ effect to measure the momentum field and large scale flows. The power of these probes is amplified by combining CMB-S4 data with galaxy surveys and Lyman alpha surveys, such as DESI, LSST, Euclid and WFIRST.

   a) CMB lensing maps from CMB-S4 will provide hi-fidelity projected mass maps that will be cross-correlated with optical survey maps. This will increase the reach and precision of the dark energy constraints, as well as provide independent checks. Papers in the literature have quantified the dark energy figure of merit (FOM) improvement of various projects with the addition of CMB lensing. Simulations need to be done to quantify the projected improvements with CMB-S4.

   b) The dark energy task force (DETF) pointed out that galaxy cluster evolution had the highest sensitivity of the DE probes considered. However, it also had the largest systematic. The issue is the uncertainty in understanding the mass scaling of the cluster observable. The thermal SZ effect has now been demonstrated to be a low scatter observable with the extraordinary feature of its brightness being redshift independent; an SZ survey probes all redshifts to a limiting mass. However, there still remain large uncertainties in the SZ observable mass scaling. CMB-S4 will be revolutionary in that it is expected to be able to calibrate the mass scaling to better than 1% through CMB lensing. This coupled with a low mass threshold will enable CMB-S4 to identify of order 100,000 clusters, probe the growth of structure to redshifts beyond $z \sim 2.5$, and will allow CMB-S4 to realize the full potential of galaxy clusters as a probe of dark energy. In combination with other Stage-IV baryon acoustic oscillation, supernova, and weak lensing surveys, a Stage-IV cluster survey similar to CMB-S4 should improve the overall dark energy figure of merit to approximately 1250, nearly a factor of two improvement than achieved without clusters.

   c) Testing GR on large scales is important for our understanding of dark energy and the underlying workings of space and matter in general. The kinematic SZ effect allows measurement on the peculiar velocity (departure from Hubble flow) of structures. By measuring the differences in kSZ between pairs of clusters with known redshifts (a synergy of CMB-S4 and optical surveys), gravity can be tested on scales of 100 Mpc and larger. In this way, CMB-S4 paired with a Stage-IV spectroscopic survey would improve constraints on the growth rate predicted by general relativity by a factor of two.

Lastly it would be an oversight not to point out the obvious: there is only one CMB sky. It holds a wealth of information on fundamental physics and the origin and evolution of the Universe. While we have learned

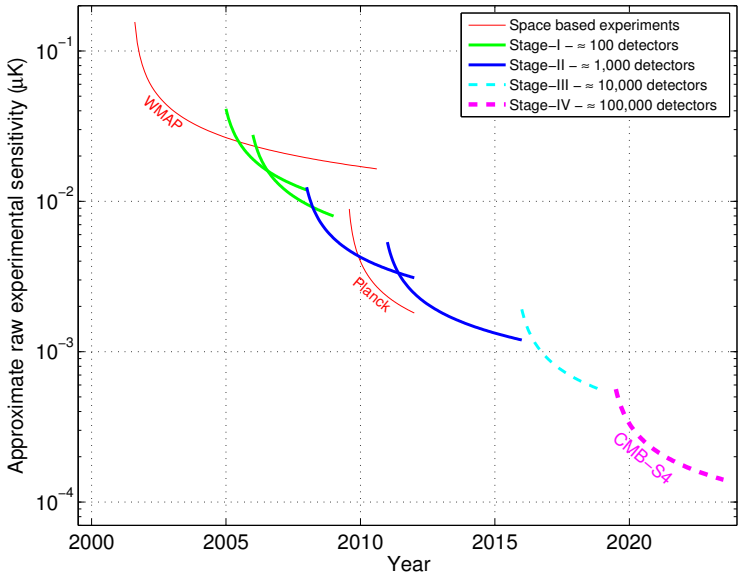

Figure 1. *Plot illustrating the evolution of the raw sensitivity of CMB experiments, which scales as the total number of bolometers. Ground-based CMB experiments are classified into Stages with Stage II experiments having O(1000) detectors, Stage III experiments having O(10,000) detectors, and a Stage IV experiment (such as CMB-S4) having O(100,000) detectors. Figure from Snowmass CF5 Neutrino planning document.*

a great deal from CMB measurements, including discoveries that have pointed the way to new physics, we have only begun to tap the information contained in CMB polarization, CMB lensing and secondary effects. CMB-S4 should be designed to maximize discovery space by producing high fidelity maps.

1.3 From science goals to CMB-S4 design

1.3.1 Conceptual design of CMB-S4

The science goals discussed above leads to a rough conceptual design of CMB-S4.

1.3.1.1 Sensitivity and detector count

The sensitivity of CMB measurements has increased enormously since Penzias and Wilson's discovery in 1965, following a Moore's Law like scaling, doubling every roughly 2.3 years. Fig. 1 shows the sensitivity of recent experiments as well as expectations for upcoming Stage 3 experiments, characterized by order 10,000 detectors on the sky, as well as the projection for a Stage 4 experiment with order 100,000 detectors. To obtain many of the CMB-S4 science goals requires of order 1 μK arcminute sensitivity over roughy 70% of the sky, which for a four year survey requires of order 500,000 CMB-sensitive detectors.

To maintain the Moore's Law-like scaling requires a major leap forward, it requires a phase change in the mode of operation of the ground based CMB program. Two constraints drive the change: 1) CMB detectors

are background limited, so more pixels are needed on the sky to increase sensitivity; and 2) the pixel count for CMB cameras are nearing saturation. Even using multichroic pixels and wide field of view optics, CMB telescopes are expected to field only tens of thousands of polarization detectors, far fewer than needed to meet the CMB-S4 science goals.

CMB-S4 thus requires multiple telescopes, each with a maximally outfitted focal plane of pixels utilizing superconducting, background limited, CMB detectors. To achieve the large sky coverage and to take advantage of the best atmospheric conditions, the South Pole and the Chilean Atacama sites are baselined, with the possibility of adding a new northern site to increase sky coverage to 100%.

1.3.1.2 Inflationary B-modes: low ℓ sensitivity, foregrounds and atmospheric noise mitigation

At the largest angular scales (low ℓ)— the angular scales that must be measured well to pursue inflationary B-modes as well as critical tests of the E-mode polarization —the CMB polarization anisotropy is highly contaminated by foregrounds. Galactic synchrotron dominates at low frequencies and galactic dust at high frequencies, as recently shown by the Planck and Planck/BICEP/KECK polarization results. Multi-band polarization measurements are required to distinguish the primordial polarized signals from the foregrounds.

Adding to the complexity of low multipole CMB observations is the need to reject the considerable atmospheric noise contributions over the large scans needed to extract the low ℓ polarization. While the spatial and temporal fluctuations of the atmosphere are not expected to be polarized, any mismatches in the polarized beams or detector gains will lead to T-P leakage. These issues can be mitigated by including additional modulations into the instrument design, such as bore-sight rotation or modulation of the entire optics with a polarization modulation scheme in front of the telescope. Implementing such modulations is easier for small telescopes, although they could in principle be implemented on large telescopes as well. The cost of a small aperture telescope is dominated by the detector array, making it feasible to deploy multiple telescopes each optimized for a single band, or perhaps multiple bands within the relatively narrow atmosphere windows.

It is therefore an attractive option for CMB-S4 to include dedicated small aperture telescopes for pursuing low-ℓ polarization. The default plan for CMB-S4 is to target the recombination bump, with E-mode and B-mode polarization down to $\ell \sim 20$. If Stage 3 experiments demonstrate that it is feasible to target the reionization bump from the ground, those techniques may be incorporated into CMB-S4. More likely, however, this is the ℓ range for which CMB-S4 will be designed to be complementary to balloon-based and satellite based measurements.

1.3.1.3 Neutrinos and dark energy: high ℓ sensitivity

At the highest angular resolution (high ℓ)— the angular scales needed for de-lensing the inflationary B-modes, constraining $N_{\rm eff}$ and Σm_ν, investigating dark energy and performing gravity tests with secondary CMB anisotropy —the CMB polarization anisotropy is much less affected by both foregrounds and atmospheric noise. In fact, it should be possible to measure the primary CMB anisotropy in E-mode polarization to multipoles a factor of a few times higher than possible in TT, thereby extending the lever arm to measure the spectral index and running of the primordial scalar (density) fluctuations. CMB-lensing benefits from ℓ_{max} of order 5000 and secondary CMB measurements are greatly improved with ℓ_{max} of order 10,000 and higher, requiring large aperture telescopes with diameters of several meters. Owing to the steep scaling of telescope cost with aperture diameter, it is likely not cost-effective to consider separate large aperture telescopes each optimized for a single frequency band.

CMB-S4 is therefore envisioned to include dedicated large aperture, wide field of view telescopes equipped with multiple band detector arrays.

1.3.2 Refining the CMB-S4 science case and key performance parameters

The rough conceptual design outlined above clearly needs to be refined. The first priorities are to determine the instrumental specifications to meet each of the science goals. We need to determine: the required resolution and sensitivity; the number of bands to mitigate foreground contamination, which is likely to be function of angular scale; the required sky coverage; the beam specifications (can we tolerate segmented primary reflectors?); the scanning strategy and instrument stability; etc.

Determining these specifications requires simulations, informed by the best available data and phenomenological models. Only when we have these specifications in hand can we design the instrument and answer such basic questions as the number and sizes of the telescopes.

1.4 The Road from Stage 3 to Stage 4

The Stage 2 and 3 experiments are logical technical and scientific stepping stones to CMB-S4. Fig. 2 shows the timeline of the CMB sensitivity and the expected improvement in a few of the key cosmological parameters. The enormous jump in sensitivity with the corresponding improvement in science reach is clear.

Finally, in Fig. 3 we show how the scientific findings (yellow), the technical advances (blue) and satellite selections (green) would effect the science goals, survey strategy and possibly the design of CMB-S4. [FEEDBACK ON THIS MOST APPRECIATED]

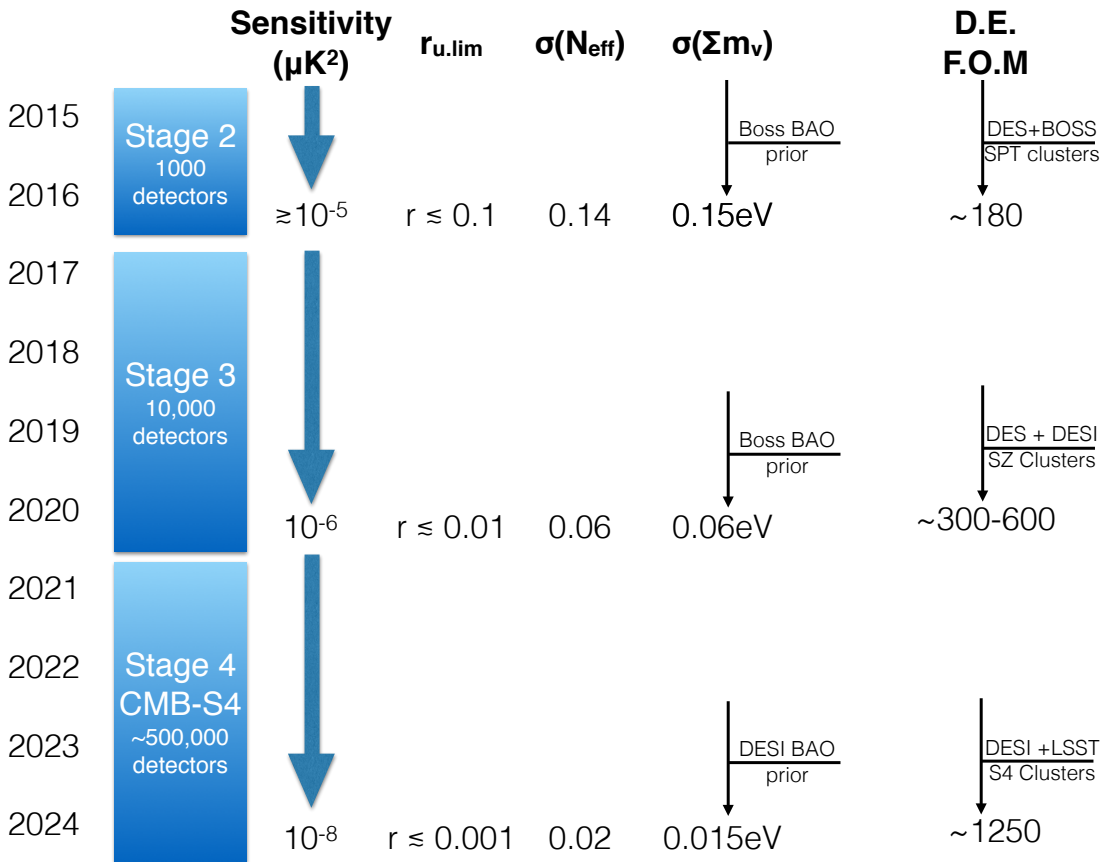

Figure 2. *Schematic timeline of evolution of Stage 3 and CMB-S4 sensitivity in μK^2 and the expected improvement in a few of the key cosmological parameters.*

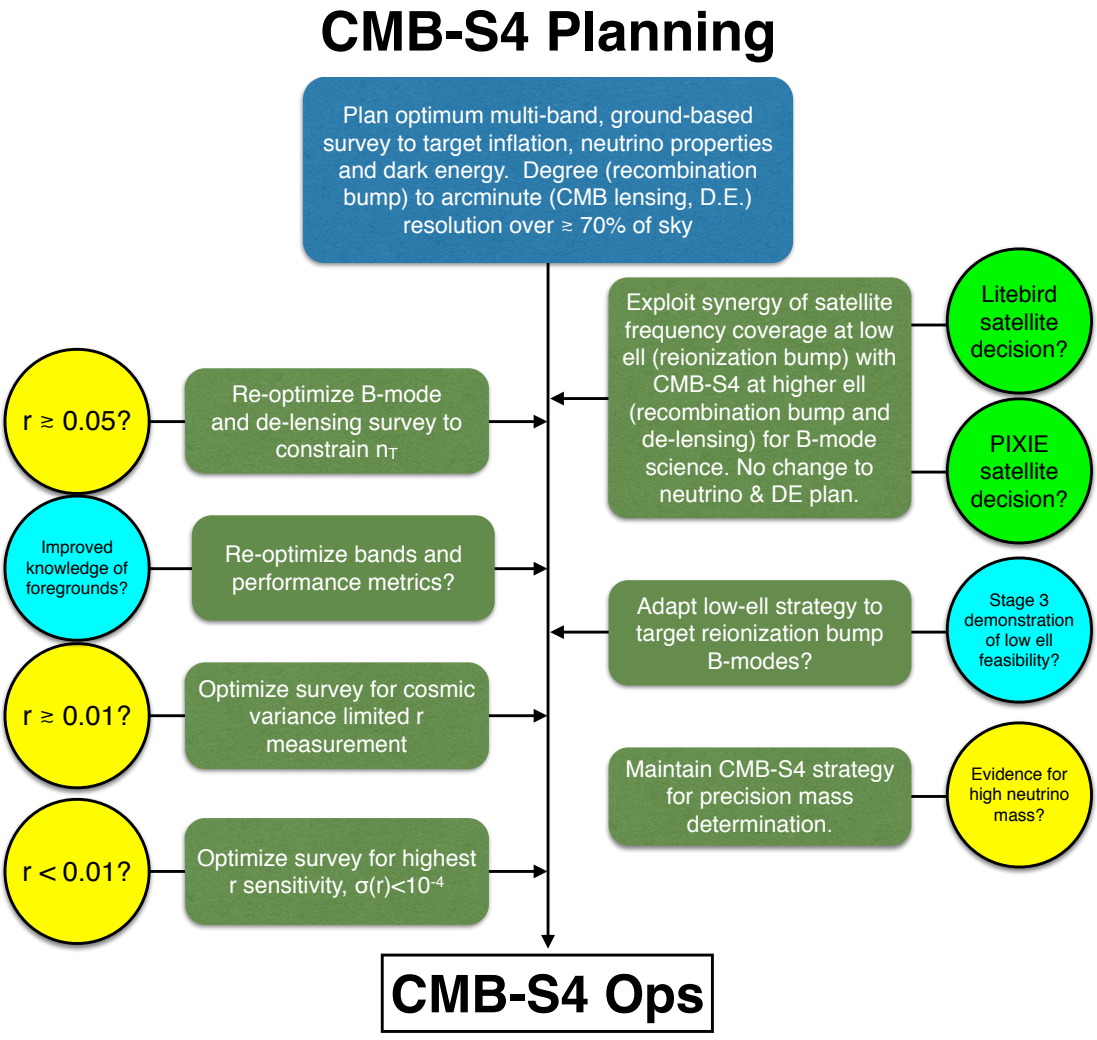

Figure 3. *Schematic flow chart showing how the scientific findings (yellow), the technical advances (blue) and satellite selections (green) would effect the science goals, survey strategy and possibly the design of CMB-S4 (green boxes) [FEEDBACK ON THIS MOST APPRECIATED]*

2

Inflation Physics from the Cosmic Microwave Background

(send feedback on this chapter to s4_inflation@cosmo.uchicago.edu)

2.1 Introduction

The small anisotropies in the cosmic microwave background radiation contain invaluable information about the primordial universe. On the one hand, they encode the properties of the primordial scalar (or density) perturbations and hence the matter sector of the primordial universe. CMB-S4 will significantly improve current constraints on primordial observables in the scalar sector, typically by a factor of at least five. On the other hand, on degree scales a polarization pattern known as B-mode polarization would reveal the existence of primordial tensor modes or gravitational waves. In the tensor sector, CMB-S4 will improve current constraints by almost two orders of magnitude. This is especially interesting because it allows this next generation instrument to reach theoretically well-motivated thresholds for the tensor-to-scalar ratio (the ratio of power in tensor modes to power in scalar modes), which consequently serves as the primary inflationary science driver for the design. A detection of primordial gravitational waves in the range accessible to this instrument would:

- Reveal a new scale of particle physics far above those accessible with terrestrial particle colliders.
- Rule out the only currently developed competitor to inflation (ekpyrotic scenario)

If, in addition, we can conclusively determine that any detected signal is dominated by vacuum fluctuations then a detection would also

- Identify the energy scale of inflation.
- Provide strong evidence that the complete theory of quantum gravity must accommodate a Planckian field range for the inflaton.
- Provide strong evidence that gravity is quantized, at least at the linear level.
- Constrain the mass of the graviton

In the absence of a detection CMB-S4 will rule out large classes of inflation models.

In Section 2.2 we review in detail what a detection of primordial gravitational waves would mean and what follow-up measurements should or could be done to further characterize any signal. Section 2.3 explains the implications of a robust upper limit of $r < 0.001$. Section 2.4 lays out what is required to achieve that goal. The final two sections describe the significant gains CMB-S4 will allow in constraining other aspects of the primordial universe, both standard and more speculative. These include characterizing the scalar power

spectrum, constraining curvature, non-Gaussianity, isocurvature modes, further probes of CMB 'anomalies' and test/constraints of cosmic strings.

2.2 Implications of a detection of primordial gravitational waves with CMB-S4

The overall evolution of the universe is well modeled by a Friedmann-Lemaître-Robertson-Walker line element

$$ds^2 = -dt^2 + a^2(t)\left[\frac{dr^2}{1-kr^2} + r^2 d\Omega^2\right], \tag{2.1}$$

where $k = \pm 1$ allows for spatial curvature and the time evolution is specified by the scale factor, $a(t)$. The Hubble parameter, $H = \dot{a}/a$, gives the rate of expansion of the universe.

The existence of primordial Helium and the cosmic microwave background radiation provide strong evidence for a hot big bang, a period during which the universe was dominated by radiation before it became dominated by matter and eventually dark energy. In the context of general relativity, observations of the cosmic microwave background furthermore provide strong evidence for a period preceding the hot big bang during which the co-moving Hubble radius, $(a|H|)^{-1}$, was decreasing with time: the measured average CMB temperature and the statistics of the measured anisotropies are the same over regions that otherwise share no causal history.

In an expanding universe a decreasing co-moving Hubble radius requires an era of accelerated expansion, $\ddot{a} > 0$, cosmic inflation. Such a period will drive the spatial curvature close to zero, in good agreement with current observations. Thus, we will assume spatial flatness and set $k = 0$ for most of the discussion, but will return to constraints on the curvature in Section 2.6. Since the period of cosmic inflation must end, there must exist a clock, or scalar degree of freedom. According to the uncertainty principle this clock must fluctuate, generating density perturbations that are adiabatic. In the most economic scenarios, these density perturbations are the seeds that grow into the anisotropies observed in the cosmic microwave background radiation and the stars and galaxies around us. Other degrees of freedom could, of course, also be present during this phase and might even be responsible for the generation of density perturbations we observe. **(Mention isocurvature modes here?)**

Alternatively, the phase of decreasing co-moving Hubble radius could have occurred during a period of decelerating contraction which must then be followed by a bounce as in the ekpyrotic or matter bounce scenarios.

For these early times, the ADM formalism provides a convenient parametrization of the line element

$$\begin{aligned} ds^2 &= -N^2 dt^2 + h_{ij}(dx^i + N^i dt)(dx^j + N^j dt) \\ h_{ij} &= a^2(t)[e^{2\zeta}\delta_{ij} + \gamma_{ij}]\,. \end{aligned} \tag{2.2}$$

The equations of motion for N (the lapse) and N^i (the shift) are the Hamiltonian and momentum constraints, while ζ ($= -\mathcal{R}$ of *Planck*) and γ_{ij} contain the dynamical scalar and tensor degrees of freedom. In scenarios with matter sources other than a scalar field there may also be vector perturbations. These rapidly decay and can be neglected unless they are actively sourced in the post-inflationary universe, e.g. by cosmic strings.

Because the equations of motion are invariant under translations and the perturbations are linear or nearly so, it is convenient to work with the Fourier transforms

$$\zeta(t,\vec{x}) = \int \frac{d^3k}{(2\pi^3)}\zeta(t,\vec{k})e^{i\vec{k}\cdot\vec{x}} + h.c. \qquad \text{and} \qquad \gamma_{ij}(t,\vec{x}) = \sum_s \int \frac{d^3k}{(2\pi^3)}\gamma_s(t,\vec{k})e_{ij}(\vec{k},s)e^{i\vec{k}\cdot\vec{x}} + h.c.\,, \quad (2.3)$$

where $e_{ij}(\vec{k},s)$ is the transverse traceless polarization tensor for the graviton. The solutions oscillate when the modes are deep inside the horizon, $k \gg aH$. By definition, the modes exit the horizon when $k = aH$ and in single-field models approach a constant outside the horizon when $k \ll aH$.

The statistical properties of the scalar and tensor fluctuations, ζ and γ_s, at times sufficiently late so that they have frozen out provide the link between the primordial era and the CMB as well as other probes of the structure of the late universe. For a universe that is statistically homogeneous and isotropic and in which the primordial fluctuations are Gaussian, the information about the statistical properties is contained in the two-point correlation functions

$$\begin{aligned}\langle\zeta(\vec{k})\zeta(\vec{k}')\rangle &= (2\pi)^3\delta^3(\vec{k}+\vec{k}')\frac{2\pi^2}{k^3}\mathcal{P}_\zeta(k)\\ \langle\gamma_s(\vec{k})\gamma_{s'}(\vec{k}')\rangle &= (2\pi)^3\delta_{ss'}\delta^3(\vec{k}+\vec{k}')\frac{2\pi^2}{k^3}\frac{1}{2}\mathcal{P}_t(k)\end{aligned} \quad (2.4)$$

where the factor of 1/2 in the second to last line accounts for the fact that the measured power includes contributions from each of the two graviton polarizations. In single field slow-roll inflation, the gauge invariant combination of metric and scalar field fluctuations that is conserved outside the horizon has the power spectrum

$$\mathcal{P}_\zeta(k) = \frac{1}{2\epsilon M_p^2}\left(\frac{H}{2\pi}\right)^2\Bigg|_{k=aH} \quad (2.5)$$

where $\epsilon = -\dot{H}/H^2$ is the first slow-roll parameter, and $M_p = 1/\sqrt{8\pi G}$ is the reduced Planck mass. As indicated, the Hubble parameter and ϵ are to be evaluated at horizon exit when the wavenumber k is equal to the inverse comoving Hubble radius. In the absence of additional sources, the tensor power spectrum generated by inflation is

$$\mathcal{P}_t(k) = \frac{8}{M_p^2}\left(\frac{H}{2\pi}\right)^2\Bigg|_{k=aH} \quad (2.6)$$

It is convenient to introduce the logarithmic derivatives of these power spectra

$$n_s(k) - 1 \equiv \frac{d\ln\mathcal{P}_\zeta}{d\ln k} \qquad \text{and} \qquad n_t(k) \equiv \frac{d\ln\mathcal{P}_t}{d\ln k}\,. \quad (2.7)$$

If the Hubble rate and slow-roll parameter only weakly depend on time as in slow-roll inflation, these will be $n_s(k) \approx 1$ and $n_t(k) \approx 0$ and can be expanded around a pivot scale $k_\star$ accessible by the CMB

$$n_s(k) - 1 = n_s - 1 + \frac{dn_s(k)}{d\ln k}\bigg|_{k_\star}\ln(k/k_\star) + \ldots \qquad \text{and} \qquad n_t(k) = n_t + \frac{dn_t(k)}{d\ln k}\bigg|_{k_\star}\ln(k/k_\star) + \ldots \quad (2.8)$$

In this approximation, the power spectra are

$$\mathcal{P}_\zeta(k) = A_s \left(\frac{k}{k_\star}\right)^{n_s - 1 + \frac{1}{2}\frac{dn_s}{d\ln k}\big|_{k=k_\star} \ln(k/k_\star) + \ldots},$$
$$\mathcal{P}_t(k) = A_t \left(\frac{k}{k_\star}\right)^{n_t + \frac{1}{2}\frac{dn_t}{d\ln k}\big|_{k=k_\star} \ln(k/k_\star) + \ldots}, \tag{2.9}$$

where A_s, A_t are the scalar and tensor amplitudes, and n_s and n_t, are the scalar and tensor spectral index, respectively, both at the pivot scale. The tensor-to-scalar ratio, r, is the relative power in the two types of fluctuations at a chosen pivot scale $k_\star$ accessible by the CMB

$$r = \frac{A_t}{A_s} \tag{2.10}$$

The power spectra of ζ and γ_s are time-independent as long as the modes are outside the horizon, and only begin to evolve once the modes of interest re-enter the horizon at late times. In particular, they set the initial conditions for the system of equations governing the time evolution of the universe from around 10^9 K when electrons and positrons have annihilated to the present. To exhibit the link between the primordial perturbations and late time observables explicitly, note that in a spatially flat universe, the contributions of primordial scalar perturbations to the angular power spectra of temperature or E-mode anisotropies are given by

$$C^{(S)}_{XX,\ell} = \int \frac{dk}{k} \mathcal{P}_\zeta(k) \left| \int_0^{\tau_0} d\tau S^{(S)}_X(k,\tau) j_\ell(k(\tau_0 - \tau)) \right|^2, \tag{2.11}$$

where $S^{(S)}_X(k,\tau)$ with $X = T, E$ are source functions that encode the physics of recombination and j_ℓ is a spherical Bessel function that encodes the (spatially flat) geometry of the universe. At linear order, scalar perturbations only contribute to angular power spectra of temperature and E-mode polarization and the cross-spectrum of temperature and E-mode polarization, while the tensor perturbations in addition generate B-mode polarization. The primordial contribution of the tensor perturbations to the angular power spectrum of B-modes is

$$C_{BB,\ell} = \int \frac{dk}{k} \mathcal{P}_t(k) \left| \int_0^{\tau_0} d\tau S^{(T)}_B(k,\tau) j_\ell(k(\tau_0 - \tau)) \right|^2. \tag{2.12}$$

where $S^{(T)}_B(k,\tau)$ is the appropriate source function.

At present, bounds on the tensor contribution to the temperature and E-mode anisotropies are comparable to constraints on the tensor-to-scalar ratio from B-mode observations. The former constraints are now cosmic variance limited. There is no limit on the latter from cosmic variance, and improvements and a potential detection with CMB-S4 will rely on measurements of B-mode polarization on degree scales.

Constraints on the amplitude of primordial tensor modes already strongly disfavor once popular inflationary models like minimally coupled chaotic inflation with a quadratic potential. We will discuss in detail what a detection of primordial gravitational waves would imply for inflation in the next several sections, but it is also important to note that a detection would rule out contracting universe scenarios. A contracting universe can also put large scales in causal contact if the scale factor a is nearly constant while the magnitude of the Hubble parameter increases. This means the spectrum of gravitational wave fluctuations will be very blue [227]. In addition the Hubble parameter at the end of the contracting phase can be approximately bounded (minimally, $H < M_p$, or $H \sim T_{\rm reheat}$) and so the value of H that sets the amplitude of tensor fluctuations on scales accessible through the CMB must be exponentially smaller. The vacuum fluctuations in a contracting universe are then far too small to be detected [82].

2.2.1 The energy scale of inflation

According to the inflationary prediction for the amplitude of primordial gravitational waves, Eq. (2.6), a detection provides a direct measurement of the Hubble scale during inflation. In single field slow-roll models, Eq. (2.5), the value of the amplitude of the power spectrum of scalar fluctuations measured by the *Planck* satellite together with the Friedmann equation $3H^2M_p^2 \approx V$ determine the energy scale of inflation in terms of r (all at the pivot scale $k_\star = 0.05$ Mpc^{-1})

$$V^{1/4} = 1.04 \times 10^{16}\text{GeV} \left(\frac{r_\star}{0.01}\right)^{1/4} , \tag{2.13}$$

so that a detection of primordial gravitational waves determines the energy scale of inflation to within a few per cent.

In more general models of inflation the relation can be modified by changing the power in the scalar sector so that a detection only determines the order of magnitude of the new energy scale. Familiar examples are models in which the speed of sound of the inflaton quanta differs from unity or multi-field models. The extent to which the relation can be modified is bounded by constraints on non-Gaussianity. **be more specific** In other examples string or particle production events source gravitational waves [110, 341]. To maximize the production of gravitational waves, the field χ creating and annihilating the quanta should be massless, since massive particles contribute a smaller quadrupole moment and are a weaker source of gravitational waves [45]. Furthermore, χ should be a stronger source of tensor than of scalar modes, because the properties of the latter are tightly constrained by current bounds on the bispectrum [46], and in some models by constraints on the running of n_s [279]. Current bounds on an equilateral bispectrum imply that scenarios in which the inflaton is directly coupled to the additional field sourcing gravitational waves cannot lead to a signal that is parameterically larger than the vacuum signal [45, 154, 283, 394]. So in this case, a detection remains a good indicator of the scale of inflation. Improved constraints on non-Gaussianity (see Section 2.5) will further restrict these scenarios. A bound $f_{\rm NL}^{\rm equil} <?$ achievable with CMB-S4 would constrain these scenarios to contribute at most xx% of any gravitational wave signal.

To evade constraints from scalar non-Gaussianity, the dynamics generating χ should be decoupled from the inflaton sector [45] (that is, only gravitationally coupled). Together with the considerations above, this suggests a scenario in which χ is a gauge field whose quanta are created by a parity violating interaction with a spectator field [110, 45], so that only modes with a definite handedness are produced [26]. The gauge fields in turn source gravity waves and scalar perturbations. Helicity conservation implies that gravitons of that same handedness are produced in much larger amount than gravitons of the opposite handedness [351], and than scalar modes [45]. In such a scenario current constraints on non-Gaussian correlations in the temperature anisotropies can be evaded if the production of χ quanta occurs only around the time the modes contributing to the multipoles relevant for the B-mode search leave the horizon [293] because constraints on non-Gaussianities are dominated by smaller scales. Reference [293] provides a model in which gravitational waves from gauge field production could be measured at a level of $r = 10^{-1}$ with a vacuum contribution of only $r = 10^{-4}$. While in that case the determination of the scale of inflation is affected by less than one order of magnitude, adjusting the parameters of the scenario, it may allow for more dramatic modifications of Eq. (2.13). However, in a regime in which the relation is strongly modified the B-mode anisotropies would be highly non-Gaussian. So in the case of a detection even the B-mode bispectrum would become observable with CMB-S4. In addition, since the signal would be parity violating, the angular bispectrum of B-modes would be dominated by $\ell_1 + \ell_2 + \ell_3 =$even, which would vanish in any theory that respects parity. Such a signal would not be confused with the vacuum fluctuations of the spacetime metric arising in single field slow-roll inflation. We return to this point in more detail in Section 2.2.4 below.

Finally, note that these secondary production mechanisms cannot be used to obtain a signal from a contracting primordial era... **does anyone know if this is true?**

Should we address these papers at all: 1410.8845, rebutted in 1508.01527, re-rebutted in 1510.06759, (different author) 1510.07956?

2.2.2 Planckian field ranges and symmetries

The spectrum of tensor fluctuations depends only on the Hubble parameter H during inflation, while the scalar power depends on both H and the evolution of the homogeneous field sourcing inflation. As a consequence, the tensor-to-scalar ratio r determines the inflaton field range in Planck units [256]

$$\frac{\Delta\phi}{M_p} = \int_0^{\mathcal{N}_\star} d\mathcal{N} \left(\frac{r}{8}\right)^{1/2} , \tag{2.14}$$

where $\mathcal{N}_\star$ is the number of e-folds between the end of inflation and the moment when the mode with $k_\star = 0.05\,\mathrm{Mpc}^{-1}$ corresponding to the CMB pivot scale exits the horizon. In many common inflationary models r is a monotonic function of $\mathcal{N}$ so that

$$\frac{\Delta\phi}{M_p} \gtrsim \left(\frac{r_\star}{8}\right)^{1/2} \mathcal{N}_\star \gtrsim \left(\frac{r}{0.01}\right)^{1/2} . \tag{2.15}$$

The value of $\mathcal{N}_\star$ is not well constrained and depends on unknown details of reheating, but $\mathcal{N}_\star \gtrsim 30$ provides a conservative lower limit, justifying the second inequality in equation (2.15). Thus, a tensor-to-scalar ratio $r > 10^{-2}$ typically corresponds to a trans-Planckian excursion in field space between the end of inflation and the epoch when the modes we observe in the CMB exit the horizon.

Unless we work in a UV complete theory such as string theory, we rely on an effective field theory description of the inflationary epoch. General relativity viewed as an effective field theory breaks down as energies approach the Planck scale because interactions between gravitons become strongly coupled. The same is true for matter coupled to general relativity, so that the effective field theory governing the inflationary period will generically have a sub-Planckian cut-off $\Lambda_{\rm UV} < M_p$. In fact, in any weakly coupled UV completion of general relativity the new degrees of freedom must enter well below the Planck scale to ensure weak coupling so that $\Lambda_{\rm UV} \ll M_p$.

According to the bound (2.15), a tensor-to-scalar ratio $r > 10^{-2}$ then requires a displacement in field space that is larger than the cut-off of the effective field theory. While this does not invalidate an effective field theory description, it has important consequences. The effective field theory was obtained by integrating out all modes parametrically heavier than the cut-off $\Lambda_{\rm UV}$ of the single-field model. In the absence of symmetries, we expect the inflaton ϕ to couple to heavy degrees of freedom χ, schematically

$$S = \int d^4x\sqrt{-g}\left[-\frac{1}{2}g^{\mu\nu}\partial_\mu\phi\partial_\nu\phi - \frac{1}{2}g^{\mu\nu}\partial_\mu\chi\partial_\nu\chi - \frac{1}{2}m^2\phi^2 - \frac{1}{2}M^2\chi^2 - \frac{1}{2}\mu\phi\chi^2 + \dots\right] . \tag{2.16}$$

By assumption, the mass of the heavy degrees of freedom to be integrated out is $M \gtrsim \Lambda_{\rm UV}$, and the dots represent various other interaction terms. Generically the dimensionful coupling μ is also expected to be of order the cut-off, $\mu \sim \Lambda_{UV}$. From the last two terms in equation (2.16), we see that displacements of ϕ by a distance comparable to the cut-off may lead to cancellations in the effective mass of the heavy degrees of freedom, and heavy states, in this case χ, may become light if ϕ is displaced by a distance large compared to the cut-off. In particular, since $\Lambda_{\rm UV} < M_p$ we should not expect potentials that are smooth over super-Planckian distances in a generic low energy effective field theory with cut-off $\Lambda_{\rm UV} < M_p$.

We can only expect potentials suitable for large-field inflation if some mass scales, in the example m and μ are well below the cut-off, or if dimensionless couplings are small. This occurs naturally if the UV theory respects a weakly broken shift symmetry $\phi \to \phi + c$ that ensures that quantum corrections from the inflaton and graviton will not introduce large corrections to the inflationary Lagrangian [251, 216, 118, 221, 103]. At the level of an effective field theory we can simply postulate such an approximate shift symmetry, but one should keep in mind that we ultimately require the existence of such a symmetry in quantum gravity.

As the best developed theory of quantum gravity, string theory is a useful framework for exploring mechanisms that allow large-field inflation to be realized even in the presence of heavy degrees of freedom. Axions are ubiquitous in string theory and provide natural candidates for the inflaton because they enjoy a shift symmetry that is weakly broken by instanton effects as well as the presence of branes or fluxes [383]. Early field theory models relied on the familiar periodic contributions to the potential generated by instantons to drive inflation [163, 9]. In string theory the periods are expected to be sub-Planckian [44, 31], while constraints on the scalar spectral index require super-Planckian axion periods so that a UV completion of these models does not currently exist. The claimed detection of primordial B-modes by BICEP2 has led to renewed interest in models in which the inflaton is an axion with a potential that is entirely due to instanton effects, and has intensified the discussion to what extent some means to achieve large field inflation via multiple axions may be incompatible with basic principles of quantum gravity [228, 334, 128, 333, 86, 40, 87, 192, 191, 234].

In addition to the familiar non-perturbative contributions that break the continuous shift symmetry to a discrete one, the presence of fluxes and branes lead to contributions to the axion potentials that break the discrete shift-symmetry as well. As the axion is displaced by one period, one unit of charge is induced, so that the axion field space becomes non-compact. As a consequence, super-Planckian decay constants are not required for super-Planckian excursions in these monodromy models [346, 274, 217, 60, 303, 275, 270, 71, 190]. Generically both contributions to the potential are present and these models predict periodic effects at some level, either directly from the periodic features in the potential or from periodic bursts of string or particle production. Unfortunately, the strength of the signal is very model dependent, and a detection of these effects with CMB-S4 is not guaranteed.

In writing (2.15), we have assumed that r is monotonic, or at least of the same order of magnitude throughout the inflationary period. One can easily construct models in which r is non-monotonic to weaken the bound [56, 201, 100]. In the case of a detection with CMB-S4 of a spectrum that is at least approximately scale-invariant, we can write the weaker bound

$$\frac{\Delta\phi}{M_p} \gtrsim \left(\frac{r}{0.3}\right)^{1/2} , \tag{2.17}$$

which bounds the distance in field space traveled during the time the modes we observe in the CMB exited the horizon. This inequality implies that even if the distance in field space traveled during this period is sub-Planckian, it is not parameterically smaller than M_p. Because general relativity is not UV complete and becomes strongly coupled at M_p, any weakly coupled UV completion will come with a scale of new physics M, e.g. the string scale, that must be parameterically smaller than the Planck scale to ensure weak coupling. This implies that we cannot avoid the question of the embedding of the inflation model into quantum gravity for $r = 0.01$ or even for $r = 0.005$ unless we assume the UV completion of general relativity is strongly coupled.

In deriving the primordial power spectra and equation (2.14), we have assumed the Bunch-Davies state. The relation between r and the scale of inflation is modified if we assume that the tensor modes (and the scalar modes) either do not start in the Bunch-Davies state [36, 107], or that the evolution during inflation will lead to departures from it. The first option generically introduces a stronger scale-dependence into the tensor spectrum [27, 158] (and additional non-Gaussianity). In addition, this way of achieving observable primordial B-modes from a low-scale model has a similar feature to large-field models: one should show that the initial state is not only acceptable from the point of view of low energy considerations, but can

be generated by pre-inflationary physics. The second option, discussed in section 2.2.1, leads to non-trivial higher n-point functions that are in principle measurable.

In summary, a conclusive detection of primordial B-modes with CMB-S4 would provide evidence that the theory of quantum gravity must accommodate a Planckian field range for the inflaton. Conversely, the absence of a detection of B-modes with CMB-S4 will mean that a large field range is not required.

A detection of r, together with high confidence that the gravitational waves are predominantly due to vacuum fluctuations, would provide the only data point for the foreseeable future that weighs in on quantum gravity.

2.2.3 Constraints on the graviton mass

Theories of massive gravity come in many flavors (see e.g. [137, 195]), and their predictions in the scalar sector differ significantly. However, by definition, the dispersion relation for the graviton in all of them is

$$\omega^2 = p^2 + m_g^2 \,, \tag{2.18}$$

where p is the physical momentum and m_g the possibly time-dependent graviton mass. As a consequence, gravitational waves necessarily have frequencies $\omega > m_g$. A detection of primordial B-mode polarization on angular degree scales may be considered as a detection of gravitational waves with frequencies $\omega \sim H_{\rm rec}$ through the quadrupole they produce in the primordial plasma, where $H_{\rm rec} \approx 3 \times 10^{-29}$ eV is the Hubble parameter at recombination. A detection then implies a model-independent bound $m_g < H_{\rm rec}$ or

$$m_g < 3 \times 10^{-29} \text{ eV} \,. \tag{2.19}$$

If the graviton mass is time-dependent, this should be interpreted as a constraint on the graviton mass around the time of recombination.

Because the perturbations in the primordial plasma before and around recombination are linear, the effect of the graviton mass is straightforward to incorporate by a simple modification of the field equation for tensor metric perturbations so that the above argument can be made more quantitative. The equation of motion for the transverse traceless metric perturbation γ takes the same form as for a minimally coupled massive scalar field,

$$\ddot{\gamma}_k(\tau) + 2\frac{\dot{a}}{a}\dot{\gamma}_k(\tau) + (k^2 + m_g^2 a^2)\gamma_k(\tau) = 0 \,. \tag{2.20}$$

Here k is the comoving momentum of the metric perturbation, and we work in the conformal coordinates so that the background cosmological metric is

$$ds^2 = a^2(\tau)(d\tau^2 - d\mathbf{x}^2) \,. \tag{2.21}$$

The consequences of this modification are discussed in detail in [138]. The most important consequence is that superhorizon modes start to oscillate around the time τ_m when $H(\tau_m) = m_g$, and their amplitude subsequently redshifts as $a^{-3/2}$. In contrast, in the massless case all modes remain frozen until they enter the horizon. This results in a suppression of the amplitude primordial B-mode for $m_g \gg H_{\rm rec}$, and a detection of B-modes would rule out this possibility. For masses around $H_{\rm rec}$, there is no suppression, but the angular power spectra are modified by the presence of a graviton mass, and a detection of primordial B-mode polarization would allow to measure the graviton mass. A detection of primordial gravitational waves with angular B-mode power spectrum consistent with that expected in general relativity would imply $m_g < 3 \times 10^{-29}$ eV.

For comparison, the current model-independent bounds on the graviton mass arise from the indirect detection of $\sim 3 \times 10^{-5}$ Hz gravitational waves through the timing of the Hulse-Taylor binary pulsar [156], and the bound on the difference in arrival times for gravitational waves with different frequencies in the recent direct detection of astrophysical gravitational waves with LIGO [6]. The resulting bounds are $m_g \lesssim 10^{-19}$ eV and $m_g \lesssim 10^{-22}$ eV, respectively.

A detection of B-mode polarization on angular degree scales consistent with the expectation in the context of general relativity would improve current bounds on the mass of the graviton by nearly seven orders of magnitude.

Measurements of B-mode polarization on the largest angular scales, possible only with a satellite, would further strengthen the bound.

2.2.4 Following up on a detection

Once a detection has been made, it becomes necessary to understand the source of the signal. In slow-roll inflation, we expect a nearly scale invariant power spectrum and a nearly Gaussian signal so that the spectral index and the bispectrum provide observables that can strengthen the interpretation of the signal. More generally, the scale-dependence of the B-mode spectrum and higher order correlations probe the contributions of sources other than vacuum fluctuations, and possible physics beyond Einstein gravity and/or minimal coupling of the inflationary matter fields to gravity. Although we do not find that these considerations affect the optimal design of CMB-S4, they are be important in order to distinguish vacuum fluctuations from secondary sources of B-modes, and because of the complementarity with other future direct detection instruments.

2.2.4.1 Distinguishing vacuum fluctuations from other particle physics sources of B-modes

As mentioned in section 2.2.1, string of particle production may generate gravitational waves that can compete with the vacuum fluctuations in the spacetime metric. In a regime in which the relation between the amplitude of tensor modes and the scale of inflation is strongly modified the B-mode anisotropies are generally highly non-Gaussian and in some cases parity violating. Such a signal is distinguishable from vacuum fluctuations with CMB-S4 provided... **Can we add a figure/some numbers?**

Scenarios in which non-Abelian gauge fields play a significant role in the inflationary dynamic are closely related. In chromo-natural inflation and gauge-flation scenarios [264, 20, 21, 18, 19, 133, 134], the central piece is a homogeneous and isotropic, flavor-space locked gauge field that helps slow the roll of the inflaton or else is the inflaton itself. For a non-Abelian field with SU(2) symmetry, this means the three flavor gauge vector potentials are mutually orthogonal in space. The stress-energy of this configuration could leave a unique imprint on a spectrum of primordial gravitational waves, which would be transferred to the B-mode spectrum in the CMB. The non-Abelian nature of the field introduces a preferred handedness onto this medium leading to an enhancement of left (or right) circularly polarized gravitational waves. Again this would lead to parity-violating EB and TB correlations [255, 175] or parity violating higher n-pt functions. If this process takes place in the post-inflationary environment, the gauge field could further impress a periodic modulation on the gravitational wave spectrum [66, 67]. Although the basic chromo-natural and gauge-flation models have been ruled out [292], these unique features are expected to be generic to any viable variations on these scenarios.

Multi-field inflationary scenarios that end with phase transitions [193, 375, 232, 365, 209, 210, 331] and models of brane-inflation in string theory [336, 212, 112] generically predict some level of vector and tensor modes actively sourced by topological defects. In particular, either a breaking of a $U(1)$ symmetry or the production of fundamental strings at the end of inflation can lead to "cosmic strings" whose B-mode spectrum is primarily generated by vector modes and peaks on small scales ($\ell \sim 600 - 1000$) and is more similar in shape to the E to B lensing signal than to the vacuum spectrum. CMB-S4 should be able to distinguish even a small contribution from such sources [369], but the precise bounds from non-detection are related to the precision with which the lensing signal can be removed. Estimates made in reference [340, 39] indicate that CMB-S4 should be able to improve the limit on cosmic string tension by at least an order of magnitude beyond the current bounds from the CMB ($G\mu \sim 10^{-7}$ [15, 12]) and may be competitive with direct detection limits from the stochastic gravitational wave background ($G\mu \sim 10^{-11}$ or 10^{-8} depending on the model assumed for string loops [35]). In addition, the spectra of different types of defects have different shapes, and should be distinguishable [368, 39]. Measuring the location of the main peak would provide valuable insights into fundamental physics. For example, in the case of cosmic superstrings the position of the peak of the B-mode spectrum constrains the value of the fundamental string coupling g_s in string theory [39].

Post-inflationary phase transitions themselves have also been proposed as a source of nearly scale-invariant gravitational waves detectable through CMB polarization (and direct detection) [238, 213]. Even for a spectrum that matches the inflationary result on small scales, any such signal can in principle be distinguished from the inflationary signal by the presence of super-horizon correlations at the time of recombination. A framework to extract specifically this bit of the signal was proposed in [53] and could be applied to robustly extract the part of any signal that must come from physics outside of the hot big bang paradigm. (**Can this be achieved with CMB-S4?**)

2.2.4.2 Probing matter and gravitational interactions at the inflationary scale

The tensor tilt as a probe of the potential and non-minimal coupling: If the amplitude of primordial B-modes is large enough to be measured, we can begin to constrain the shape of the spectrum. The simplest inflation scenarios all predict a red spectrum for gravitational waves, and the canonical single field consistency relation fixes $n_t = -r/8$. For a single field with a sound speed less than one, or multiple fields, $n_t/r < -1/8$ instead [323]. However, allowing the inflaton to couple to higher curvature terms can produce a blue tilt [52]. A detection of primordial gravitational waves on CMB scales would allow precise predictions, especially relevant for a blue index, for the amplitude expected on the much smaller scales accessible to direct detection. The recent detection of gravitational waves by LIGO, as well as the beginning of operation of the LISA pathfinder instrument, open an exciting new era of gravitational wave science. If CMB-S4 also sees a signal, LIGO and future instruments may be particle physics detectors as well as astrophysical observatories. A recent analysis in [241] shows the complementarity between observations over a wide range of scales in constraining the spectrum (although one must assume a constant tilt n_t over many orders of magnitude).

The tensor amplitude and field content that modifies the scalar power: Since non-minimal inflation models with multiple fields or a small sound speed for a single degree of freedom predict a tensor-to-scalar ratio that is suppressed, a detection of gravitational waves of can be used to constrain the physics that produces the suppression in these scenarios. For single clock scenarios, this link is relatively straightforward [51] and a detection of r can provide an upper limit on the speed of sound (and so a limit on non-Gaussianities). For multi-field scenarios many more details of the model must be specified [330], but r together with bounds on isocurvature and local type non-Gaussianities may aid in model discrimination.

Other signatures of a modified gravitational sector: Coupling the inflaton to higher curvature terms can also introduce parity violation in the spectrum of primordial gravitational waves [254, 23, 109, 361]. Reference [361] contains some example amplitudes of the coupling that would be detectable for a detection of $r = 0.05$; reference [173] discusses distinguishability of chiral gravity waves from other possible sources of parity violation, such as uniform cosmic birefringence. In addition, the momentum structure of the three-point function of gravitational waves would also be a sensitive probe of possible extensions of Einstein gravity [262]. However, the amplitude of the three point correlations between tensors alone in both standard inflation and extensions is small, at most $f_{\rm NL}^{\rm tensor} \lesssim 1$ [263, 262]. So while any constraint on the gravitational three-point function would be a useful data point for secondary sources, it is unlikely to be significant for vacuum fluctuations. Finally, it is worth noting that, if primordial gravitational waves were indeed chiral, they may present themselves first through a non-vanishing cross-correlation of B-modes with temperature, as demonstrated in Ref. [109].

2.3 Lessons from upper limits

A detection of primordial gravitational waves has profound implications. Even excluding the presence of gravitational waves at a level observable by CMB-S4 has important consequences for the theory of inflation. Current constraints already strongly disfavor models that were plausible candidates such as chaotic inflation with a quadratic potential [65]. Upper limits from CMB-S4 would rule out entire classes of inflationary models.

We first present a version of an argument developed in [288, 332, 114] that does not rely on microscopic details of inflationary models. In the limit $\epsilon \ll 1$, equations (2.5) and (2.7) lead to a differential equation

$$\frac{d\ln\epsilon}{d\mathcal{N}} - (n_s(\mathcal{N}) - 1) - 2\epsilon = 0\,, \tag{2.22}$$

where $\mathcal{N}$ is the number of e-folds until the end of inflation, and $n_s(\mathcal{N})-1$ denotes the spectral index evaluated for the mode which exits the horizon $\mathcal{N}$ e-folds before the end of inflation. Note that ϵ is small (but positive) during inflation and $\epsilon \sim 1$ when inflation ends. If ϵ is a monotonic function of $\mathcal{N}$ this implies $n_s(\mathcal{N}) - 1 \leq 0$ in agreement with observations.

Denoting the number of e-folds before the end of inflation at which the CMB pivot scale exits the horizon as $\mathcal{N}_\star$, the departure from a scale invariant spectrum observed by the *Planck* satellite is $\mathcal{O}(1/\mathcal{N}_\star)$. While this could be a coincidence, it would find a natural explanation if

$$n_s(\mathcal{N}) - 1 = -\frac{p+1}{\mathcal{N}}\,, \tag{2.23}$$

up to subleading corrections in an expansion in large $\mathcal{N}$ for some real p. Under this assumption, the general solution to equation (2.22) is

$$\epsilon(\mathcal{N}) = \frac{p}{2\mathcal{N}}\frac{1}{1 \pm (\mathcal{N}/\mathcal{N}_{\rm eq})^p}\,, \tag{2.24}$$

where we have chosen to parameterize the integration constant by $\mathcal{N}_{\rm eq}$ so that the magnitudes of the first and second term in the denominator become equal when $\mathcal{N} = \mathcal{N}_{\rm eq}$. We take $\mathcal{N}_{\rm eq} > 0$ and indicate the choice of sign for the integration constant by '$\pm$'.

Assuming the epoch during which the modes we observe in the CMB exit is not special so that $\mathcal{N}_\star \gg \mathcal{N}_{\rm eq}$ or $\mathcal{N}_\star \ll \mathcal{N}_{\rm eq}$, equation (2.22) leads to four classes of solutions

$$\text{I.}\quad \epsilon(\mathcal{N}) = \frac{p}{2\mathcal{N}}\,, \tag{2.25}$$

$$\text{II.}\quad \epsilon(\mathcal{N}) = \frac{p}{2\mathcal{N}}\left(\frac{\mathcal{N}_{\rm eq}}{\mathcal{N}}\right)^p \quad \text{with} \quad p>0 \quad \text{and} \quad \mathcal{N}_{\rm eq} \ll \mathcal{N}_\star\,, \tag{2.26}$$

$$\text{III.}\quad \epsilon(\mathcal{N}) = \frac{|p|}{2\mathcal{N}}\left(\frac{\mathcal{N}}{\mathcal{N}_{\rm eq}}\right)^{|p|} \quad \text{with} \quad p<0 \quad \text{and} \quad \mathcal{N}_{\rm eq} \gg \mathcal{N}_\star\,, \tag{2.27}$$

$$\text{IV.}\quad \epsilon(\mathcal{N}) = \frac{1}{2\mathcal{N}\ln \mathcal{N}_{\rm eq}/\mathcal{N}} + \frac{p}{4\mathcal{N}} + \ldots \quad \text{with} \quad |p| \ll \frac{1}{\ln \mathcal{N}_{\rm eq}/\mathcal{N}_\star} \quad \text{and} \quad \mathcal{N}_{\rm eq} \gg \mathcal{N}_\star\,. \tag{2.28}$$

As we explain in what follows, if CMB-S4 does not detect primordial B-modes, only class II with $\mathcal{N}_{\rm eq} \lesssim 1$ will remain viable, the rest will be disfavored or excluded.

The value of $\mathcal{N}_\star$ depends on the post-inflationary history of the universe. Equation (2.23) implies that a measurement of the spectral index and its running would determine p and hence $\mathcal{N}_\star$, but unfortunately a measurement of the running at a level of $(n_s-1)^2$ is out of reach for CMB-S4. A given reheating scenario predicts $\mathcal{N}_\star$, but the space of reheating scenarios is large. Instantaneous reheating leads to $\mathcal{N}_\star \approx 57$ for $k_\star = 0.05{\rm Mpc}^{-1}$, smaller values correspond to less efficient reheating. We will assume $47 < \mathcal{N}_\star < 57$ for the following discussion.

Current constraints on n_s and r from [65] disfavor class III at just over 2σ relative to class II. Furthermore, the best-fit of class III occurs for $p \approx 0$ where classes I, II, and III degenerate so that class III need not be discussed seperately. Class IV is disfavored at $2-3\sigma$ relative to class II. As a consequence we focus on classes I and II in what follows.

For class I, constraints from the *Planck* satellite and the BICEP2 and *Keck Array* experiments [65] translate into $p = 0.32 \pm 0.16$ at $1\,\sigma$, and favor models with inefficient reheating. At the best-fit point in this class, $r = 0.044$ and $n_s = 0.973$, which is currently disfavored relative to class II at $1-2\,\sigma$. Upper limits on r directly translate into constraints on p. A $1\,\sigma$ upper limit on the amount of primordial gravitational waves from CMB-S4 at a level of $r < 0.001$ would imply $p < 0.013$ and effectively rule out this class as it degenerates into class II in this limit.

For class II the tensor-to-scalar ratio is naturally smaller than in class I as long as p is of order unity because $\mathcal{N}_\star \gg \mathcal{N}_{\rm eq}$. Under the additional assumption that the scaling (2.26) should be valid until the end of inflation we have $\mathcal{N}_{\rm eq} \simeq 1$. In this case, current data from [65] imply $p = 0.67 \pm 0.24$ after marginalization over $\mathcal{N}_\star$. The best-fit occurs for $p = 0.83$ and for instantaneous reheating so that in this class the data favors models with efficient reheating. At the best-fit point, $r = 0.004$ and $n_s = 0.968$. An upper limit of $r < 0.001$ would disfavor this scenario relative to scenarios with $\mathcal{N}_{\rm eq} \ll 1$ at approximately $2\,\sigma$. The precise significance depends slightly on the true value of the spectral index. Similarly, for an upper limit of $r < 0.001$, the regime with $p \ll 1$ and equivalently class I would be disfavored relative to class II with $\mathcal{N}_{\rm eq} \ll 1$ at $3\,\sigma$. To disfavor the scenario with $\mathcal{N}_{\rm eq} \simeq 1$ at approximately $3\,\sigma$ relative to $\mathcal{N}_{\rm eq} \ll 1$ would require an upper limit of $r \lesssim 5 \times 10^{-4}$.

In summary, in the absence of a detection of primordial gravitational waves, CMB-S4 would place constraints on n_s and r that are strong enough to rule out or disfavor all models that naturally explain the observed value of the scalar spectral index in the sense that $n_s(\mathcal{N}) - 1 \propto 1/\mathcal{N}$ and in which the behavior (2.25)-(2.28) provides a good approximation until the end of inflation.

To understand the implications better, let us discuss the models that underlie the classes favored by current data, classes I and II. The potentials can be obtained from

$$\frac{d\phi}{d\mathcal{N}} = M_p^2 \frac{V'}{V} \qquad \text{and} \qquad \left(\frac{d\phi}{d\mathcal{N}}\right)^2 = 2\epsilon M_p^2 \,, \tag{2.29}$$

where M_p is the reduced Planck mass.

Class I corresponds to models of chaotic inflation with monomial potentials $V(\phi) = \mu^{4-2p}\phi^{2p}$ already considered in [250]. The most commonly studied examples were $p = 1, 2$, both of which are now ruled out or strongly constrained [65]. Models with fractional powers $1/3 < p < 1$ that are still viable candidates have naturally appeared in in the study of large-field models of inflation in string theory [346, 274, 159]. If gravitational waves are not observed with CMB-S4, these would be ruled out.

Provided $p \neq 1$, class II corresponds to potentials of the form

$$V(\phi) = V_0 \exp\left[-\left(\frac{\phi}{M}\right)^{\frac{2p}{p-1}}\right] , \tag{2.30}$$

with $M = \sqrt{\alpha(p)\mathcal{N}_{\rm eq}}M_p$ where $\alpha(p)$ is of order unity for the range of p of interest. For $p > 1$ inflation occurs when $\phi \ll M$. In this regime, the potential behaves like a hilltop model $V(\phi) \approx V_0(1-(\phi/M)^n)$ with $n = 2p/(p-1)$. For $0 < p < 1$ inflation occurs for $\phi \gg M$ and $V(\phi) \approx V_0(1-(M/\phi)^n)$ with $n = 2p/(1-p)$. In the limit $p \to 0$ in which classes I, II, III become degenerate, the ϕ-dependence becomes logarithmic.

For the special case $p = 1$ the dependence on the inflaton in (2.30) becomes exponential and in the inflationary regime the potential is well approximated by $V(\phi) \approx V_0\,(1-\exp\,(-\phi/M))$ with $M = \sqrt{\mathcal{N}_{\rm eq}}M_p$. There are many examples of models with a potential with this asymptotic behavior for $\phi \gg M$. Some of them are the Starobinsky model [353], Higgs inflation [335, 62], an early example of chaotic inflation [178], and the T-model [215].

If only the asymptotic forms of the potentials agree with (2.30), equation (2.23) will not be exact and the departures from (2.30) will be encoded in the subleading terms that vanish more rapidly than $1/\mathcal{N}$ in the limit $\mathcal{N} \to \infty$. Unfortunately, just like the running of the scalar spectral index, the subleading contributions are typically too small to be detected.

Note that $\mathcal{N}_{\rm eq}$ sets the characteristic scale in field space. For $\mathcal{N}_{\rm eq}$ of order unity, the variation of the inflaton is naturally given in units of the reduced Planck mass while for $\mathcal{N}_{\rm eq} \ll 1$ the characteristic scale in field space is sub-Planckian.

This allows us to rephrase the lesson we can draw from an upper limit on r from CMB-S4.

In the absence of a detection, CMB-S4 would rule out or disfavor all models that naturally explain the observed value of the scalar spectral index and in which the characteristic scale in field space equals or exceeds the Planck scale.

Unfortunately, because of the scaling $M \propto \sqrt{\mathcal{N}_{\rm eq}}$ it will only be possible to obtain constraints $M \lesssim M_p$ but not $M \ll M_p$. It should also be kept in mind that a natural explanation of the value of the scalar spectral index is not guaranteed and its value could be an accident. That a natural explanation is possible is, however, encouraging.

2.4 CMB data products and simulations required to achieve goals for PGW

Figure 4 is a place-holder forecast done by Victor Buza with Colin Bischoff and John Kovac.

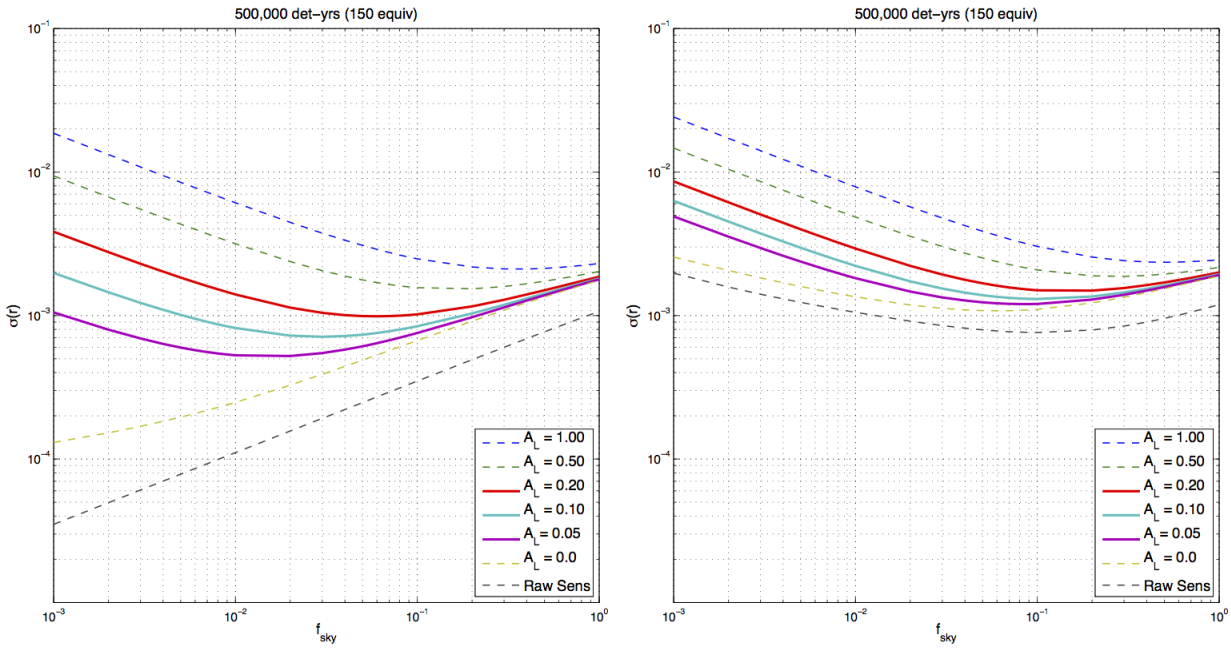

Figure 4. *Forecasted uncertainty on r, assuming $r = 0$ (left panel) and $r = 0.01$ (right panel). The forecasting procedure assumes an amount of delensing achieved, so we show several cases from complete delensing ($A_{\rm L} = 0$) to no delensing ($A_{\rm L} = 1$). The cases $A_{\rm L} = 0.05$ to 0.2 are highlighted as we expect what is achieved will be in this range.*

2.5 Improved constraints on primordial density perturbations

All current data are consistent with primordial density perturbations that are adiabatic, Gaussian, and nearly scale invariant. Because of its high angular resolution, CMB-S4 will significantly improve current constraints on the scale dependence of the primordial power spectrum of scalar perturbations, on departures from Gaussianity, and on departures from adiabatic perturbations. In fact, it will measure anisotropies in both the temperature and E-mode polarization of the CMB to cosmic variance over the entire range of multipoles that is not contaminated by unresolved foregrounds. As a consequence, it will place the strongest constraints achievable by any ground-based CMB experiment on all observables that benefit from the number of modes measured, such as the primordial power spectrum and higher order correlations.

2.5.1 The power spectrum of primordial density perturbations

The density perturbations are close to scale invariant but not exactly so. In the context of ΛCDM, *Planck* has measured the scalar spectral index to be $n_s = 0.9677 \pm 0.0060$ and has established $n_s - 1 < 0$ at more than $5\,\sigma$. CMB-S4 will improve current constraints on the spectral index by more than a factor two to $\sigma(n_s) = 0.0028$, and will provide valuable constraints on the space of inflationary models.

As mentioned in section 2.3, a measurement of the running of the scalar spectral index with a precision of a few parts in ten thousand would allow a measurement of p in equation (2.23), or equivalently $\mathcal{N}_\star$. This precision cannot be achieve with CMB-S4, but with a precision of one part in a thousand, it will test the idea that the lack of power on large angular scales might be explained by scale dependence of the spectral index [277].

Models of inflation that achieve super-Planckian inflaton displacements from repeated circuits of a sub-Planckian fundamental period may give rise to oscillatory features in the spectrum or primordial perturbations. The features may arise either from instanton effects or from periodic bursts of particle or string production. A search for such features is well motivated even though the amplitude is model-dependent and may be undetectably small. A detection would provide clues about the microscopic origin of the inflaton, the absence of a detection can constrain the parameters space of these models in interesting ways. CMB-S4 would tighten the constraints on the amplitude of features in the primordial power spectrum by a factor three.

2.5.2 Higher order correlations

Any detection of departures from Gaussianity would shed light on the interactions either of the inflaton with itself or between the inflaton and other degrees of freedom. The lowest order correlation function that encodes departures from Gaussianity is the 3*pt*-function

$$\langle \zeta(\vec{k}_1)\zeta(\vec{k}_2)\zeta(\vec{k}_3)\rangle = (2\pi)^3\delta(\vec{k}_1+\vec{k}_2+\vec{k}_3)B(k_1,k_2,k_3)\,, \tag{2.31}$$

where invariance under rotations and translations guarantee that the bispectrum $B(k_1, k_2, k_3)$ only depends on the magnitudes k_1, k_2, and k_3. A model independent search for the bispectrum, or equivalently the angular bispectrum $b_{\ell_1\ell_2\ell_3}$, is not computationally tractable, and in practice searches place constraints on the amplitudes $f_{\rm NL}$ of certain theoretically motivated functional forms, or shapes.

A detection of the most widely studied local shape would have far reaching theoretical implications. A detection of this shape would rule out all models of single clock inflation [116]. In addition, such a signal would open the door to significant cosmic variance on all scales from coupling of fluctuations within our observed volume to any super-Hubble modes [295, 253, 296]. Indeed, there would be room for a significant shift between the observed amplitude of scalar fluctuations (and so the observed r) and the mean value of fluctuations on much larger scales. Any scenario that predicts local non-Gaussianity together with fluctuations on scales much larger than our observed volume predicts a probability distribution for our observed $f_{\rm NL}^{\rm local}$. Many well-motivated scenarios predict a small mean value. These include the simplest modulated reheating scenario [390] and ekpyrotic cosmology [243], both of which predict mean values of $f_{\rm NL}^{\rm local} \sim 5$. Currently the strongest constraints on the local shape come from the *Planck* 2015 temperature and polarization analysis which give $f_{\rm NL}^{\rm local} = 0.8 \pm 5.0$ [15]. A noise-free cosmic variance limited CMB experiment is expected to produce constraints on $f_{\rm NL}^{\rm local}$ with 1σ error bars of about 3 [233]. Therefore the improvement expected of CMB-S4 over current limits is slightly less than a factor of two. This is not sufficient to reach the interesting theoretical

threshold around $|f_{\rm NL}^{\rm local}| \lesssim 1$ [25], but will still reduce the space of viable models or hint at a detection. CMB-S4 could, for example, provide hints for the modulated reheating scenario or ekpyrotic cosmology at roughly $2\,\sigma$. The simplest curvaton scenario, which predicts $f_{\rm NL} = -5/4$ [257], will unfortunately be out of reach.

In models with a single clock, the symmetry breaking pattern underlying inflation guarantees that the fluctuations are governed by the action

$$S = \int d^4x\sqrt{-g}\left[-\frac{M_p^2\dot{H}}{c_s^2}\left(\dot{\pi}^2 - c_s^2\frac{(\partial_i\pi)^2}{a^2}\right) + M_p^2\dot{H}\left(1-\frac{1}{c_s^2}\right)\left(\dot{\pi}^3 - \dot{\pi}\frac{(\partial_i\pi)^2}{a^2}\right) + M_3^4\dot{\pi}^3 + \dots\right], \quad (2.32)$$

where at leading order $\zeta = H\pi$ and the omissions represent terms higher order in fields, derivatives, or both. In the presence of an approximate continuous shift symmetry, the coefficients in this action are approximately constant in time and there are only two linearly independent shapes. Current constraints on the equilateral and orthogonal shapes are $f_{\rm NL}^{\rm equil} = -4 \pm 43$ and $f_{\rm NL}^{\rm ortho} = -26 \pm 21$, both (68% CL) [15]. Because of its high angular resolution, CMB-S4 can improve these constraints by about a factor two which would further tighten existing constraints on the speed of sound during inflation and the strong coupling scale in single-clock models of inflation. In addition, the tighter constraints on the equilateral shape would constrain scenarios with secondary production of gravitational waves.

Especially in models in which the inflaton is an axion, there is only an approximate discrete shift symmetry. In these models instanton contributions to the potential and periodic bursts of particle or string production naturally lead to periodic features in the bispectrum. If moduli in the underlying string constructions do not evolve appreciably, instanton contributions lead to oscillations with a constant amplitude in the logarithm of k. In general, moduli evolve during inflation and cause a drift in the frequency and a scale-dependent amplitude [160]. At present, these shapes have not yet been constrained systematically. Often these contributions will lead to counter-parts in the power spectrum and are expected to be detected there first [54], but this need not be the case [55]. So a search for these more general shapes is well motivated, and as for the scale invariant shapes CMB-S4 will improve constraints by about a factor two.

(Beyond the bispectrum)

2.5.3 Isocurvature

To be added

2.6 Constraints on other fundamental physics: spatial curvature, birefringence, primordial magnetic fields, cosmic strings, axions...

2.6.1 Spatial Curvature

Despite the fact that inflation drives the spatial curvature to zero at the level of the background evolution, it predicts small, but non-zero curvature for a typical observer. The curvature measured in a Hubble patch receives contributions from long wavelength perturbations and is expected to be $|\Omega_k| < 10^{-4}$. A

measurements of Ω_k exceeding this expectation would contain important information about the process responsible for inflation. In particular, if $|\Omega_k|$ is found to be considerably larger than this value, it would tell us that the inflaton was not slowly rolling when scales slightly larger than our observable horizon exited the horizon. Furthermore, observations of large negative Ω_k would falsify eternal inflation, while observation of positive and large Ω_k would be consistent with false vacuum eternal inflation [186, 229].

Current constraints on this parameter from the CMB alone are $\Omega_k = 0.005^{+0.016}_{-0.017}$. Including baryon acoustic oscillation (BAO) data tightens the bound to $\Omega_k = 0.000 \pm 0.005$. CMB-S4 is expected to constrain spatial curvature at a level of $\sigma(\Omega_k) \approx 10^{-3}$. A detection at this level would have profound implications for the inflationary paradigm.

2.6.2 Cosmic Birefringence

The simplest dynamical way to model the accelerated expansion of the universe is to invoke a new slowly evolving scalar field that dominates its energy budget (the quintessence models for DE). Such a field generically couples to photons through the Chern-Simons term in the electromagnetic Lagrangian, causing linear polarization of photons propagating cosmological distances to rotate—the effect known as cosmic birefringence [97]. In the case of the CMB, such rotation converts the primordial E mode into B mode, producing characteristic TB and EB cross-correlations in the CMB maps [218, 174]. Even though there is no firm theoretical prediction for the size of this effect, if observed, it would be a clear smoking-gun evidence for physics beyond the standard model. Previous studies have used quadratic estimator formalism to constrain this effect [172], with the best current limit coming from sub-degree scale polarization measurements with POLARBEAR [17] (< 0.33 deg^2 for the amplitude of a scale-invariant rotation-angle power spectrum). A promising way to pursue search for cosmic birefringence in the future is measurement of the off-diagonal EB cross correlations on small angular scales. **Put in more specific predictions for S4?**

2.6.3 Primordial Magnetic Fields

The origin of the microgauss (μG) strength magnetic fields in galaxies and galaxy clusters is one of the long standing puzzles in astrophysics [140]. It is challenging to explain such fields solely based on the dynamo mechanism without there being some initial seed field. However, if magnetic fields were present in the early universe, they would remain frozen in the cosmic plasma and collapse with the rest of the matter to form the galactic fields [182], or at least provide the seeds for the dynamo. A primordial magnetic field (PMF) could be produced in the aftermath of cosmic phase transitions [370] or in specially designed inflationary scenarios [367, 327]. Detecting their signatures in the CMB temperature and polarization would decisively prove their primordial origin. Aside from explaining the galactic fields, bounds on PMF have profound implications for our understanding of the early universe. They help constrain theories of inflation [77], models of the QCD and electroweak phase transitions [94] and baryogenesis [371].

A stochastic PMF affects CMB in several ways. Magnetic stress-energy induces scalar, vector and tensor mode perturbations in the metric, and the Lorentz force generates vorticity in the photon-baryon fluid [359, 260, 248, 344, 304]. Dissipation of PMF on small scales dumps energy into the plasma, which produces spectral distortions and affects the recombination history [240]. Finally, Faraday Rotation (FR) of CMB polarization converts some of the E-modes into B-modes [237, 321].

Stochastic PMF has two potentially observable frequency independent contributions to the B-mode spectrum [344]. One comes from the passive, or uncompensated tensor mode, which is generated by the PMF before neutrino decoupling. For nearly scale-invariant PMF, the spectrum of this component is indistinguishable from the inflationary gravity wave signal. The amplitude of this tensor contribution is proportional to $B_{1\mathrm{Mpc}}^4[\ln(a_\nu/a_{\mathrm{PMF}})]^2$, where $B_{1\mathrm{Mpc}}$ is the PMF strength smoothed over 1Mpc, a_ν is the scale factor at neutrino decoupling and a_{PMF} is the scale factor at which PMF was generated. The other is the PMF vector mode which peaks at $l \sim 2000$, with the precise peak position dependant on the PMF spectrum. The vector-mode contribution is independent of a_{PMF}.

Planck data limits the magnetic field strength to $B_{1\mathrm{Mpc}} < 4.4$ nanogauss (nG) at the 95% confidence level [14]. Similar bounds were recently obtained by POLARBEAR [17] based on their B-mode spectrum alone.

2.6.4 Cosmic Strings

Cosmic strings can at most contribute O(1%) to the total CMB temperature anisotropy [12, 252, 242], however, they can still generate observable B-modes. As shown in [285], the bounds on cosmic strings obtained solely from the POLARBEAR [10] and BICEP2 [11] B-mode spectra are comparable to those from temperature spectra. CMB-S4 polawill be able to reveal the presence of cosmic strings through their B-mode signature even if strings contribute as little as 0.1% to the CMB temperature anisotropy [39].

2.6.5 Anomalies

Several unexpected features have been observed in the temperature of the CMB sky at relatively low-l or large angular scales. Some of these were first noticed in COBE data, and all have been seen in both WMAP and Planck maps. These include:

- a lack of correlation on the largest angular scales;
- alignment of the lowest multipole moments with one another and with the geometry and motion of the Solar System;
- a hemispherical asymmetry or dipolar modulation of the power;
- greater power in odd-parity modes than in even-parity ones.

Compared to the expectations of the best-fit inflationary ΛCDM model, the individual p-values of these features are in the per mille to per cent level, and therefore each anomaly has a frequentist probability at approximately the 3-sigma level or higher. Since certain pairs of anomalies are uncorrelated in ΛCDM, in combination they nominally represents a very significant detection of anomalous behaviour.

There are however two possible concerns before one can conclude that the CMB large-angle pattern is truly anomalous. First, these features were identified a posteriori and are characterized by statistics that were devised after the anomalies were first noted. Second, there is no physical understanding of how the collection of such features could arise. In order to help address or resolve these concerns, it is therefore crucial to obtain additional information about the large-scale primordial fluctuations, and to devise a successful model or other explanation.

The observed features can have two possible origins: either our cosmological model is incomplete and requires a modification (the new physics hypothesis), or we just happen to live in a realization of that model that is statistically unlikely (the fluke hypothesis). Meanwhile, cosmologists have effectively exhausted their ability to obtain further independent CMB temperature data that can test these anomalies, as observations are already cosmic-variance limited at the relevant angular scales.

It has been suggested that one may nevertheless make observational progress, at least in the frequentist sense, even in the absence of an alternative model. This can occur in two ways:

1. In the fluke hypothesis the conditional probability distributions of ΛCDM for correlation functions of CMB polarization (and other observables) with CMB temperature and with one another are altered by the observed temperature anomalies (Dvorkin et al 2008, Copi et al 2013, Yoho et al. 2013).
2. In the new physics hypothesis, a given phenomenological model that explains the anomalies will have observational consequences for other observable quantities [Yoho et al. 2015]. For example, the absence of large-angle correlations in T may reflect a lack of long-distance correlation in a fundamental physical quantity like the potential; similarly, a hemispherical asymmetry in TT power could cause a similar asymmetry in EE.

A variety of ideas have been proposed to explain the anomalies, ranging from Solar system dust artifacts to anisotropic models of inflation (for a summary, see Copi et al, 2016). Unfortunately, none of those ideas lead to a convincing explanation, as it is simply difficult to find models that explain the alignments of the largest primordial structures in the universe while at the same time lowering the amplitude of large-angle temperature correlations (e.g. Gordon et al, 2005).

Additional information from polarization on the largest angular scales would be of great help. Polarization probes only those epochs where a large number of free electrons saw a temperature quadrupole, i.e. just at photon decoupling and later at reionization, whereas the intensity maps probe the complete line of sight to the last scattering surface.

To give two examples: If the lack of correlation is an intrinsic property of the inflationary power spectrum, then it should be reflected by a suppression of the reionization bump in the polarization. And if the observed alignments are due to some nearby superclusters and voids, then the supercluster plasma might also leave its imprint on the polarization.

S4, alone or in combination with other data, can begin to explore both the cosmological and the fluke explanation for the origin of the observed anomalies. For example, ΛCDM instructs us how to remove the part of the E-mode signal that is correlated to temperature; the remainder should be Gaussian random and statistically isotropic. If it contains a hemispherical anomaly (especially one aligned with the temperature asymmetry), that would be evidence against the fluke hypothesis [Copi, Knox, ODwyer and Starkman, contribution to March 9/10 S4 meeting, in preparation].

Add connections to axion physics. eg 1601.03049

2.7 Summary

CMB-S4 is an ideal tool to test the inflationary paradigm and competing theories of the early universe. On the one hand, its exquisite sensitivity will allow a detection of degree scale B-modes in the CMB or achieve upper limits on the amount of B-mode polarization that improve current constraints on the tensor-to-scalar

ratio by almost two orders of magnitude. In particular, it is sensitive enough to detect the level of B-mode polarization predicted in a wide range of well-motivated inflationary models. In doing so, it would provide invaluable information about physics at energy scales far outside the reach of any terrestrial particle physics experiment. In the absence of a detection it would exclude large classes of inflationary models. On the other hand, with its high angular resolution, it will measure anisotropies in both the temperature and E-mode polarization of the CMB to cosmic variance over the entire range of multipoles that is not contaminated by unresolved foregrounds, and it will extend our window to the early universe by almost one e-fold beyond the reach of current experiments. As a consequence, it will provide the best constraints achievable by any ground-based CMB experiment on any observable that benefits from the number of modes measured, such as the primordial power spectrum, and hence the spectral index, its running, features in the power spectrum, as well as higher order correlations.

3

Neutrino Physics from the Cosmic Microwave Background

(send feedback on this chapter to s4_neutrinos@cosmo.uchicago.edu)

3.1 Introduction

Direct interactions between neutrinos and observable matter effectively ceased about one second after the end of inflation. Nevertheless, the total energy density carried by neutrinos was comparable to other matter sources through today. As a result, the gravitational effect of the neutrinos is detectable both at the time of recombination and in the growth of structure at later times [2], leaving imprints in the temperature and polarization spectrum as well as in CMB lensing.

CMB-S4 can improve our understanding of neutrino physics in regimes of interest for both cosmology and particle physics. Arguably the most important parameters of interest will be the sum of the neutrino masses $\sum m_\nu$ and the effective number of neutrino species, $N_{\rm eff}$. These two parameters have natural targets that are within reach of a CMB-S4 experiment:

- $\sum m_\nu \gtrsim 58$ meV is the lower bound guaranteed by observations of solar and atmospheric neutrino oscillations. A CMB experiment with $\sigma(\sum m_\nu) < 20$ meV would be guaranteed a detection of a least 3σ.
- $\Delta N_{\rm eff} > 0.027$ is predicted for any light particle that was in thermal equilibrium with the standard model. A CMB experiment producing $\sigma(N_{\rm eff}) \lesssim 0.01$ would be sensitive to all models in this very broad class of extensions of the Standard Model, which includes a wide range of axions and axion-like particles.

Current CMB data already provides a robust detection of the cosmic neutrino background at $> 10\sigma$. A CMB-S4 experiment will provide an order of magnitude improvement in sensitivity that opens a new window back to the time of neutrino decoupling and beyond.

Section 2 will review the motivation for studying neutrino masses with cosmological probes, and specifically with the CMB. We will explain why cosmology is sensitive to $\sum m_\nu$ via different probes and how it is complementary to the laboratory-based experimental neutrino effort. Section 3 will review the physics of $N_{\rm eff}$ and its role as probe of the CνB and as sensitive tool for beyond the Standard model physics. We will emphasize the unique impact $N_{\rm eff}$ has on the CMB that makes it distinguishable from other extensions of ΛCDM. In Section 4, we will discuss the implications for a variety of well motivated models, including sterile neutrinos and axions. In Section 5, we will discuss the relation between CMB and BBN based constraints.

3.2 Neutrino Mass

3.2.1 Theory Review

Cosmic background neutrinos are nearly as abundant in the universe as CMB photons. In the standard cosmological model, neutrinos cease to scatter with other particles at temperatures $\sim 1\,\mathrm{MeV}$. The relic neutrinos are relativistic at decoupling but as the universe expands and cools the neutrino momenta redshift as $p_\nu \propto 1/a$ and eventually the energy of relic neutrinos comes to be dominated by their rest mass, rather than the momentum. The energy density in nonrelativistic neutrinos therefore contributes to the matter budget of the universe today. The neutrinos, however, were relativistic for much of the history of the Universe so their gravitational clustering is qualitatively different from that of cold dark matter (CDM) particles. This difference can be used to distinguish the neutrino and cold dark matter contributions to the matter density [206, 245, 5]. In this section, we review how neutrino mass affects the evolution of the neutrino energy density and the gravitational clustering of matter in the universe.

As discussed more detail in the $N_{\rm eff}$ section, cosmic background neutrinos have been detected indirectly through their contribution to the energy density in radiation in the early universe. The current CMB constraints from $N_{\rm eff}$ are in excellent agreement with the standard model expectation of three neutrino and anti-neutrino states each described by a relativistic thermal Fermi-Dirac distribution [13]. The phase space for each neutrino and anti-neutrino state is given by

$$f_\nu(p) = \frac{1}{e^{ap/(k_B T_\nu)} + 1} \tag{3.1}$$

where $T_\nu \approx 1.95K$ or $k_B T_\nu \approx 1.68 \times 10^{-4}\mathrm{eV}$ is the temperature today. Note that the spectral shape of the neutrino phase space distribution is preserved with the expansion of the universe so relic neutrinos will retain the relativistic Fermi-Dirac momentum distribution inherited from decoupling even if the individual neutrinos become non-relativistic.

The neutrino energy density is given by

$$\rho_\nu = \sum_i \int \frac{d^3\mathbf{p}}{(2\pi\hbar)^3} \frac{\sqrt{p^2 + m_{\nu i}^2}}{e^{ap/(k_B T_\nu)} + 1} \tag{3.2}$$

where $m_{\nu i}$ are the three neutrino mass eigenstates. For $T_\nu/a \gg m_{\nu i}$ the neutrino energies are dominated by their momenta and the total energy density behaves like radiation

$$\begin{aligned} \rho_\nu\Big|_{\rm early} &\approx \frac{7\pi^2}{40} \frac{(k_B T_\nu)^4}{\hbar^3 c^3} \frac{1}{a^4} \\ &\propto a^{-4} \end{aligned} \tag{3.3}$$

While for $T_\nu/a \ll m_{\nu i}$ the energy density behaves like matter

$$\begin{aligned} \rho_\nu\Big|_{\rm late} &\approx \sum_i m_{\nu i} \bar{n}_\nu \\ &\propto a^{-3} \end{aligned} \tag{3.4}$$

where $\bar{n}_\nu$ is the number of neutrinos and antineutrinos in each mass eigenstate

$$\bar{n}_\nu = \int \frac{d^3\mathbf{p}}{(2\pi\hbar)^3} \frac{2}{e^{ap/(k_B T_\nu)} + 1} \approx \frac{113}{a^3} \mathrm{cm}^{-3}\,. \tag{3.5}$$

For a neutrino of mass $m_{\nu i}$ the transition between these two regimes ($T_\nu(a) \sim m_{\nu i}$) occurs at redshift $z_{nr} \sim 300(m_{\nu i}/0.05\text{eV})$. Using Eq. (3.4) the fractional energy density in neutrinos today can be written as

$$\Omega_\nu h^2 \approx \frac{\sum_i m_{\nu i}}{93\,\text{eV}}\,. \tag{3.6}$$

The individual masses of the neutrino states are unknown but neutrino oscillation data specifies the square of two mass splittings $\Delta m^2_{12} = 7.54 \times 10^{-5}\text{eV}$, $|\Delta m^2_{13}| \approx 2.4 \times 10^{-3}\text{eV}$ [299]. These mass splittings, in combination with the neutrino number density, give a lower limit on the contribution of neutrinos to the cosmic energy budget

$$\Omega_\nu h^2 \gtrsim 0.0006\,. \tag{3.7}$$

At $z \ll z_{NR}$ the matter density of the universe, which enters into the Hubble equation, is the sum of the CDM, baryon, and massive neutrino energy densities $\Omega_m = \Omega_c + \Omega_b + \Omega_\nu$. Whereas, at $z \gg z_{nr}$ the matter density is solely the baryon and CDM parts and neutrinos contribute to the radiation density.

Neutrinos do not participate in gravitational collapse until late times when they have become nonrelativistic. Prior to this transition, the neutrinos *free-stream* out of gravitational wells, leaving the CDM and baryons behind [76, 258, 205, 206]. Primordial fluctuations in the neutrino density are therefore damped away on scales smaller than the horizon at z_{nr}. In comoving units, this scale corresponds to a wave number

$$k_{nr} \equiv a_{nr} H(a_{nr})/c \approx 0.003 \left(\frac{\Omega_m}{0.3}\frac{m_\nu}{0.05\,\text{eV}}\right)^{1/2} h/\text{Mpc}\,. \tag{3.8}$$

Once the neutrinos are non-relativistic, their finite velocity dispersion still prevents them from clustering on scales smaller than the typical distance a neutrino travels in a Hubble time, $v_\nu/H(a)$ where $v_\nu \approx 3.15 T_\nu/(a m_\nu)$ the mean neutrino velocity. In analogy with the Jeans criterion for gravitational collapse, the neutrino free-streaming scale is defined by [76, 245]

$$k_{fs}(a) \equiv \sqrt{\frac{3}{2}}\frac{aH(a)}{v_\nu(a)} \approx 0.04\, a^2 \sqrt{\Omega_m a^{-3} + \Omega_\Lambda}\left(\frac{m_\nu}{0.05\text{eV}}\right) h/\text{Mpc} \tag{3.9}$$

in comoving coordinates.

On scales larger than k_{nr} (adiabatic) perturbations in the density of neutrinos, baryons, and CDM are coherent and can be described by a single perturbation to the total matter density $\delta_m = \delta\rho_m/\rho_m$. On smaller scales where the neutrino perturbations have decayed, only the perturbations to the CDM and baryons remain so that $\delta_m = (\Omega_c + \Omega_b)/\Omega_m \delta_{cb}$. The remaining CDM and baryon perturbations also grow more slowly because the neutrino energy density contributes to the expansion rate, but not to the source potentials. These two effects cause a suppression in the amplitude and the growth rate of matter perturbations wavenumbers $k > k_{fs}$ relative to a universe with massless neutrinos (and also relative to density perturbations with $k < k_{nr}$). The net change in the amplitude of perturbations with $k > k_{nr}$ primarily depends on the fractional energy density in massive neutrinos but retains a small sensitivity to the individual neutrino masses through a dependence on a_{nr}.

An estimate of the effect of massive neutrinos on the growth of structure can be made by studying the evolution of matter perturbations in the two regimes $k \ll k_{fs}$ and $k \gg k_{fs}$. In the synchronous gauge, linear perturbations to the matter density with wavenumbers $k \ll k_{fs}$ evolve as

$$\ddot{\delta}_m + 2H(a)\dot{\delta}_m - \frac{3}{2}\Omega_m H_0^2 a^{-3}\delta_m = 0 \quad \text{for} \quad k \ll k_{nr} \tag{3.10}$$

which has solutions $\delta_m \propto a$, $a^{-\frac{3}{2}}$ during the matter dominated era.

On scales where the neutrino perturbations have decayed, perturbations to matter density are just in the CDM and baryon components

$$\delta_m(k \gg k_{fs}) \approx (\delta\rho_c + \delta\rho_b)/\rho_m = (1 - f_\nu)\delta_{cb} \tag{3.11}$$

where $f_\nu = \Omega_\nu/\Omega_m$ and $\delta_{cb} = (\delta\rho_c + \delta\rho_b)/(\rho_c + \rho_b)$, but the neutrino energy density still contributes to the Hubble friction. In this limit, linear perturbations to the CDM and baryon density evolve as

$$\ddot{\delta}_m + 2H(a)\dot{\delta}_m - \frac{3}{2}\Omega_{cb}H_0^2 a^{-3}\delta_m = 0 \quad \text{for} \quad k \gg k_{fs} \tag{3.12}$$

where $\Omega_{cb} = \Omega_c + \Omega_b$ and $\Omega_{cb} < \Omega_m$ for a cosmology with massive neutrinos. Equation (3.12) has the approximate solutions during the matter dominated era of $\delta_{cb} \propto a^{1-\frac{3}{5}f_\nu}, a^{-\frac{3}{2}+\frac{3}{5}f_\nu}$ for $f_\nu \ll 1$.

The matter dominated solutions give a simple estimate of the net effects of massive neutrinos on the amplitude of matter perturbations. For fixed $\Omega_c h^2$, the evolution of perturbations in a cosmology with $f_\nu \neq 0$ is the same as a cosmology with $f_\nu = 0$. After a_{nr}, the perturbations with $k \gg k_{fs}$ grow more slowly (according to Eq. (3.12), the growing mode solution grows as $\propto a^{1-3/5f_\nu}$) than those with $k \ll k_{fs}$ (according to Eq. (3.10), $\propto a$). At scale-factor a during the matter dominated era, the total difference in growth or perturbations with $k \gg k_{fs}$ is roughly

$$\frac{\delta_{cb}(k \gg k_{fs}, a|f_\nu)}{\delta_{cb}(k \gg k_{fs}, a|f_\nu = 0)} \sim \left(\frac{a}{a_{nr}}\right)^{-3/5f_\nu} . \tag{3.13}$$

The resulting difference in the amplitude of the matter power spectra is then

$$\frac{P_{mm}(k \gg k_{fs}, a|f_\nu)}{P_{mm}(k \gg k_{fs}, a|f_\nu = 0)} \sim (1 - 2f_\nu)\frac{P_{cc}(k \gg k_{fs}, a|f_\nu)}{P_{cc}(k \gg k_{fs}, a|f_\nu = 0)} \sim \left(1 - 2f_\nu - \frac{6}{5}f_\nu \ln\left(a/a_{nr}\right)\right) . \tag{3.14}$$

On the other hand, the evolution of the large scale modes is identical,

$$\frac{P_{mm}(k \ll k_{fs}, a|f_\nu)}{P_{mm}(k \ll k_{fs}, a|f_\nu = 0)} = 1 . \tag{3.15}$$

The above expression overestimates the effect of neutrino mass by assuming the transition from relativistic to non-relativistic is instantaneous. It also ignores the effects of the cosmological constant at late times. Using the true evolution of δ_{cb} through a_{nr} and allowing for the cosmological constant gives

$$\frac{P_{mm}(k \gg k_{fs}|f_\nu)}{P_{mm}(k \gg k_{fs}|f_\nu = 0)} \approx 1 - 6f_\nu \tag{3.16}$$

at $a = 1$. Note that this expression assumes fixed $\Omega_c h^2$, $\Omega_b h^2$ so that matter-radiation equality is not changed by neutrino mass and that and $\Omega_\Lambda = 1 - \Omega_m$ is fixed by adjusting h so that the onset of cosmological constant domination is also unchanged. Alternatively, assuming fixed Ω_m and decreasing Ω_{cb} to account for Ω_ν makes matter-radiation equality, which occurs while the neutrinos are relativistic, slightly later so that the suppression is increased to

$$\frac{P_{mm}(k \gg k_{fs}|f_\nu)}{P_{mm}(k \gg k_{fs}|f_\nu = 0)} \approx (1 - 8f_\nu) . \tag{3.17}$$

3.2.2 Observational Signatures and Target

Massive neutrinos contribute to the critical density as

$$\Omega_\nu h^2 \simeq \frac{\sum m_\nu}{93\,\mathrm{eV}} . \tag{3.18}$$

As discussed above, the signature of massive neutrinos manifests through the energy density Ω_ν making its transition from relativistic radiation to non-relativistic matter as its temperature drops; the transition occurs at around $z_{\rm nr} \sim 2000 m_\nu/1\,{\rm eV}$. During the epoc when neutrinos are relativistic, they free-stream out of the over-dense regions and washes out the matter fluctuations on small scales. This effect turns off roughly at scales larger than the horizon scale at the redshift $z_{\rm nr}$. Thus, comparison of the amplitudes of the fluctuations at large and small scales probes neutrino mass.

The amplitudes at large scales are precisely measured through primordial CMB fluctuations in both TT and EE power spectra, except for the uncertainty from the optical depth τ, which we discuss later. The large scale structure (LSS) measures the small scales; this is the area where we expect significant improvement through CMB S4.

3.2.3 CMB Lensing

Likely the cleanest probe of the neutrino mass in the CMB is through gravitational lensing, which directly measures the matter distribution along the line of sight. To be concrete, in the limber approximation, the lensing power spectrum is given by

$$C_\ell^{\phi\phi} = \frac{8\pi^2}{\ell^2}\int_0^{\chi_\star} \chi d\chi P_\Psi(\ell/\chi;\eta_0-\chi)\frac{(\chi_\star-\chi)^2}{\chi_\star\chi} \tag{3.19}$$

$$P_\psi(k;\eta) = \frac{9\Omega_m^2(\eta)H^4(\eta)}{8\pi^2}\frac{P_{mm}(k;\eta)}{k} \tag{3.20}$$

where χ ($\chi_\star$) is the co-moving distance (to the last scattering surface) and η (η_0) is conformal time (today). More details regarding CMB lensing, including current and future measurements, will be discussed in Chapter **.

For the purposes of the neutrino mass measurement, the advantage of lensing over other probes is that it is largely free of astrophysical uncertainties. As we see from the lensing power spectrum, we are directly sensitive to the matter power spectrum (rather than a biased tracer) and the relevant scales are in the linear regime where modeling should be reliable.

The primary challenges for the lensing measurement are degeneracies with other cosmological parameters. The two primary degeneracies in ΛCDM are

- Optical depth, τ: The suppression of small scale power at low redshift requires a reliable measurement of the amplitude of the power spectrum at high redshift. In principle, this is measured by the primary CMB anisotropies, but the overall normalization is degenerate with τ for $\ell \gtrsim 20$. A precise measurement of τ is therefore crucial to calibrate the suppression at low redshifts. This degeneracy can be broken by ... .
- Ω_m : The amount of lensing is controlled by the total amount of matter. Therefore, we can compensate for a suppression from neutrinos by increasing the matter power spectrum. This degeneracy will be broken by DESI BAO measurements of the expansion history.

In addition to degeneracies in ΛCDM there can be degeneracies with possible extensions. Most notably:

- $N_{\rm eff}$: The density of neutrinos after they become non-relativistic is given by $\rho_\nu \simeq m_\nu n_\nu$ where n_ν is the number density. Therefore, we only measure the mass if we know the number density to sufficient

accuracy. Fortunately, as we will discuss in the next section, measurements of the neutrino energy density from the primary CMB will be sufficiently accurate as to make this degeneracy insignificant under plausible assumptions.

In principle, measurement of the free streaming scale directly in the matter power spectrum would separate the neutrino mass from most other physical quantities. Unfortunately, given current limits on the neutrino mass, the change to the shape of the lensing potential power spectrum is not expected to drive future constraints.

Status of current observations – Planck has provided a strong constraint of $\sum m_\nu < 0.194$ eV when combining both temperature and polarization data with the CMB lensing power spectrum and external data. A weaker constraint of $\sum m_\nu < 0.492$ eV can be derived using only the temperature and polarization data. This constraint arises through the effect of massive neutrinos on the primordial TT and EE power spectra. For sufficiently large masses, the neutrinos do not behave as radiation around the time of recombination which impacts the damping tail and locations of the acoustic peaks. Improvements in the limits on the sum of the neutrino masses will be driven primarily by lensing given that current limits imply that the neutrinos are effectively massless from the point of view of the primary CMB anisotropies. External data will continue to be important in breaking the degeneracy with Ω_b.

3.2.4 Other Cosmological Probes

3.2.4.1 SZ Cluster Abundance

Abundance of galaxy clusters also gives us a measure of the amplitudes at small scales ($\simeq 0.1h\mathrm{Mpc}^{-1}$). In particular, the mass function of clusters is strongly sensitive to σ_8 and therefore, in principle, clusters counts are sensitive to the sum of the neutrino mass through the same suppression of small scale power. CMB datasets can be used to measure the abundance through the Sunyaev-Zel'dvich (SZ) effect. The size of the SZ signal does not provide a direct measurement of the mass of the cluster as it is directly sensitive to the free electrons in the cluster. As a result, determining the mass function requires calibration of the mass-signal relation.

3.2.4.2 Cross-correlations with External Datasets

3.2.4.3 Relation to Other Surveys

3.2.5 Forecasts

3.2.6 Relation to Lab Experiments

One of the more interesting connections between cosmological measurements of neutrino mass and terrestrial experiments is the complementarity between cosmological neutrino mass measurements and the search for neutrinoless double beta decay (NLDBD). NLDBD is a hypothetical decay mode of certain nuclei where two neutrons convert to two protons and two electrons with no emission of neutrinos. The observation of NLDBD would be transformational demonstrating that neutrinos are Majorana particles and revealing a

new lepton-number-violating mechanism for mass generation. This new physics could potentially explain both the smallness of neutrino masses and matter-antimatter asymmetry in the universe.

Initial results from the current generation of NLDBD searches limit the NLDBD half life, $T^{0\nu}_{1/2}$, to be larger than $\sim 2 \times 10^{25}$ years [**?**, **?**, **?**]. The full sensitivity of these experiments is expected to be in the range of $10^{25} - 10^{26}$ years [**?**]. Planning and technology development is already underway for next generation "ton-scale" NLDBD searches which would achieve sensitivities of $10^{27} - 10^{28}$ years [**?**].

We can illustrate the connection between NLDBD searches to cosmological determinations of neutrino mass by examining the silmplest case where NLDBD is mediated by exchange of light Majorana neutrinos. Within the context of this mechanism, we can define an "effective neutrino mass," $m_{\beta\beta}$, given by

$$m^2_{\beta\beta} = (\sum_i U^2_{ei} m_{\nu i})^2 \tag{3.21}$$

where $m_{\nu i}$ are the light neutrino masses and U_{ei} is the usual PMNS mixing matrix only including two unknown Majorana phases. The NLDBD half-life is then given by

$$(T^{0\nu}_{1/2})^{-1} = G^{0\nu} \cdot (M^{0\nu})^2 \cdot m^2_{\beta\beta}, \tag{3.22}$$

where $G^{0\nu}$ is a phase space integral and $M^{0\nu}$ is the nuclear matrix element. In this simple scenario, the signal from NLDBD experiments can be directly related to other measures of neutrino mass. Figure 5 illustrates this relationship between the effective neutrino mass and the lightest neutrino mass including limits and sensitivities of current and next generation NLDBD searches.

The complementarity between cosmological neutrino mass measurement and NLDBD can be understood by considering scenarios where NLDBD experiments either observe or fail to observe NLDBD. In the absence of a signal in next generation NLDBD searches, a cosmological measurement constraining $\sum_i m_{\nu i} > 100$ meV (corresponding to either the inverted hierarchy or a minimum neutrino mass of 50 meV) would strongly point to neutrinos being primarily Dirac particles (see Fig. 5). On the other hand, if NLDBD is observed, equation 3.21 shows that cosmological measurements of $\sum_i m_{\nu i}$ are sensitive to the physics governing neutrino mass generation. For example, Fig. 6 shows that in the inverted mass hierarchy cosmological measurements together with NLDBD measurements can constrain one of the Majorana phases. Perhaps even more interesting would be the situation where cosmological and NLDBD measurements violate equation 3.21 indicating new physics beyond the simple model of light Majorana neutrino mediated decay.

Cosmological measurements of the summed neutrino masses also complement direct measurements of the neutrino mass using radioactive decay. These kinematic measurements of neutrino mass focus on one of two processes, beta-decay or electron-capture, where the decay spectra near the decay endpoint is particularly sensitive to the mass of the lightest neutrino (add Figure of b-decay and e-capture endpoint spectra).

Current kinematic measurements from Mainz [**?**] and Troitsk [**?**] limit the neutrino mass to < 2.0 eV. The KATRIN experiment [**?**] will begin taking data in 2016 and is expected to improve this limit by a factor of ten. The spectroscopic techniques of KATRIN are unlikely to improve beyond the 0.2 eV limit because of the final state spectrum of the source itself, specifically rotational-vibrational states of molecular Tritium. As such, the community is in the process of developing new approaches to kinematic measurements of the neutrino mass. One of the new approaches is a calorimetric measurement of the electron-capture spectrum of ^{163}Ho. The calorimetric measurement of the ^{163}Ho endpoint is insensitive to the details of the source configuration and may provide an avenue for eventually surpassing the KATRIN sensitivity. Interestingly, upcoming experiments such as ECHO, HOLMES, and NuMECS utilize multiplexed superconducting detectors, the

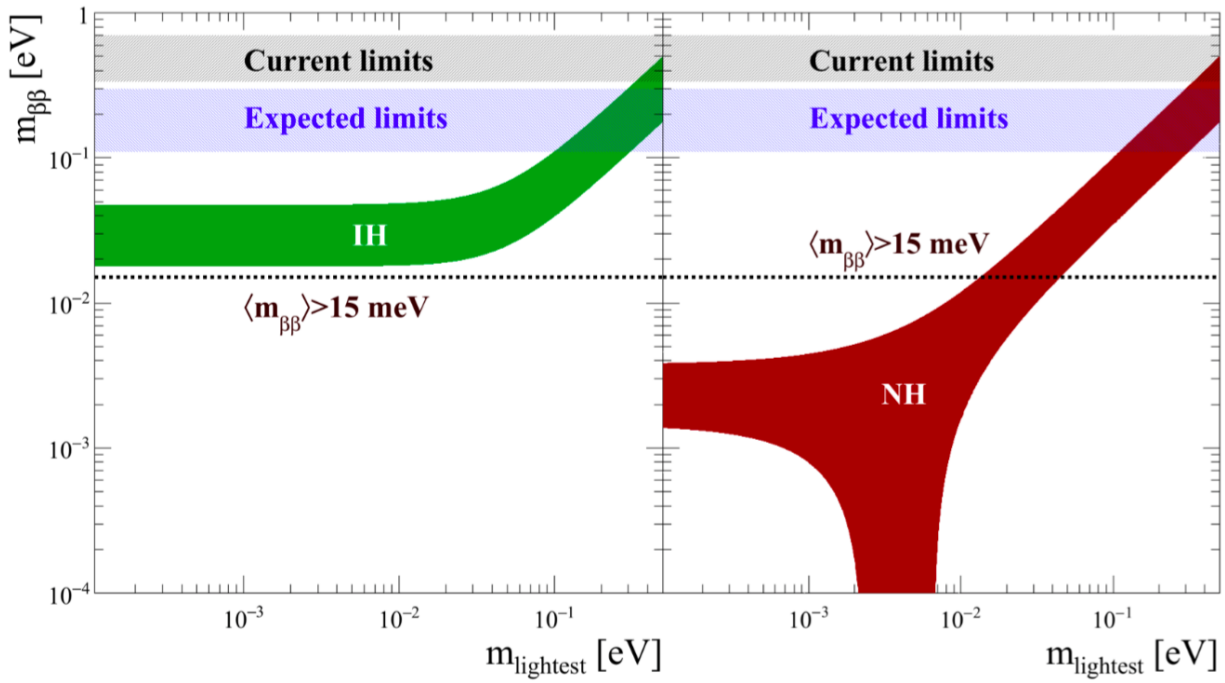

Figure 5. *Plot of effective neutrino mass versus the mass of the lightest neutrino in the scenario where NLDBD is mediated by light neutrino exchange. Left corresponds to the inverted hierarchy (green band) and right corresponds to the normal hierarchy (red band). Current limits and expected sensitivities rom current generation NLDBD experiments are shown by gray and blue bands. Next generation "ton-scale" NLDBD searches will have sensitivities down to $m_{\beta\beta} > 15$ meV (dashed line). Figure from [?]*

same technology baselined for the CMB-S4 experiment. Another promising direction for direct neutrino mass measurement is the frequency-based technique employed by the Project-8 experiment. Project-8 aims to measure the beta-decay spectrum of Tritium by measuring the frequency of cyclotron radiation emitted by the decay electrons when trapped in a magnetic field. An exciting aspect to this frequency-based technique is the potential to trap atomic Tritium which is not subject to the rotational-vibrational excitations of molecular Tritium. A spectroscopic measurement using atomic Tritium could eventually achieve sensitivities of < 0.04 eV, a level comparable to cosmological measurements.

The relation between cosmological measurement from CMB-S4, kinematic constraints constraints expected from KATRIN [], and upcoming long-baseline oscillation experiments is shown in Fig. 7. The three approaches to neutrino mass and mixing are complementary and the combination of their results will either reveal new physics in the neutrino sector or provide a definitive measure of the full neutrino mass spectrum.

Possible anomalies found in short baseline oscillation experiments (LSND, MiniBoon, etc.) may be explained as an active-sterile neutrino oscillation. Parameters required to these fits typically lead to thermalization of the sterile species in the early universe before neutrino decoupling, resulting in non-standard $N_{\rm eff}$ and contribution to $\sum_\nu m_\nu$. Further description can be found below in Section 3.4.1.

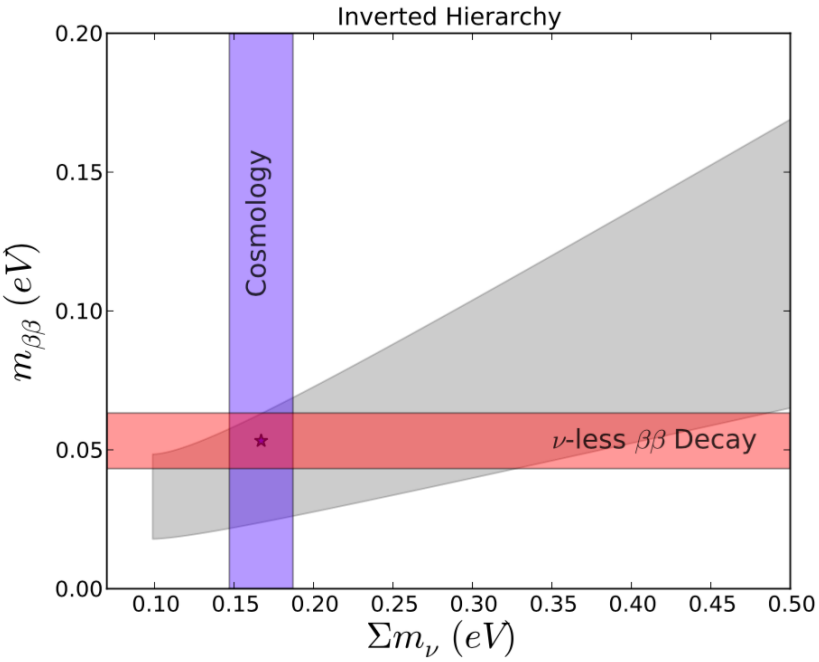

Figure 6. *Relationship between effective neutrino mass as measured by NLDBD experiments versus* $\sum_i m_{\nu i}$ *as measured by cosmology for the inverted hierarchy. The gray band corresponds to a region allowed by existing measurements where the width of the band is determined by the unknown Majorana phase.*

3.3 Effective Number of Neutrinos

The angular power spectrum of the cosmic microwave background (CMB) at small angular scales is quite sensitive to the radiation content of the early universe, usually parametrized by a quantity $N_{\rm eff}$ which will be defined more precisely below. In the standard models of cosmology and particle physics, $N_{\rm eff}$ is a measure of the energy density of the cosmic neutrino background. More generally, however, $N_{\rm eff}$ receives contributions from all forms of radiation apart from photons which are present in the early universe. Due to its sensitivity to $N_{\rm eff}$, the CMB can be used as a tool to probe physics of the standard model and beyond which are difficult to measure through other means. Here we will give an overview of the theoretical issues related to $N_{\rm eff}$ and outline the expectations from the standard model.

3.3.1 Thermal History of the Early Universe

In this section, we will give a sketch of the thermal history of the standard hot big bang universe when the temperature of the plasma was falling from about 10^{11} K to about 10^8 K following Section 3.1 of [380]. For other reviews see [135, 299]. During this era, there are two events of particular interest: neutrinos decoupled from the rest of the plasma, and a short time later electrons and positrons annihilated, heating the photons relative to the neutrinos. Our task is to follow how these events impact the evolution of the energy densities of the photons and neutrinos.

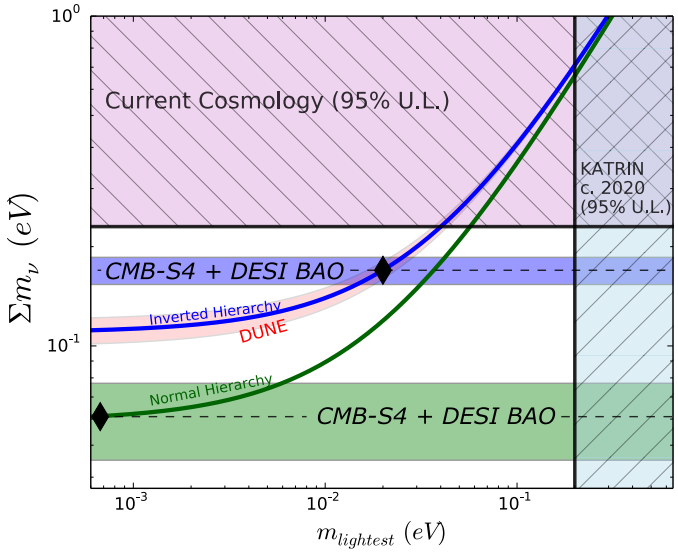

Figure 7. *Shown are the current constraints and forecast sensitivity of cosmology to the neutrino mass in relation to the neutrino mass hierarchy. In the case of an "inverted hierarchy," with an example case marked as a diamond in the upper curve, the CMB-S4 (with DESI BAO prior) cosmological constraints would have a very high-significance detection, with 1σ error shown as a blue band. In the case of a normal neutrino mass hierarchy with an example case marked as diamond on the lower curve, CMB-S4 would detect the lowest $\sum m_\nu$ at $\gtrsim 3\sigma$. Also shown is the sensitivity from the long baseline neutrino experiment (DUNE) as the pink shaded band, which should be sensitive to the neutrino hierarchy. Figure adapted from the Snowmass CF5 Neutrino planning document.*

For massless particles described by the Fermi-Dirac or Bose-Einstein distributions, the energy density is given by

$$\rho(T) = \begin{cases} g\frac{\pi^2 k_B^4}{30\hbar^3 c^3}T^4 & \text{Boson} \\ \frac{7}{8}g\frac{\pi^2 k_B^4}{30\hbar^3 c^3}T^4 & \text{Fermion} \end{cases} \tag{3.23}$$

where g counts the number of distinct spin states. The entropy density for massless particles is given by

$$s(T) = \frac{4\rho(T)}{3T}\,. \tag{3.24}$$

It is convenient to define a quantity $g_\star$ which counts the spin states for all particles and antiparticles, with an additional factor $\frac{7}{8}$ for fermions. With this definition, the total energy density and entropy density of the universe during radiation domination are given by

$$\begin{aligned} \rho(T) &= g_\star \frac{\pi^2 k_B^4}{30\hbar^3 c^3}T^4\,, \\ s(T) &= \frac{4}{3}g_\star \frac{\pi^2 k_B^4}{30\hbar^3 c^3}T^3\,. \end{aligned} \tag{3.25}$$

In an expanding universe, the first law of thermodynamics implies that for particles in equilibrium, the comoving entropy density is conserved

$$a^3 s(T) = \text{const}\,. \tag{3.26}$$

One straightforward consequence of this conservation is that for radiation in free expansion, the temperature evolves as the inverse of the scale factor

$$T \propto \frac{1}{a}\,. \tag{3.27}$$

Let us now apply this to the physics of the early universe.

At a temperature of 10^{11} K ($k_B T \sim 10$ MeV), the universe was filled with photons, electrons and positrons, and neutrinos and antineutrinos of three species, all in thermal equilibrium with negligible chemical potential, along with a much smaller density of baryons and dark matter both of which are unimportant for the present discussion. As the temperature of the plasma dropped below about 10^{10} K (about 1 second after the end of inflation), the rate of collisions between neutrinos and electrons and positrons could no longer keep up with the expansion rate of the universe, and neutrinos began to fall out of equilibrium and begin a free expansion. This is just above the temperature for which $m_e c^2 \sim k_B T$, and so for slightly lower temperatures electrons and positrons rapidly disappeared from equilibrium. We will simplify the discussion by assuming that neutrinos decoupled instantaneously before electron-positron annihilation and comment below how a more detailed calculation modifies the results. Non-zero neutrino masses can safely be neglected here as long as $m_\nu c^2 \lesssim 1$ keV which is guaranteed by current observational bounds.

From this point on, we will distinguish the temperature of neutrinos T_ν from that of the photons T_γ. Before neutrino decoupling, frequent interactions kept neutrinos and photons in equilibrium, ensuring they had a common falling temperature. After the universe became transparent to neutrinos, the neutrinos kept their relativistic Fermi-Dirac distribution with a temperature which fell as the inverse of the scale factor. The photons, on the other hand, were heated by the annihilation of the electrons and positrons. Comoving entropy conservation allows us to compute the relative temperatures at later times.

After neutrino decoupling, but before electron positron annihilation, the thermal plasma contained two spin states of photons, plus two spin states each of electrons and positrons, which means that during this period,

$$\mathcal{N}_{\rm before} = 2 + \frac{7}{8}(2+2) = \frac{11}{2}\,. \tag{3.28}$$

After electron positron annihilation, only the two spin states of photons remained, and so

$$\mathcal{N}_{\rm after} = 2\,. \tag{3.29}$$

Since $T_\nu \propto a^{-1}$ during this period, we can express the condition of comoving entropy conservation as follows

$$\frac{\mathcal{N}_{\rm before} T_{\gamma,{\rm before}}^3}{T_{\nu,{\rm before}}^3} = \frac{\mathcal{N}_{\rm after} T_{\gamma,{\rm after}}^3}{T_{\nu,{\rm after}}^3}\,. \tag{3.30}$$

Using the fact that $T_{\gamma,{\rm before}} = T_{\nu,{\rm before}}$, we find as a result

$$\frac{T_{\gamma,{\rm after}}}{T_{\nu,{\rm after}}} = \left(\frac{11}{4}\right)^{1/3}\,. \tag{3.31}$$

We find that in the instantaneous neutrino decoupling limit, the annihilation of electrons and positrons raised the photons relative to the neutrinos by a factor of $(11/4)^{1/3} \simeq 1.401$.

After electron positron annihilation, assuming three species of light neutrinos and antineutrinos, each with one spin state, the radiation density of the universe is

$$\rho_r = \frac{\pi^2 k_B^4}{30\hbar^3 c^3}\left[2T_\gamma^4 + 3\frac{7}{8}T_\nu^4\right] = \frac{\pi^2 k_B^4}{15\hbar^3 c^3}\left[1 + 3\,\frac{7}{8}\left(\frac{4}{11}\right)^{4/3}\right] T_\gamma^4\,. \tag{3.32}$$

It is conventional to define a quantity $N_{\rm eff}$ which gives the radiation energy density in terms of the effective number of neutrino species as

$$\rho_r = \frac{\pi^2 k_B^4}{15\hbar^3 c^3}\left[1 + \frac{7}{8}\left(\frac{4}{11}\right)^{4/3} N_{\rm eff}\right] T_\gamma^4\,. \tag{3.33}$$

In the instantaneous neutrino decoupling approximation described above, we found $N_{\rm eff} = 3$. In the real universe, however, decoupling of neutrinos is not instantaneous, and the residual coupling of neutrinos at the time of electron positron annihilation increases $N_{\rm eff}$ by a small amount in the standard model.

The current best estimate of $N_{\rm eff}$ in the standard model is $N_{\rm eff} = 3.046$ [266]. Very unlike photon decoupling at temperature $T \sim 0.2$ eV, active neutrino decoupling at $T \sim 10\,{\rm MeV} - 0.1\,{\rm MeV}$ takes place over many tens of Hubble times, with the result that we expect distortions in the relic neutrino energy spectra relative to thermal-shaped, Fermi-Dirac black bodies. Standard model physics Boltzmann neutrino transport calculations show that these distortions could change $N_{\rm eff}$ from 3 to something close to 3.05. This result is largely due to (1) the incomplete decoupling of neutrinos during electron-positron annihilation and (2) QED plasma effects. While both effects have been calculated independently quite accurately, there is some theoretical uncertainty in this quantity due to the various numerical approximations that are made in the calculations when both effects are included simultaneously (see e.g. [184] for discussion).

3.3.2 Natural Target

As will be discussed in more detail below, the CMB angular power spectrum is sensitive to the value of $N_{\rm eff}$ in our universe. Measurement of the value of $N_{\rm eff}$ provides a huge amount of insight into the early universe, and is in fact an observational probe of the conditions at very early times, well before recombination. Even within the standard model, $N_{\rm eff}$ provides an observational handle on the thermal history back to about one second after the end of inflation. The true power of measuring $N_{\rm eff}$, however, comes from the realization that it is sensitive not just to the neutrinos of the standard model, but it in fact receives contributions from all forms of radiation apart from photons present in the early universe and is thus a probe of new physics.

Collider experiments are known to provide a measurement of the number of neutrino species (or more precisely the number of species of fermions coupling to the Z boson with mass below $m_Z/2$) and find very close agreement with three families of light active neutrinos [337]. Cosmological measurements of $N_{\rm eff}$ provide complimentary constraints and are sensitive to the total energy density of radiation whether constituted of active neutrinos or other light species.

If the measured value of $N_{\rm eff}$ exceeds the standard model prediction, it would be an indication that there is additional radiation content in the early universe or that the thermal history is somehow modified. Additional radiation which contributes to $N_{\rm eff}$ is often referred to as dark radiation. There is a huge number of possible sources for dark radiation, including sterile neutrinos [3, 358, 79], gravitational waves [81, 355, 278], dark photons [7, 220, 123], and many more [90, 382]. It is also possible that the measured value of $N_{\rm eff}$ could be found below the standard model prediction. This can happen if for example photons are heated relative to neutrinos after decoupling [354, 74].

One of the features that make $N_{\rm eff}$ a compelling theoretical target, is the degree to which broad classes of models fall into two basic levels of $\Delta N_{\rm eff}$. As illustrated in Figure 10, any species that was in thermal equilibrium with the standard model degrees of freedom produces a characteristic correction to $N_{\rm eff}$ that depends only on its spin and its freeze-out temperature. For freeze-out after the QCD phase transition, one finds $\Delta N_{\rm eff} \gtrsim 0.3$. Freeze-out before the QCD phase transition instead produces $\Delta N_{\rm eff} > 0.027$. This first category has been tested by Planck. The second category, which is sensitive freeze-out temperatures as early as reheating, falls into the level of sensitivity attainable by CMB Stage IV.

The contributions to $N_{\rm eff}$ from hot thermal relics are relatively easy to understand from the discussion of neutrino decoupling. After freeze-out, the temperature of a relativistic specifics redshift like a^{-1} and therefore is only diluted relative to the Standard model when energy is injected. The annihilation of heavy standard

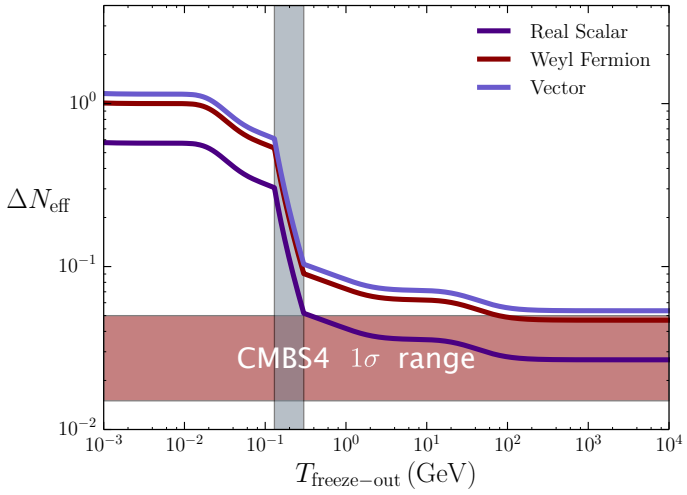

Figure 8. *Contribution to $N_{\rm eff}$ from a massless field that was in thermal equilibrium with the Standard model at temperatures $T > T_{\rm freeze}$. For $T_{\rm freeze} \gg m_{\rm top}$, these curves saturate with $\Delta N_{\rm eff} > 0.027$. The region in red shows the range of forecasts for $\sigma(N_{\rm eff})$ for plausible CMB-S4 configurations.*

model particles into photons conserves the comoving entropy and therefore, the diluted temperature of a relic before neutrino decoupling is given by

$$\left(\frac{T_{\rm relic}}{T_\nu}\right)^3 = \frac{g_\star^{\nu-\rm freeze-out}}{g_\star^{\rm relic\,freeze-out}} = \frac{43/4}{g_\star^{\rm relic\,freeze-out}}\,, \tag{3.34}$$

where $g_\star$ is defined as above to be the number of independent spin states including an additional factor of $\frac{7}{8}$ for fermions. The order of magnitude difference in $\Delta N_{\rm eff}$ before and after the QCD phase transition comes from order of magnitude drop in $g_\star$ below the QCD scale. At temperatures well above to top mass, the standard model gives $g_\star = 106.75$.

Even a measurement of $N_{\rm eff}$ which agrees with the standard model prediction to high precision would be very interesting due to the constraints it would place on physics beyond the standard model. Some specific implications for sterile neutrinos, axions and other popular models will be discussed below. Broadly speaking, constraining $\Delta N_{\rm eff}$ at the 10^{-2} level would constrain a wide variety of models that are consistent with current cosmological, astrophysical, and lab-based constraints. Furthermore, because of the sharp change in $\Delta N_{\rm eff}$ at the QCD phase transition, the improvement from current constraints to projections for CMB-Stage IV can be quite dramatic.

For the minimal scenario of a single real scalar, reaching $\sigma(N_{\rm eff}) \sim 1 \times 10^{-2}$ would push the constraint on freeze-out temperatures from electroweak scale to the reheat temperature. Nevertheless, a measurement a factor of a few times larger would still be extraordinarily valuable, for higher spin fields, multiple light scalars and modifications to the thermal history up to the electroweak scale. This broad reach to extremely high energies and very early times demonstrates the discovery potential for a precision measurement of $N_{\rm eff}$ with the CMB. Furthermore, the CMB power spectrum has the ability to distinguish among certain types of dark radiation based on the behavior of its density perturbations [98, 50]. This point will be discussed further below.

3.3.3 Observational Signatures

Cosmic neutrinos play to two important roles in the CMB that are measured by $N_{\rm eff}$. They contribute to the total energy in radiation which controls the expansion history and, indirectly, the damping tail of the power spectrum. The fluctuations of neutrinos and any other free streaming radiation also produces a constant shift in the of phase the acoustic peaks. These two effects drive both current and future constraints on $N_{\rm eff}$.

The effect of neutrinos on the damping tail has historically driven the constraint on $N_{\rm eff}$ in the CMB. The largest effect is from the mean free path of photons, which introduces a suppression $e^{-(k/k_d)^2}$ of short wavelength modes, with [391]

$$k_d^{-2} = \int \frac{da}{a^3 \sigma_T n_e H} \frac{R^2 + \frac{16}{15}(1+R)}{6(1+R)^2} \ , \tag{3.35}$$

where R is the ratio of the energy in baryons to photons, n_e is the density of free electrons and σ_T is the Thompson cross-section. The damping scale is sensitive to the energy in all radiation through $H \propto \sqrt{\rho_{\rm radiation}}$ during radiation domination (which is applicable at high ℓ), and is therefore sensitive to $N_{\rm eff}$ or any form of dark radiation. At this level, this also illustrates the degeneracy with n_e which may be altered by the helium fraction, Y_p.

In reality, the effect on the damping tail is actually subdominant to the change to the scale of matter radiation equality and the location of the first acoustic peak [202]. As a result, the effect on neutrinos on the damping tail is more accurately represented by holding the first acoustic peak fixed. This changes the sign of the effect on the damping tail, but the intuition for the origin of the effect (and degeneracy) remain applicable.

In addition to the effect on the Hubble expansion, perturbations in neutrinos affect the photon-baryon fluid through their gravitational influence. The contributions from neutrinos are well described by a correction to the amplitude and the phase of the acoustic peaks in both temperature and polarization [47]. The phase shift is a particularly compelling signature as it is not degenerate with other cosmological parameters [47, 50]. This effect is the result of the free-streaming nature of neutrinos that allows propagation speeds of effectively the speed of light (while the neutrinos are relativistic). This effect is sensitive to any gravitationally coupled light thermal relics.

E-mode polarization will play an increasingly important role for several reasons. First of all, the acoustic peaks are sharper in polarization which makes measurements of the peak locations more precise, and therefore aid the measurement of the phase shift. The second reason is that polarization breaks a number of degeneracies that would also affect the damping tail [50].

Status of current observations – Planck has provided a strong constraint on $N_{\rm eff} = 3.15 \pm 0.23$ when combining both temperature and polarization data. The addition of polarization data has both improved the constraint on $N_{\rm eff}$ and reduced the impact of the degeneracy with Y_p. Recently, the phase shift from neutrinos has also been established directly in the Planck temperature data [161]. This provides the most direct evidence for presence of free-steaming radiation in the early universe, consistent with the cosmic neutrino background.

3.3.4 Forecasts

3.4 Sterile Neutrinos and Axions

3.4.1 Sterile Neutrinos

A number of recent neutrino oscillation experiments have anomalies that are possible indications of four or more mass eigenstates. The first set of anomalies are in short baseline oscillation experiments: first, in the Liquid Scintillator Neutirno Detector (LSND) experiment, where electron antineutrinos were observed in a pure muon antineutrino beam [37]. The MiniBooNE Experiment also sees an excess of electron neutrinos and antineutrinos in their muon neutrino beam [22]. Two-neutrino oscillation interpretations of the results indicate mass splittings of $\Delta m^2 \approx 1$ eV^2 and mixing angles of $\sin^2 2\theta \approx 3 \times 10^{-3}$ [22]. Another anomaly arises from re-evaluations of reactor antineutrino fluxes that indicate an increased flux of antineutrinos as well as a lower neutron lifetime and commensurately increase the antineutrino events from nuclear reactors by 6%. This brought previous agreement of reactor antineutrino experiments to have a $\sim$6% deficit [281, 208]. Another indication consistent with sterile neutrinos are in radio-chemical gallium experiments for solar neutrinos. In their calibrations, a 5-20% deficit of the measured count rate was found when intense sources of electron neutrinos from electron capture nuclei were placed in proximity to the detectors. Such a deficit could be produced by a > 1 eV sterile neutrino with appreciable mixing with electron neutrinos [41, 167]. Some simultaneous fits to the short baseline anomalies and reactor neutrino deficits, commensurate with short baseline constraints, appear to prefer at least two extra sterile neutrino states [108, 235], but see Ref. [166]. Because such neutrinos have relatively large mixing angles, they would be thermalized in the early universe with a standard thermal history, and affect primordial nucleosynthesis [4].

In addition, there are combinations of CMB plus LSS datasets that are in tension, particularly with a smaller amplitude of fluctuations at small scale than that inferred in zero neutrino mass models. This would be alleviated with the presence of massive neutrinos, extra neutrinos, or both. In particular, cluster abundance analyses [389, 16] and weak lensing analyses [49] indicate a lower amplitude of fluctuations than zero neutrino mass [168]. Baryon Acoustic Oscillation measures of expansion history are affected by the presence of massive neutrinos, and nonzero neutrino mass may be indicated [61], though 2015 Planck results show a lack of such alleviation in cases with massive or extra neutrinos [13].

There is a potential emergance of both laboratory and cosmological indications of massive and, potentially, extra neutrinos. However, the combined requirements of the specific masses to produce the short baseline results, along with mixing angles that require thermalized sterile neutrino states, are inconsistent at this point with cosmological tension data sets [214, 28]. The tension data sets are not highly significant at this point ($\lesssim 3\sigma$), and there are a significant set of proposals for short baseline oscillation experiment follow up [1]. Future high-sensitivity probes of neutrino mass and number such as CMB-S4 will be able to definitively test for the presence of extra neutrino number and mass consistent with sterile neutrinos.

3.4.2 Axion-like Particles

A ubiquitous component of extensions of the Standard model are axions and/or axion-like particles (ALPs). Axions have been introduced to solve the strong-CP problem [309], the hierarchy problem [181] and the

naturalness of inflation [163]. Furthermore, they appear generically in string theory, in large numbers, leading to the qualitative phenomena describe as the string axiverse [34].

ALPs typically appear as (pseudo)-Goldstone bosons of some high energy global symmetry. At low energy, the mass of the ALP is protected by an approximate shift symmetry of the general form $a \to a + c$ where a is the axion and c is a constant (for non-abelian Goldstone bosons, this transformation will include higher order terms in a). We will define an ALP to be any such particle where all of the couplings of the axion to the Standard model respect such a symmetry. This symmetry may be softly broken with an explicit mass term, although this is highly restricted in the case of the QCD axion.

Two couplings of particular interest for axion phenomenology are the coupling to gluons and photons,

$$\frac{1}{4} g_{a\gamma\gamma} a \tilde{F}_{\mu\nu} F^{\mu\nu} \ , \qquad \frac{1}{4} g_{agg} a \tilde{G}_{\mu\nu} G^{\mu\nu} \ . \tag{3.36}$$

These couplings typically appear as the consequence of chiral anomalies. The coupling of the axion to gluons is what makes the solution to the strong-CP problem possible. The coupling to photons is somewhat model dependent but typically arises in conjunction with the gluon coupling. In addition or instead of these coupling, a variety of possible couplings to matter may also be included.

Two very common features of these models are that the axions are typically light (in many cases, $m \ll 1$ eV) and their interactions are suppressed by powers of f_a. These two features make ALPs a particularly compelling target. Because of the small masses, they will often behave as relativistic species in the CMB. Furthermore, because their production rate will scale as T^{2n+1}/f_a^{2n} for some $n \geq 1$, they are likely to be thermalized at high temperatures. Given that $\Delta N_{\rm eff} > 0.027$ under such circumstances, a CMB experiment with sensitivity at this level will be sensitive to a very wide range of ALP models.

Status of current observations – Current constrains on ALPs arise from a combination of experimental [180], astrophysical [325] and cosmological [272] probes. Current cosmological constraints are driven by several effects that depend on the mass of the axion. For axion masses greater than 100 eV, stable thermal ALPs are easily excluded because they produce dark matter abundances inconsistent with observations. By including the free streaming effects of thermal QCD-axions, Planck data [131] combined with local measurements provide the constrain $m_a < 0.525$ eV (95 % CL). At larger masses, ALPs become unstable and can be constrained by the change to $N_{\rm eff}$ from energy injection as well as from spectral distortions and changes to BBN [91, 161]

Implications for CMB Stange IV – Sensitive to $N_{\rm eff}$ of order $\sigma(N_{\rm eff}) \simeq 10^{-2}$ has the sensitive to probe then entire mass range of ALPs down to $m_a = 0$ under the assumption that it thermalized in the early universe. Interpreting such bounds in terms of the couplings of axions is more complicated [88] and can depend on assumptions about the reheating temperature. For high (but plausible) reheat temperatures of 10^{10} GeV, CMB stage IV would be sensitive to $g_{a\gamma\gamma}$, $g_{agg} \gtrsim 10^{-13}{\rm GeV}^{-1}$ [], which exceeds current constraints and future probes for a range of possible axion masses (including the QCD axion).

3.5 Complementarity of CMB and BBN

Primordial light element abundances have historically been an interesting observational test of hot big bang cosmology. The process by which light elements form in the early universe known as big bang nucleosynthesis (BBN) was worked out theoretically in the early days of the development of the hot big bang model of cosmology [24]. It is a process which depends on all four fundamental forces, that unfolded during the first three minutes of our current phase of expansion, and which has long provided a useful constraint on physics

beyond the standard model. The current observational limits on primordial abundances overall show good agreement with the predictions of standard BBN. Primordial light element abundances are sensitive to the radiation content of the universe as measured through $N_{\rm eff}$, which also affects the angular power spectrum of the CMB. Combining these two probes provides useful insight into the physics of the early universe which neither could achieve alone.

3.5.1 Standard Big Bang Nucleosynthesis

In this section, we will briefly review the physics of big bang nucleosynthesis in the standard model. For more extensive reviews see for example [380, 299, 121].

At temperatures above $k_B T \sim 1$ MeV, weak interactions kept neutrons and protons in thermal equilibrium, fixing their number densities to have the ratio $n_n/n_p = e^{-Q/k_B T}$, where $Q = 1.293$ MeV is the mass difference between neutrons and protons. At lower temperatures, interactions which convert protons to neutrons could not keep up with the expansion rate, leaving free neutron beta decay as the only channel by which protons and neutrons interconverted. The initial ratio of their number densities at the freeze-out temperature $k_B T_{\rm fr} \simeq 0.8$ MeV was therefore

$$n_n/p_n = e^{-Q/k_B T_{\rm fr}} \simeq 1/5\,. \tag{3.37}$$

After freeze-out, neutrons decayed until becoming bound into nuclei. This process proceeded primarily through two-body processes, starting with the formation of deuterium. The very small number density of baryons compared to that of photons (parametrized through $\eta \equiv n_b/n_\gamma$) delayed the start of these nuclear reactions until well after the temperature dropped below the binding energy of deuterium due to photo-dissociation of deuterium. The condition of the onset of deuterium formation is set by requiring that the number of photons per baryon with energy above the binding energy of deuterium drops below unity

$$\eta^{-1} e^{-|B_D|/k_B T_D} \simeq 1\,. \tag{3.38}$$

With the deuterium binding energy given by $|B_D| = 2.23$ MeV, and $\eta \sim 6 \times 10^{-10}$, we find that deuterium begins to form when the temperature drops below about $k_B T_D \simeq 0.1$ MeV. By this time, due to free neutron decay, the neutron to proton ratio had dropped to about $n_n/n_p \simeq 1/7$. Once deuterium was able to form, nearly all of the neutrons quickly became bound into the most energetically favorable light nucleus, which is ^{4}He. We can estimate the mass fraction of primordial ^{4}He, $Y_p \equiv \frac{\rho(^4\mathrm{He})}{\rho_b}$ to be

$$Y_p = \frac{2(n_n/n_p)}{1 + n_n/n_p} \simeq 0.25\,. \tag{3.39}$$

In addition to ^{4}He, BBN produces a small amount of D, ^{3}He, ^{6}Li, and ^{7}Li (and also ^{7}Be which subsequently decays by electron capture to ^{7}Li). While Y_p is primarily sensitive to the neutron lifetime, the primordial abundances of the other light elements depend in complicated ways various nuclear rates and generally require numerical computation (see for example [377, 120, 312]).

Standard BBN is a one parameter model, depending only on the baryon to photon ratio η. The theory predicts several abundances which can be used to fix η and check the consistency of the theory, or alternatively, to constrain new physics. Current observations agree quite well with the predictions of standard BBN, with the exception of ^{7}Li. It is unclear whether this disagreement points to a problem with the astrophysical

determination of the primordial abundance or a problem with the standard theory. The cosmological lithium problem remains unsolved [155]. From here on, however, we will ignore the lithium problem and focus on how measurements of the other abundances (primarily D and ^{4}He) can be used to constrain the physics of the early universe.

3.5.2 Beyond the Standard Model

Moving beyond standard BBN, measurements of primordial abundances have the ability to constrain many deviations from the standard thermal history and the standard model of particle physics. Because BBN is sensitive to all fundamental forces, changes to any force can in principle impact light element abundances. Of primary interest for our purpose is that BBN is sensitive to the expansion rate between about one second and a few minutes after the end of inflation. The expansion rate is in turn determined by the radiation content of the universe during this period, and thus BBN is sensitive to $N_{\rm eff}$.

More specifically, the expansion rate determines the freeze-out temperature setting the initial ratio of neutrons to protons and the amount of time free neutrons have to decay. Additional radiation compared to the standard model gives a higher expansion rate, which leads to a higher freeze-out temperature and less time for free neutron decay, leading to a larger primordial ^{4}He abundance. The freeze-out temperature also depends weakly on the distribution function of electron neutrinos, though this is subdominant to the dependence $N_{\rm eff}$ for small non-thermal distortions [342].

Historically, Y_p had provided the best constraint on $N_{\rm eff}$. Recent advancements in the determination of primordial deuterium abundance have made constraints on $N_{\rm eff}$ from deuterium competitive with those from Y_p [111]. The precision with which primordial abundances constrain $N_{\rm eff}$ is now comparable to that of constraints the CMB power spectrum, and there is no evidence for deviation from the standard model [13].

3.5.3 Complementarity with the CMB

The CMB can be used to quite precisely constrain η by measurement of the baryon fraction of the critical density, which is related to η by

$$\Omega_b h^2 \simeq \frac{\eta \times 10^{10}}{274}\,. \tag{3.40}$$

Using the value of η determined from CMB measurements as an input for BBN makes standard BBN a theory without free parameters which agrees very well with all observations (apart from the aforementioned disagreement with the observed lithium abundance). The CMB and BBN are sensitive to the baryon density measured at different times. While BBN is sensitive to the baryon to photon ratio up to a few minutes after the end of inflation, the CMB is sensitive to the baryon density at much later times, closer to recombination about 380,000 years later. Combining constraints from BBN and CMB on the baryon fraction therefore allows constraints on models where the photon or baryon density changes between these times.

The precision with which the CMB can constrain $N_{\rm eff}$ will soon come to surpass the constraints from BBN, but the value of the latter will not be totally eclipsed. BBN and the CMB probe the physics at different times, and so combining constraints can give insight into models where $N_{\rm eff}$ changes in time. If it were measured for example that $N_{\rm eff}^{\rm BBN} < N_{\rm eff}^{\rm CMB}$, this could be explained by the late decay of some unstable particles [157, 280, 200]. Alternatively, if observations revealed that $N_{\rm eff}^{\rm BBN} > N_{\rm eff}^{\rm CMB}$, this might signal late photon heating [90, 282].

The power spectrum of the CMB is also directly sensitive to Y_p. Since helium recombines earlier than hydrogen, the density of helium present at the time of recombination affects the free electron density, and thereby affects the damping tail of the CMB (though in a way which can be distinguished from the effects of $N_{\rm eff}$) [47, 202, 161, 50]. The degeneracy between Y_p and $N_{\rm eff}$ is more strongly broken with precise CMB polarization data.

CMB-Stage IV will provide constraints on $N_{\rm eff}$ which are about an order of magnitude better than the current best constraints, and will also improve on the measurement of Y_p by about a factor of two compared to the current best astrophysical measurements. Combined with measurements of other primordial abundances, this will help to provide a very thorough check of our understanding of the early universe and provide the opportunity to discover physics beyond the standard model.

4

Dark Energy and Dark Matter

4.1 Dark Energy and Modified Gravity

(send feedback on this chapter to s4_de@cosmo.uchicago.edu)

The enigma of cosmic acceleration is among the most challenging problems in physics. Our most basic understanding about gravity – that objects fall towards one and other under mutual gravitational attraction – simply does not apply on the largest distance scales. Instead, gravity is apparently repulsive at large distances and late times; the scale of spacetime itself is currently not only expanding but accelerating. The implication is either that our understanding of gravity is incomplete, or some other causative agent – dark energy – with exotic gravitational properties fills the universe. In both cases, new physics is required beyond the four fundamental forces described by the Standard Model and general relativity.

The working hypothesis is that the cosmic acceleration is due to an exquisitely small cosmological constant, that Einstein's general relativity is valid from millimeter to beyond gigaparsec scales, and that dark matter consists of a single species of a cold, collisionless particle. Yet none of these offer insight or reflect the unity of physics demonstrated elsewhere as in the Standard Model of particle physics.

In particular, the cosmological constant suffers from a naturalness problem whose resolution may lie in a dynamical dark energy, quintessence. Theories of quintessence posit a new scalar field and predict a variety of testable phenomena. They can also unveil new links to dark matter, neutrino physics, and cosmic parity violation. In their most general form, they represent a scalar-tensor theory of gravity which can be described by the effective field theory (EFT) of cosmic acceleration in the linear regime. CMB-S4 can provide the hard evidence needed to pare down these possibilities and potentially discover clues to the enigma of cosmic acceleration that will enable the development of compelling theoretical alternatives to the cosmological constant.

In summary, the current observational evidence suggests a new frontier for physics at low energies and weak coupling, implied by the cosmological scales that characterize cosmic acceleration.CMB lensing, thermal SZ cluster counts and mass measurements, and the kinematic SZ effect all measure the influence of cosmic acceleration on the growth of structure. As such, CMB-S4 would be capable of helping to answer basic questions about dark energy and gravity in a manner complementary to ongoing precision measurements of the expansion history.

4.1.1 Models and parameters

In this section, we briefly review the models and frameworks that have been proposed over the past years to test dark energy and modified gravity. These fall into three families: "trigger", equations of motion, and theory parametrizations. The first ones are aimed at testing and falsifying the standard model of ΛCDM, a cosmological constant with cold dark matter, and are agnostic as to its alternatives. Given precise measurements from primary CMB anisotropy of the high redshift universe, all low redshift observables related

to the expansion history and growth of structure are potential triggers. Trigger parameters thus have the benefit that their relationship to the raw observables can be made as direct as desired. The drawback is that deviant values for the trigger may not have any physical motivation. Instead they help pare down the possibilities for the more model dependent and theory oriented tests.

In the next section we discuss the cluster abundance, CMB lensing and pairwise kinematic SZ effects as the building blocks of triggers when combined with other measurements such as BAO and SNIa. CMB-S4 will also enhance the precision and robustness of these other tests by measurements of the primary E-mode polarization. For example the cold dark matter $\Omega_c h^2$ and effective relativistic degrees of freedom $N_{\rm eff}$ enter into the calibration of the BAO scale as well as inferences on H_0.

In addition to triggers based on the expansion history, CMB-S4 provides triggers based on the growth of structure. The ΛCDM model predicts that the growth of structure will slow in a precisely known manner as the expansion starts to accelerate. For example the rms amplitude of linear matter fluctuations at the $8h^{-1}$Mpc scale $\sigma_8(z)$ is a trigger parameter that can be closely associated with the cluster abundance. The linear growth rate index γ is another that is closely related to peculiar velocities and the kSZ observables.

The second way of parametrizing deviations from ΛCDM is by modifying the equations of motion for dark energy in a manner consistent with conservation laws. These have the benefit of attempting to tie distance and growth tests together in a physical, yet still phenomenological manner. The next step up in complexity from a cosmological constant is a model where the dark energy is dynamical but spatially smooth relative to the dark matter. In these models, the expansion history can deviate from that of ΛCDM due to evolution in the dark energy equation of state $w(z)$, yet still predict the growth of structure. A common parameterization of this phenomenology is

$$w(z) = w_0 + w_a \frac{z}{1+z}. \tag{4.1}$$

The figure of merit defined by the DETF is the inverse area of the 95% CL region in the $w_0 - w_a$ plane.

There are generalizations of this type of parameterization that separate the expansion history from the growth of structure. A complete parametrization for observables for scalar-tensor theories in the linear regime would include in addition the gravitational slip or effective anisotropic stress (the ratio of the space curvature potential and Newtonian potential), the effective Newton constant, and c_T the speed of tensor perturbations. [intentionally vague on which notation to use: forecaster will decide the favorite one and supply details. Possibly add graviton mass as it is mentioned in Inflation chapter.]

The last way of studying deviations from ΛCDM consists in directly testing theories beyond it. Given the lack of a compelling specific theory to test, we can still make progress by parameterizing all possible Lagrangians for fluctuations that are consistent with the given symmetry. This approach maintains a strong connection with the underlying theory at the price of complicating the relation to the raw data.

More specifically, a systematic implementation of this approach is the effective field theory (EFT) of cosmic acceleration [185, 70], inspired by the EFT of inflation described in the Inflation Chapter [115, 102, 381, 113, 307, 211]. The EFT of cosmic acceleration describes the cosmological phenomenology of all universally coupled single scalar field dark energy and modified gravity models. Specifically, the EFT action is constructed in a unitary gauge to preserve isotropy and homogeneity of the cosmological background and

reads:

$$\mathcal{S}_{\rm EFT} = \int d^4x\sqrt{-g}\ \ \Big\{\frac{m_0^2}{2}\left[1+\Omega(\tau)\right]R + \Lambda(\tau) - c(\tau)\,a^2\delta g^{00} + \frac{M_2^4(\tau)}{2}\left(a^2\delta g^{00}\right)^2 \\ -\frac{\bar{M}_1^3(\tau)}{2}\,a^2\delta g^{00}\,\delta K^\mu_{\ \mu} - \frac{\bar{M}_2^2(\tau)}{2}\left(\delta K^\mu_{\ \mu}\right)^2 - \frac{\bar{M}_3^2(\tau)}{2}\,\delta K^\mu_{\ \nu}\,\delta K^\nu_{\ \mu} \\ +m_2^2(\tau)\left(g^{\mu\nu}+n^\mu n^\nu\right)\partial_\mu(a^2g^{00})\partial_\nu(a^2g^{00}) + \frac{\hat{M}^2(\tau)}{2}\,a^2\delta g^{00}\,\delta\mathcal{R} + \dots\Big\} \\ +S_m[g_{\mu\nu},\chi_m] \tag{4.2}$$

where R is the four-dimensional Ricci scalar, δg^{00}, $\delta K^\mu_{\ \nu}$, $\delta K^\mu_{\ \mu}$ and $\delta\mathcal{R}$ are, respectively, the perturbations of the upper time-time component of the metric, the extrinsic curvature and its trace and the three dimensional spatial Ricci scalar of constant-time hypersurfaces. Finally, S_m denotes the action for all the matter fields conventionally considered in cosmology.

In the action (4.2), the extra scalar degree of freedom is hidden inside metric perturbations. To study the dynamics of linear perturbations, however, it is convenient to make it explicit by means of the Stückelberg technique i.e. performing an infinitesimal coordinate transformation such that $\tau \to \tau + \pi$, where the field π describes the extra propagating degree of freedom. This approach allows us to maintain a direct link to the underlying theory so that we can keep under control its theoretical viability while exploring the cosmological implications of any of the models included in this language [328].

Since the choice of the unitary gauge breaks time diffeomorphism invariance, each operator allowed by the residual symmetry, in action (4.2), can be multiplied by a time-dependent coefficient that we shall call EFT function. To fully specify the phenomenology of linear perturbations only a restricted set of EFT functions are needed. These can be either parametrized to explore agnostically the space of dark energy and modified gravity models [169, 69, 310, 171] or can be fixed to reproduce exactly the phenomenology of some model of interest such as $f(R)$ gravity, quintessence and, more generally, the Horndeski class of theories and beyond [170, 165, 164].

4.1.2 CMB Dark Energy Observables

4.1.2.1 Cluster abundance and mass

Clusters of galaxies are sensitive to the content, geometry, and growth of structure in the universe. In the report of the DETF, they were highlighted as having the highest sensitivity to dark energy parameters but simultaneously the largest astrophysical systematic due to uncertainties in the mass scaling of the cluster observables. In the "Stage IV" era of dark energy probes, CMB-S4 will play a critical role in overcoming this challenge.

Clusters of galaxies are the most massive ($\sim 10^{14}$-10^{15} $M_\odot$) objects in the universe to have underwent gravitational collapse, having formed from regions ∼10-40 Mpc. This property makes clusters representative of the overall content of the universe, and also makes them important tracers of the evolution of large-scale structure, sampling the most extreme peaks in the large-scale matter distribution. These properties have enabled clusters to make important contributions to cosmology: the discovery of dark matter in the Coma cluster [393], providing early evidence for $\Omega_m < 1$ [384, 136, 42], and constraining the physical nature of dark matter [106]. More recently, measurements of clusters have been used to constrain the properties of dark energy and modifications to gravity [374, 267, 326, 59, 268, 269]. In the future era of "Stage IV"

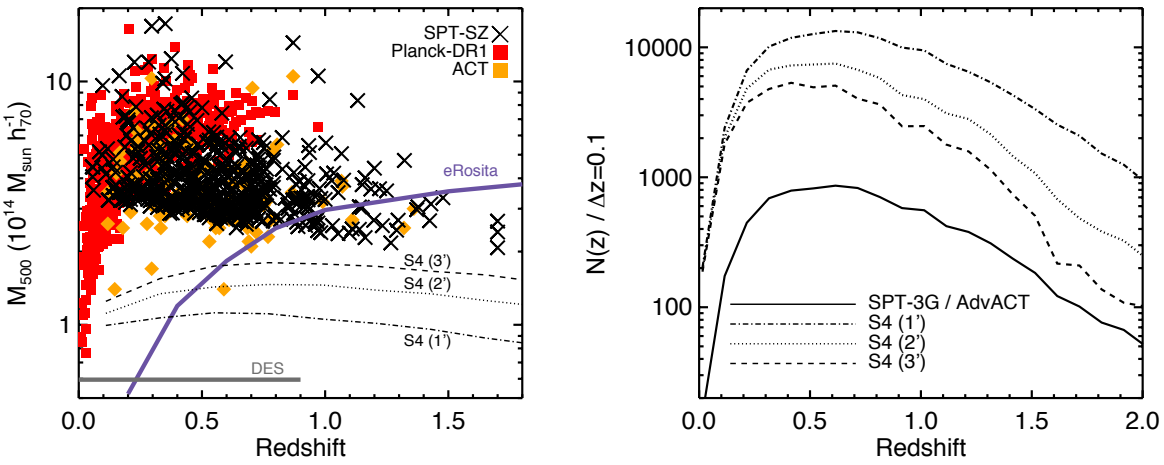

Figure 9. *(Left) The 50% mass-completeness limits for three possible CMB-S4 instrumental configurations with either 1, 2, or 3 arc minute angular resolution. For comparison, this can be compared with existing SZ-selected cluster catalogs from Planck [316], SPT-SZ [68], and ACT [189], and future thresholds expected for the optical Dark Energy Survey and the X-ray eRosita survey [311]. (Right) The projected cluster counts for the three possible CMB-S4 configurations described above. For comparison, the projected cluster counts from the SPT-3G [58] and AdvACT surveys.*

dark energy facilities such as DESI and LSST, measurements of the abundance of galaxy clusters can make complementary and competitive constraints on the dark energy equation of state and deviations from General Relativity [379].

CMB measurements find clusters through the inverse Compton scattering of CMB photons off of intra-cluster gas, otherwise known as the Sunyaev-Zel'dovich (SZ) effect [360]. SZ cluster surveys have two important advantages: the SZ surface brightness is redshift independent, and the integrated SZ signal is expected to be a relatively low-scatter cluster observable [290, 291, 239]. These properties enable SZ surveys to provide relatively clean, mass-limited cluster catalogs out to high-redshift ($z > 1$). Since the first SZ-discovered clusters were report in 2009 [352], SZ surveys have produced catalogs of over 1000 SZ-selected clusters extending out to $z \sim 1.7$ [373, 329, 189, 315, 68, 316].

Figure 10 shows an estimate of the mass sensitivity, expressed as the one-sigma mass uncertainty as a function of redshift, for two possible CMB-S4 configurations and compares them to planned CMB experiments. In Figure 9, we show projections for the mass-threshold and total cluster counts for three possible CMB-S4 configurations. The 50% mass-completeness threshold for the CMB-S4 cluster survey would be relatively flat with redshift out to $z \sim 2$. The mass-threshold increases from $\sim$1-2 $\times$ 10^{14} $M_{\odot}$, going from a CMB-S4 angular resolution of 1 to 3 arc-minutes, which is >2 times lower than current SZ surveys even in the worse case scenario for CMB-S4. In addition, the lower mass threshold and larger sky area of CMB-S4, would translate to a nearly $\sim$100 fold increase in the number of SZ-identified clusters. At a 99% purity threshold, for a configuration with a 1, 2, and arc-minute angular resolution, CMB-S4 would identify $\sim$40,000, 70,000, and 140,000 clusters, respectively.

CMB-S4 will also enable a new means of calibrating cluster masses through CMB lensing. Accurate masses are crucial for catalogs to provide constraints on dark energy and modified gravity. With sufficient angular resolution, CMB-S4 opens tremendous possibilities for measuring cluster, more generally halo masses. Figure

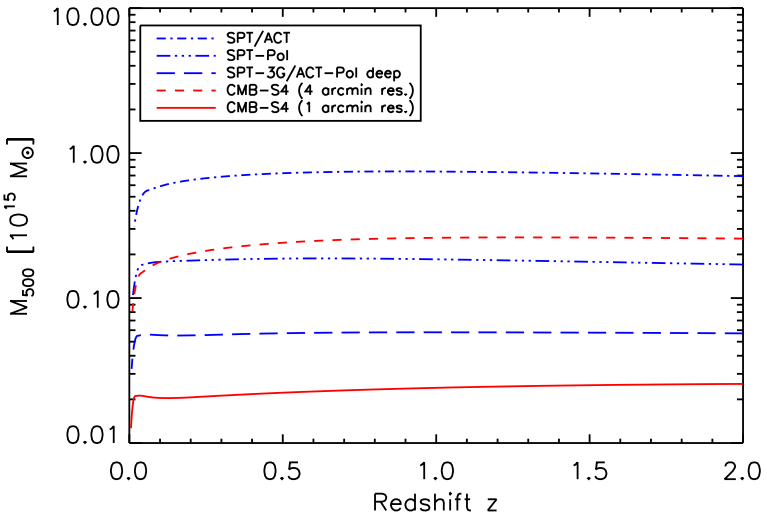

Figure 10. *Cluster mass sensitivity of CMB lensing.*

10 shows an estimate of the mass sensitivity, expressed as the one-sigma mass uncertainty as a function of redshift, for two possible CMB-S4 configurations and compares them to planned CMB experiments.

The estimation is made assuming foreground subtraction to reach the quoted CMB map noise level at the given angular resolution. The method (Melin & Bartlett 2015) employs an optimal filter matched to the NFW profile and applied to reconstructions of the lensing potential with a quadratic estimator (Hu & Okamoto 2002). The method has already been successfully applied to the Planck cluster cosmology sample of more than 400 objects (Planck Collaboration XXIV 2015). This figure shows the sensitivity obtained with just CMB temperature lensing reconstruction. Including polarization will significantly improve it. We see that the mass sensitivity remains flat with redshift, a remarkable property that enables mass estimation out to redshifts unreachable with galaxy shear measurements. This is a powerful and unique capability of CMB lensing. The figure also demonstrates the important gains attained with high angular resolution. At one arcmin resolution, S4 achieves a mass sensitivity of $2 \times 10^{13} M_{\odot}$ with temperature alone. This unprecedented sensitivity not only ensures robust mass estimation for cluster cosmology over the large redshift interval where S4 will detect clusters through the SZ effect, but also paves the way to numerous cluster and large-scale structure studies. The rapidly increasing science reach enabled by high angular resolution, approaching one arcmin, is an important consideration in CMB-S4 objectives.

4.1.2.2 Lensing

As described in the Lensing Chapter, the CMB lensing deflection map measures the projected mass density all the way back to the decoupling epoch at $z \sim 1100$, with the majority of the contributions coming from $z > 1$. CMB lensing is also dominated by structure on large scales in the linear regime. Thus, CMB lensing provides a clean probe of a particular integral over the linear growth of structure, e.g. $\sigma_8(z)$, weighted by distances. The lensing power spectrum shape is predicted from the background cosmology; shape deviations indicate scale-dependent effects on the growth, including those caused by modified gravity or the gravitational

effects of dark energy. CMB lensing complements other dark energy probes by providing a handle on effects at high redshift, e.g. in so-called early dark energy scenarios.

Cross-correlating the CMB lensing with other tracers of structure further permits extraction of information about the growth rate of structure in the universe that is localized in redshift. To the extent that other tracers have well-understood redshift distributions, cross-correlating a set of them to the CMB constitutes a tomographic study probing the evolution of the dark energy and its impact on the growth rate. The Lensing Chapter catalogs two broad categories of other tracers: galaxy density fields (and by extension the CIB) and galaxy shear maps. Combining lensing maps with maps of large scale flows from the kSZ will provide further constraints on the dark energy.

Another key contribution from CMB lensing to the study of dark energy will be its complementarity to other Stage IV experiments, including DESI and LSST, as well as EUCLID and WFIRST. (CMB Lensing chapter already mentions forecasting the improvement on calibrating multiplicative bias for LSST would it make sense to move that here?) Not only will CMB lensing provide a new redshift kernel for tomography studies, it will also validate or improve the calibration for LSST, increasing its DE FOM by a factor of xxx.

4.1.2.3 Kinematic SZ

CMB-S4 will map with unprecedented precision the momentum field of the large scale structure via measurements of the kinematic Sunyaev Zel'dovich (kSZ) effect. Multi-frequency data can be used to remove other foregrounds and isolate the kSZ signal. CMB-S4 measurements with sufficient angular resolution can be used to reconstruct the diffuse kSZ anisotropy signal enabling sub-percent precision measurements of the amplitude of the matter density fluctuations σ_8 (see for example [92]) while measurements of the patchy kSZ can place strong constraints on the time and duration of reionization.

The combination of CMB-S4 with data from galaxy surveys will be able to measure the kSZ effect associated with galaxy clusters, which is proportional to their peculiar momentum. The large scale structure momentum field is an important cosmological observable that can place strong constraints on the cosmological parameters [63, 236, 286, 287] complementary to density fluctuations field measurements. The mean pairwise velocity of galaxy clusters is sensitive to both the growth of structure and the expansion history of the universe and it is an excellent probe for gravity on large scales. Being a differential measurement it is also particularly stable against residual foregrounds that might survive the frequency cleaning process. In [286, 287] it has been shown that a S4 survey with high resolution can constrain the redshift dependent growth of structure at $\lesssim 5\%$ precision in generic models allowing also for a redshift dependent equation of state of the dark energy. These measurements will be able to distinguish dark energy from modified gravity and will provide complementary constraints to redshift space distortions and weak lensing measurements, probing larger physical scales.

kSZ pairwise measurements can also constrain the sum of neutrino masses $M_\nu = \sum m_\nu$ with a 1σ uncertainty of 0.030eV for a 1 arcmin CMB-S4 overlapping 10000 deg^2 with a galaxy survey able to identify $M > 10^{13} M_\odot$ clusters. With a 5 arcmin resolution separating the CMB background from the kSZ signal would be more difficult, providing $\sigma_{M_\nu} = 0.076$eV (de Bernardis et al., in preparation). These forecasts include only priors on the 6 standard cosmological parameters from Planck temperatures data and show the potential of the kSZ pairwise signal to provide constraints on the neutrino mass.

4.2 Dark Matter

We have learned from many different experiments (weak and strong lensing, studies of the Bullet Cluster, the Cosmic Microwave Background, etc) that approximately 84% of all the matter in the universe is composed of dark matter, which is not accounted for by the Standard Model of particles. However, the particle nature of dark matter remains unknown.

There are various types of experiments trying to shed light on this question: direct detection experiments, indirect detection experiments, and collider experiments. An alternative observable where Dark Matter interactions can modify the Standard Model prediction is the CMB power spectrum. CMB-Stage IV will have the sensitivity to detect new cosmological signatures originating from various types of dark matter interaction. In the sections below, we will discuss some of these possible scenarios.

4.2.1 Dark Matter Annihilation

One of the leading candidates for dark matter are the Weakly Interactive Massive Particles (WIMPs). If dark matter consists of WIMPs, we would expect these particles to self-annihilate. The annihilation of dark matter produces a shower of very energetic particles, that injects energy into the universe, ionizing the matter in it.

This extra source of ionization has distinctive effects on the Cosmic Microwave Background (CMB): it suppresses the CMB temperature and polarization fluctuations at small angular scales, and it enhances the CMB polarization fluctuations at large angular scales due to the extra scattering of photons off free electrons [101, 301]. CMB temperature and polarization spectra can constrain the parameter $p_{\rm ann} = f\langle\sigma v\rangle/m_{\rm DM}$, where f is the fraction of energy deposited into the plasma, $\langle\sigma v\rangle$ is the velocity-weighted cross section, and $m_{\rm DM}$ is the mass of the DM particle. Current constraints coming from WMAP 9-year data, Planck, ACT, SPT, BAO, HST and SN data excluded Dark Matter masses below 26 GeV at the 2σ level, assuming that all the energy is deposited in the plasma [261]. CMB-Stage IV is expected to tighten these constraints by a factor of 10 [388]. Ref. [388] found that the main factor that improves the limit in $m_{\rm DM}$ is the sky coverage $f_{\rm sky}$. This is because the constraints are mostly sample variance limited. Fig. 11 shows the dependence on $f_{\rm sky}$, and the small dependence on detector number and beam size.

Dark-matter annihilation also leads to growing ionization fraction perturbations and amplified small-scale cosmological perturbations, leaving an imprint on the CMB bispectrum [143].

4.2.2 Non-standard Dark Matter Interactions

Near the epoch of CMB last scattering, dark matter accounts for about 65% of the energy budget of the Universe, hence making the CMB a particularly good probe of potential new physics in the dark matter sector. Of particular relevance to CMB-S4 studies, the presence of new dark matter interactions with light degrees of freedom [177, 96, 179, 259, 129, 38, 73, 162, 183, 324, 265, 8, 30, 153, 343, 84, 219, 276, 220, 372, 132, 43, 105, 124, 150, 149, 122, 85, 386, 142, 72, 385, 147, 104, 29, 89, 244] can leave subtle imprints on the temperature and polarization CMB power spectra. The introduction of such non-minimal dark matter models has been primarily (but not exclusively) motivated in the literature by potential shortcomings of the standard cold dark matter scenario at small sub-galactic scales [127, 231, 284, 392, 297, 80, 305, 378, 308, 230, 300, 306].

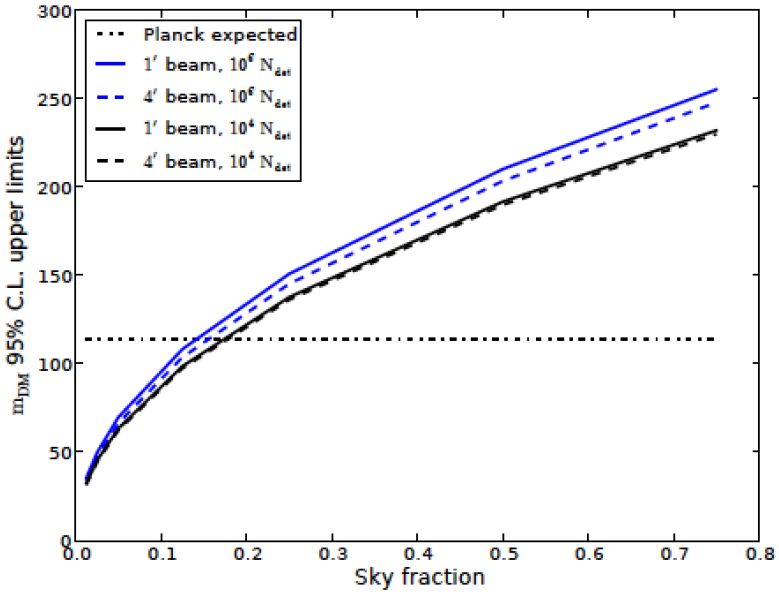

Figure 11. *95 % CL upper limit on $m_{\rm DM}$ in GeV as a function of sky coverage, $f_{\rm sky}$. The blue/black lines correspond to $10^6/10^4$ detectors. The solid/dashed lines correspond to 1'/4' beams. The dashed/dotted lines show the limit from Planck for a thermal cross section and 100% of the energy absorbed by the plasma (it was expected from Fisher forecasts and then confirmed by the Planck collaboration measurements).*

While these issues are far from settled, they motivate the search for other non-minimal dark matter signatures in complementary data sets (such as the CMB) that could indicate whether or not dark matter can be part of the solution.

4.2.2.1 Dark Matter-Baryon Scattering

A possible non-standard dark matter scenario is that in which dark matter scatters off baryons in the early universe. In this scenario, there is a drag force produced by the baryons on the dark matter fluid, which affects the CMB temperature and polarization power spectra and the matter power spectrum. Ref. [142] has done a model-independent analysis on the Dark Matter-Baryon interactions using CMB temperature data from the *Plack satellite*, and the Layman-α forest data from the *Sloan Digital Sky Survey*, as a tracer of the matter fluctuations. This analysis suggests that the constraints could become significantly better with better temperature data on small scales, and additional polarization data at large and small scales. Therefore, an experiment such as CMB-S4 would have a large impact on these constraints.

4.2.2.2 Dark Matter-Dark Radiation Interaction

Dark matter interacting with light (or massless) dark radiation has been put forward [89, 244] as a potential solution to the small discrepancy between the amplitude of matter fluctuations inferred from CMB measurements and those inferred from cluster number counts and weak lensing measurements. CMB-S4

measurements of the lensing power spectrum have the potential to significantly improve constraints on dark matter interacting with light degrees of freedom in the early Universe.

The key equations governing the evolution of cosmological fluctuations for this broad class of non-minimal dark matter models are presented in Ref. [126]. Essentially, the new dark matter physics enters entirely through the introduction of dark matter and dark radiation opacities, which, similarly to the photon-baryon case, prohibit dark radiation free-streaming at early times and provides a pressure term that opposes the gravitational growth of dark matter density fluctuations. The impact of this new physics on CMB fluctuations has been studied in detail in Ref. [122] and we briefly review it here. First, the presence of extra dark radiation mimics the presence of extra neutrino species and affects the expansion history of the Universe, possibly modifying the epoch of matter-radiation equality, the CMB Silk damping tail, and the early Integrated Sachs-Wolfe effect. However, unlike standard free-streaming neutrinos, the dark radiation forms a tightly-coupled fluid at early times, leading to distinct signatures on CMB fluctuations which include a phase and amplitude shift of the acoustic peaks (see e.g. Ref. [47, 125, 161]). Second, the dark radiation pressure prohibits the growth of interacting dark matter fluctuations on length scales entering the causal horizon before the epoch of dark matter kinematic decoupling. This weakens the depth of gravitational potential fluctuations on these scales, hence affecting the source term of CMB temperature fluctuations. Finally, the modified matter clustering in the Universe due to nonstandard dark matter properties will affect the lensing of the CMB as it travel from the last-scattering surface to us. For interacting dark matter models that are still allowed by the current Planck data, this latter effect is where CMB-S4 can significantly improve the constraints on these non-minimal theories.

Given the large array of possible dark matter theories to constrain, we use the Effective THeory Of Structure formation (ETHOS) [126] to systematically parametrize the deviations from standard cold dark matter. Within ETHOS, the impact of having all or a fraction of dark matter interacting with dark radiation can be captured with a handful of "effective" parameters which entirely determine the structure of the linear matter power spectrum. The most relevant parameters are [126]

$$\Xi_{\rm ETHOS} = \Big\{\omega_{\rm DR}, f_{\rm int}, \{a_n, \alpha_l\}\Big\}, \tag{4.3}$$

where $\omega_{\rm DR} = \Omega_{\rm DR}h^2$ is the physical energy density in dark radiation in units of the critical density of the Universe, $f_{\rm int}$ is the fraction of the total dark matter density that interacts with dark radiation, and where a_n and α_l are parameters describing the size of the interaction cross section and its angular dependence, respectively. The coefficients a_n enter directly into the calculation of the dark matter drag opacity $\dot{\kappa}_\chi$ as:

$$\dot{\kappa}_\chi = -\omega_{\rm DR}\sum_n \left(\frac{2+n}{3}\right) a_n \frac{(1+z)^{n+1}}{z_{\rm D}^n}, \tag{4.4}$$

where $z_{\rm D}$ is a normalization scale. Choosing the latter to correspond to the dark matter decoupling redshift ensures that the a_n coefficients are of order unity. The index n is directly related to the nature of the physical process coupling dark matter and dark radiation: a non-vanishing a_n coefficient implies a scattering process characterized by the matrix element $|\mathcal{M}|^2 \propto (p_{\rm DR}/m_\chi)^{n-2}$, where $p_{\rm DR}$ is the incoming momentum of the dark radiation and m_χ is the dark matter mass. Since the decoupling of dark matter from dark radiation is given by the approximate criterion $-\dot{\kappa}_\chi = H$, the magnitude of the ETHOS coefficients a_n set the scale at which the CMB lensing power spectrum departs from its ΛCDM counterpart. We use the ETHOS parametrization to illustrate that CMB-S4 can provide competitive constraints on partially interacting dark matter theories.

We illustrate in Fig. 12 the impact of different interacting dark matter models on the CMB lensing power spectrum. In the top panel, we show four partially-interacting dark matter models parametrized by their ETHOS opacity coefficient and for which only 5% of the total amount of dark matter is interacting. We

display the fractional difference between the ETHOS models and a standard ΛCDM model with vanishing neutrino mass. For comparison, we also illustrate the difference for a standard massive neutrino ΛCDM model with $\sum m_\nu = 0.06$ meV. Interestingly, the damping of the lensing power spectrum has a different shape than that caused by massive neutrinos. Given the expected performance of CMB-S4 in measuring the lensing power spectrum, all the model illustrated there (which are currently allowed by Planck data) could be ruled out, significantly improving our knowledge about interacting dark matter. The lower panel of Fig. 12 is similar, but illustrates how the fractional difference in the CMB lensing power spectrum is affected as the fraction of interacting dark matter is varied from 5 to 2 percents. Again, this illustrates that CMB-S4 can provide very tight constraints on the fraction of interacting dark matter.

Since non-standard dark matter models affect primarily the large CMB lensing multipoles, the constraining power of CMB-S4 on interacting dark matter is largely independent of the specific choice of $\ell_{\rm min}$. We foresee that the main difficulty in constraining non-standard dark matter theories with CMB-S4 will be the proper modeling of non-linearities in the matter power spectrum, which are quite important for $\ell > 500$. We note that recent progress has been made in this direction [376].

4.2.3 Ultralight axions

Non-thermally produced ultralight axions (ULAs) with masses in the range 10^{-33} eV $\leq m_a \leq 10^{-20}$ eV are well motivated by string theory, can contribute to either the dark matter or dark energy components of the Universe, depending on their masses, and are distinguishable from DE and CDM in cosmological observables. The current best constraints from the primary CMB TT power, and WiggleZ galaxy redshift survey were made in [199]. Our fiducial axion energy density is chosen to be consistent with these constraints.

The degeneracies of the axions with other cosmological parameters, such as $N_{\rm eff}$ or m_ν, vary depending on the axion mass (see Fig. 13, right panel). Dark energy-like axions with masses around 10^{-33} eV change the late-time expansion rate and therefore the sound horizon, changing the location of the acoustic peaks. This has degeneracies with the matter and curvature content. Heavier axions ($m_a \gtrsim 10^{-26}$ eV) affect the expansion rate in the radiation era and reduce the angular scale of the diffusion distance, leading to a boost in the higher acoustic peaks, which has a degeneracy with $N_{\rm eff}$.

In both of these cases, improved errors on the temperature and polarization power spectrum, coupled with constraints on the Hubble constant (for the lightest axions) from Baryon Acoustic Oscillations, lead to improvements in the error on allowed axion energy density of a factor of three from these spectra alone.

In the matter power spectrum, and thus CMB lensing power, light axions suppress clustering power, suggesting a degeneracy with effects of massive neutrinos that must be broken to make an unambiguous measurement of neutrino mass using the CMB. The above-mentioned effects in the expansion rate break this degeneracy for some axion masses. There remains a significant degeneracy between axions and massive neutrinos $m_a = 3 \times 10^{-29}$ eV and $\Sigma m_\nu = 60$ meV. Effort should be made to break this degeneracy and distinguish the effects of non-thermal axions from massive neutrinos for an unambiguous detection of neutrino mass using the CMB.

We show the forecasted constraints on the axion energy density from S4 including lensing in the left panel of Figure 13 (for fixed neutrino mass of $\Sigma m_\nu = 0.06$ eV). Adding in information from the lensing reconstruction using S4 will improve constraints on axion DM significantly. A percent-level measurement of the lensing deflection power at multipoles $\ell > 1000$ leads to an improvement in the error on the axion energy density of a factor of eight relative to the current Planck constraints, for an axion mass of $m_a = 10^{-26}$ eV. This represents an ability to test the component nature of dark matter, and thus the CDM paradigm, at the

percent level. Furthermore, since $\Omega_a \propto f_a^2$ this improves the expected constraint on the axion decay constant from 10^{17} GeV with Planck to 10^{16} GeV with S4, testing the predictions of the "string axiverse scenario [33].

For higher mass axions there is a strong degeneracy between CDM and axions. Using high-ℓ lesing measurements, S4 breaks this degeneracy at larger masses than Planck. However, this degeneracy is still significant and care should be taken in interpreting the constraints on the energy density shown in Fig. 13. Constraints at $m_a \gtrsim 10^{-24}$ eV are driven by the improved measurement of the total matter density, and do not allow one to distinguish such axions from CDM at high precision. Achieving further improvement in the mass constraint will require improved understanding of non-linear clustering of axions. These constraints represent the absolute lower bound on DM particle mass from cosmology. If this bound can be improved and the degeneracy broken up to 10^{-23} eV, the CMB will begin to make contact to the "Fuzzy DM axion model [203, 271].

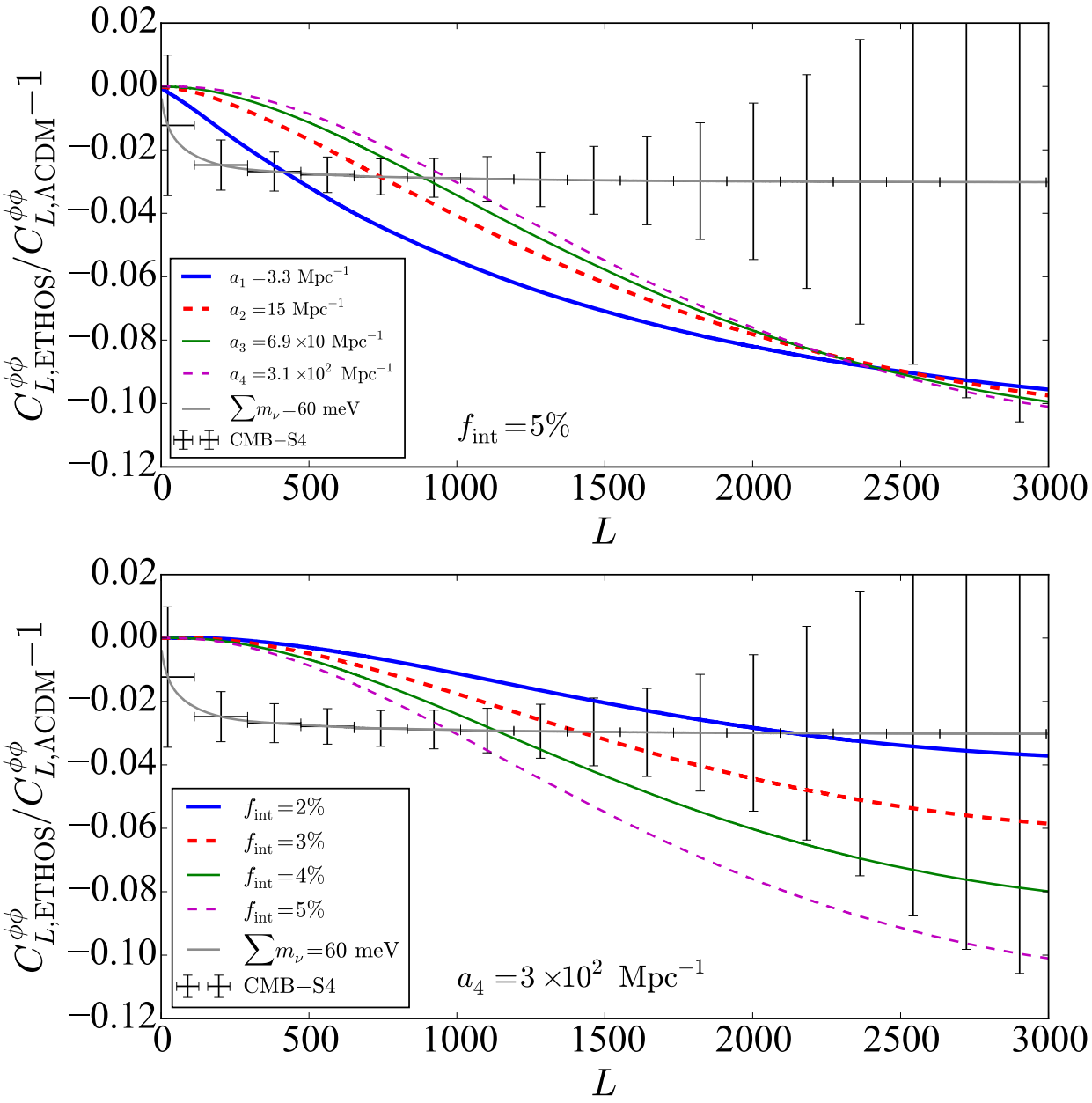

Figure 12. Top panel*: Fractional difference of the CMB lensing spectrum between a standard ΛCDM model (with massless neutrinos) and four different ETHOS models with opacity coefficients a_n given in the legend. In all models shown, 5% of the dark matter is allowed to interact with dark radiation. For comparison, we also display a standard massive neutrino model with $\sum m_\nu = 0.06$ meV.* Lower panel*: Similar to the top panel, but we now vary the fraction of dark matter that can interact with dark radiation, for a fixed opacity coefficient of $a_4 = 3 \times 10^2$ Mpc^{-1}.*

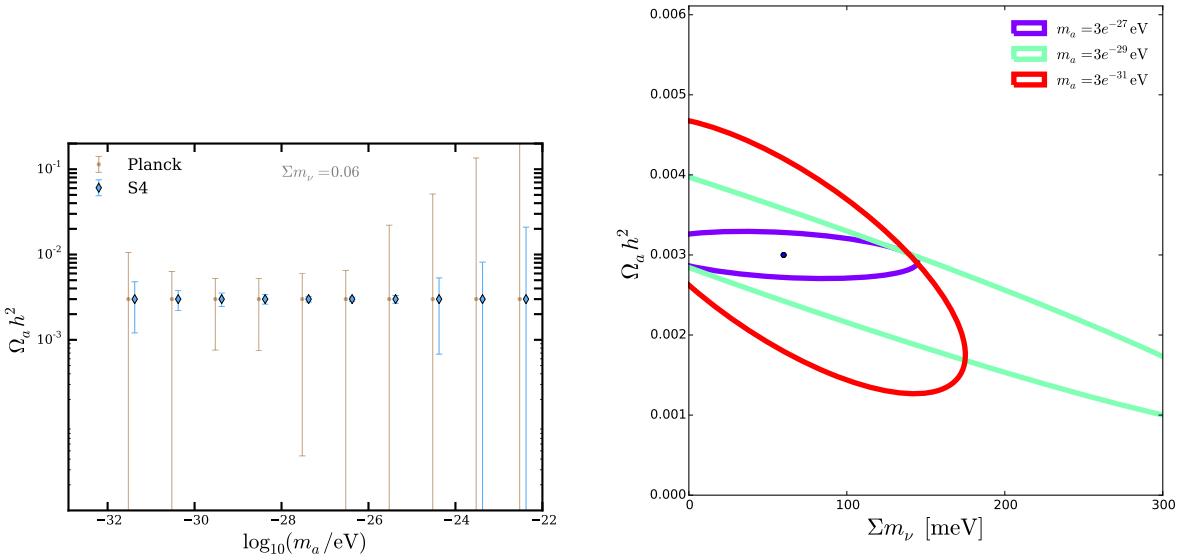

Figure 13. *(Left: Constraints on the axion energy density as a function of axion mass at fixed neutrino mass $\Sigma m_\nu = 0.06$ eV. Over the 'fuzzy' dark matter region, S4 allow for percent-level constraints on an axion component, improving significantly on current constraints. Right: Degeneracy of axions with massive neutrinos. There is a significant degeneracy for $m_a = 3 \times 10^{-29}$ eV and $\Sigma m_\nu = 60$ meV.*

5

CMB Lensing

(send feedback on this chapter to s4_lensing@cosmo.uchicago.edu)

5.1 Introduction to CMB Lensing

As CMB photons travel from the last scattering surface to Earth, their travel paths are bent by interactions with intervening matter in a process known as *gravitational lensing*. This process distorts the observed pattern of CMB anisotropies, which has two important consequences:

• CMB lensing encodes a wealth of statistical information about the entire large-scale structure (LSS) mass distribution, which is sensitive the properties of neutrinos and dark energy.

• CMB lensing distortions obscure our view of the primordial Universe, limiting our power to constrain inflationary signals; removing this lensing noise more cleanly brings the early Universe and any inflationary signatures into sharper focus.

Gravitational lensing of the CMB can be measured by relying on the fact that the statistical properties of the primordial CMB are well known. The primordial (un-lensed) CMB anisotropies are statistically isotropic. Gravitational lensing shifts the apparent arrival direction of CMB photons, which breaks the primordial statistical isotropy; lensing thus correlates previously independent Fourier modes of the CMB temperature and polarization fields. These correlations can be used to make maps of the LSS projected along the line-of-sight; see the discussion in Section 5.2.1.

A CMB-S4 experiment will make radical improvements in CMB lensing science: high sensitivity will enable lensing maps that have much higher signal to noise; the high polarization sensitivity will allow lensing maps that are much less sensitive to foreground contamination; multi-frequency coverage will greatly reduce foreground contamination in the temperature-based lensing estimates, allowing lensing maps with higher resolution; large area coverage will provide maps for cross-correlation with large scale structure for next generation surveys, including Euclid and LSST.

The information contained in lensing mass maps can be accessed and used in several ways. First, the power spectrum of the lensing deflection map is sensitive to any physics that modifies how structure grows, such as dark energy, modified gravity, and the masses of neutrinos. In Section 5.2.2, we discuss how the lensing power spectrum is measured, and in Section 5.6, we give parameter forecasts combining primordial CMB power spectrum and CMB lensing power spectrum measurements. Second, lensing mass maps can be compared to other tracers of LSS at lower redshifts such as the distribution of galaxies and optical weak lensing shear maps. By cross correlating, for example, CMB lensing and optical shear mass maps, which are each derived from lensed sources at widely differing redshifts, one can enhance dark energy constraints and improve the calibration of systematic effects. Cross-correlation science with CMB lensing maps is discussed in Section 5.3. Finally, lensing distortions partially obscure potential signatures of cosmic inflation in the primordial

B-mode polarization signal. With precise measurements, this lensing-induced noise can be characterized and removed in a procedure known as "delensing." Because B-mode polarization measurements from CMB-S4 are expected to be lensing-noise dominated, delensing will be critical to maximize the information we can infer about cosmic inflation; see the discussion in Section 5.4.

We discuss systematics from astrophysical and instrumental effects that can impact the lensing signal as well as ways to mitigate them in Section 5.5. Section 5.6 describes forecasted parameter constraints when including CMB lensing measurements as well as the instrument requirements for CMB-S4 to maximize the science gain from CMB lensing.

5.2 Measuring CMB Lensing

5.2.1 Constructing a Lensing Map

A map of the CMB lensing deflection field is a direct probe of the projected matter distribution that exists in the observable Universe. This lensing map is a fundamental object for nearly all areas of CMB lensing science: it is used to measure the lensing power spectrum, measure cross correlations between CMB lensing and external data sets, and to de-lens maps of the B-mode polarization.

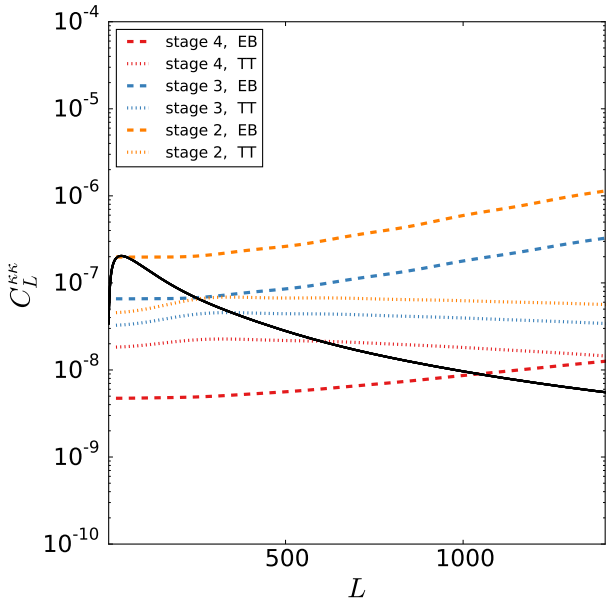

Figure 14. *Signal and noise-per-mode curves for three experiments. "Stage 2" is meant to represent a current-generation survey like SPTpol or ACTPol and has $\Delta_T = 9\mu$K-'; "Stage 3" is an imminent survey like SPT-3G or AdvACT, with $\Delta_T = 5\mu$K-'; and "Stage 4" has a nominal noise level of $\Delta_T = 1\mu$K-'. These noise-per-mode curves do not depend on the area of sky surveyed. All experiments assume a 1.4' beam. [note: iterative delensing not yet performed perfectly for stage 4 curves – more accurate calculation in progress.]*

To date, all maps of the lensing field have been constructed using the quadratic estimator by Hu & Okamoto 2002. This estimator uses information about the off-diagonal mode-coupling in spherical harmonic space

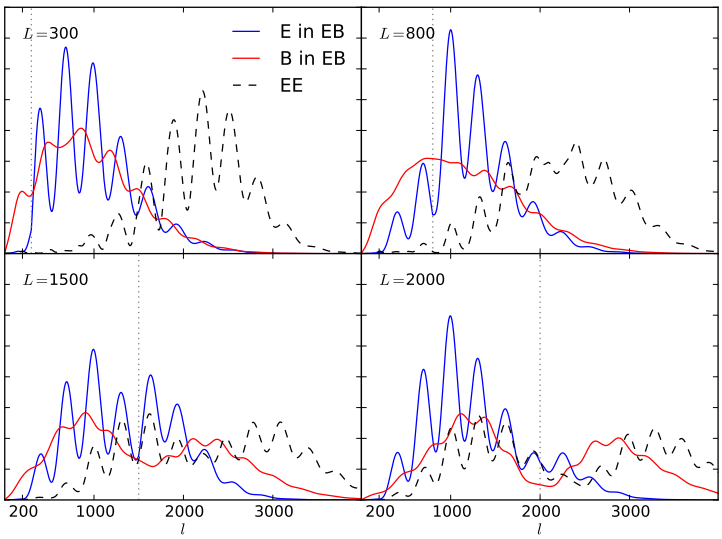

Figure 15. *Contributions from CMB scales (ℓ) to lensing reconstruction on four lensing scales (L). The EB estimator is expected to be the main channel for lensing science with CMB-S4. On degree and sub-degree scales, $L = 300$ and 800, the estimator uses B and E modes at $\ell \sim 1000$. On scales of several arcmin, $L = 1500$ and 2000, the estimator uses B modes on significantly smaller scales. Figure taken from Pearson et al. 2014*

that lensing induces to reconstruct the deflection field. An estimate for the amount of lensing on a given scale is obtained by averaging over pairs of CMB modes in harmonic space separated by this scale. CMB-S4 will greatly improve over existing measurements by having high angular resolution at high sensitivity to both temperature and polarization.

One way that the high angular resolution and sensitivity of CMB-S4 improves upon the Planck measurement is simply by increasing the number of CMB modes imaged on scales smaller than the Planck beam. Imaging CMB modes between $l = 2000$ and 4000, which can be achieved with CMB-S4 yields considerable gain in the accuracy of the lensing power spectrum measurement.

However, the primary reason for the increased power of CMB-S4 lensing measurements is this experiment's ability to measure CMB polarization with unprecedented sensitivity. To date, all CMB lensing results have had their signal-to-noise dominated by lensing reconstructions based on CMB temperature data (cite). Such lensing measurements in temperature are limited for two reasons. First, they are limited by systematic biases from astrophysical foregrounds and atmospheric noise. Second, the signal-to-noise on lensing measurements from temperature is intrinsically limited by the cosmic variance of the unlensed CMB temperature field. Due to the unprecedented sensitivity of CMB-S4, the bulk of the lensing signal-to-noise will now be derived from CMB polarization data; polarization lensing reconstruction will allow CMB-S4 to overcome both of these limitations. First, the challenges of astrophysical emission and atmospheric noise are much reduced in polarization data. Second, low-noise polarization lensing measurements are not limited by primordial CMB cosmic variance, because they make use of measurements of the B-mode polarization, which contains no primordial signal on small scales. To fully exploit the lack of limiting primordial signal in the B-mode polarization, maximum likelihood lensing reconstruction algorithms can be used, which use iteration to surpass the quadratic estimator. This iterative lensing reconstruction procedure is discussed in more detail in Section 5.4.

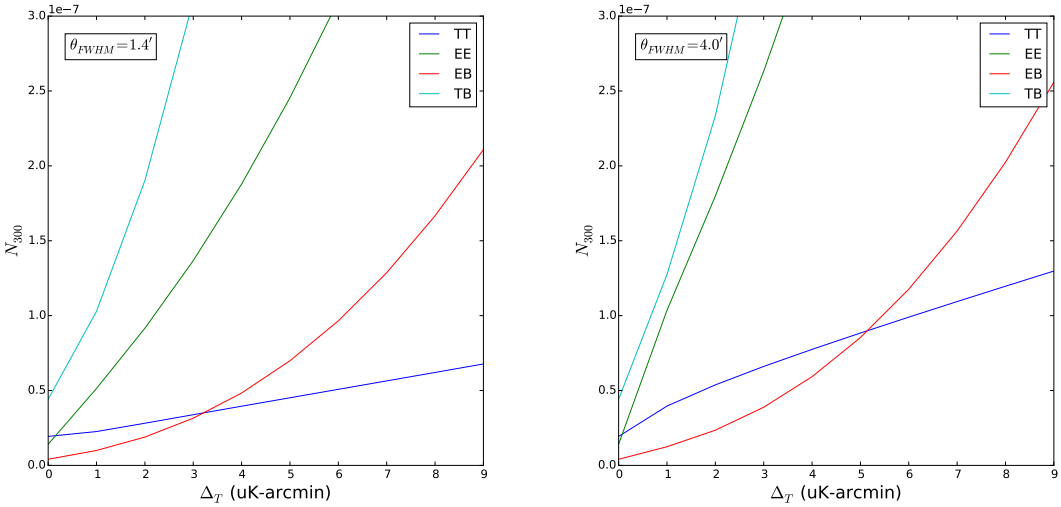

Figure 16. *Noise per mode in the lensing field for different lensing estimators at $L = 300$. Left panel is for 1.4 arcmin resolution, and right panel is for 4 arcmin resolution. For a 1.4 and 4 arcmin resolution experiment, the EB polarization estimator yields lower noise than the temperature estimator, below 3uk-arcmin and 5uk-arcmin noise in temperature respectively.*

5.2.2 Lensing Power Spectrum

The power spectrum of reconstructed CMB lensing maps is a measure of the matter power spectrum integrated over redshift. The lensing power spectrum has a broad redshift response kernel, with most of the contribution coming from $z \sim 1-5$, with a peak at $z \sim 2$ (see Figure 19). Most of the scales probed by the lensing power spectrum are on sufficiently large scales that they are mainly in the linear regime. As such, the lensing power spectrum is sensitive to physics which affects the growth of structure on large scales and at high redshift, such as the mass of the neutrinos.

The latest measurements of the CMB lensing autospectrum, as of early 2016, are shown in Figure 17. The first detections were obtained by the Atacama Cosmology Telescope (ACT; Das+ 2011) and South Pole Telescope (SPT; van Engelen+ 2012) teams, who analyzed maps of several hundreds of square degrees yielding precisions on the lensing power spectrum of approximately 25% and 18% respectively. The Planck collaboration has since provided all-sky lensing maps whose precision on the power spectrum amplitude is approximately 4% in the 2013 data release and 2.5% in the 2015 data release. The first detections of the lensing autospectrum using CMB polarization, which is ultimately a more sensitive measure of lensing for low-noise maps, have also been obtained (Story+2013, Polarbear 2014).

There has been rapid improvement in these measurements over the period of just a few years. Early detections of the CMB lensing autospectrum were not sample variance limited over a broad range in L and were only covering a relatively small sky area; the power spectrum of the noise in the CMB lensing reconstruction in the 2015 Planck data release is approximately equal to the lensing power spectrum only at its peak of $L \sim 40$, but smaller scales are noise-dominated and therefore not limited only by sample variance. Lensing reconstructions from current ground-based surveys (like SPTPol, ACTPol, PolarBear) are strongly signal-dominated below $L \sim 200$ and noise-dominated on smaller scales. However, they have been obtained over relatively small sky areas of several hundreds of degrees. A ground-based survey such as CMB-S4, with wide

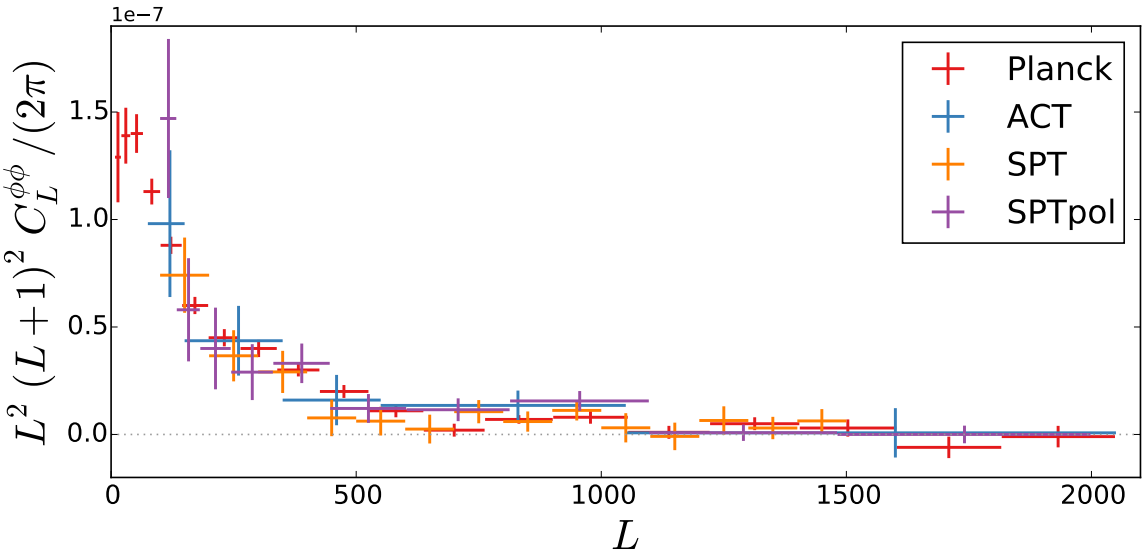

Figure 17. *Compendium of lensing power spectrum measurements, since first discovery in 2011. [POLARBEAR not yet included]*

sky coverage, low-noise, and high resolution, will provide a sample-variance-limited measurement to scales below $L \sim 1000$ (see Figure 18) over a wide area.

Such a measurement holds the promise to qualitatively improve our understanding of cosmology. While the cosmological parameters describing the standard Lambda-Cold Dark Matter model have been precisely measured, extensions to this model can be constrained by including growth or geometrical information at a new redshift. From the redshifts probed by CMB lensing, extensions to the standard model such as a non-minimal mass for the sum of the neutrinos, a dark energy equation of state deviating from the vacuum expectation, and a non-zero curvature of the Universe can all be probed to much higher precision than with the primordial CMB alone.

5.3 Cross Correlations with CMB Lensing

Cross-correlating CMB lensing maps with other probes of large-scale structure provides a powerful source of information inaccessible to either measurement alone. Because the CMB last-scattering surface is extremely distant, the CMB lensing potential includes contributions from a wide range of intervening distances extending to high redshift; as a result, many other cosmic observables trace some of the same LSS that lenses the CMB. These cross-correlations can yield high-significance detections, are generally less prone to systematic effects, and given the generally lower redshift distribution of other tracers, are probing LSS in exactly the redshift range relevant for dark energy studies (see Figure 19). With CMB-S4, cross-correlations will transition from detections to powerful cosmological probes.

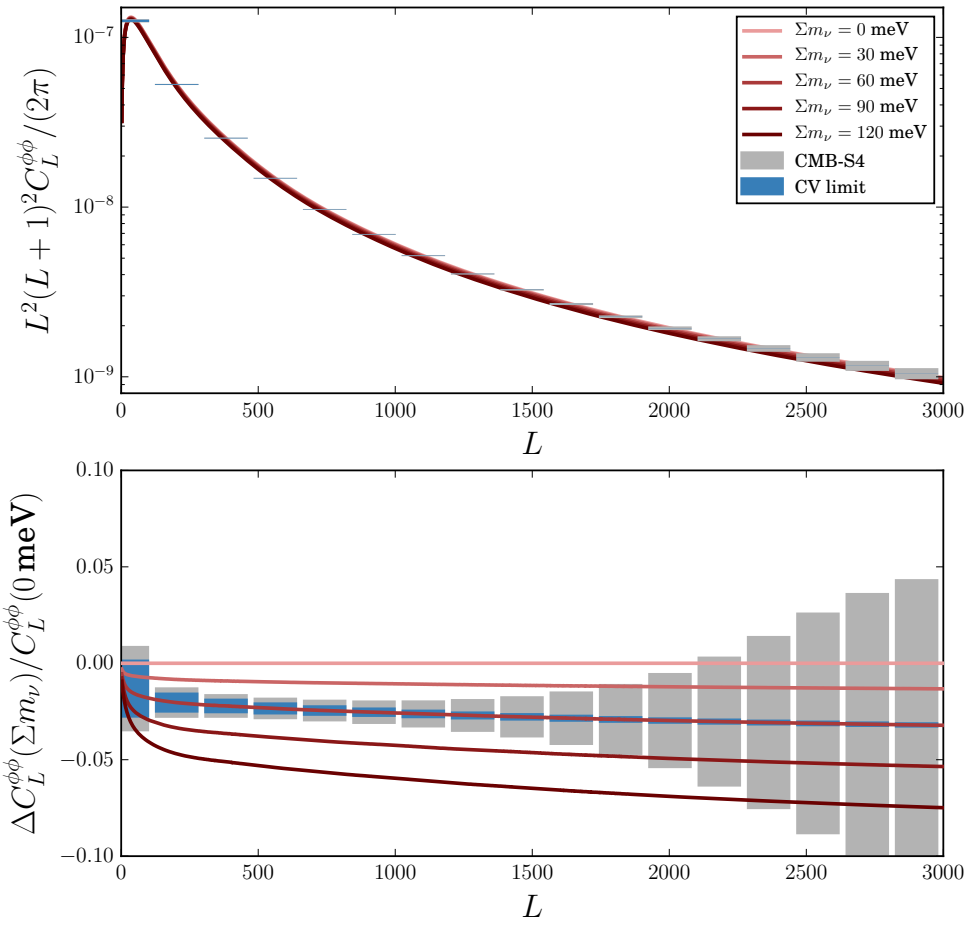

Figure 18. *Constraining neutrino mass with CMB-S4. Top: lensing power spectra for multiple neutrino masses (curves) together with forecasted errors for S4. Bottom: residual from curve at zero neutrino mass. Error boxes are shown centered at the minimal value of* 60 *meV. S4 will be targeted to resolve differences in neutrino mass of 20 meV.*

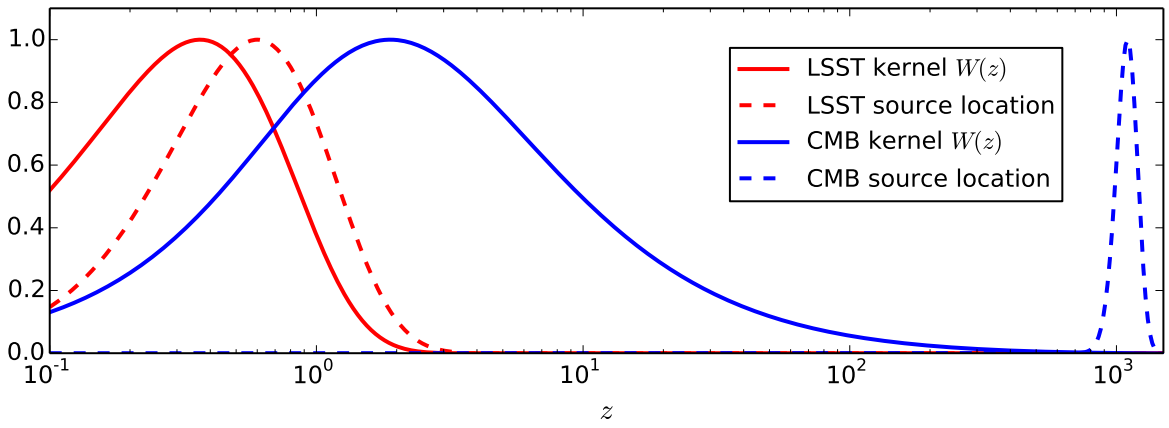

Figure 19. *Redshift kernel for CMB lensing (blue solid) and for cosmic shear with LSST (red solid), together with the expected redshift distribution of LSST galaxies (red dashed) and the CMB source redshift (blue dashed).*

5.3.1 CMB Lensing Cross Galaxy Density

Galaxies form in the peaks of the cosmic density field; thus the distribution of galaxies traces the underlying dark matter structure – which contributes to the CMB lensing potential. Cross-correlating galaxy density distributions with CMB lensing is highly complementary to galaxy clustering measurements. Galaxy surveys measure luminous matter while CMB lensing maps directly probe the underlying dark matter structure. Thus these correlations provide a clean measurement of the relation between luminous matter and dark matter. Cross-correlations between independent surveys are more robust against details of selection functions or spatially inhomogeneous noise that could add spurious power to auto-correlations. Additionally, while CMB lensing maps are projected along the line-of-sight, galaxy redshift surveys provide information about the line-of-sight distance; thus correlating redshift slices of galaxy populations allow for tomographic analysis of the CMB lensing signal (see, e.g., SPT/DES 2015). These properties can lead to improved constraints on cosmology: for example, with LSST galaxies, it has been shown that including cross-correlation with CMB lensing can substantially improve constraints on neutrino masses (Pearson & Zahn 2013).

CMB lensing was first detected using such a cross-correlation (Smith+ 2007, Hirata+ 2008). Since these first detections, cross-correlation analyses have been performed with tracers at many wavelengths, including optically-selected sources (Bleem+ 2012, Sherwin+ 2012, Planck 2013 XVII, SPT/DES 2015, Pullen+ 2014), infrared-selected sources (Bleem+ 2012, Geach+ 2013, DiPompeo 2015), X-ray-selected galaxy clusters (Planck 2013 XVIII), sub-mm-selected galaxies (Bianchini+ 2014,2015) and maps of flux from unresolved dusty star-forming galaxies (Holder+ 2013, Hanson+ 2013, Planck 2013 XVIII, van Engelen+ 2015).

On the timescale of the S4 experiment, a number of large surveys are expected be complete, including DESI, Euclid, and LSST. Due to the high number density of objects detected, wide areal coverage, and accurate redshifts, the precision of cross-correlation measurements with these surveys will be much higher than those performed to date. For example, the amplitude of cross-correlation between the S4 convergence map and the galaxy distribution from LSST is expected to be measured to XXX%.

5.3.2 CMB Lensing Cross Galaxy Shear

There have been several recent detections of the cross-correlation between lensing of the CMB and cosmic shear (Hand+ 2015, Liu+ 2015, Kirk+2016), demonstrating the emergence of a new cosmological tool.

Cosmic shear tomography is the measurement of cosmic shear of distant galaxies as a function of redshift, providing the ability to reconstruct the 3D mass distribution. CMB lensing offers similar signal-to-noise as cosmic shear surveys but provides the most distant source possible, allowing this 3D reconstruction to extend to the edge of the observable universe and providing a high-redshift anchor for dark energy studies.

CMB lensing, as a probe that is highly complementary to galaxy shear, can also be used as an external calibration for cosmic shear studies. It has been shown (Vallinotto 2012, Vallinotto 2013, Das+ 2013) that CMB lensing, galaxy clustering, and cosmic shear taken together can in principle cross-calibrate each other while still providing precise constraints on cosmological parameters. This has been successfully applied to existing surveys (Liu+ 2015, Baxter+ 2016) as a proof of principle; CMB-S4 will be a powerful tool for precision cosmology.

5.3.3 CMB Halo Lensing

In addition to constructing CMB lens maps of matter fluctuations on relatively large scales ($>\sim$ 5 arcmin) as discussed in the preceding sections, one can also make CMB lens maps capturing arcminute-scale matter distributions. Such small-scale measurements capture lesning of the CMB by individual dark matter halos, as opposed to lensing by larger scale structure represented by the clustering of halos. This small-scale lensing signature, called CMB halo lensing, allows one to obtain measurements of the mass of these halos.

Using CMB halo lensing, CMB-S4 will be sensitive to halo masses in the range of $10^{13}M_{\odot}$ to $10^{15}M_{\odot}$. This corresponds to halos belonging to galaxy groups and galaxy clusters. As discussed in Chapter 3, measuring the abundance of galaxy clusters as a function of mass and redshift provides a direct handle on the growth of matter perturbations and consequently, on the equation of state of Dark Energy. Galaxy clusters can be identified internally in CMB maps through their wavelength-dependent imprint caused by the thermal Sunyaev-Zeldovich (tSZ) effect. However, the scaling between the tSZ observable, which is sensitive to baryonic physics, and the cluster mass, which is dominated by dark matter is not precisely constrained. Calibration of this mass scaling and scatter is currently the dominant systematic for extracting Dark Energy constraints from cluster abundance measurements.

Weak lensing of galaxies behind the galaxy cluster is a promising method for mass calibration since it is directly sensitive to the total matter content of the cluster. Reconstructing the mass profiles of clusters using measurements of the shapes of distant galaxies in deep photometric surveys is an active research program; however, it is often limited by the poor accuracy of source redshifts and the availability of sufficient galaxies behind the cluster, especially for very high-redshift clusters. CMB halo lensing has an advantage here since the CMB is a source of light which is behind every cluster, has a well defined source redshift, and well understood statistical properties.

A general approach for obtaining the average mass of a sample of clusters using CMB halo lensing is to reconstruct the lensing deflection field using a variation of the standard quadratic estimator, stack the reconstructed lens maps at the positions of the clusters, and fit the resulting signal to a cluster profile (e.g NFW). A modified quadratic estimator is used to reconstruct small-scale lensing signals since the standard estimator tends to underestimate the signal from massive clusters (Hu, Dedeo, Vale 2007). This modified

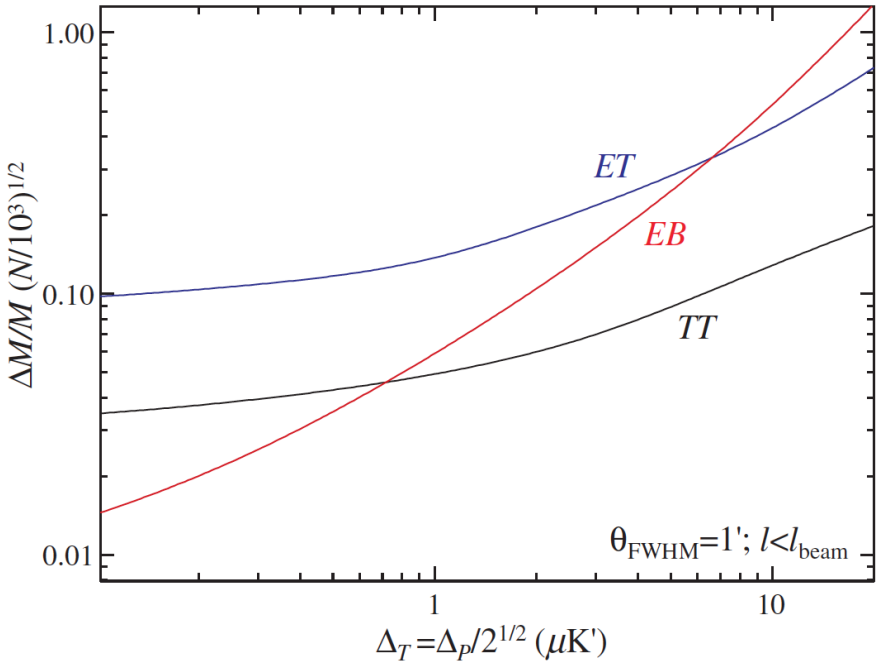

Figure 20. *Lensing sensitivity to halos of a given mass M as a function of instrumental noise. Figure from Hu, DeDeo, Vale 2007.*

estimator makes use of the fact that halo lensing induces a dipole pattern in the CMB that is aligned with the background gradient of the primordial CMB. The halo lensing signal can be measured with both temperature and polarization estimators, which can be used to cross check each other and reduce systematics.

CMB experiments have only very recently reached the sensitivity required to detect the lensing signal on scales of dark matter halos. The first detections were reported in 2015 by ACTPol (Madhavacheril+2015), SPT (Baxter+2015), and Planck (Planck 2015 XXIV). CMB-S4 will be capable of providing precision mass calibration for thousands of clusters which will be an independent cross check of galaxy shear mass estimates and will be indispensable for high-redshift clusters. Figure 20 shows that an arcminute resolution experiment with a sensitivity of around 1μK-arcmin can determine the mass of 1000 stacked clusters to $\sim 5\%$ using temperature maps and independently to $\sim 5\%$ using polarization maps. The primary systematic in temperature maps is contamination from the thermal SZ effect and radio and infrared galaxies coincident with the halos. This systematic can be mitigated using multi-frequency information due to the spectral dependence of the thermal SZ effect and galaxy emission, a procedure that requires the high sensitivity at multiple frequencies of CMB-S4. Halo lensing from polarization maps is relatively free of these systematics, and ultimately may be the cleanest way to measure halo masses, which requires the high polarization sensitivity provided by CMB-S4.

5.4 Delensing

To probe an inflationary gravity wave signal it is important to have low-noise B-mode polarization maps. However, for instrumental noise levels below $\Delta_P \simeq 5\mu$K-arcmin in polarization, the dominant source of

noise is no longer instrumental, but instead is from the generation of B-mode polarization by lensing of E-mode polarization from recombination (see Figure 21). This B-mode lensing signal has a well-understood amplitude, but the sample variance in these modes in the CMB maps leads to increased noise in estimates of the inflationary B-modes. Unlike other sources of astrophysical B-mode fluctuations in the map, it cannot be removed with multifrequency data. Fortunately, this signal can be removed using map-level estimates of both the primordial E-mode map and the CMB lensing potential ϕ with a technique called delensing. However, this procedure requires precise maps of both the E-modes and of the gravitational lensing potential (which can be obtained from the CMB-S4 data itself).

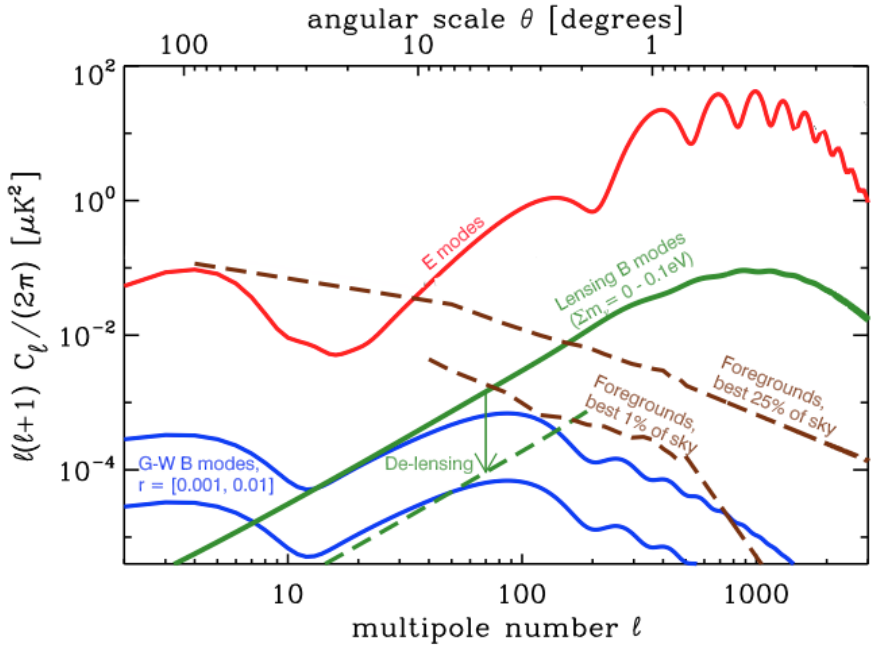

Figure 21. *The green curve is the power spectrum of lens-induced E-to-B mixing. Delensing can reduce the amplitude of this effect by large factors (green dashed curve) yielding lower effective noise in B-mode maps.[Will add 5uK-arcmin noise curve to plot]*

Moreover, delensing will be a crucial part of the reconstruction of the CMB lensing field for CMB-S4, even for science goals like measuring the neutrino mass. This is because at low noise levels the standard quadratic reconstruction of lensing using the EB estimator (Hu & Okamoto 2001) can be improved upon by cleaning the B-mode CMB maps of the lens-induced B-mode fluctuations and then performing lens reconstruction again. This procedure can be repeated until CMB maps cleaned of the lensing signals are produced (See Figure 22).

Delensing in principle can be a perfect procedure: in the limit of no instrumental noise or primordial B modes, the lensing potential and the primordial E-mode map can be perfectly imaged (Hirata/Seljak 2003). However, the finite noise in a CMB-S4 survey will lead to residual lensing B modes which cannot be removed and will act as a noise floor for studying primordial B-modes from tensors. In particular, as shown in Figure 15, it is important to have high-angular resolution maps in order to obtain the small-scale E and B fluctuations needed for the EB quadratic lensing estimator.

Potential systematic biases with the delensing procedure are similar to those for measuring the lensing power spectrum. The impact of polarized dust and polarized synchrotron emission from the Galaxy as well as the

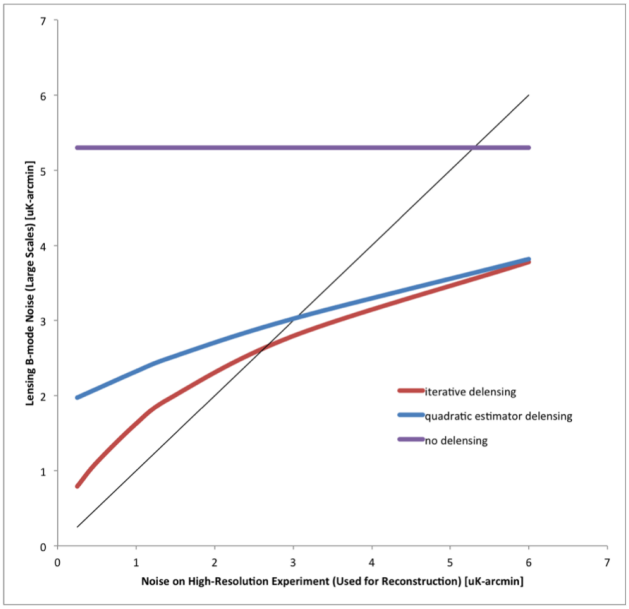

Figure 22. *The B-mode noise on large scales as a function of the noise level used in EB-based lens reconstruction. The purple line is for no delensing and shows that lens-induced E to B mixing manifests as an effective 5 uK-arcmin white noise level. The blue curve shows the improvement possible when using a lens reconstruction to remove this source of effective noise. The red curve shows further improvement when the delensing is performed in an iterative fashion.*

impact of polarized extragalactic emission on the reconstructed lensing field are discussed in Section 5.5.1 as well as ways to mitigate them.

Additionally, rather than using an estimate of the CMB lensing field obtained internally from the CMB itself, it is also possible to use other tracers of large-scale structure which are correlated with CMB lensing (Smith+ 2010). In particular the dusty, star-forming galaxies that comprise the cosmic infrared background (CIB) are strongly correlated with CMB lensing due to their redshift distribution which peaks near $z \sim 2$ (Sherwin+ 2014; Simard+ 2014). The level of correlation can be as high as 80% (Planck 2013 XVIII) and can in principle be improved using multifrequency maps of the CIB which select different emission redshifts (Sherwin+ 2014). However, as shown in (Smith+2010), the gain from delensing with external galaxy tracers is modest, and delensing internally with CMB maps holds far more promise.

5.5 Systematic Effects and Mitigation

The quadratic estimators used for lens reconstruction search for departures from statistical isotropy. The lens effect locally changes the CMB power spectrum via shear and dilation effects (e.g. Bucher+2011). Other sources of deviation from statistical isotropy can thus be confused with lensing effects; these can be of both instrumental and astrophysical origin.

5.5.1 Astrophysical Systematics

Extragalactic sources and tSZ clusters in temperature maps can be troublesome for lensing estimates in two ways: they tend to cluster more strongly in overdense regions (i.e, are non-Gaussian), an effect which lensing estimators can mistakenly attribute to lensing, while individual sources show up as strong local deviations from statistical isotropy.

Planck (2013) removed the effect of Poisson sources in the CMB four-point function from their lensing autospectrum which left untreated would have shifted their measured lensing power spectrum amplitude by 4%, a 1σ shift. For an experiment with lower map noise level and smaller beam, such as CMB-S4, sources can be found and removed to much fainter flux thresholds, making this a much smaller effect. The largest sources of bias thus come from the three-point and four-point correlation functions of the non-Gaussian clustering of sources and non-Gaussian clustering between the sources and the lensing field. These biases can be as large as several percent (van Engelen+2013, Osborne+2013) and their amplitude is highly model-dependent in temperature-based CMB lensing estimates. However, the extragalactic sources and tSZ clusters that can cause large sources of bias in temperature-based CMB lensing estimates are expected to be nearly unpolarized and therefore not a concern for polarization-based lensing estimates. In addition, sensitive multi-frequency temperature measurements should be able to spectrally remove these foregrounds through their unique frequency signatures. In addition, a robust campaign to measure these non-Gaussianities in the CMB data should allow a careful empirical understanding of these effects, an approach known as "bias-hardening" (Osborne+ 2013).

Galactic dust is likely to be the largest source of contamination for polarization-based lensing estimates, but the dominant signal there is on large scales. Higher-frequency polarized data (such as Planck 353 GHz) should give a good template for this spurious signal.

5.5.2 Instrumental and Modeling Systematics

Given the unprecedented precision targeted by CMB-S4 lensing measurements, the effects of instrumental systematic errors must be investigated and well-controlled. Since lensing results in a remapping or distortion of the sky, beam systematics are a particular concern.

The main beam systematics that affect CMB measurements are commonly described by differential gain, differential beamwidth, differential ellipticity, as well as differential pointing and rotation. In Smith et al. 2003, the impact of all these beam systematics on lensing measurements and hence on r and $\sum m_\nu$ was investigated using a Fisher matrix formalism. It was found that for an S4-type experiment, with 1μK-arcmin noise and a ~ 3 arcmin beam, the beam characterization from planets or other point sources will be sufficiently accurate that the biases arising from differential gain, differential beamwidth and differential ellipticity are less than one tenth of the one-sigma error on key parameters. Differential pointing and rotation must be controlled to within 0.02 arcmin and 0.02 degrees respectively in order to be similarly negligible.

While ideally the instrument can be designed or shown using measurements to have systematic errors that are negligible, one can also estimate residual beam systematics directly from the data, in a manner analogous to bias hardening. Many beam systematics result in a known mode-coupling (Yadav/Su/Zaldarriaga); their levels can hence be estimated by quadratic estimators and projected out, though complications due to the scan strategy must be accounted for. This method of beam-hardening was first demonstrated in (Planck 2013).

Another challenge in making high precision lensing power spectrum measurements is, given a set of cosmological parameters, predicting the actual observed lensing power spectrum. One example for such a challenge is the presence of higher-order biases, which have been previously neglected. For instance, often the Gaussianity of the lensing potential is assumed; however, if the full large scale structure non-linearity is taken into account, biases result that can affect measurements at the one-sigma level over many bandpowers. Another such challenge is that the lensing power spectrum itself may not be exactly known, due to astrophysical or baryonic effects which modify the mass distribution. While this is a challenge for optical weak lensing measurements, investigations with simulations have found that such baryonic effects can be neglected for CMB lensing, at least at the precision achievable by CMB-S4 (cite paper incl. Battaglia).

5.6 Parameter Forecasts with Lensing

Since CMB lensing is a sensitive probe of the matter power spectrum, CMB lensing measurements added to measurements of the primordial CMB power spectrum serve to significantly tighten parameter constraints. In particular, measurements of the CMB lensing autospectrum yield tight constraints on the sum of the masses of the neutrinos ($\sum m_\nu$). Cross correlations of CMB lensing maps with maps of galaxy density and galaxy shear can provide tight constraints on the dark energy equation of state (w) and modified gravity. Delensing B-mode polarization maps can also give strong constraints on the tensor-to-scalar ratio (r) from inflationary primordial gravity waves, as well as tighten constraints on the number of neutrino species ($N_{\rm eff}$).

Below we forecast these parameter constraints including CMB lensing or delensing. [Just did neutrino mass so far. Other parameters in progress. Adding cross with LSST shear also in progress.] Table 5-1 shows the expected error on the neutrino mass with just the primordial CMB alone and after including CMB lensing. We also show how Baryon Acoustic Oscillation (BAO) measurements from DESI tighten neutrino mass constraints further.

Table 5-1. *Constraints on neutrino mass from CMB-S4 primodial CMB measurements plus CMB lensing and BAO measurements from DESI. Inputs to these forecasts are discussed in Section 5.6. These constraints are robust to modest variations in instrument resolution and sensitivity.*

$\sigma(\sum m_\nu)$ meV	**S4 Primordial**	**S4 Primordial +Lens**	**S4 Primordial +Lens+DESI**
1' , 1μK'	324	55	18
3' , 1μK'	336	56	19
1' , 5μK'	378	60	20
3' , 5μK'	395	61	20

The assumptions input into these forecasts are that we assume no foregrounds and only white instrumental noise. Removing foregrounds will inflate the errorbars by XX [work in progress to calculate] . Since most of the lensing signal-to-noise is coming from the EB lensing estimator (see Figure 16), white noise may be a reasonable assumption if leakage of atmospheric noise in temperature maps into polarization maps can be prevented via a half-wave plate or some alternative. We also assume CMB-S4 will observe 40% of the sky, and we include Planck primordial CMB data in the non-overlapping region of the sky ($65\% - 40\% = 25\%$ of sky). For both CMB-S4 and Planck, we use temperature modes between $l = 50 - 3000$, and polarization modes between $l = 50 - 5000$. We also include Planck low-ell data between modes $l = 2 - 50$. Given that there is covariance between the CMB power spectrum (2-point function) and the CMB lensing power spectrum (4-point function) because lensing induces peak-smearing in the former, we forecast Table I assuming unlensed

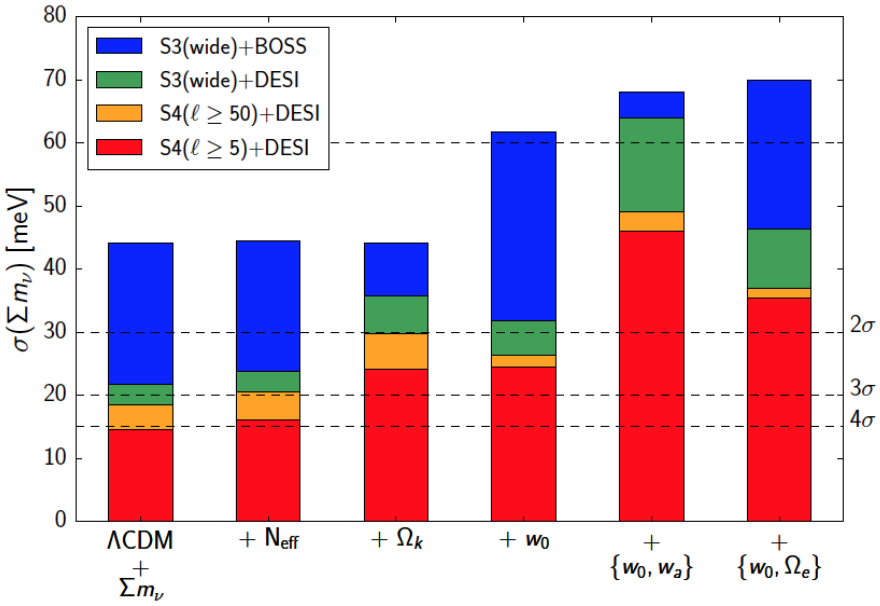

Figure 23. *Constraints on total neutrino mass from various CMB surveys and with and without large-scale structure data included. In the minimal seven-parameter model (left bar) with all data included (red), the minimal neutrino mass of 60 meV can be detected at 4σ; the plot shows how this number degrades when including less data or when freeing up additional cosmological parameters. Figure from Allison et al 2015.*

CMB power spectra plus the CMB lensing 4-point function. [Note: work to include covariance between 2-point and 4-point is in progress. We also did not include iterative lensing here yet - in progress.]

In Table 5-1, we see that 1-sigma errors on the sum of the neutrino masses of 60 meV is possible combing CMB-S4 lensing measurements with measurements of the primordial CMB from CMB-S4 and Planck. Table 5-1 also shows the large improvement in neutrino mass constraint that CMB lensing measurements offer. When BAO data from DESI is added to this, neutrino mass errors of about 20 meV are achievable, which would yield a 4-sigma detection of the neutrino mass sum in the minimal mass scenario (also see Figure 23).

We also vary the resoltuion and sensitivity of CMB-S4 and explore the impact on neutrino mass constraints. We find that, given the assumptions above, the neutrino mass constraints are robust to modest variation in resolution (between 1 and 3 arcmin) and sensitivity (between 1uK-arcmin to 5uK-arcmin in temperature). However, we point out that a higher-resolution of 1 arcmin, as opposed to 3 arcmin, would make high-ell foreground removal more effective. High resolution on the scale of an arcminute is also critical for CMB halo lensing science as discussed in Section 5.3.3. Additionally, increased sensitivity gives more weight to the EB lensing estimator (see Figure 16), which is relatively free from foreground systematics and atmospheric noise.

6

Simulations and Data Analysis

(send any feedback on this chapter to tcrawfor@kicp.uchicago.edu and jdborrill@lbl.gov)

6.1 Introduction

Extracting science from a CMB dataset is a complex, iterative process requiring expertise in both physical and computational sciences. In this chapter we start with an overview of the data analysis pipeline before diving more deeply into its subsets - time-orderd data processing, component separation and the estimation of statistics and parameters. We then discuss the drivers for, and corresponding structure of, the simulation pipeline, and describe in detail its sky modeling and data simulation subsets. Finally we assemble the full simulation and data analysis pipeline, noting its inherently iterative structure, and discuss its critical uses in forecasting and validation and verification, before concluding with a discussion of some key implementation issues. Throughout our goal is to describe the current state of the art, note the particular challenges posed by CMB-S4, and describe how they might be addressed.

6.2 Data Analysis Overview

The reduction of a CMB data set typically proceeds in a sequence of steps:

Pre-processing: The raw time-ordered detector data are calibrated and gross time-domain systematics are either removed (typically by template subtraction, filtering or marginalization) or flagged. The goal here is to make the real data match a model that will underpin all subsequent analyses.

Map-making: At each observing frequency, estimates of the intensity I and the Stokes Q- and U-polarizations of the sky signal are extracted from the cleaned time-ordered data based on their spatial stationarity, typically using some degree of knowledge of the instrument's noise properties.

Component separation: If sufficient frequenciy maps are available, the CMB can be separated from the various foreground sky components based on its unique spectral invariance (in CMB units).

Power spectrum estimation: The six auto- and cross-angular power spectra of the CMB temperature T and E- and B-mode polarizations are estimated from the CMB and/or frequency maps, and corrected for E- to B-mode lensing.

Parameter estimation: The best-fit parameters for any cosmological model are derived by comparing the theoretical TT, TE, EE and BB CMB power spectra that they would induce with the data and their uncertainties.

This reduction essentially consists of a series of changes of basis for the data, from time samples to map pixels to spectral multipoles to cosmological parameters, with each basis-change reducing the data volume, increasing the signal-to-noise, and exposing a different class of systematic effects for mitigation.

Note however that the data can only remain a sufficient statistic at each step in the reduction if we also propagate its full covariance matrix. Since this is an $\mathcal{N}_b \times \mathcal{N}_b$ matrix in the dimension of the basis, its construction, manipulation and reduction pose the greatest computational challenge to this analysis. In particular the full pixel-domain data covariance matrix is generally dense and unstructured, requiring $O(\mathcal{N}_p^3)$ operations to build and $O(\mathcal{N}_p^2)$ bytes to store. All the major drivers of CMB science - polarization sensitivity, higher resolution, larger sky coverage - push us towards larger pixel counts, with an instrument mapping a fraction of the sky f_{sky} with a beam of b arcminutes covering $O(10^9\, f_{sky}/b^2)$ pixels per IQU-component. For the last decade or more the computational intractability of the resulting pixel-domain matrices has forced us to replace explicit covariance propagation with Monte Carlo methods in all but a limited set of small sky fraction/low resolution cases.

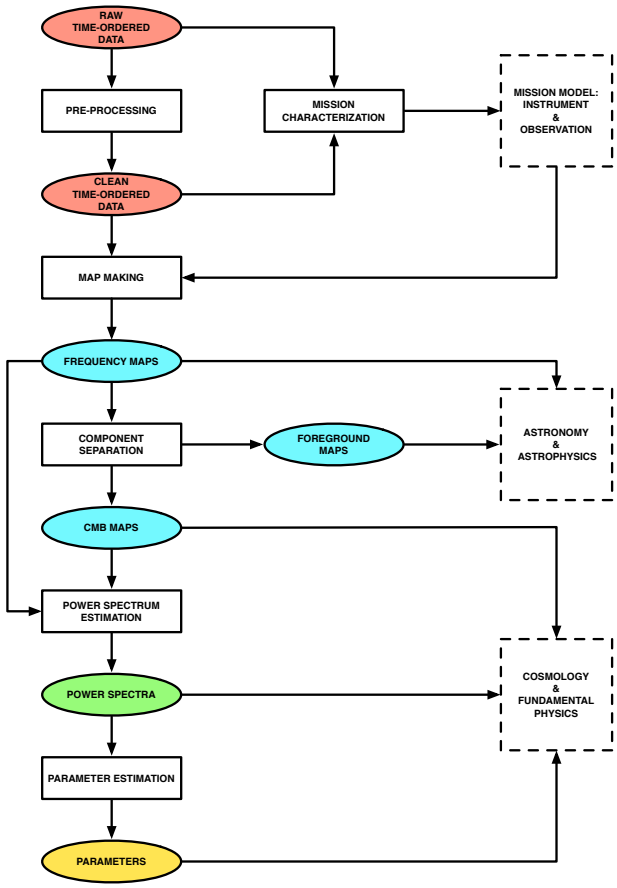

Figure 24. *The CMB data analysis pipeline*

Beyond this basic data reduction, the full analysis pipeline (Figure 24)[1] also includes mission characterization and science exploitation branches. Time domain data are extensively used to build a model of the mission, comprising the instrument and the observation. For the instrument this modeling can include such steps as determining beam profiles and estimating noise properties (including cross-correlations); for the observation, it includes reconstructing the detector pointing and polarization orientation from telescope sensor data, and incorporating atmosphere records in the data-flagging. The resulting mission model then feeds

[1] In all pipeline figures ovals represent data objects in the various domain (red for time, blue for pixel, green for multipole and yellow for parameter) and rectangles represent data processing steps.

back into all of the ensuing data reduction and interpretation. The primary science exploitation derives cosmology and fundamental physics results from the various correlation functions of the CMB maps, from the power spectra's energy scale of inflation and neutrino mass to the higher-order statistics' measures of non-Gaussianity and the lensing potential. In addition the frequency maps represent important astronomical and astrophysical observations, particularly when the frequency sampling is sufficient to isolate individual foreground components along with the CMB.

6.3 Time-Ordered Data Processing

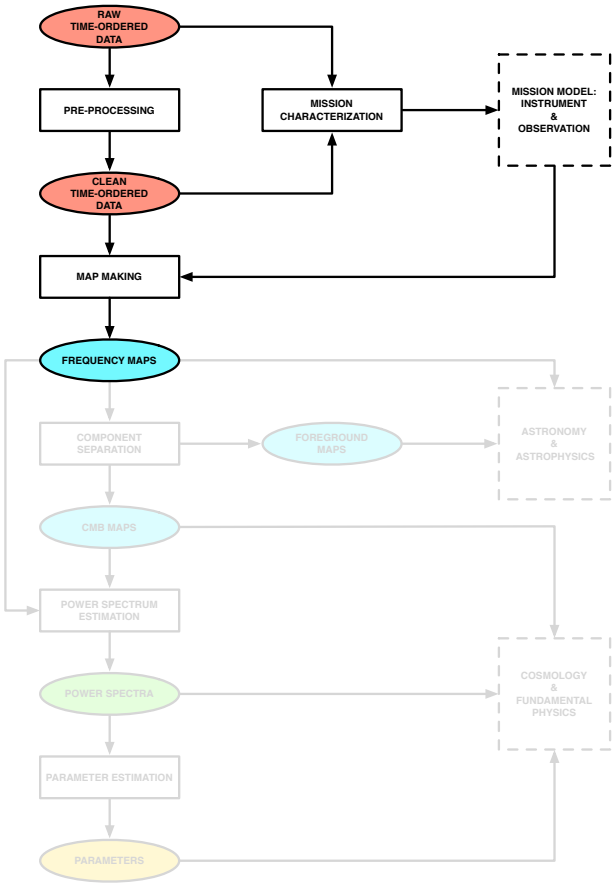

Figure 25. *The time-ordered data processing subset of the CMB data analysis pipeline*

6.3.1 Pre-Processing and Mission Characterization

systematics mitigation: filtering, template-subtraction, marginalization

mission model building: pointing reconstruction, beam measurement, bandpass mismatch, noise estimation, systematics

6.3.2 Map-Making

Map-making is the stage of the analysis when the major compression of the time-ordered data happens and some estimate of the sky signal is produced at each observing frequency. It is usually a linear operation,

characterized by some operator, $\mathbf{L}$, which transforms the input time-ordered data, $\mathbf{d}$, into a pixel domain map, $\mathbf{m}$, e.g., [362],

$$\mathbf{m} = \mathbf{L}\mathbf{d}, \tag{6.1}$$

typically under the condition that the estimator is unbiased over the statistical ensemble of instrumental noise realizations, i.e.,

$$\langle \mathbf{m} - \mathbf{s} \rangle = 0, \tag{6.2}$$

where $\mathbf{s}$ is the underlying pixelized sky signal. Given the usual model for the time-ordered data as the sum of sky-synchonous signal and time-varying noise,

$$\mathbf{d} = \mathbf{A}\mathbf{s} + \mathbf{n}, \tag{6.3}$$

for a pointing matrix $\mathbf{A}$, this condition leads to,

$$\langle \mathbf{m} - \mathbf{s} \rangle = (\mathbf{L}\mathbf{A} - \mathbf{1})\mathbf{s} + \langle \mathbf{n} \rangle = (\mathbf{L}\mathbf{A} - \mathbf{1})\mathbf{s}, \tag{6.4}$$

as the average noise is assumed to vanish. Hence,

$$\mathbf{L}\mathbf{A} = \mathbf{1}, \tag{6.5}$$

which is solved by,

$$\mathbf{L} = (\mathbf{A}^{\mathrm{T}}\mathbf{W}\mathbf{A})^{-1}\mathbf{A}^{\mathrm{T}}\mathbf{W}. \tag{6.6}$$

Here the matrix $\mathbf{W}$ is an arbitrary positive definite weight matrix, and different choices of $\mathbf{W}$ lead to different estimates of the sky signal.

- If $\mathbf{W}$ is taken to be the inverse of the time-domain noise covariance, i.e., $\mathbf{W} = \mathbf{N}^{-1}$, then the sky signal estimate, $\mathbf{m}$, will correspond to the **maximum likelihood** and **minimum variance** solution.
- If $\mathbf{W}$ is taken to be proportional to some diagonal matrix minus some low-rank correction, i.e. $\mathbf{W} \propto \mathbf{1} - \mathbf{T}\mathbf{T}^{\mathrm{T}}$, with $\mathbf{T}$ assumed to be column-orthogonal, then the modes defined by its columns are marginalized over, effectively removing them from the solution. This approach includes as a special case so-called **destriping** map-making, e.g., [322, 224], which has gained recognition thanks to its successful applications to the Planck data, e.g., [223, 366, 319, 314], and is therefore of potential interest to any experiments aiming to cover a large fraction of the sky. More generally, however $\mathbf{T}$ can be constructed to remove any unwanted modes present in the time domain data, e.g., [357, 93, 139].
- If $\mathbf{W}$ is taken to be diagonal, then the map-making solution corresponds to **binning**, i.e. the weighted co-addition of the samples falling within each pixel.

If the instrument beams display complex, non-axially symmetric structure, the proper estimation of the sky signal may require correcting for their effects at the map level, leading to the so-called **deconvolution** map-making [32, 188, 225]. However, further work is needed to demonstrate the effectiveness of such an approach in general.

If map-making is used primarily as a data compression operation on the way to deriving constraints on the statistical properties of the sky signal (such as its power spectra), one may choose to relax the condition in Eq. (6.2) in favor of the more computationally tractable, albeit potentially biased, sky estimate,

$$\mathbf{m} = (\mathbf{A}^{\mathrm{T}}\mathrm{diag}(\mathbf{W})\mathbf{A})^{-1}\mathbf{A}^{\mathrm{T}}\mathbf{W}\mathbf{d}, \tag{6.7}$$

where diag($\mathbf{W}$) denotes the diagonal part of $\mathbf{W}$. In this approach any bias is then corrected at the next level of the data processing, e.g., [198]. This approach has been proven to be very effective, at least in the context of experiments with small sky coverage, e.g., [119, 338, 364, 64].

Formally the linearity of the mapmaking operation permits the propagation of the uncertainty due to the instrumental noise from time- to pixel-domain as

$$\hat{\mathbf{N}} = \mathbf{L}\mathbf{N}\mathbf{L}^{\mathrm{T}}, \tag{6.8}$$

which leads to a particularly simple expression for maximum likelihood estimators

$$\hat{\mathbf{N}} = (\mathbf{A}^{\mathrm{T}}\mathbf{N}^{-1}\mathbf{A})^{-1}. \tag{6.9}$$

However, as noted above, due its size the computational cost involved in computating such pixel-domain noise correlations make them impractical for all but special cases today, and the uncertainty is either carried over to the next stages of the data processing in implicit form or the final uncertainty is estimated using Monte Carlo simulations.

6.4 Component Separation

Authors: Mark Ashdown, Jonathan Aumont, Carlo Baccicalupi, Josquin Errard, Maude Le Jeune

Key challenges:

- validation - are we using the right algorithms for the (as yet unknown) real foregrounds
- verification - are these algorithms right given our (as yet flawed) simulations

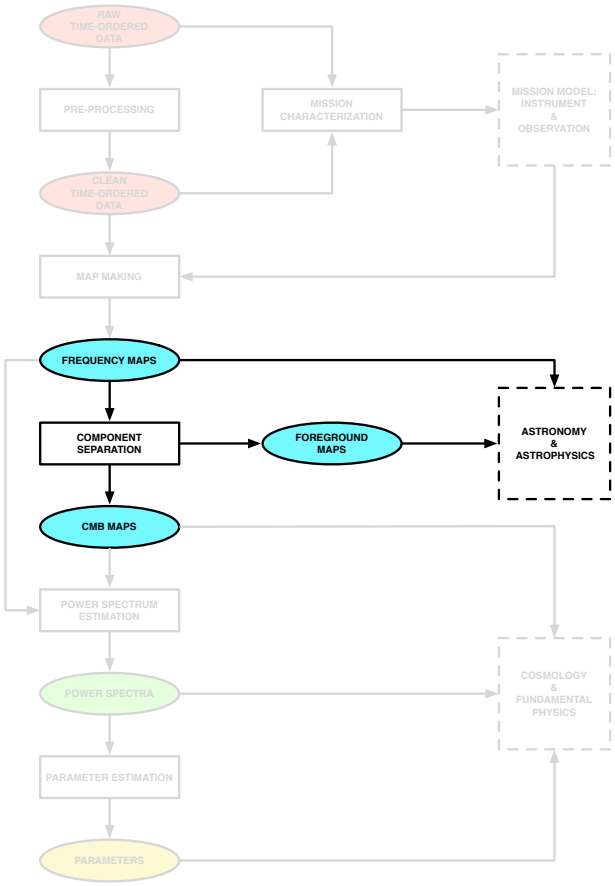

Figure 26. *The component separation subset of the CMB data analysis pipeline*

This section discusses the algorithms and methods for disentangling different sources of sky emission in multi-frequency maps. We first present the motivations and the general ideas of existing approaches. We then give some specifics of parametric and blind methods. Finally, we summarize several questions which might be answered by follow-up studies.

6.4.1 Introduction

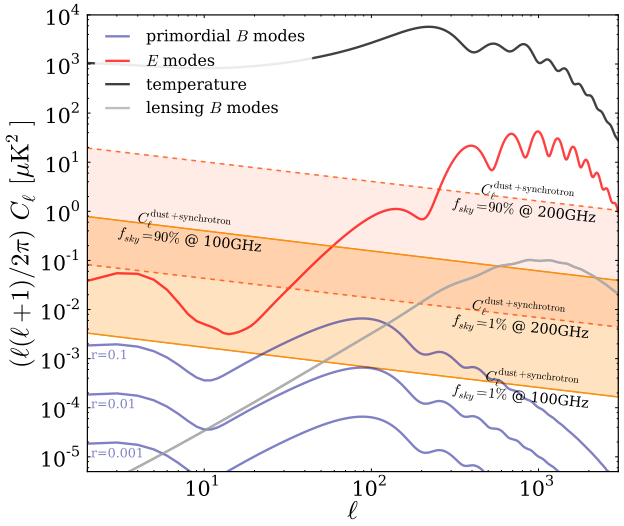

Figure 27. *Angular power spectra showing primordial B modes, lensing B modes, total intensity, and E modes, as well as the total contribution of polarized B-mode foregrounds (dust plus synchrotron), expected on the cleanest* $1-90\%$ *of the sky, at* 100 *and* 200 *GHz. Note that, as these results are derived from Planck data at intermediate and high Galactic latitudes, sensitive primarily to the large scale foreground pattern in polarization and are not therefore optimized for high-resolution, small scale instruments, there is potential for discovery of small patches of sky (e.g.,* $f_{\rm sky} \leq 5\%$*) with a signal differing than those indicated here. From [146].*

6.4.1.1 Motivations

Recent measurements by BICEP2/Keck/Planck [65] confirm that on degree scales, where CMB-S4 is expected to search for the imprint of B modes from primordial GWs, the contamination from polarized foreground emission is comparable to or higher than the cosmological signal at 150 GHz and in one of the cleaner patches of the sky. Given that 150 GHz is expected to be close to the minimum of foreground contamination vs. CMB signal, this is likely to be the case at all frequencies and all but the smallest fractions of the sky. Given the power law behavior in ℓ found on larger scales by Planck and WMAP [313, 302], foregrounds are expected to be even more relevant at larger angular scales. Foregrounds are expected to be subdominant with respect to the B-mode lensing signal on the scale of a few arcminutes (see Figure 27); nevertheless, dust polarization fractions around 10% (comparable to observed levels) have been shown to have non-negligible impact on the 4-point function used for achieving lensing extraction [151]. Therefore, component separation is a necessary and important step in gaining insight into the amplitude of primordial GWs, as well as the neutrino masses and dark energy abundances through CMB lensing studies.

6.4.1.2 Definition of component separation

Broadly defined, the process of component separation would generally

- include any data processing that characterizes and exploits correlations between observations at multiple frequencies
- use external constraints and physical modeling
- aim at distinguishing between different physical sources of emission.

The general data modeling reads

$$d_p = \sum_{\mathrm{comp,p}} a_p^{\mathrm{comp}} s_p^{\mathrm{comp}} + n_p \equiv \mathbf{A}\, s_p + n_p \tag{6.10}$$

where the vector d_p contains the measured signal in each observing band, $\mathbf{A}$ is the so-called mixing matrix which encapsulates the emission law a_p^{comp} of each component, s_p is a vector containing the unknown CMB and foregrounds amplitude and n_p is a vector containing the noise level at each observing band. The index p refers to sky pixels (θ, ϕ), or modes of a spherical harmonic decomposition (ℓ, m), or a set of Fourier modes (k_x, k_y), etc. Note that this modeling assumes spatial templates s_p that are the same in all observing bands.

Component separation aims at inverting Eq. 6.10, to estimate the foregrounds-disentangled CMB signal encapsulated in s_p, as well as the foreground templates which are relevant for testing and updating our knowledge of astrophysical processes (and hence improve the sky model), as illustrated in Fig. 26. The estimate $\tilde{s}_p$ of the true sky templates s_p — given $\mathbf{A}$, d_p and the statistical properties of the noise — minimizes the following χ^2:

$$\chi^2 \equiv \sum_p |s_p - \tilde{s}_p|^2 \tag{6.11}$$

and can be taken to have the following general form

$$\tilde{s}_p = \mathbf{W}\, d_p \tag{6.12}$$

where the weighting operator $\mathbf{W}$ is chosen to optimize some criterion regarding $\tilde{s}_p$ and s_p (variance of the cleaned map, unbiasedness, etc.) while keeping statistical consistency and robustness. In particular, a common requirement for all component separation algorithms is the ability of propagating errors due to foreground subtraction, while having the flexibility of including foreground modeling and external constraints in a transparent way.
Component separation is then defined as a method of estimating the mixing matrix $\mathbf{A}$ and finding the weighting $\mathbf{W}$ that provides closest possible estimate $\tilde{s}_p$ to the true sky signal.

For example, a solution to Eqs. 6.11 and 6.12 is obtained by taking $\mathbf{W} \equiv \left(\mathbf{A}^T \mathbf{N}^{-1} \mathbf{A}\right)^{-1} \mathbf{A}^T \mathbf{N}^{-1}$ with $\mathbf{N} \equiv \langle n_p^T n_p \rangle$, leading to an unbiased estimate of the sky. As mentioned below, this expression can be changed (see, e.g., [130]), depending on the desired level of generality and complexity and on the level of prior knowledge of the sky signal.

Studies have demonstrated the applicability of classes of component separation algorithms to certain simulated multi-frequency datasets, either balloon-borne or ground-based, and targeting limited frequency ranges and sky areas [356, 152, 151]. Results indicate that generally, for a frequency range extending from 90 to 250 GHz, polarized foregrounds may be removed effectively through a multi-frequency combination, at the price of enhancing the white noise contribution due to channel mixing; moreover, a possible bias may be introduced if, at the lowest frequency interval edge, the synchrotron component is not negligible: lower frequency templates/data are required to avoid such a contribution [148]. The most comprehensive application of component separation to data, in terms of completeness of algorithms and frequency range, is represented by Planck [313], although the targeted CMB components in that analysis (total intensity and E-mode polarization) are not the same as in the CMB-S4 case.

6.4.2 Description of methods

The CMB extraction may be achieved essentially through two basic concepts: the fitting of foreground unknowns along with CMB, or the minimization of the variance of a linear combination of the data, constrained to have the frequency scaling of a black body. The first class of algorithms, known as "parametric", makes the maximum use of prior knowledge of foreground emission. By contrast, the second class, known as "blind", makes the minimum set of assumptions. These two broad classes and other possibilities are discussed in turn below.

- **Parametric** – The overall idea of these methods boils down to two steps: 1) the estimation of the mixing matrix, $\mathbf{A}$; and 2) the inversion of Eq. 6.10 to recover an estimate of the sky signal, s_p. Parametric methods assumes that the mixing matrix, used in Eq. 6.10, has a functional form which is known and which can be parametrized by so-called "spectral" parameters β, i.e. $\mathbf{A} = \mathbf{A}(\beta)$. The functional form of $\mathbf{A}$ being fixed, the estimation of the mixing matrix is therefore equivalent to an estimation of the parameters β. The parameters of the model are determined via a fitting procedure, often performed over sky pixels. This can be achieved by maximizing the following so-called "spectral" likelihood [83, 144]:

$$-2\log\mathcal{L}(\beta) = -\sum_p \left(\mathbf{A}^T\mathbf{N}^{-1}d\right)^T \left(\mathbf{A}^T\mathbf{N}^{-1}\mathbf{A}\right)^{-1} \left(\mathbf{A}^T\mathbf{N}^{-1}d\right). \tag{6.13}$$

  Any deviation between the true mixing matrix $\mathbf{A}$ and the estimated $\tilde{\mathbf{A}} \equiv A(\tilde{\beta})$ leads to the presence of foreground residuals in the reconstructed component maps.

- **Blind** – By assuming that sky components are statistically independent, blind methods aim at recovering these with an a priori unknown mixing matrix. Blind methods make minimal assumptions about the foregrounds and focus on the CMB reconstruction from its well known black body spectral energy distribution. The Internal Linear Combination (ILC, [363]) belongs to this class of methods. It only uses the CMB column of the mixing matrix elements (noted a hereafter) to perform the minimum variance reconstruction, cf. Eq. 6.12:

$$\tilde{s}_p = \sum_{i=0}^{i=m} w_i d_{p,i} \tag{6.14}$$

  with $\sum_i w_i a_i = 1$, leading to the following solution:

$$w_i = a^T N^{-1}(a^T N^{-1} a)^{-1} \tag{6.15}$$

  In this scheme, no attempt is made to design a foreground model. The decorrelation property between CMB and foregrounds alone is used to project out the contamination into a m-1 subspace (with m being the number of frequency maps).

  The main caveat in this method is its well known bias ([194, 130], etc) which comes from empirical correlation between the CMB and the foregrounds. The ILC bias is proportional to the number of detectors m and inversely proportional to the number of pixels used to compute N. In order to reduce this effect, one could think of reducing the foreground subspace size by adding further constraints. The SEVEM template fitting method ([273], etc) follows this idea, by building some foreground templates with a combination of a subset of the input frequency maps.

  The semi-blind SMICA method [95] also works at containing the foreground in a smaller dimension space, but in a more general way. The idea of Independent Component Analysis (ICA) is to blindly

recover the full mixing matrix **A** by using the independence property of the different components. As we know that they are spatial correlations between the foregrounds, the ICA principle is used to disentangle the CMB from the noise and the foregrounds taken as a whole.

The main advantage of such blind of semi-blind methods is their ability to face any unknown and/or complex foreground contamination, to reconstruct a clean CMB signal. This is a big advantage when real data comes, one can then focus on instrumental effects, or data set combination issues at first, and leave the complex task of the foreground modeling and reconstruction for a future analysis step.

Moreover, in a framework like SMICA, the level of blindness can be adjusted via the plugin of any parametric component to its flexible engine as described in [95], allowing for a step by step fine grain design of the foreground model.

- **Template fitting** – In this variant, emission laws are not modeled, and the analysis is reduced to the maximisation of a likelihood over the CMB contribution and the amplitudes of each foreground component (see, e.g., [222]).

For all of the approaches discussed above, Eq. 6.12 can be implemented equivalently with any representations of the map—i.e. pixel, harmonic, wavelet, etc. The resulting component separation is independent of this choice as long as the linear data modeling (Eq. 6.10) holds. This complementarity, and the internal comparison of results through these pipelines has been proven to be relevant in actual analysis of Planck data [313]. That said, the difference between domain of application will lie in the computational needs: for high number of sky pixels, the implementation of Eq. 6.12 might be significantly more efficient in harmonic space.

6.4.3 Questions to be addressed during follow-up studies

- **E/B or Q/U basis of analysis** – Component separation between CMB radiation and its foregrounds can be performed either dealing with Stokes parameters Q and U maps of the sky in real space or Fourier space, and either before or after the separation between the E and B modes. Several approaches have been followed by CMB experiments so far [176, 320, 65], and each of them has some advantages and some caveats. For example, processing Q/U data in the map domain simplifies the treatment of foreground components that have non-Gaussian and/or non-stationary spatial distributions. However, in the Q and U basis, the CMB E and B modes are mixed and the CMB E modes will be the dominant contribution to the variance at intermediate and small scales in the CMB observing frequencies, limiting the accuracy of the separation. To overcome this limitation, E and B observables can be constructed in Fourier space. The separation of the B-mode components (primordial CMB, Galactic foregrounds, lensing, etc.) can then be done in the angular power spectrum domain (where the final accuracy might be limited by the cosmic variance associated to foregrounds), in the two-dimensional, phase-full Fourier domain (where the treatment of non-stationary components will be complicated) or in the map domain (where the final accuracy might be limited by ringing of the foregrounds due to the non-local transformation). While for Q and U the problem we face is analogous in terms of foreground vs CMB balance, for E and B that is not: E is more similar to Q and U, but in the B channel separation is more challenging. We have the capability and will analyze in both domains, to validate and cross-check the stability of the mixing matrix recovery. Although these different approaches are currently giving satisfactory results on simulated data, these effects will become crucial at the sensitivity of CMB-S4 and merit a dedicated study.

- **Combining data from multiple instruments** – Ground-based instruments heavily filter time streams because of atmosphere contamination, ground emission, etc to perform projections on the sky. In particular, large angular scales are usually suppressed anisotropically, and this suppression is corrected in the power spectrum estimate. In order to perform component separation using various observations, component separation methods will require the use of maps derived from common filters. As stressed already, in recent analysis a first B modes foreground cleaning was implemented in a multi-site fashion, i.e. by combining different probes, i.e. BICEP2, Keck Array and Planck [65]. A template fitting analysis was implemented with the primary objective to minimize the variance in the CMB solution, by achieving a linear combination of the data, which turned out in a reduction of the power observed from the ground, which is interpreted as cleaning of the Galactic dust, and sets the current limit on B modes from primordial GWs. The independent reduction of the data required an additional layer in the analysis, made by the simulated scans of the Planck data through the filtering by the ground observatories, along with validation through simulations of the whole procedure. The necessity for CMB-S4 will be to have a combined data reduction, a single pipeline reducing and combining different datasets. With a common filtering implemented from scratch in a multi-site experiment, the latter a posteriori combination would be built-in, thus avoiding the extra layer and increasing confidence and robustness of results.

- **Various resolutions** – under the approximation that the mixing matrix is not significantly varying under the largest resolution, the impact of various resolutions can be propagated to the noise level of the final CMB map through the CMB x CMB term of $\left(\mathbf{A}^T\mathbf{N}^{-1}\mathbf{A}\right)^{-1}$ as given by Eq. 6.12 with $\mathbf{W} \equiv \left(\mathbf{A}^T\mathbf{N}^{-1}\mathbf{A}\right)^{-1}\mathbf{A}^T\mathbf{N}^{-1}$. Beam for each frequency channel would appear in the expression of the noise covariance matrix

$$\mathbf{N}(i) \equiv \mathbf{N}(i)_\ell = (\sigma_i)^2 \exp\left[\frac{\ell(\ell+1)\theta^2_{\rm FWHM}}{8\log(2)}\right] \tag{6.16}$$

  where i is a frequency channel and σ_i is the noise level in the corresponding map. The noise variance in the reconstructed CMB map, i.e. after component separation, would then be given by

$$N_\ell^{\text{post comp sep}} = \left[\left(\mathbf{A}^T\left(\mathbf{N}_\ell\right)^{-1}\mathbf{A}\right)^{-1}\right]_{\rm CMBxCMB} \tag{6.17}$$

  The effective beam of this noise is degraded compared to a simple quadratically combined noise, but this obviously depends on the involved beams sizes and on the importance of given channels to perform the foregrounds cleaning.

- **Atmosphere residuals** – Atmosphere residuals appear at large scales in ground-based CMB observations, and they scale with frequency in a similar way as dust, $\propto \nu^\beta$ [145]. Having redundant frequencies among the different observatories could help mitigating the atmospheric and astrophysical foregrounds. Furthermore, the small intrinsic polarization of the atmosphere [48, 145] will limit the contamination to component separation of the polarized signals. Still, this effect will have to be investigated quantitatively with realistic simulations.

6.5 Statistics and Parameters

In this section, we discuss the process of going from sky maps at different frequencies—or, in light of the previous section, foreground-cleaned CMB maps and an estimate of foreground residuals—to post-map products such as angular power spectra, estimates of lensing potential ϕ, and finally cosmological parameters, as well as covariance estimates for all of these quantities. We briefly describe the current practice for this process, then we address specific challenges anticipated in the CMB-S4 era.

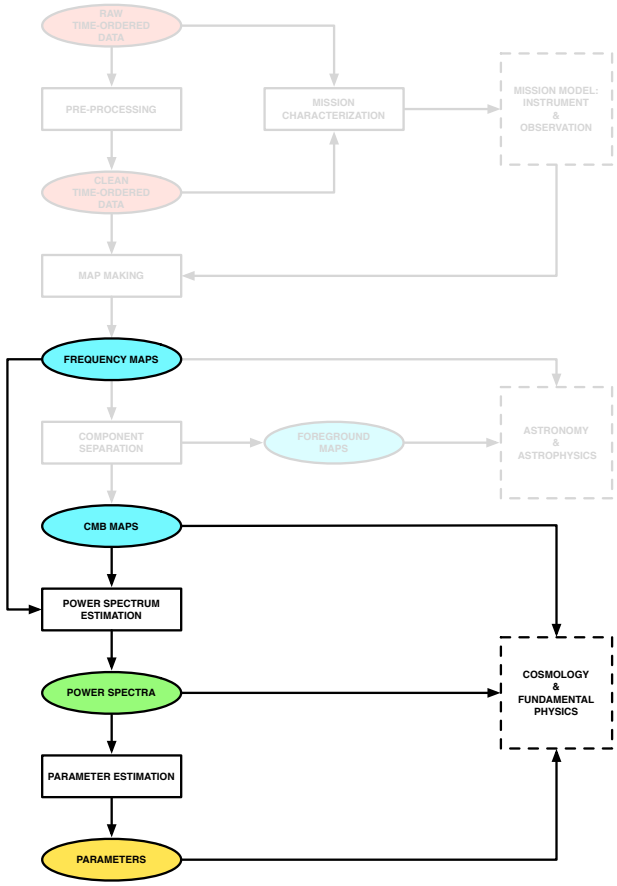

Figure 28. *The statistics and parameters subset of the CMB data analysis pipeline*

6.5.1 Current practice

Early measurements of CMB temperature anisotropy, with comparatively few map pixels or angular modes measured, often used maximum-likelihood methods to produce maps of the sky (e.g., [387]) and either a direct evaluation of the full likelihood or a quadratic approximation to that likelihood to go from maps to angular power spectra (e.g., [75]). With the advent of the WMAP and Planck space missions, which would map the entire sky at sub-degree resolution, it became apparent that computing resources could not compete with the $\mathcal{O}(N^3)$ scaling of the full-likelihood approach (e.g., [78]). The solution for power spectrum analysis

that has been adopted by most current CMB experiments is a Monte-Carlo-based approach advocated in [197]. In this approach, a biased estimate of the angular power spectrum of the data is obtained by simply binning and averaging the square of the spherical harmonic transform of the sky map. That estimate (known as the "pseudo-C_ℓ spectrum") is related to the unbiased estimate that would be obtained in a maximum-likelihood procedure through the combined effect of noise bias, sky windowing, and any filtering applied to the data before or after mapmaking (including the effects of instrument beam and pixelization). These effects are estimated by "observing" and analyzing simulated data and constructing a matrix describing their net influence on simulated data. This matrix is inverted, and the inverse matrix is applied to the pseudo-C_ℓs to produce the final data product. It is expected that some version of this Monte-Carlo treatment will also be adopted for CMB-S4.

Pseudo-C_ℓ methods are also now commonly used in analysis of CMB polarization anisotropy [320, 289, 117]. An added complication in polarization analyses is that pseudo-C_ℓ methods do not cleanly separate E and B modes (e.g., [99]). "Pure" B-mode estimators can be constructed that suppress the spurious B-mode contribution from estimating E and B on a cut sky with pseudo-C_ℓ methods [348]), but other analysis steps (such as particular choices of filtering) can produce spurious B modes that are immune to the pure estimators [226]. These can also be dealt with using Monte-Carlo methods, either by estimating the statistical bias to the final B-mode spectrum or by constructing a matrix representing the effect of any analysis steps on the true sky [64]. The latter approach involves constructing an $N_{\rm pixel}$-by-$N_{\rm pixel}$ matrix, equal in size to the full pixel-pixel covariance, and will not be feasible for high-resolution CMB-S4 data but could be used in analyzing lower-resolution data.

In addition to the two-point function of CMB maps, higher-order statistics of the maps have recently been of great interest to the community. In particular, the four-point function encodes the effect of gravitational lensing, and estimators can be constructed to go from CMB temperature and polarization maps to estimates of CMB lensing ϕ and the associated covariance (e.g., [204, 298]). These quadratic estimators are the first step in an iterative estimation of the true likelihood, and in the weak-lensing limit they are nearly optimal; as a result, they remain the state of the art for estimating the large-scale ϕ from CMB lensing (e.g., [318]). The computational burden involved in this step of the analysis is unlikely to be significantly greater for CMB-S4 than for Planck.

The final step in the analysis of a CMB data set is the estimation of cosmological parameters from the various post-map statistics discussed above. This involves estimating the likelihood of the data given a model parameterized by the standard six ΛCDM parameters, possible extensions of the cosmological model, and any nuisance parameters involving the instrument, foregrounds, and other sources of systematic uncertainty. The current industry standard for this part of the analysis are Monte-Carlo Markov-Chain (MCMC) methods, in particular the implementation in CosmoMC [246], and it is expected that CMB-S4 will use similar methods. There will be several aspects of the CMB-S4 dataset, however, that will necessitate going beyond what past analyses have done at this step. First of all, the data from several different telescopes and cameras will need to be combined in as lossless a fashion as possible—such that combining at the parameters stage may be sub-optimal. Further, as shown by [65], foregrounds cannot be ignored in the estimation of the B-mode power spectrum, even in the cleanest parts of the sky and in the least contaminated observing bands. Foreground modeling will be used to mitigate the contamination, but there will be foreground residuals (both from noise and imperfect modeling), and these need to be properly characterized and accounted for in parameter extraction. Similarly, algorithms to separate the B-mode power spectra from a background of gravitational waves and from lensing of E modes (so-called "de-lensing", see the CMB Lensing chapter for details) will leave an uncertain level of lensing residuals in the primordial B-mode spectrum, and this residual will need to be treated properly. Finally, for information from angular power spectra and lensing potential ϕ to be properly combined, the covariance between the two-point and four-point functions of the CMB needs to be taken into account.

6.5.2 Challenges

As discussed in the previous section, some of the avenues in the analysis that need to be re-addressed for an experiment such as CMB-S4 are:

- The combination of data from different telescopes and cameras (with different heritage and observation/analysis techniques) without significant loss of information.
- The impact of uncertainties in foreground modeling on cosmological parameters, particularly the tensor-to-scalar ratio r.
- The covariance between different observables (i.e., the lensed CMB power spectrum and the reconstructed lensing potential power spectrum)
- The separation of the gravitational lensing signal and the primordial B-mode signal, lowering the effective lensing background (these algorithms are known as "delensing"), the impact of delensing on cosmological parameters.

We treat each of these challenges individually in the sections below.

6.5.2.1 Combining different data sets

At what stage in the analysis does it make the most sense to combine data from different experiments? One possibility is to estimate angular power spectra or even cosmological parameters from every data set individually and combine them at that stage. This would be computationally efficient but sub-optimal from a sensitivity standpoint unless every experiment covered fully independent patches of the sky. For any overlap between data sets, combining at the map or time-ordered data stage (adding before squaring) will lead to lower final uncertainties than combining at the power spectrum stage (squaring before adding). Of course, the earlier in the analysis we choose to combine data, the more work it will be to standardize the data between experiments—the time-ordered data is generally quite instrument-specific, the maps less so, etc. The trade-off between maximizing constraining power and possibly placing undue burdens on the individual experiment pipelines will need to be balanced in answering this question.

6.5.2.2 Foreground-related uncertainty on cosmological parameters

To separate the CMB signal from the contaminating signals of Galactic and extragalactic foregrounds, data from multiple bands will be combined, either in a cross-spectrum analysis or, as detailed in Section 6.4, by making linear combinations of maps in different bands to produce a "pure-CMB" map for power spectrum estimation. In either case, an underlying model of foreground behavior is assumed—even if that model is simply an assumption regarding the level to which the spectral behavior of foregrounds varies over the sky. Any model of foreground behavior is by definition imperfect, and the resulting component separation or frequency-cross-spectrum fit will have leakage between the foreground and CMB components. At the sensitivity levels attainable by CMB-S4, these residuals have the potential to dominate the error budget on cosmological parameters and, more troublingly, to significantly bias the best-fit parameter values if they are not properly taken into account.

Section 6.7 discusses the baseline plan for, and challenges involved in, modeling Galactic and extragalactic foregrounds. It is likely that more information will be needed—from Stage-3 experiments, or from a possible

dedicated, balloon-borne CMB foreground mission—before we can confidently assess the level to which foregrounds will limit the final parameter constraints from CMB-S4 and how flexible we will need to make the underlying foreground models that inform component separation and parameter extraction.

6.5.2.3 CMB lensing covariances for CMB S4

The measured lensing power spectrum is given by a 4-point function of the lensed CMB. This is not statistically independent from the lensed CMB 2-point function, because both depend on the same observed, lensed CMB maps. As a consequence, measured lensing power spectra and lensed CMB power spectra may be correlated. This correlation should be taken into account when combining these measurements to avoid spurious double counting of information. For the specific case of Planck this correlation is negligible [339]. However, the level of correlation depends on experiment specifications and the multipole range where power spectra have high signal-to-noise. The correlation should thus be included in analyses that combine 2- and 4-point measurements unless it is known to be negligible for a specific experiment.

For CMB-S4, the best lensing measurements are expected to come from the auto-power spectrum of EB reconstruction. Its covariance with the lensed EE and BB power spectra depends on six-point functions of the lensed CMB, e.g. $\langle EBEBEE\rangle$. Although many terms contribute, the dominant effect is expected from only a few contributions [339]:

- First, there are signal contributions to the covariance of the form

$$\mathrm{cov}(\hat{C}^{EE}_{l,\mathrm{expt}},\, \hat{C}^{\hat{\phi}_{EB}\hat{\phi}_{EB}}_{L})_{\mathrm{signal}} = \frac{\partial C^{EE}_{l}}{\partial C^{\phi\phi}_{L}} \frac{2}{2L+1} (C^{\phi\phi}_{L})^2, \tag{6.18}$$

$$\mathrm{cov}(\hat{C}^{BB}_{l,\mathrm{expt}},\, \hat{C}^{\hat{\phi}_{EB}\hat{\phi}_{EB}}_{L})_{\mathrm{signal}} = \frac{\partial C^{BB}_{l}}{\partial C^{\phi\phi}_{L}} \frac{2}{2L+1} (C^{\phi\phi}_{L})^2, \tag{6.19}$$

  where $\hat{C}$ are data power spectra, and C_{expt} are power spectra of observed (noisy, beam-deconvolved) CMB fluctuations $X \in \{E, B\}$:

$$\langle \hat{C}^{XX}_{l,\mathrm{expt}} \rangle = C^{XX}_{l,\mathrm{expt}} = C^{XX}_{l} + \left(\frac{\sigma_X}{T_{\mathrm{CMB}}}\right)^2 e^{l(l+1)\sigma^2_{\mathrm{FWHM}}/(8\ln 2)}. \tag{6.20}$$

  The signal covariance in Eqs. (6.18) and (6.19) arises because cosmic variance fluctuations of the true lensing potential (i.e. fluctuations of matter along the line of sight) modify the lensing reconstruction power as well as the lensed EE and BB power spectra. Formally, this follows from the connected part of the lensed CMB 6-point function.

- Second, a noise covariance follows from the disconnected 6-point function,

$$\mathrm{cov}(\hat{C}^{EE}_{l,\mathrm{expt}},\, \hat{C}^{\hat{\phi}_{EB}\hat{\phi}_{EB}}_{L})_{\mathrm{noise}} = \frac{2}{2l+1} (C^{EE}_{l,\mathrm{expt}})^2 \frac{\partial(2\hat{N}^{(0)}_{L})}{\partial \hat{C}^{EE}_{l,\mathrm{expt}}}, \tag{6.21}$$

  and similarly for BB. This noise covariance arises because fluctuations of the CMB and instrumental noise change both the Gaussian reconstruction noise $N^{(0)}$ and the CMB power spectra. It is however cancelled if the Gaussian $N^{(0)}$ reconstruction noise is subtracted in a realization-dependent way [141, 187, 294, 339]

$$\hat{C}^{\hat{\phi}\hat{\phi}}_{L} \to \hat{C}^{\hat{\phi}\hat{\phi}}_{L} - 2\hat{N}^{(0)}_{L} + N^{(0)}_{L}. \tag{6.22}$$

For the specific case of $EBEB$ reconstruction, the realization-dependent $\hat{N}^{(0)}$ is

$$\hat{N}_L^{(0)} = \frac{\left|A_L^{EB}\right|^2}{2L+1} \sum_{l_1,l_2} \left|g_{l_1 l_2}^{EB}(L)\right|^2 \frac{1}{2} \left[\hat{C}_{l_1,\mathrm{expt}}^{EE} C_{l_2,\mathrm{expt}}^{BB} + C_{l_1,\mathrm{expt}}^{EE} \hat{C}_{l_2,\mathrm{expt}}^{BB}\right], \tag{6.23}$$

where A^{EB} is the estimator normalization and g^{EB} is the optimal weight given by [298]

$$g_{l_1 l_2}^{EB}(L) = -i \, \frac{C_{l_1}^{EE} {}_2F_{l_2 L l_1} - C_{l_2}^{BB} {}_2F_{l_1 L l_2}}{C_{l_1,\mathrm{expt}}^{EE} C_{l_2,\mathrm{expt}}^{BB}} \tag{6.24}$$

with lensed spectra in numerator and denominator [247, 187], and

$${}_{\pm s}F_{l_1 L l_2} = [-l_1(l_1+1) + L(L+1) + l_2(l_2+1)] \sqrt{\frac{(2l_1+1)(2L+1)(2l_2+1)}{16\pi}} \begin{pmatrix} l_1 & L & l_2 \\ \pm s & 0 & \mp s \end{pmatrix}. \tag{6.25}$$

In the square brackets in Eq. (6.23) one of the CMB power spectra is replaced by a data power spectrum. On average, $\langle \hat{N}_L^{(0)} \rangle = N_L^{(0)}$. This realization-dependent $\hat{N}^{(0)}$ subtraction also follows more formally from optimal trispectrum estimation (see Appendix B in [339] and Appendix D in [317]).

- A third covariance contribution arises from the connected trispectrum part of the CMB 6-point function. If realization-dependent $\hat{N}^{(0)}$ subtraction is used, the dominant remaining term is expected to be (at leading order in ϕ, see also Eq. (D4) of [339]; similarly for BB)

$$\mathrm{cov}(\hat{C}_{l,\mathrm{expt}}^{EE}, \hat{C}_L^{\hat{\phi}^{EB}\hat{\phi}^{EB}}) = 2 \, \frac{C_L^{\phi\phi}}{A_L^{EB}} \, \frac{\partial(2\hat{N}_L^{(0)})}{\partial \hat{C}_{l,\mathrm{expt}}^{EE}} \, \frac{2}{2l+1} (C_{l,\mathrm{expt}}^{EE})^2. \tag{6.26}$$

Similarly to avoiding the noise covariance with the realization-dependent $\hat{N}^{(0)}$ subtraction, the signal covariance could in principle also be avoided by delensing CMB power spectra with the estimated lensing reconstruction, e.g. by forming [339]

$$\hat{C}_{l,\mathrm{expt}}^{EE} \to \hat{C}_{l,\mathrm{expt}}^{EE} - \sum_L \frac{\partial C_l^{EE}}{\partial C_L^{\phi\phi}} \left(\frac{C_L^{\phi\phi}}{\langle \hat{C}_L^{\hat{\phi}\hat{\phi}} \rangle}\right)^2 (\hat{C}_L^{\hat{\phi}\hat{\phi}} - 2\hat{N}_L^{(0)}), \tag{6.27}$$

or by applying more advanced delensing methods. However this has not yet been tested in practice and makes only sense if lensing reconstructions have sufficient signal-to-noise. In general, forming linear combinations of measured lensing and CMB power spectra as in Eqs. (6.22) and (6.27) does simplify covariances, but it cannot add any new information as long as correct covariances are used.

Since more covariance contributions arise from other couplings of the CMB 6-point function, it should be tested against simulations if the above contributions are sufficient. In practice, it is then favorable to use analytical covariances because they are less noisy than those derived from simulations.

On top of the cross-covariance between 2-point CMB power spectra and 4-point lensing power spectra, both power spectra can also have non-trivial auto-covariances. Covariances between CMB power spectra have been computed in [350, 249, 57]. They contain similar building blocks as the covariances above [57]. Covariances between two 4-point lensing power spectra involve the lensed CMB 8-point function. While many covariance contributions are cancelled when using realization-dependent $\hat{N}^{(0)}$ subtraction [187], other contributions may be relevant for future experiments. Finally, the discussion above applies to the standard quadratic lensing reconstruction estimators and may change for maximum-likelihood lensing estimators [196].

6.5.2.4 Delensing

For noise levels below $\Delta_P \simeq 5\mu$K-arcmin, the dominant source of effective noise in B-mode maps is the fluctuation induced by the lensing of E-modes from recombination. This signal has a well-understood amplitude, and unlike other sources of astrophysical fluctuation in the map, it cannot be removed with multifrequency data. Instead it must be removed using map-level estimates of both the primordial E-mode maps and the CMB lensing potential ϕ.

As discussed in the dedicated CMB lensing chapter, delensing will be a crucial portion of the reconstruction of the CMB lensing field. This is because at low noise levels a quadratic reconstruction of lensing using the EB estimator [207] can be improved upon by cleaning the CMB maps of the lens-induced B-mode fluctuations, and then performing lens reconstruction again. In effect, the quadratic estimate of [207] is effectively the first step in an iterative scheme to find the maximum-likelihood solution for the lensing and primordial fields [196]. CMB maps cleaned of the lensing signals will thus likely be produced as part of the CMB lensing analysis procedure.

The finite noise in the CMB-Stage IV survey will lead to residual lensing B-modes which cannot be removed and will act as a noise floor for studying B modes from tensors. The amplitude of these residual lensed B-modes are discussed in the dedicated lensing chapter as a function of the angular resolution and the noise level of the S4 survey; in particular, it is crucial to have high-angular resolution maps in order to measure the small-scale E- and B-modes fluctuations needed for the EB quadratic lensing estimator.

The concerns with the delensing procedure are similar to those for measuring the lensing power spectrum. The impact of polarized dust and synchrotron emission from the Galaxy, and the impact of polarized point sources on small scales on the lensing reconstruction are addressed in chapter IV. Left untreated the effects may be large; however the use of multi-frequency data together with the application of dedicated point-source estimators can mitigate these effects.

Additionally, rather than using an estimate of the CMB lensing field obtained from the CMB itself, it is also possible to use other tracers of large-scale structure which are correlated with CMB lensing [349]. In particular the dusty, star-forming galaxies that comprise the cosmic infrared background (CIB) are strongly correlated with CMB lensing, due to their redshift distribution which peaks near $z \sim 2$ [345, 347]. The level of correlation is approximately 80% [318] and can in principle be improved using multifrequency maps of the CIB which select different emission redshifts [345].

Delensing can also impact the measurement of features of the CMB spectrum on small scales, in particular the CMB damping scale and the precise location of the acoustic peaks in harmonic space. Effects that can change these observables include changes in the effective number of neutrino species, the primordial helium fraction, and running of the spectral index of fluctuations. Using completely unlensed CMB spectra, rather than lensed spectra, can improve constraints on these parameters [50]. While the delensing procedure will not completely recover the unlensed CMB fluctuations for the S4 experiment, the low noise levels will enable the primordial CMB fluctuations to be measured with good enough fidelity that delensing should have a non-negligible impact on these parameter constraints.

6.6 Simulation Overview

Simulations of a CMB mission's data play a number of critical roles; specifically they are required for

- Forecasting: informing the design and development of a mission to ensure that it is capable of meeting its science goals.
- Validation and verification: ensuring that all of our data analysis tools meet their requirements and specifications.
- Uncertainty quantification and debiasing: providing an alternative to the full data covariance matrix when this is computationally intractable.

As shown in Figure 29, given a mission model (both instrument and observation) and a sky model (both CMB and extra-galactic and galactic foregrounds) we can generate a simulation of the mission data in any of its domains. However, there is an inevitable trade-off between how representative the simulation is of real data and the complexity of the input models and computational cost of generating the simulation. The choice of the simulation data domain will then be determined by the balance between the realism requirements and the complexity/cost constraints for the particular task at hand.

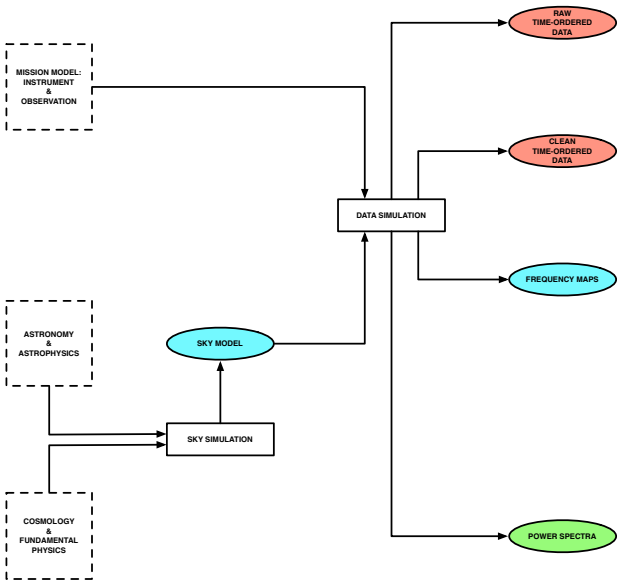

Figure 29. *The CMB simulation pipeline*

The generation of the input mission and sky models are themselves far from trivial tasks. The mission model is typically derived from pre-deployment measurements of the instrument properties refined by characterization from the data themselves, together with ancilliary telescope and environmental data characterizing the observation; the sky model requires its own dedicated simulation capability which - since it is independent of the details of any single mission - can be a community-wide endeavor.

6.7 Sky Modeling

The capability of CMB-S4 to address its science program crucially depends on the possibility to separate the signals of interest from astrophysical emission originating from various astrophysical processes, and on the accuracy of the characterization of foreground residuals after such cleaning is performed.

The polarised CMB is mostly contaminated by diffuse emission from the interstellar medium of our own Milky Way. Both synchrotron and thermal dust are highly polarised (at the level of tens of per cents, depending on the observed region). Their integrated emission dominates over both the CMB E-modes and the CMB B-modes on large angular scales, and cannot be safely neglected at scales where B-modes from gravitational lensing dominate without robust analyses of their impact on lensing science. Other components, such as spinning dust, free-free emission, emission of molecular lines such as CO, could in principle be polarized at a lower level, of order 1-2 per cent or less, but measurements or upper limits are scarce, and not sufficient at this stage for robust predictions of the polarized amplitude of their emission over large patches of sky. For low angular resolution observations, the presence of polarized extragalactic radio and infrared sources constitutes an additional source of contamination, which must be removed with a combination of masking or subtracting individual sources, and modeling residuals at the power-spectrum level.

Massive galaxy clusters are easily detected in atmospheric windows below 217 GHz (and in particular around 150 GHz) as decrements in high angular resolution maps of total sky emission fluctuations. The detection of low-mass, distant galaxy clusters, however, will suffer from confusion with fluctuations of the CIB emission (which can be locally positive or negative), and from contamination by radio and infrared sources in the cluster halos. Accurate determination of the clusters' profiles, of their integrated Compton parameter Y that serves as a mass-proxy for cosmological constraints, and of cluster peculiar velocities along the line of sight via the kinematic SZ effect, will require sufficient frequency coverage at high angular resolution (of order 1-2$'$) to separate the various SZ components (thermal SZ, relativistic corrections, and kinematic SZ) as well as sources of astrophysical confusion. In particular, it is plausible that high angular resolution observations of the positive side of the SZ effect (at frequencies above 217 GHz) will be required to fully exploit the sensitivity of CMB-S4 for galaxy cluster science.

More precise estimations of the impact of foreground emission on these main science targets of CMB-S4 hence require realistic simulations of the sky emission, that can be used to investigate the effectiveness of component separation techniques and assess the impact of residual contamination from foregrounds on the main scientific products (degradation of the error bars and possible biases). The place of such modelling in the CMB simulation and data analysis pipeline is shown in Figure 30.

A sky model is useful only as far as it captures adequately the characteristics of real sources of sky emission that play an essential role in the performance of cleaning techniques and on the amplitude and statistical properties of residual contamination after such cleaning is performed. The key characteristics of sky emission for foreground cleaning are:

- The coherence and decoherence of diffuse emission across observed frequencies, which is key to identifying foreground emission in the form of patterns that scale with an emission law different from that of the CMB;
- The existence or not of a simple parametric emission law for each component emission, such as power laws (for synchrotron) or modified blackbody emission (for dust components);
- The absolute level of foreground emission (in particular for those components that do not scale simply as a function of frequency, such as the superposition of many individual sources with a specific emission law each);

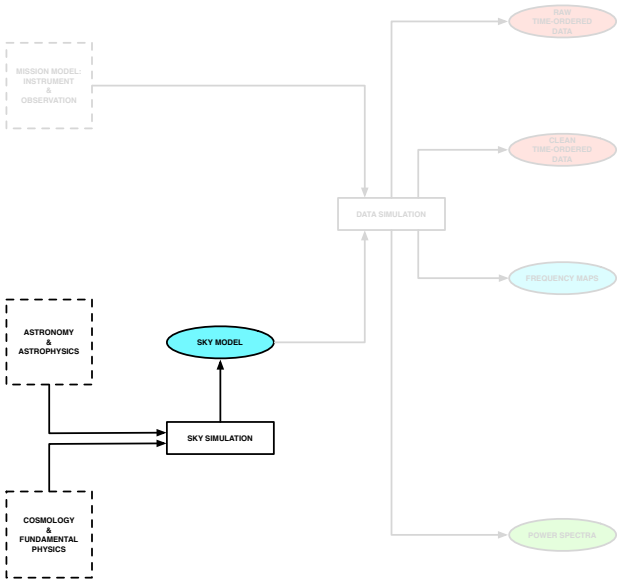

Figure 30. *The sky modeling subset of the CMB simulation pipeline*

- Whether or not emissions for which the level of polarization is unknown or unclear (including possible surprises) are above the sensitivity objectives of CMB-S4, or can be safely neglected;
- The self-consistency of extragalactic emission (in particular CIB and SZ clusters) and CMB lensing. In particular, CIB as observed by Planck and by future instruments can be used to generate a proxy for the lensing potential, which can be used to partially de-lens the CMB B-modes.

The key challenges for a usable sky model are hence:

- The reliability of models based on observations at angular resolution lower than that of CMB-S4, integrated in broad frequency bands, and with a sensitivity limit at least an order of magnitude worse than what will be achieved with CMB-S4; the complexity of sky emission below current sensitivity limits must be extrapolated on the basis of existing knowledge and theoretical models, taking into account past experience when orders of magnitude in sensitivity were gained;
- The self-consistency of CMB secondary anisotropies (lensing, SZ emission from hot intra-cluster gaz and filaments, late ISW) and extra-Galactic foregrounds (CIB, radio and infrared sources) is crucial to both de-lensing, and to extragalactic science; generating reliable models over the entire Hubble volume is challenging, the evaluation of errors of such models even more so;
- The practical usability of the model (software engineering aspects for generating many simulations).

6.7.1 The sky modeling pipeline

The emission of the sky will be modeled as the sum of emission of different components, identified either by their emission process (e.g. Galactic synchrotron, due to electrons spiralling in the Galactic magnetic field), or by their region of origin (e.g. emission of a particular extragalactic source). These emissions, as

a function of sky pixel and frequency, must then be band-integrated and beam-integrated to produce total emission maps as observed by the instrument. We decompose this simulation pipeline into two main steps: the multicomponent model of sky emission, which does not depend on the instrument, and the integration of this emission in the instrumental response.

6.7.1.1 The multi-component sky model

6.7.1.2 Sky emission observations

6.7.2 The Galactic interstellar medium

Strong evidence exists for variability of the physical properties of the interstellar medium of the Milky Way as a function of the line of sight, and hence as a function of region of emission. Hence, in each line of sight the total ISM emission is the superposition of emission from various regions. Even assuming that each such region has a simple parameteric emission law, such as a power law or a modified blackbody, the superposition of such emission cannot be modeled with a single simple emission law. Modeling the Galactic ISM for future sensitive surveys such as CMB-S4 requires modeling this complexity at the appropriate level. It seems reasonable to use a multi-layer approach, in which each ISM component is modeled as a superposition of several layers, with a simple (although pixel-dependent and polarization dependent) emission law for each such layer.

6.7.2.1 Synchrotron

A baseline model we use here has a power law scaling with a modestly spatially varying spectral index. The emission templates are the Haslam 408 MHz data reprocessed by [**?**], and the WMAP 7-year 23 GHz Q/U maps [**?**] smoothed to 3 degree FWHM and with smaller scales added using the PSM code [**?**] The spectral index map is derived using a combination of the Haslam 408 MHz data and WMAP 23 GHz 7-year data [**?**] The same scaling is used for intensity and polarization. This is the same prescription as used in the Planck Sky Model's v1.7.8 'power law' option, but with the Haslam map updated to the Remazeilles version.

Extensions to this model that we are exploring include a curved power law model with a single isotropic curvature index, and a polarization spectral index that steepens with Galactic latitude by $\delta\beta \sim 0.2$ from low to high latitude, as this is currently consistent with WMAP and Planck data.

6.7.2.2 Thermal dust

A baseline model we consider has thermal dust modelled as a single component modified blackbody. We use dust templates for emission at 545 GHz in intensity and 353 GHz in polarisation from the Planck-2015 analysis, and scale these to different frequencies with a modified black-body spectrum using the spatially varying dust temperature and emissivity obtained from the Planck data using the Commander code (Planck Collaboration 2015, arXiv:1502.01588). This therefore assumes the same spectral index for polarization as for intensity. These templates are smoothed to degree scale.

Variations on this model that appear consistent with current data are a more strongly varying emissivity, e.g. up to $\sigma \sim 0.2$ dispersion on degree scales, in addition to different prescriptions for small-scale behaviour that account for turbulence in the magnetic field. A two (or more) component model for the dust, composed of

the spatially varying sum of silicon and carbonaceous dust, each with a different emissivity, is also physically motivated.

6.7.2.3 Spinning dust

In polarization the spinning dust, or anomalous microwave emission, is nominally unpolarized, but a fractional polarization of a few percent is physically possible and not excluded by current data. We construct a possible polarized model for this using the intensity templates for spinning dust from the Planck-2015 Commander fits, combined with the thermal dust polarization angles and an overall polarization fraction.

6.7.2.4 Free-free

6.7.2.5 Atomic and molecular lines

6.7.3 CMB Secondary Anisotropies and Extragalactic Sources

The key challenges for the extragalactic sky models of CMB-S4 are to provide fast and self-consistent simulations of CMB secondary anisotropies and extragalactic sources. These models will allow us to make more realistic forecasts. In our cosmological analyses they will allows us to Monte Carlo over the underlying astrophysical uncertainties of these secondaries and sources. Our plan to meet these challenges is modular and can be broken down as follows:

- We will use full hydrodynamical simulations of cosmological volume as the basis to parametrically model the complicated *gastrophysical* processes associated with extragalactic foregrounds.
- As the backbone of our model we will require fast simulations of growth of structure that generate halo catalogs for a large set of cosmological parameters.
- To have self-consistent maps we will have a flexible pipeline that generates simulated all sky maps which applies the parametric models from the hydrodynamical simulations to our backbone large-scale structure simulations and halo catalogs.

Hydrodynamical simulations of cosmological volumes are currently available which we can already use to model extragalactic foregrounds. These simulations will be used for the development and testing phases of the simulation pipeline. However, they are limited in their size and sub-grid modeling accuracy, and thus will not meet our accuracy requirements of CMB-S4. We will develop new full hydrodynamical simulations of cosmological volumes that include a variety of physical processes. An essential requirement of these simulations will be to capture growth and evolution of galaxies to cluster-size halos throughout cosmic time at a sufficient spatial resolution. Hydrodynamic simulations of this size and scale are already computationally feasible, the challenges will be the appropriate modeling of radiative cooling, star formation, and feedback processes in order to capture the global stellar and gas contents of these halos.

There are many different approaches already developed to provide us with the underlying large-scale structure simulations that will we build our extragalactic model upon. They vary in speed which tend to inversely scale with accuracy. A benefit of our modular and flexible approach is that we do not need to limit ourselves to one approach. In fact we will compare the various approaches to see how they bias our answers. It is in

these simulations where we will vary cosmological parameters assuming that they only affect the growth of structure and not the *gastrophysical* properties of extragalactic foregrounds.

Our final product will be all sky maps. They will be in HEALPIX format (or some other format) to seamlessly interface with galactic and CMB simulated maps. The map products will include:

- Optical galaxies that correspond to the various overlapping surveys including LSST.
- Radio and dusty star-forming galaxy point sources.
- Unresolved CIB.
- Projected density maps (both total and gas) of the large-scale structure.
- Thermal and kinetic SZ maps.

We will explore the parameter space for each of the maps listed above and provide a sufficient number of realizations that we can marginalize over the many model uncertainties. For example, the lensing field can be constructed through a proper ray-tracing method from the projected density maps or via the Born approximation. Our self-consistent extragalactic sky model allows us to test various sources of contamination and systematic biases in our estimators. Additionally, any cross-correlation analyses can easily be checked and evaluated using these maps. **All the simulation products we create will become public.**

6.8 Data Simulation

The data simulation subset of the CMB simulation pipeline (Figure 31) takes the sky model and applies the mission model to it to generate a simulated data set for that mission. The mission model consists of two parts; the instrument model defines the data acquisition system (telescope, detectors, read-out), while the observation model defines its deployment (scanning strategy, environment). Depending on the degree of detail of the sky, instrument and observation model that we include, the resulting data set can be in any of the data domains - time-ordered (raw or clean), map, or spectral. Inevitably there is a trade-off between the realism of the simulation and the complexity and cost both of generating the model inputs and of performing the simulation, with the choice reflecting both the requirements of the subsequent analyses of the data set and the availability of computational resources.

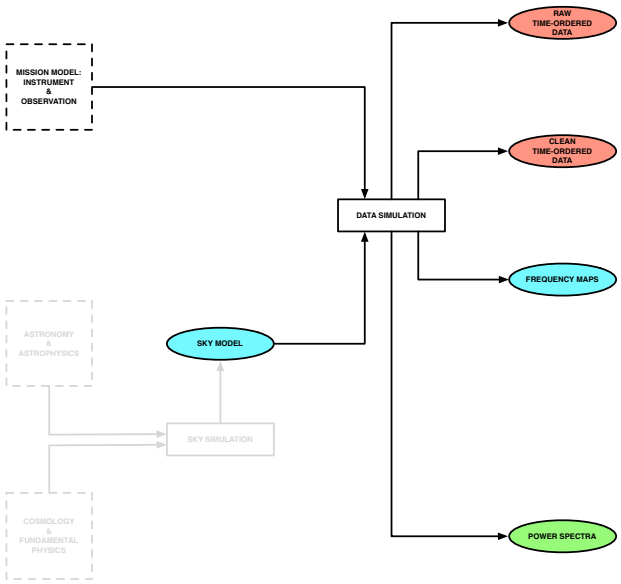

Figure 31. *The data simulation subset of the CMB simulation pipeline*

At the most detailed level, the observation model includes the telescope pointing (typically sampled more sparsely that the detectors), and its environment (comprising the atmosphere and surroundings for a ground-based telescope). Correspondingly, the instrument model includes each detector's polarized 4π-beam and bandpass (defining the optical power incident on the detector for a given pointing), and a model of its electronics and readout (defining the recorded output data resulting from that optical power).

6.8.1 Time Domain

TOD simulations are necesserily the most expensive to perform, but provide the most precise representation of the mission data. In particular they enable the injection of the full range of systematic effects into the data to assess strategies for their mitigation and to quantify any residuals. As such they are critical for the quantification of uncertainties due to inherently temporal data components such as noise. The TOD simulation is separated into signal and noise components, which are then added prior to the reduction of the total TOD.

For the signal simulation for a given detector, we first apply the detector's bandpass to the sky model, component by component, to build up the total sky for that detector. We then reconstruct the detector pointing from the overall telescope pointing model and generate the astrophysical sky signal for each pointing by convolving the sky model map with the 4π beam. The astrophysical sky signal is added to additional simulated signals from atmospheric signal fluctuations and ground pickup (both of which will obviously induce correlated signals across the detectors), and the total signal is propagated through a simple model of the optics to include the polarization angle rotations and optical efficiencies of the optical stages. This results in the total millimeter-wave power incident on the detector. For simulating the clean TOD this is sufficient. However, for the raw TOD we now need to apply a physical model of the detector system and associated readout to convert the optical power into detector output. The details of the physical model depend on the detector technology, but as an example we consider a transition-edge superconducting (TES) bolometer read out with a multiplexed SQUID amplifier. The simulation would then need to model the flow of heat in the TES absorber and the flow of current and magnetic flux through the SQUID readout. Variations in ambient magnetic field could also be added at this stage. Such a simulation would also need to incorporate detector-detector correlations induced by crosstalk or thermal fluctuations. Additional filters applied by the readout electronics would also be included, including digitization with an analog to digital converter. For MKID or coherent receivers, the physical model would be different in detail, but would include a similarly detailed model.

For the noise simulation we can simply generate a white noise timestream and convolve it with the detector's noise power spectral density (PSD), given in either analytic or numerical form. Cross-correlated noise can be included by simulating multiple noise timestreams each with their own PSD, with some being common to multiple detectors, while piecewise stationary noise simply requires us to use the appropriate PSD for each stationary interval.

6.8.2 Map Domain

Apply symmetric beam in harmonic space, or effective beam (built up over pointings), to bandpassed map.

Use hitmap or 3x3 white noise covariance matrix (built up over pointings) to generate noise map.

6.8.3 Spectral Domain

Model residuals (noise, systematics, component separation, etc) in spectral domain.

6.9 The Simulation and Data Analysis Pipeline

The overall simulation and data analysis pipeline (Figure 32) can now be seen as both a top-down data reduction process and a wrap-around refinement of our mission and sky modeling. Typically the two phases are interleaved, with each new data reduction improving our mission and sky models, which are in turn fed back into an improved data reduction.

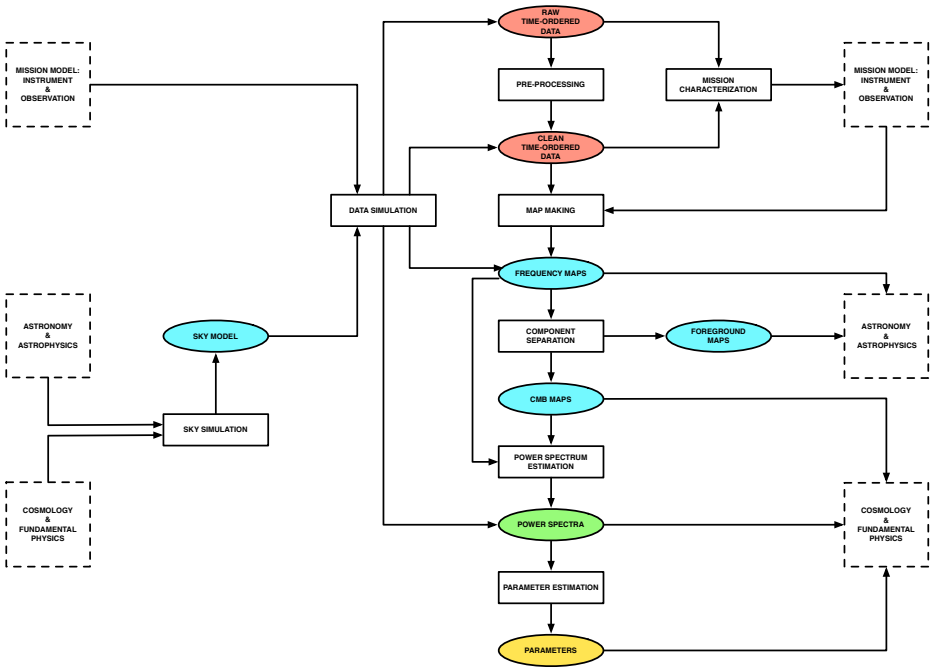

Figure 32. *The full CMB simulation and data analysis pipeline*

For CMB-S4 the most critical uses of this pipeline (or subsets thereof) are currently in forecasting and validation and verification. Further, the very discussion of such a pipeline provides a natural context in which to consider important implementation issues.

6.10 Forecasting

We emphasize the importance of accurate forecasting for CMB-S4. Forecasting efforts for Stage 1 and 2 experiments were hampered by lack of experience with previous deep polarization maps and little knowledge of high latitude Galactic foregrounds. Forecasting for CMB-S4 will be built on the solid foundation of map-derived evaluations of instrumental noise performance and astrophysical foreground levels from the Stage 2 experiments and the Planck satellite.

The forecasting approach will combine Fisher matrix-derived estimates of power spectrum errors with detailed map-level simulations. The spectral-domain projections are computationally easy, making them useful to explore the large parameter space of instrument and survey configurations. Map-domain simulations are used to ground the spectral-domain projections in reality and to challenge them with cases of real world astrophysical complexity. To gain the benefit of this complementarity, it is important that we maintain compatibility between these two forecasting approaches and establish agreement between them for simple questions before proceeding to more difficult tests.

A key input to the forecasting process are full-season noise maps from existing Stage 2 experiments, which encode actual noise performance and have been verified by null tests on real datasets. Performance of CMB-S4 can be estimated by rescaling these noise maps, which already contain reality factors such as detector yield, weather, observing efficiency, and filtering of sky modes. Systematic errors should be included in the projections, with unknown systematics allowed at a level that scales with the map noise used for jackknife null tests. Forecasting should also include our best knowledge of the astrophysical foregrounds and account for the impact of component separation on CMB-S4 science goals. The forecasting inputs will improve as we acquire data from Stage 3 experiments, which will produce deeper noise maps and better assessments of foregrounds, as well as demonstrations of new techniques and technologies in development for Stage 4.

Here we describe the main approaches used by our community for forecasting the expected performance of CMB-S4. The central considerations for assessing the expected performance for large-scale B-modes are Galactic foregrounds, ability to delens the data, and a realistic assessment of instrument noise at large scales. For the smaller-scale polarization two-point functions (TE, EE) and the lensing four-point function ($\kappa\kappa$), extragalactic foregrounds and instrumental noise are the key considerations. To forecast the return of the thermal Sunyaev-Zel'dovich effects, an estimate of the expected cluster counts as a function of mass and redshift is the core statistic, combined with an estimate of how well the masses can be calibrated using overlaps with weak lensing surveys. For the kinetic Sunyaev-Zeldovich effect, extragalactic foregrounds and overlap with spectroscopic surveys must all be considered.

6.10.1 Limits on the tensor-to-scalar ratio

6.10.1.1 Spectrum-based domain forecasting

Power spectra are the primary tool used for CMB analysis. Forecasting the power spectrum uncertainty and resulting parameter constraints for CMB-S4 is an efficient and powerful tool to explore trade-offs in experiment design.

The bandpower covariance matrix describes the raw sensitivity of all auto and cross-spectra obtained between maps of T, E, and/or B modes at multiple observing frequencies, as well as the signal and noise correlations that exist between these spectra. This covariance matrix includes contributions from the sample variance

of signal fields (CMB and foreground) and instrumental noise, including signal×noise terms. The signal variance depends on the assumed sky model, which can be modified to explore optimistic or pessimistic scenarios. As discussed above, estimates of the noise variance should be obtained by rescaling of noise levels that have actually been obtained by Stage 2 experiments (or Stage 3, when available). Only these scaled noise levels will include all the small "reality factors" that are incurred in operating a CMB experiment.

We will explicitly account for the impact of systematic errors by including them in the bandpower covariance matrix. For constraining tensor-to-scalar ratio, we are particularly concerned with effects that add B-mode power to maps. Even if the bandpowers are debiased using accurate simulations of such a systematic, it will still leave behind a noise floor due to its sample variance. Unknown and unforseen sources of spurious signal in CMB-S4 will ultimately be constrained by jackknife null tests, which analyze a map constructed from the difference of two data subsets. The statistical power of the null test is set by the noise level of the maps, since any signal contributions should difference away. We can acknowledge this limitation by including in our projections an unknown systematic that adds B modes at the level of the null test uncertainty. Errors that are multiplicative in the signal, such as an absolute calibration error in the map, are best handled by adding nuisance parameters to the signal model.

Once we have a projection for the bandpower covariance matrix of CMB-S4, we can derive constraints on a parametrized model of cosmological and foreground signals via the Fisher information matrix. While we are most interested in parameter r, it is necessary to also consider the amplitude, spectrum, and spatial distribution of the dust and synchrotron foregrounds (see [65] for an example). The Fisher matrix formalism allows us to calculate the marginalized error on each parameter, with priors if desired, or to explore the degeneracies between parameters.

By compressing the data down to power spectra, it is feasible to use this technique to evaluate a wide range of survey designs. The parametrized signal model is also quite flexible and can include complications such as dust–synchrotron correlation or spatially varying foreground spectral indices. The limitation is that by considering the power spectrum only we are treating all signals as Gaussian, an approximation which must break down at some point for foregrounds. For this reason, it is important to have the ability to spot check the spectrum-based forecasts against map-based forecasts at specific choices of signal model.

6.10.1.2 Map-based domain forecasting

Foregrounds are intrinsically non-Gaussian, so it is beneficial to consider approaches directly in map space, to check the robustness of spectrum-based approaches, in particular in the case of pessimistic foregrounds where the spectral indices or dust emissivities have non-trivial spatial variation. Here one of the approaches our community uses is a Bayesian model fitting method, where the foregrounds are described parametrically using a physical model for each component.

Using this method, maps of the CMB plus Galactic foreground sky and expected noise are simulated at each of the CMB-S4 frequencies and integrated across the expected bandpasses, using Galactic models as described for example in Section 6.7. Simulations at ancillary frequencies that might be provided by other experiments, for example the Planck data, can also be included in the same way. A parameterized model is then fit to the simulated maps, for example fitting the CMB, thermal dust, and synchrotron in small pixels, and typically the synchrotron spectral index and dust emissivity and temperature in larger pixels of order degree-scale or larger. The BB power spectrum of the foreground-marginalized CMB map is then estimated using e.g., the MASTER [197] algorithm or a pixel-based likelihood, and converted into an estimate of r and its uncertainty. Our community has at least two such codes that can perform this procedure (Commander and BFoRe).

This method allows for an assessment of the expected bias on r if the model does not match the simulation, and shows how much the expected uncertainty on r would increase if more complicated foreground models are explored e.g. [**?**, **?**]. It is more computationally expensive than spectral-domain forecasts though, so we limit this approach to a smaller subset of explorations.

6.10.2 Limits on parameters from TT/TE/EE/$\kappa\kappa$

To forecast the expected constraints on cosmological parameters from TT/TE/EE and $\kappa\kappa$ for CMB-S4, many of our community's codes use a Fisher matrix method, which assumes that the resulting parameter distributions are close to Gaussian. Some forecasts are performed using full MCMC simulations if the parameters are known to be highly non-Gaussian.

For CMB-S4, the method we follow is to combine CMB-S4 specifications with other available datasets, for example the data from Planck and expected measurements of Baryon Acoustic Oscillations and other low redshift data.

For the noise levels of Planck, we assume that a data release including reliable polarization data will have happened before CMB-S4 data is taken, and forecast results that include TE and EE data and also large-scale polarization from HFI at multipoles lower than CMB-S4 is expected to reach. This follows approaches in e.g. [**?**].

Our community uses two approaches to these Fisher forecasts, either considering the unlensed maps and the lensing convergence map as the basic statistics, or the lensed power spectra of those maps together with the reconstructed $\kappa\kappa$ spectrum. In the case of the power spectrum approach, to compute the Fisher matrix for the CMB we use the lensed power spectrum between each pair of fields X, Y:

$$\hat{C}_\ell^{XY} = \frac{1}{2\ell+1}\sum_{m=-\ell}^{m=\ell} x^*_{\ell m} y_{\ell m}. \tag{6.28}$$

The estimated power spectrum is Gaussian distribution to good approximation at small scales. In this case a full-sky survey has

$$-2\ln\mathcal{L}(\boldsymbol{\theta}) = -2\sum_\ell \ln p(\hat{C}_\ell|\boldsymbol{\theta}) = \sum_\ell \Big[(\hat{C}_\ell - C_\ell(\boldsymbol{\theta}))^\top \mathbb{C}_\ell^{-1}(\boldsymbol{\theta})\big(\hat{C}_\ell - C_\ell(\boldsymbol{\theta})\big) + \ln\det(2\pi\mathbb{C}_\ell(\boldsymbol{\theta}))\Big] \tag{6.29}$$

where $\hat{C}_\ell = (\hat{C}_\ell^{TT}, \hat{C}_\ell^{TE}, ...)$ contains auto- and cross-spectra and $\mathbb{C}_\ell$ is their covariance matrix. Discarding any parameter dependence in the power spectrum covariance matrix gives

$$F_{ij} = \sum_\ell \frac{\partial C_l^\top}{\partial\theta_i}\mathbb{C}_\ell^{-1}\frac{\partial C_l}{\partial\theta_j}. \tag{6.30}$$

Here the covariance matrix for the power spectra has elements

$$\mathbb{C}(\hat{C}_l^{\alpha\beta}, \hat{C}_l^{\gamma\delta}) = \frac{1}{(2l+1)f_{\rm sky}}\big[(C_l^{\alpha\gamma}+N_l^{\alpha\gamma})(C_l^{\beta\delta}+N_l^{\beta\delta}) + (C_l^{\alpha\delta}+N_l^{\alpha\delta})(C_l^{\beta\gamma}+N_l^{\beta\gamma})\big], \tag{6.31}$$

where $\alpha, \beta, \gamma, \delta \in \{T, E, B, \kappa_c\}$ and $f_{\rm sky}$ is the effective fractional area of sky used.

The second approach we consider is to construct the Fisher matrix using the unlensed temperature and polarization fields, and the lensing convergence field, rather than the suite of lensed two-point spectra and the lensing four-point function. Both approaches give consistent estimates.

The CMB lensing reconstruction noise is calculated using the [?] quadratic-estimator formalism. Our nominal approach is to neglect non-Gaussian terms in the power spectrum covariance. We also avoid including information from both lensed BB and the four-point $\kappa\kappa$, as they are covariant. The BB spectrum will not contribute as significantly to S4 constraints, compared to $\kappa\kappa$, and has a highly non-Gaussian covariance [?].

To address the issue of possible extragalactic foregrounds, we set a maximum multipole for the recoverable information of $\ell^T_{\rm max} = 3000$ and $\ell^P_{\rm max} = 4000$ for CMB-S4, as foregrounds are expected to be limiting at smaller scales. We also set a minimum multipole due to the challenge of recovering large-scales from the ground, and consider in general $\ell = 50$. We include Planck data at the scales $\ell < \ell_{\rm min}$.

When relevant, we can also add information from Baryon Acoustic Oscillation (BAO) experiments. This can be done by adding the BAO Fisher matrix

$$F^{\rm BAO}_{ij} = \sum_k \frac{1}{\sigma^2_{f,k}} \frac{\partial f_k}{\partial \theta_i} \frac{\partial f_k}{\partial \theta_j} \tag{6.32}$$

where $f_k = r_s/d_V(z_k)$ is the sound horizon at photon-baryon decoupling r_s over the volume distance d_V to the source galaxies at redshift z_k. We also follow standard approaches to including other low redshift probes.

6.10.2.1 Instrument and atmospheric noise

Noise spectra are generated assuming the sum of white noise and atmospheric noise. The white noise part is given by

$$N^{\alpha\alpha}_\ell = (\Delta T)^2 \exp\left(\frac{\ell(\ell+1)\theta^2_{\rm FWHM}}{8\ln 2}\right) \tag{6.33}$$

for $\alpha \in \{T, E, B\}$, where ΔT (ΔP for polarization) is the map sensitivity in μK-arcmin and $\theta_{\rm FWHM}$ is the beam width.

To estimate the atmospheric noise level in intensity, we consider levels at the South Pole and in Chile. For Chile, we base this estimate on current data from ACT and POLARBEAR. For the South Pole, we use data from SPT and BICEP as a guide. We then make the assumption that the atmospheric noise will scale down with observation time for detector arrays within a telescope, and will be uncorrelated for physically separated telescopes. For polarization our nominal estimate is white noise, assuming that the tiny intrinsic polarization of the atmosphere, potentially combined with the use of polarization modulators, minimizes atmospheric contamination.

6.10.3 Limits on parameters from tSZ/kSZ

To estimate the expected tSZ cluster counts from S4, we use.

6.11 Validation and Verification

How do we validate and verify the pipeline elements and whole?

6.12 Implementation Issues

6.12.1 Time-Ordered Data Volume & High Performance Computing

The quest for ever-fainter signals in the CMB drives us to gather ever-larger time-ordered data (TOD) sets to obtain the necessary signal-to-noise to uncover them. As Figure 33 shows, the volumes of ground-based, balloon-borne and satellite CMB data sets have exhibited exponential growth over the last 20 years and are anticipated to do so again over the next. Moreover, for suborbital experiments the exponent exactly matches that of Moore's Law for the growth of computing capability, where we us as a proxy here the peak performance of the flagship high performance computing (HPC) system at the DOE's National Energy Research Scientific Computing (NERSC) Center at any epoch (reflecting the widespread use of NERSC for CMB data analyses over the last 20 years).

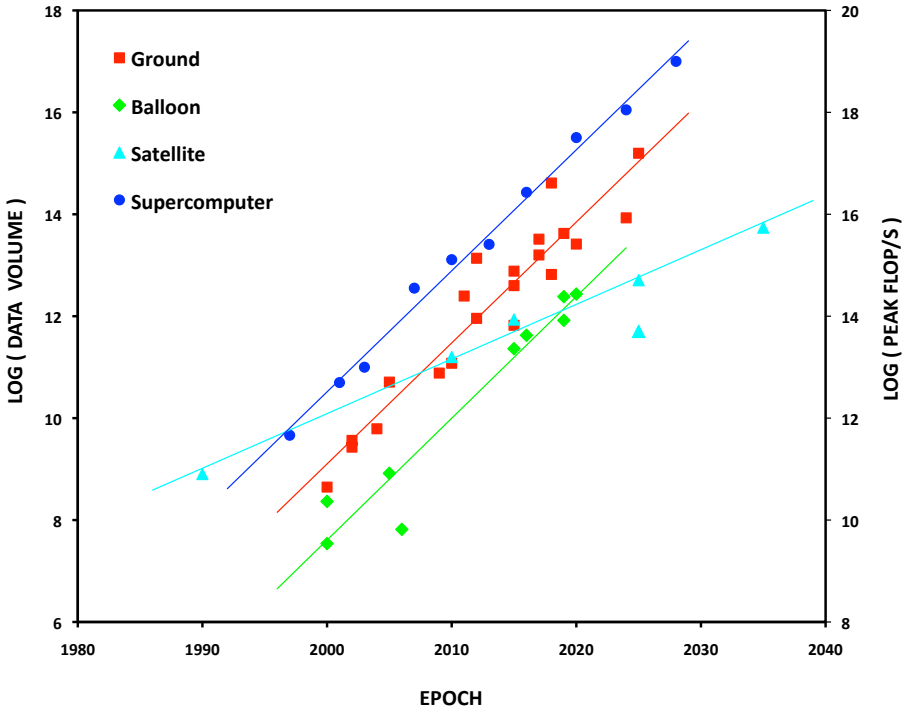

Figure 33. *Exponential growth of CMB time-ordered data volume and HPC capability: 1990 – 2030.*

Furthermore, in the absence of a full covariance matrix we rely on Monte Carlo methods for uncertainty quantification and debiasing, and to achieve the desired percent-level statistical uncertainty requires us to simulate and reduce 10^4 realizations of the data. Taken together, this implies that all TOD-processing steps (in simulation or analysis) (Figure 34 must employ algorithms that scale no worse than linearly in the number of samples, and that these algorithms must *collectively* be implemented efficiently on the largest high performance computing (HPC) platforms available to us.

The most massive Monte Carlo sets generated to date have been the Full Focal Plane (FFP) sets in support of the analysis of the Planck satellite data, with FFP8 comprising 10^4 realizations of the mission reduced to $O(10^6)$ maps. Key to achieving this scale has been an aggressive optimization of the software stack,

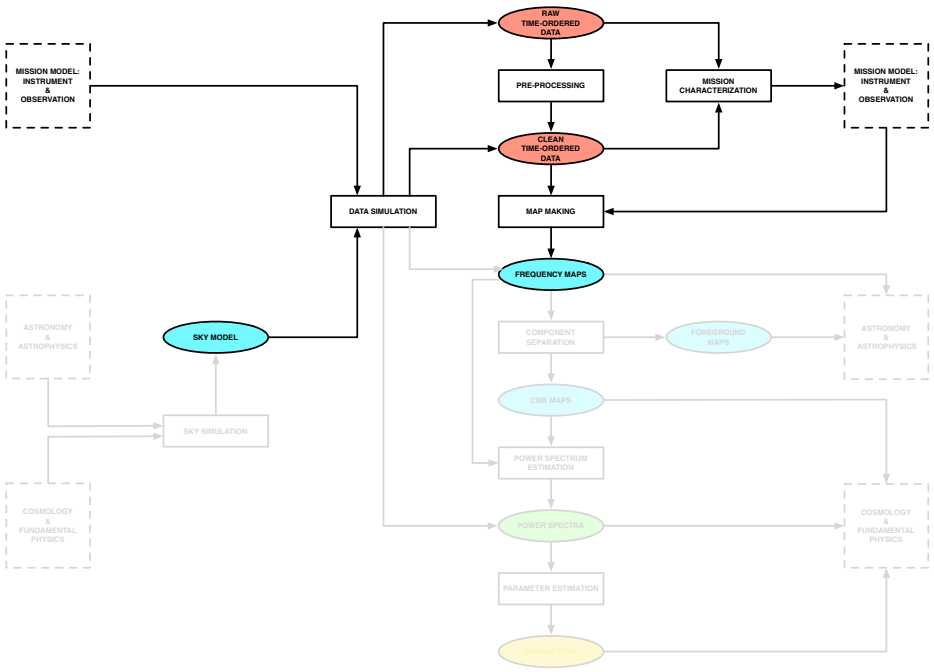

Figure 34. *Time-ordered data processing elements of the CMB simulation and data analysis pipeline.*

coupled with system-specific tuning over 6 generations of NERSC supercomputer. In particular wherever possible TOD input/output (IO) is removed from the pipeline so that, for example, instead of pre-computing the TOD and then pre-processing/mapping it, each realization is generated on demand and passed to the analysis pipeline in memory. While this necessitates the re-simulation of a realization should further analysis be required, it is still very substantially faster than writing it to disk and reading it back in. Similarly, inter-process communication is optimized by using a hybridized MPI/OpenMP implementation that employs explicit message passsing for inter-node, and threading for intra-node, communication.

A critical challenge for CMB-S4 will be to develop this capability for a dataset 1000x the size of Planck's on the coming generations of energy-constrained HPC architectures, with their increased heterogeneity and deeper memory hierarchies. In the short term such systems will be based on either graphical programming unit (GPU) or many integrated core (MIC) technologies; in the longer term the path to Moore's Law is unclear.

6.12.2 Application Interfaces, Data Objects and Formats

References

[1] K. N. Abazajian et al. Light Sterile Neutrinos: A White Paper. 2012.

[2] K. N. Abazajian et al. Neutrino Physics from the Cosmic Microwave Background and Large Scale Structure. *Astropart. Phys.*, 63:66–80, 2015.

[3] Kevork Abazajian, George M. Fuller, and Mitesh Patel. Sterile neutrino hot, warm, and cold dark matter. *Phys. Rev.*, D64:023501, 2001.

[4] Kevork N. Abazajian. Telling three from four neutrinos with cosmology. *Astropart. Phys.*, 19:303–312, 2003.

[5] K.N. Abazajian, E. Calabrese, A. Cooray, F. De Bernardis, S. Dodelson, et al. Cosmological and Astrophysical Neutrino Mass Measurements. *Astropart.Phys.*, 35:177–184, 2011.

[6] B. P. et al. Abbott. Observation of gravitational waves from a binary black hole merger. *Phys. Rev. Lett.*, 116:061102, Feb 2016.

[7] Lotty Ackerman, Matthew R. Buckley, Sean M. Carroll, and Marc Kamionkowski. Dark Matter and Dark Radiation. *Phys. Rev.*, D79:023519, 2009. [,277(2008)].

[8] Lotty Ackerman, Matthew R. Buckley, Sean M. Carroll, and Marc Kamionkowski. Dark Matter and Dark Radiation. *Phys. Rev. D*, 79:023519, 2009.

[9] Fred C. Adams, J. Richard Bond, Katherine Freese, Joshua A. Frieman, and Angela V. Olinto. Natural inflation: Particle physics models, power law spectra for large scale structure, and constraints from COBE. *Phys. Rev.*, D47:426–455, 1993.

[10] P. A. R. Ade et al. A Measurement of the Cosmic Microwave Background B-Mode Polarization Power Spectrum at Sub-Degree Scales with POLARBEAR. *Astrophys. J.*, 794(2):171, 2014.

[11] P. A. R. Ade et al. Detection of B-Mode Polarization at Degree Angular Scales by BICEP2. *Phys. Rev. Lett.*, 112(24):241101, 2014.

[12] P. A. R. Ade et al. Planck 2013 results. XXV. Searches for cosmic strings and other topological defects. *Astron. Astrophys.*, 571:A25, 2014.

[13] P. A. R. Ade et al. Planck 2015 results. XIII. Cosmological parameters. 2015.

[14] P. A. R. Ade et al. Planck 2015 results. XIX. Constraints on primordial magnetic fields. 2015.

[15] P. A. R. Ade et al. Planck 2015 results. XVII. Constraints on primordial non-Gaussianity. 2015.

[16] P. A. R. Ade et al. Planck 2015 results. XXIV. Cosmology from Sunyaev-Zeldovich cluster counts. 2015.

[17] Peter A. R. Ade et al. POLARBEAR Constraints on Cosmic Birefringence and Primordial Magnetic Fields. *Phys. Rev.*, D92:123509, 2015.

[18] Peter Adshead, Emil Martinec, and Mark Wyman. Gauge fields and inflation: Chiral gravitational waves, fluctuations, and the Lyth bound. *Phys. Rev.*, D88(2):021302, 2013.

[19] Peter Adshead, Emil Martinec, and Mark Wyman. Perturbations in Chromo-Natural Inflation. *JHEP*, 09:087, 2013.

[20] Peter Adshead and Mark Wyman. Chromo-Natural Inflation: Natural inflation on a steep potential with classical non-Abelian gauge fields. *Phys. Rev. Lett.*, 108:261302, 2012.

[21] Peter Adshead and Mark Wyman. Gauge-flation trajectories in Chromo-Natural Inflation. *Phys. Rev.*, D86:043530, 2012.

[22] A. A. Aguilar-Arevalo et al. Improved Search for $\bar{\nu}_\mu \to \bar{\nu}_e$ Oscillations in the MiniBooNE Experiment. *Phys. Rev. Lett.*, 110:161801, 2013.

[23] Stephon Alexander and Jerome Martin. Birefringent gravitational waves and the consistency check of inflation. *Phys. Rev.*, D71:063526, 2005.

[24] R. A. Alpher, H. Bethe, and G. Gamow. The origin of chemical elements. *Phys. Rev.*, 73:803–804, 1948.

[25] Marcelo Alvarez et al. Testing Inflation with Large Scale Structure: Connecting Hopes with Reality. 2014.

[26] Mohamed M. Anber and Lorenzo Sorbo. N-flationary magnetic fields. *JCAP*, 0610:018, 2006.

[27] Aditya Aravind, Dustin Lorshbough, and Sonia Paban. Bogoliubov Excited States and the Lyth Bound. *JCAP*, 1408:058, 2014.

[28] Maria Archidiacono, Nicolao Fornengo, Carlo Giunti, Steen Hannestad, and Alessandro Melchiorri. Sterile neutrinos: Cosmology versus short-baseline experiments. *Phys. Rev.*, D87(12):125034, 2013.

[29] Maria Archidiacono, Steen Hannestad, Rasmus Sloth Hansen, and Thomas Tram. Cosmology with self-interacting sterile neutrinos and dark matter - A pseudoscalar model. *Phys. Rev. D*, 91(6):065021, 2015.

[30] Nima Arkani-Hamed, Douglas P. Finkbeiner, Tracy R. Slatyer, and Neal Weiner. A Theory of Dark Matter. *Phys. Rev. D*, 79:015014, 2009.

[31] Nima Arkani-Hamed, Lubos Motl, Alberto Nicolis, and Cumrun Vafa. The String landscape, black holes and gravity as the weakest force. *JHEP*, 06:060, 2007.

[32] C. Armitage and B. D. Wandelt. Deconvolution map-making for cosmic microwave background observations. *Phys. Rev. D*, 70(12):123007, December 2004.

[33] A. Arvanitaki, S. Dimopoulos, S. Dubovsky, N. Kaloper, and J. March-Russell. String axiverse. *Phys. Rev.* **D** , 81(12):123530, June 2010.

[34] Asimina Arvanitaki, Savas Dimopoulos, Sergei Dubovsky, Nemanja Kaloper, and John March-Russell. String Axiverse. *Phys. Rev.*, D81:123530, 2010.

[35] Z. Arzoumanian et al. The NANOGrav Nine-year Data Set: Limits on the Isotropic Stochastic Gravitational Wave Background. 2015.

[36] Amjad Ashoorioon, Konstantinos Dimopoulos, M. M. Sheikh-Jabbari, and Gary Shiu. Non-Bunch?Davis initial state reconciles chaotic models with BICEP and Planck. *Phys. Lett.*, B737:98–102, 2014.

[37] C. Athanassopoulos et al. Evidence for nu/mu –¿ nu/e neutrino oscillations from lsnd. *Phys. Rev. Lett.*, 81:1774–1777, 1998.

[38] Fernando Atrio-Barandela and Sacha Davidson. Interacting hot dark matter. *Phys. Rev. D*, 55:5886–5894, 1997.

[39] A. Avgoustidis, E. J. Copeland, A. Moss, L. Pogosian, A. Pourtsidou, and Daniele A. Steer. Constraints on the fundamental string coupling from B-mode experiments. *Phys. Rev. Lett.*, 107:121301, 2011.

[40] Thomas C. Bachlechner, Cody Long, and Liam McAllister. Planckian Axions and the Weak Gravity Conjecture. *JHEP*, 01:091, 2016.

[41] John N. Bahcall, P. I. Krastev, and E. Lisi. Limits on electron-neutrino oscillations from the GALLEX Cr-51 source experiment. *Phys. Lett.*, B348:121–123, 1995.

[42] N.A. Bahcall and X. Fan. The most massive distant clusters: Determining ω and σ_8. *Astrophys. J.*, 504:1, 1998.

[43] Marco Baldi. Structure formation in Multiple Dark Matter cosmologies with long-range scalar interactions. *Mon. Not. Roy. Astron. Soc.*, 428:2074, 2013.

[44] Tom Banks, Michael Dine, Patrick J. Fox, and Elie Gorbatov. On the possibility of large axion decay constants. *JCAP*, 0306:001, 2003.

[45] Neil Barnaby, Jordan Moxon, Ryo Namba, Marco Peloso, Gary Shiu, and Peng Zhou. Gravity waves and non-Gaussian features from particle production in a sector gravitationally coupled to the inflaton. *Phys. Rev.*, D86:103508, 2012.

[46] Neil Barnaby and Marco Peloso. Large Nongaussianity in Axion Inflation. *Phys. Rev. Lett.*, 106:181301, 2011.

[47] Sergei Bashinsky and Uros Seljak. Neutrino perturbations in CMB anisotropy and matter clustering. *Phys. Rev.*, D69:083002, 2004.

[48] E. S. Battistelli, G. Amico, A. Baù, L. Bergé, É. Bréelle, R. Charlassier, S. Collin, A. Cruciani, P. de Bernardis, C. Dufour, L. Dumoulin, M. Gervasi, M. Giard, C. Giordano, Y. Giraud-Héraud, L. Guglielmi, J.-C. Hamilton, J. Landé, B. Maffei, M. Maiello, S. Marnieros, S. Masi, A. Passerini, F. Piacentini, M. Piat, L. Piccirillo, G. Pisano, G. Polenta, C. Rosset, M. Salatino, A. Schillaci, R. Sordini, S. Spinelli, A. Tartari, and M. Zannoni. Intensity and polarization of the atmospheric emission at millimetric wavelengths at Dome Concordia. *Mon. Not. Roy. Astron. Soc.*, page 3009, May 2012.

[49] Richard A. Battye and Adam Moss. Evidence for Massive Neutrinos from Cosmic Microwave Background and Lensing Observations. *Phys. Rev. Lett.*, 112(5):051303, 2014.

[50] Daniel Baumann, Daniel Green, Joel Meyers, and Benjamin Wallisch. Phases of New Physics in the CMB. 2015.

[51] Daniel Baumann, Daniel Green, and Rafael A. Porto. B-modes and the Nature of Inflation. *JCAP*, 1501(01):016, 2015.

[52] Daniel Baumann, Hayden Lee, and Guilherme L. Pimentel. High-Scale Inflation and the Tensor Tilt. *JHEP*, 01:101, 2016.

[53] Daniel Baumann and Matias Zaldarriaga. Causality and Primordial Tensor Modes. *JCAP*, 0906:013, 2009.

[54] Siavosh R. Behbahani, Anatoly Dymarsky, Mehrdad Mirbabayi, and Leonardo Senatore. (Small) Resonant non-Gaussianities: Signatures of a Discrete Shift Symmetry in the Effective Field Theory of Inflation. *JCAP*, 1212:036, 2012.

[55] Siavosh R. Behbahani and Daniel Green. Collective Symmetry Breaking and Resonant Non-Gaussianity. *JCAP*, 1211:056, 2012.

[56] Ido Ben-Dayan and Ram Brustein. Cosmic Microwave Background Observables of Small Field Models of Inflation. *JCAP*, 1009:007, 2010.

[57] A. Benoit-Lévy, K. M. Smith, and W. Hu. Non-Gaussian structure of the lensed CMB power spectra covariance matrix. *Phys. Rev.* **D** , 86(12):123008, December 2012.

[58] B. A. Benson, P. A. R. Ade, Z. Ahmed, S. W. Allen, K. Arnold, J. E. Austermann, A. N. Bender, L. E. Bleem, J. E. Carlstrom, C. L. Chang, H. M. Cho, S. T. Ciocys, J. F. Cliche, T. M. Crawford, A. Cukierman, T. de Haan, M. A. Dobbs, D. Dutcher, W. Everett, A. Gilbert, N. W. Halverson, D. Hanson, N. L. Harrington, K. Hattori, J. W. Henning, G. C. Hilton, G. P. Holder, W. L. Holzapfel, K. D. Irwin, R. Keisler, L. Knox, D. Kubik, C. L. Kuo, A. T. Lee, E. M. Leitch, D. Li, M. McDonald, S. S. Meyer, J. Montgomery, M. Myers, T. Natoli, H. Nguyen, V. Novosad, S. Padin, Z. Pan, J. Pearson, C. L. Reichardt, J. E. Ruhl, B. R. Saliwanchik, G. Simard, G. Smecher, J. T. Sayre, E. Shirokoff, A. A. Stark, K. Story, A. Suzuki, K. L. Thompson, C. Tucker, K. Vanderlinde, J. D. Vieira, A. Vikhlinin, G. Wang, V. Yefremenko, and K. W. Yoon. SPT-3G: A Next-Generation Cosmic Microwave Background Polarization Experiment on the South Pole Telescope. In *Society of Photo-Optical Instrumentation Engineers (SPIE) Conference Series*, volume 9153 of *Society of Photo-Optical Instrumentation Engineers (SPIE) Conference Series*, July 2014.

[59] B. A. Benson, T. de Haan, J. P. Dudley, C. L. Reichardt, K. A. Aird, K. Andersson, R. Armstrong, M. L. N. Ashby, M. Bautz, M. Bayliss, G. Bazin, L. E. Bleem, M. Brodwin, J. E. Carlstrom, C. L. Chang, H. M. Cho, A. Clocchiatti, T. M. Crawford, A. T. Crites, S. Desai, M. A. Dobbs, R. J. Foley, W. R. Forman, E. M. George, M. D. Gladders, A. H. Gonzalez, N. W. Halverson, N. Harrington, F. W. High, G. P. Holder, W. L. Holzapfel, S. Hoover, J. D. Hrubes, C. Jones, M. Joy, R. Keisler, L. Knox, A. T. Lee, E. M. Leitch, J. Liu, M. Lueker, D. Luong-Van, A. Mantz, D. P. Marrone, M. McDonald, J. J. McMahon, J. Mehl, S. S. Meyer, L. Mocanu, J. J. Mohr, T. E. Montroy, S. S. Murray, T. Natoli, S. Padin, T. Plagge, C. Pryke, A. Rest, J. Ruel, J. E. Ruhl, B. R. Saliwanchik, A. Saro, J. T. Sayre, K. K. Schaffer, L. Shaw, E. Shirokoff, J. Song, H. G. Spieler, B. Stalder, Z. Staniszewski, A. A. Stark, K. Story, C. W. Stubbs, R. Suhada, A. van Engelen, K. Vanderlinde, J. D. Vieira, A. Vikhlinin, R. Williamson, O. Zahn, and A. Zenteno. Cosmological Constraints from Sunyaev-Zel'dovich-selected Clusters with X-Ray Observations in the First 178 deg^2 of the South Pole Telescope Survey. *Astrophys. J.*, 763:147, February 2013.

[60] Marcus Berg, Enrico Pajer, and Stefan Sjors. Dante's Inferno. *Phys. Rev.*, D81:103535, 2010.

[61] Florian Beutler et al. The clustering of galaxies in the SDSS-III Baryon Oscillation Spectroscopic Survey: Signs of neutrino mass in current cosmological datasets. *Mon. Not. Roy. Astron. Soc.*, 444:3501, 2014.

[62] Fedor L. Bezrukov and Mikhail Shaposhnikov. The Standard Model Higgs boson as the inflaton. *Phys. Lett.*, B659:703–706, 2008.

[63] Suman Bhattacharya and Arthur Kosowsky. Dark Energy Constraints from Galaxy Cluster Peculiar Velocities. *Phys. Rev.*, D77:083004, 2008.

[64] BICEP2 Collaboration, P. A. R. Ade, R. W. Aikin, D. Barkats, S. J. Benton, C. A. Bischoff, J. J. Bock, J. A. Brevik, I. Buder, E. Bullock, C. D. Dowell, L. Duband, J. P. Filippini, S. Fliescher, S. R. Golwala, M. Halpern, M. Hasselfield, S. R. Hildebrandt, G. C. Hilton, V. V. Hristov, K. D. Irwin, K. S. Karkare, J. P. Kaufman, B. G. Keating, S. A. Kernasovskiy, J. M. Kovac, C. L. Kuo, E. M. Leitch, M. Lueker, P. Mason, C. B. Netterfield, H. T. Nguyen, R. O'Brient, R. W. Ogburn, A. Orlando, C. Pryke, C. D. Reintsema, S. Richter, R. Schwarz, C. D. Sheehy, Z. K. Staniszewski, R. V. Sudiwala, G. P. Teply, J. E. Tolan, A. D. Turner, A. G. Vieregg, C. L. Wong, and K. W. Yoon. Detection of B-Mode Polarization at Degree Angular Scales by BICEP2. *Physical Review Letters*, 112(24):241101, June 2014.

[65] BICEP2/Keck and Planck Collaborations, P. A. R. Ade, N. Aghanim, Z. Ahmed, R. W. Aikin, K. D. Alexander, M. Arnaud, J. Aumont, C. Baccigalupi, A. J. Banday, and et al. Joint Analysis of BICEP2/Keck Array and Planck Data. *Physical Review Letters*, 114(10):101301, March 2015.

[66] Jannis Bielefeld and Robert R. Caldwell. Chiral Imprint of a Cosmic Gauge Field on Primordial Gravitational Waves. *Phys. Rev.*, D91(12):123501, 2015.

[67] Jannis Bielefeld and Robert R. Caldwell. Cosmological consequences of classical flavor-space locked gauge field radiation. *Phys. Rev.*, D91(12):124004, 2015.

[68] L. E. Bleem, B. Stalder, T. de Haan, K. A. Aird, S. W. Allen, D. E. Applegate, M. L. N. Ashby, M. Bautz, M. Bayliss, B. A. Benson, S. Bocquet, M. Brodwin, J. E. Carlstrom, C. L. Chang, I. Chiu, H. M. Cho, A. Clocchiatti, T. M. Crawford, A. T. Crites, S. Desai, J. P. Dietrich, M. A. Dobbs, R. J. Foley, W. R. Forman, E. M. George, M. D. Gladders, A. H. Gonzalez, N. W. Halverson, C. Hennig, H. Hoekstra, G. P. Holder, W. L. Holzapfel, J. D. Hrubes, C. Jones, R. Keisler, L. Knox, A. T. Lee, E. M. Leitch, J. Liu, M. Lueker, D. Luong-Van, A. Mantz, D. P. Marrone, M. McDonald, J. J. McMahon, S. S. Meyer, L. Mocanu, J. J. Mohr, S. S. Murray, S. Padin, C. Pryke, C. L. Reichardt, A. Rest, J. Ruel, J. E. Ruhl, B. R. Saliwanchik, A. Saro, J. T. Sayre, K. K. Schaffer, T. Schrabback, E. Shirokoff, J. Song, H. G. Spieler, S. A. Stanford, Z. Staniszewski, A. A. Stark, K. T. Story, C. W. Stubbs, K. Vanderlinde, J. D. Vieira, A. Vikhlinin, R. Williamson, O. Zahn, and A. Zenteno. Galaxy Clusters Discovered via the Sunyaev-Zel'dovich Effect in the 2500-Square-Degree SPT-SZ Survey. *Ap. J. Suppl.* , 216:27, February 2015.

[69] Jolyon Bloomfield. A Simplified Approach to General Scalar-Tensor Theories. *JCAP*, 1312:044, 2013.

[70] Jolyon K. Bloomfield, anna . Flanagan, Minjoon Park, and Scott Watson. Dark energy or modified gravity? An effective field theory approach. *JCAP*, 1308:010, 2013.

[71] Ralph Blumenhagen, Cesar Damian, Anamaria Font, Daniela Herschmann, and Rui Sun. The Flux-Scaling Scenario: De Sitter Uplift and Axion Inflation. 2015.

[72] C. Boehm, J. A. Schewtschenko, R. J. Wilkinson, C. M. Baugh, and S. Pascoli. Using the Milky Way satellites to study interactions between cold dark matter and radiation. *Mon. Not. Roy. Astron. Soc.*, 445:L31–L35, 2014.

[73] Celine Boehm, Alain Riazuelo, Steen H. Hansen, and Richard Schaeffer. Interacting dark matter disguised as warm dark matter. *Phys. Rev. D*, 66:083505, 2002.

[74] Cline Boehm, Matthew J. Dolan, and Christopher McCabe. A Lower Bound on the Mass of Cold Thermal Dark Matter from Planck. *JCAP*, 1308:041, 2013.

[75] J.R̃. Bond, A.H̃. Jaffe, and L. Knox. Estimating the power spectrum of the cosmic microwave background. *Phys. Rev.* **D** , 57:2117–2137, February 1998.

[76] J. R. Bond and A. S. Szalay. The Collisionless Damping of Density Fluctuations in an Expanding Universe. *Astrophys. J.*, 274:443–468, 1983.

[77] Camille Bonvin, Chiara Caprini, and Ruth Durrer. Magnetic fields from inflation: the transition to the radiation era. *Phys. Rev.*, D86:023519, 2012.

[78] J. Borrill. The challenge of data analysis for future CMB observations. In L. Maiani, F. Melchiorri, and N. Vittorio, editors, *3K cosmology*, volume 476 of *American Institute of Physics Conference Series*, pages 277–282, May 1999.

[79] Alexey Boyarsky, Oleg Ruchayskiy, and Mikhail Shaposhnikov. The Role of sterile neutrinos in cosmology and astrophysics. *Ann. Rev. Nucl. Part. Sci.*, 59:191–214, 2009.

[80] Michael Boylan-Kolchin, James S. Bullock, and Manoj Kaplinghat. Too big to fail? The puzzling darkness of massive Milky Way subhaloes. *Mon. Not. Roy. Astron. Soc.*, 415:L40, 2011.

[81] Latham A. Boyle and Alessandra Buonanno. Relating gravitational wave constraints from primordial nucleosynthesis, pulsar timing, laser interferometers, and the CMB: Implications for the early Universe. *Phys. Rev.*, D78:043531, 2008.

[82] Latham A. Boyle, Paul J. Steinhardt, and Neil Turok. The Cosmic gravitational wave background in a cyclic universe. *Phys. Rev.*, D69:127302, 2004.

[83] W. N. Brandt, C. R. Lawrence, A. C. S. Readhead, J. N. Pakianathan, and T. M. Fiola. Separation of foreground radiation from cosmic microwave background using multifrequency measurements. *ApJ*, 424:1, 1994.

[84] Torsten Bringmann. Particle Models and the Small-Scale Structure of Dark Matter. *New J. Phys.*, 11:105027, 2009.

[85] Torsten Bringmann, Jasper Hasenkamp, and Jorn Kersten. Tight bonds between sterile neutrinos and dark matter. *JCAP*, 1407:042, 2014.

[86] Jon Brown, William Cottrell, Gary Shiu, and Pablo Soler. Fencing in the Swampland: Quantum Gravity Constraints on Large Field Inflation. *JHEP*, 10:023, 2015.

[87] Jon Brown, William Cottrell, Gary Shiu, and Pablo Soler. On Axionic Field Ranges, Loopholes and the Weak Gravity Conjecture. 2015.

[88] Christopher Brust, David E. Kaplan, and Matthew T. Walters. New Light Species and the CMB. *JHEP*, 12:058, 2013.

[89] Manuel A. Buen-Abad, Gustavo Marques-Tavares, and Martin Schmaltz. Non-Abelian dark matter and dark radiation. *Phys. Rev.*, D92(2):023531, 2015.

[90] Davide Cadamuro, Steen Hannestad, Georg Raffelt, and Javier Redondo. Cosmological bounds on sub-MeV mass axions. *JCAP*, 1102:003, 2011.

[91] Davide Cadamuro and Javier Redondo. Cosmological bounds on pseudo Nambu-Goldstone bosons. *JCAP*, 1202:032, 2012.

[92] Erminia Calabrese et al. Precision Epoch of Reionization studies with next-generation CMB experiments. *JCAP*, 1408:010, 2014.

[93] C. M. Cantalupo, J. D. Borrill, A. H. Jaffe, T. S. Kisner, and R. Stompor. MADmap: A Massively Parallel Maximum Likelihood Cosmic Microwave Background Map-maker. *The Astrophysical Journal Supplement Series*, 187:212–227, March 2010.

[94] Chiara Caprini, Ruth Durrer, and Geraldine Servant. Gravitational wave generation from bubble collisions in first-order phase transitions: An analytic approach. *Phys. Rev.*, D77:124015, 2008.

[95] J.-F. Cardoso, M. Le Jeune, J. Delabrouille, M. Betoule, and G. Patanchon. Component Separation With Flexible Models - Application to Multichannel Astrophysical Observations. *IEEE Journal of Selected Topics in Signal Processing*, 2:735–746, November 2008.

[96] E. D. Carlson, M. E. Machacek, and L. J. Hall. Self-interacting dark matter. *Ap. J.* , 398:43–52, October 1992.

[97] S. M. Carroll. Quintessence and the Rest of the World: Suppressing Long-Range Interactions. *Physical Review Letters*, 81:3067–3070, October 1998.

[98] Zackaria Chacko, Yanou Cui, Sungwoo Hong, and Takemichi Okui. Hidden dark matter sector, dark radiation, and the CMB. *Phys. Rev.*, D92:055033, 2015.

[99] A. Challinor and A. Lewis. Lensed CMB power spectra from all-sky correlation functions. *Phys. Rev.* **D** , 71(10):103010–+, May 2005.

[100] Arindam Chatterjee and Anupam Mazumdar. Bound on largest $r \lesssim 0.1$ from sub-Planckian excursions of inflaton. *JCAP*, 1501(01):031, 2015.

[101] Xue-Lei Chen and Marc Kamionkowski. Particle decays during the cosmic dark ages. *Phys. Rev.*, D70:043502, 2004.

[102] Clifford Cheung, Paolo Creminelli, A. Liam Fitzpatrick, Jared Kaplan, and Leonardo Senatore. The Effective Field Theory of Inflation. *JHEP*, 0803:014, 2008.

[103] Kiwoon Choi and Sang Hui Im. Realizing the relaxion from multiple axions and its UV completion with high scale supersymmetry. *JHEP*, 01:149, 2016.

[104] Xiaoyong Chu and Basudeb Dasgupta. Dark Radiation Alleviates Problems with Dark Matter Halos. *Phys. Rev. Lett.*, 113(16):161301, 2014.

[105] James M. Cline, Zuowei Liu, and Wei Xue. Millicharged Atomic Dark Matter. *Phys. Rev. D*, 85:101302, 2012.

[106] D. Clowe, M. Bradač, A. H. Gonzalez, M. Markevitch, S. W. Randall, C. Jones, and D. Zaritsky. A direct empirical proof of the existence of dark matter. *Ap. J. Lett.*, 648:L109–L113, September 2006.

[107] Hael Collins, R. Holman, and Tereza Vardanyan. Do Mixed States save Effective Field Theory from BICEP? 2014.

[108] J. M. Conrad, C. M. Ignarra, G. Karagiorgi, M. H. Shaevitz, and J. Spitz. Sterile Neutrino Fits to Short Baseline Neutrino Oscillation Measurements. *Adv. High Energy Phys.*, 2013:163897, 2013.

[109] Carlo R. Contaldi, Joao Magueijo, and Lee Smolin. Anomalous CMB polarization and gravitational chirality. *Phys. Rev. Lett.*, 101:141101, 2008.

[110] Jessica L. Cook and Lorenzo Sorbo. Particle production during inflation and gravitational waves detectable by ground-based interferometers. *Phys. Rev.*, D85:023534, 2012. [Erratum: Phys. Rev.D86,069901(2012)].

[111] Ryan Cooke, Max Pettini, Regina A. Jorgenson, Michael T. Murphy, and Charles C. Steidel. Precision measures of the primordial abundance of deuterium. *Astrophys. J.*, 781(1):31, 2014.

[112] Edmund J. Copeland, Robert C. Myers, and Joseph Polchinski. Cosmic F and D strings. *JHEP*, 06:013, 2004.

[113] Paolo Creminelli, Guido D'Amico, Jorge Norena, and Filippo Vernizzi. The Effective Theory of Quintessence: the $w < -1$ Side Unveiled. *JCAP*, 0902:018, 2009.

[114] Paolo Creminelli, Sergei Dubovsky, Diana Lopez Nacir, Marko Simonovic, Gabriele Trevisan, Giovanni Villadoro, and Matias Zaldarriaga. Implications of the scalar tilt for the tensor-to-scalar ratio. *Phys. Rev.*, D92(12):123528, 2015.

[115] Paolo Creminelli, Markus A. Luty, Alberto Nicolis, and Leonardo Senatore. Starting the Universe: Stable Violation of the Null Energy Condition and Non-standard Cosmologies. *JHEP*, 0612:080, 2006.

[116] Paolo Creminelli and Matias Zaldarriaga. Single-Field Consistency Relation for the 3-Point Function. *JCAP*, 0410:006, 2004.

[117] A. T. Crites, J. W. Henning, P. A. R. Ade, K. A. Aird, J. E. Austermann, J. A. Beall, A. N. Bender, B. A. Benson, L. E. Bleem, J. E. Carlstrom, C. L. Chang, H. C. Chiang, H.-M. Cho, R. Citron, T. M. Crawford, T. de Haan, M. A. Dobbs, W. Everett, J. Gallicchio, J. Gao, E. M. George, A. Gilbert, N. W. Halverson, D. Hanson, N. Harrington, G. C. Hilton, G. P. Holder, W. L. Holzapfel, S. Hoover, Z. Hou, J. D. Hrubes, N. Huang, J. Hubmayr, K. D. Irwin, R. Keisler, L. Knox, A. T. Lee, E. M. Leitch, D. Li, C. Liang, D. Luong-Van, J. J. McMahon, J. Mehl, S. S. Meyer, L. Mocanu, T. E. Montroy, T. Natoli, J. P. Nibarger, V. Novosad, S. Padin, C. Pryke, C. L. Reichardt, J. E. Ruhl, B. R. Saliwanchik, J. T. Sayre, K. K. Schaffer, G. Smecher, A. A. Stark, K. T. Story, C. Tucker, K. Vanderlinde, J. D. Vieira, G. Wang, N. Whitehorn, V. Yefremenko, and O. Zahn. Measurements of E-Mode Polarization and Temperature-E-Mode Correlation in the Cosmic Microwave Background from 100 Square Degrees of SPTpol Data. *Astrophys. J.*, 805:36, May 2015.

[118] Csaba Csaki, Nemanja Kaloper, Javi Serra, and John Terning. Inflation from Broken Scale Invariance. *Phys. Rev. Lett.*, 113:161302, 2014.

[119] T. Culverhouse, P. Ade, J. Bock, M. Bowden, M. L. Brown, G. Cahill, P. G. Castro, S. E. Church, R. Friedman, K. Ganga, W. K. Gear, S. Gupta, J. R. Hinderks, J. Kovac, A. E. Lange, E. Leitch, S. J. Melhuish, Y. Memari, J. A. Murphy, A. Orlando, R. Schwarz, C. O'Sullivan, L. Piccirillo, C. Pryke, N. Rajguru, B. Rusholme, A. N. Taylor, K. L. Thompson, A. H. Turner, E. Y. S. Wu, M. Zemcov, and QUaD Collaboration. The QUaD Galactic Plane Survey. I. Maps and Analysis of Diffuse Emission. *The Astrophysical Journal*, 722:1057–1077, October 2010.

[120] Richard H. Cyburt, Brian D. Fields, and Keith A. Olive. The NACRE thermonuclear reaction compilation and big bang nucleosynthesis. *New Astron.*, 6:215–238, 2001.

[121] Richard H. Cyburt, Brian D. Fields, Keith A. Olive, and Tsung-Han Yeh. Big Bang Nucleosynthesis: 2015. 2015.

[122] Francis-Yan Cyr-Racine, Roland de Putter, Alvise Raccanelli, and Kris Sigurdson. Constraints on Large-Scale Dark Acoustic Oscillations from Cosmology. *Phys. Rev. D*, 89(6):063517, 2014.

[123] Francis-Yan Cyr-Racine and Kris Sigurdson. Cosmology of atomic dark matter. *Phys. Rev.*, D87(10):103515, 2013.

[124] Francis-Yan Cyr-Racine and Kris Sigurdson. The cosmology of atomic dark matter. *Phys. Rev. D*, 87:103515, 2013.

[125] Francis-Yan Cyr-Racine and Kris Sigurdson. Limits on Neutrino-Neutrino Scattering in the Early Universe. *Phys. Rev.*, D90(12):123533, 2014.

[126] Francis-Yan Cyr-Racine, Kris Sigurdson, Jesus Zavala, Torsten Bringmann, Mark Vogelsberger, and Christoph Pfrommer. ETHOS - An Effective Theory of Structure Formation: From dark particle physics to the matter distribution of the Universe. 2015.

[127] W. J. G. de Blok and S. S. McGaugh. The Dark and visible matter content of low surface brightness disk galaxies. *Mon. Not. Roy. Astron. Soc.*, 290:533–552, 1997.

[128] Anton de la Fuente, Prashant Saraswat, and Raman Sundrum. Natural Inflation and Quantum Gravity. *Phys. Rev. Lett.*, 114(15):151303, 2015.

[129] A. A. de Laix, R. J. Scherrer, and R. K. Schaefer. Constraints on Self-interacting Dark Matter. *Ap. J.* , 452:495, October 1995.

[130] J. Delabrouille and J.-F. Cardoso. Diffuse Source Separation in CMB Observations. In V. J. Martínez, E. Saar, E. Martínez-González, and M.-J. Pons-Bordería, editors, *Data Analysis in Cosmology*, volume 665 of *Lecture Notes in Physics, Berlin Springer Verlag*, pages 159–205, 2009.

[131] Eleonora Di Valentino, Elena Giusarma, Massimiliano Lattanzi, Olga Mena, Alessandro Melchiorri, and Joseph Silk. Cosmological Axion and neutrino mass constraints from Planck 2015 temperature and polarization data. *Phys. Lett.*, B752:182–185, 2016.

[132] Roberta Diamanti, Elena Giusarma, Olga Mena, Maria Archidiacono, and Alessandro Melchiorri. Dark Radiation and interacting scenarios. *Phys. Rev. D*, 87:063509, 2013.

[133] Emanuela Dimastrogiovanni, Matteo Fasiello, and Andrew J. Tolley. Low-Energy Effective Field Theory for Chromo-Natural Inflation. *JCAP*, 1302:046, 2013.

[134] Emanuela Dimastrogiovanni and Marco Peloso. Stability analysis of chromo-natural inflation and possible evasion of Lyth?s bound. *Phys. Rev.*, D87(10):103501, 2013.

[135] A. D. Dolgov. Neutrinos in cosmology. *Phys. Rept.*, 370:333–535, 2002.

[136] M. Donahue, G. M. Voit, I. Gioia, G. Luppino, J. P. Hughes, and J. T. Stocke. A Very Hot High-Redshift Cluster of Galaxies: More Trouble for $\Omega_0 = 1$. *Ap. J.* , 502:550–557, August 1998.

[137] S. L. Dubovsky. Phases of massive gravity. *JHEP*, 10:076, 2004.

[138] Sergei Dubovsky, Raphael Flauger, Alexei Starobinsky, and Igor Tkachev. Signatures of a Graviton Mass in the Cosmic Microwave Background. *Phys. Rev.*, D81:023523, 2010.

[139] R. Dünner, M. Hasselfield, T. A. Marriage, J. Sievers, V. Acquaviva, G. E. Addison, P. A. R. Ade, P. Aguirre, M. Amiri, J. W. Appel, L. F. Barrientos, E. S. Battistelli, J. R. Bond, B. Brown, B. Burger, E. Calabrese, J. Chervenak, S. Das, M. J. Devlin, S. R. Dicker, W. Bertrand Doriese, J. Dunkley, T. Essinger-Hileman, R. P. Fisher, M. B. Gralla, J. W. Fowler, A. Hajian, M. Halpern, C. Hernández-Monteagudo, G. C. Hilton, M. Hilton, A. D. Hincks, R. Hlozek, K. M. Huffenberger, D. H. Hughes, J. P. Hughes, L. Infante, K. D. Irwin, J. Baptiste Juin, M. Kaul, J. Klein, A. Kosowsky, J. M. Lau, M. Limon, Y.-T. Lin, T. Louis, R. H. Lupton, D. Marsden, K. Martocci, P. Mauskopf, F. Menanteau, K. Moodley, H. Moseley, C. B. Netterfield, M. D. Niemack, M. R. Nolta, L. A. Page, L. Parker, B. Partridge, H. Quintana, B. Reid, N. Sehgal, B. D. Sherwin, D. N. Spergel, S. T. Staggs, D. S. Swetz, E. R. Switzer, R. Thornton, H. Trac, C. Tucker, R. Warne, G. Wilson, E. Wollack, and Y. Zhao. The Atacama Cosmology Telescope: Data Characterization and Mapmaking. *The Astrophysical Journal*, 762:10, January 2013.

[140] Ruth Durrer and Andrii Neronov. Cosmological Magnetic Fields: Their Generation, Evolution and Observation. *Astron. Astrophys. Rev.*, 21:62, 2013.

[141] C. Dvorkin and K. M. Smith. Reconstructing patchy reionization from the cosmic microwave background. *Phys. Rev.* **D** , 79(4):043003, February 2009.

[142] Cora Dvorkin, Kfir Blum, and Marc Kamionkowski. Constraining Dark Matter-Baryon Scattering with Linear Cosmology. *Phys. Rev. D*, 89(2):023519, 2014.

[143] Cora Dvorkin, Kfir Blum, and Matias Zaldarriaga. Perturbed Recombination from Dark Matter Annihilation. *Phys. Rev.*, D87(10):103522, 2013.

[144] H. K. Eriksen, C. Dickinson, C. R. Lawrence, C. Baccigalupi, A. J. Banday, K. M. Górski, F. K. Hansen, P. B. Lilje, E. Pierpaoli, M. D. Seiffert, K. M. Smith, and K. Vanderlinde. Cosmic Microwave Background Component Separation by Parameter Estimation. *ApJ*, 641:665–682, April 2006.

[145] J. Errard, P. A. R. Ade, Y. Akiba, K. Arnold, M. Atlas, C. Baccigalupi, D. Barron, D. Boettger, J. Borrill, S. Chapman, Y. Chinone, A. Cukierman, J. Delabrouille, M. Dobbs, A. Ducout, T. Elleflot, G. Fabbian, C. Feng, S. Feeney, A. Gilbert, N. Goeckner-Wald, N. W. Halverson, M. Hasegawa, K. Hattori, M. Hazumi, C. Hill, W. L. Holzapfel, Y. Hori, Y. Inoue, G. C. Jaehnig, A. H. Jaffe, O. Jeong, N. Katayama, J. Kaufman, B. Keating, Z. Kermish, R. Keskitalo, T. Kisner, M. Le Jeune, A. T. Lee, E. M. Leitch, D. Leon, E. Linder, F. Matsuda, T. Matsumura, N. J. Miller, M. J. Myers, M. Navaroli, H. Nishino, T. Okamura, H. Paar, J. Peloton, D. Poletti, G. Puglisi, G. Rebeiz, C. L. Reichardt, P. L. Richards, C. Ross, K. M. Rotermund, D. E. Schenck, B. D. Sherwin, P. Siritanasak, G. Smecher, N. Stebor, B. Steinbach, R. Stompor, A. Suzuki, O. Tajima, S. Takakura, A. Tikhomirov, T. Tomaru, N. Whitehorn, B. Wilson, A. Yadav, and O. Zahn. Modeling Atmospheric Emission for CMB Ground-based Observations. *Astrophys. J.*, 809:63, August 2015.

[146] J. Errard, S. M. Feeney, H. V. Peiris, and A. H. Jaffe. Robust forecasts on fundamental physics from the foreground-obscured, gravitationally-lensed CMB polarization. *ArXiv e-prints*, September 2015.

[147] Miguel Escudero, Olga Mena, Aaron C. Vincent, Ryan J. Wilkinson, and Celine Boehm. Exploring dark matter microphysics with galaxy surveys. *jcap*, 1509(09):034, 2015.

[148] T. Essinger-Hileman, A. Ali, M. Amiri, J. W. Appel, D. Araujo, C. L. Bennett, F. Boone, M. Chan, H.-M. Cho, D. T. Chuss, F. Colazo, E. Crowe, K. Denis, R. Dünner, J. Eimer, D. Gothe, M. Halpern, K. Harrington, G. C. Hilton, G. F. Hinshaw, C. Huang, K. Irwin, G. Jones, J. Karakla, A. J. Kogut, D. Larson, M. Limon, L. Lowry, T. Marriage, N. Mehrle, A. D. Miller, N. Miller, S. H. Moseley, G. Novak, C. Reintsema, K. Rostem, T. Stevenson, D. Towner, K. U-Yen, E. Wagner, D. Watts, E. J. Wollack, Z. Xu, and L. Zeng. CLASS: the cosmology large angular scale surveyor. In *Society of Photo-Optical Instrumentation Engineers (SPIE) Conference Series*, volume 9153 of *Society of Photo-Optical Instrumentation Engineers (SPIE) Conference Series*, page 1, July 2014.

[149] Ji Ji Fan, Andrey Katz, Lisa Randall, and Matthew Reece. Dark-Disk Universe. *Phys. Rev. Lett.*, 110:211302, 2013.

[150] JiJi Fan, Andrey Katz, Lisa Randall, and Matthew Reece. Double-Disk Dark Matter. *Phys. Dark Univ.*, 2:139–156, 2013.

[151] Y. Fantaye, C. Baccigalupi, S. M. Leach, and A. P. S. Yadav. CMB lensing reconstruction in the presence of diffuse polarized foregrounds. *JCAP*, 12:017, December 2012.

[152] Y. Fantaye, F. Stivoli, J. Grain, S. M. Leach, M. Tristram, C. Baccigalupi, and R. Stompor. Estimating the tensor-to-scalar ratio and the effect of residual foreground contamination. *JCAP*, 8:001, August 2011.

[153] Jonathan L. Feng, Manoj Kaplinghat, Huitzu Tu, and Hai-Bo Yu. Hidden Charged Dark Matter. *jcap*, 0907:004, 2009.

[154] Ricardo Z. Ferreira and Martin S. Sloth. Universal Constraints on Axions from Inflation. *JHEP*, 12:139, 2014.

[155] Brian D. Fields. The primordial lithium problem. *Ann. Rev. Nucl. Part. Sci.*, 61:47–68, 2011.

[156] Lee Samuel Finn and Patrick J. Sutton. Bounding the mass of the graviton using binary pulsar observations. *Phys. Rev. D*, 65:044022, Jan 2002.

[157] Willy Fischler and Joel Meyers. Dark Radiation Emerging After Big Bang Nucleosynthesis? *Phys. Rev.*, D83:063520, 2011.

[158] Raphael Flauger, Daniel Green, and Rafael A. Porto. On squeezed limits in single-field inflation. Part I. *JCAP*, 1308:032, 2013.

[159] Raphael Flauger, Liam McAllister, Enrico Pajer, Alexander Westphal, and Gang Xu. Oscillations in the CMB from Axion Monodromy Inflation. *JCAP*, 1006:009, 2010.

[160] Raphael Flauger, Liam McAllister, Eva Silverstein, and Alexander Westphal. Drifting Oscillations in Axion Monodromy. 2014.

[161] Brent Follin, Lloyd Knox, Marius Millea, and Zhen Pan. First Detection of the Acoustic Oscillation Phase Shift Expected from the Cosmic Neutrino Background. *Phys. Rev. Lett.*, 115(9):091301, 2015.

[162] Robert Foot. Mirror matter-type dark matter. *Int. J. Mod. Phys.*, D13:2161–2192, 2004.

[163] Katherine Freese, Joshua A. Frieman, and Angela V. Olinto. Natural inflation with pseudo - Nambu-Goldstone bosons. *Phys.Rev.Lett.*, 65:3233–3236, 1990.

[164] Noemi Frusciante, Georgios Papadomanolakis, and Alessandra Silvestri. An Extended action for the effective field theory of dark energy: a stability analysis and a complete guide to the mapping at the basis of EFTCAMB. 2016.

[165] Noemi Frusciante, Marco Raveri, Daniele Vernieri, Bin Hu, and Alessandra Silvestri. Horava Gravity in the Effective Field Theory formalism: from cosmology to observational constraints. 2015.

[166] C. Giunti and E. M. Zavanin. Appearancedisappearance relation in $3 + N_s$ short-baseline neutrino oscillations. *Mod. Phys. Lett.*, A31(01):1650003, 2015.

[167] Carlo Giunti and Marco Laveder. Statistical Significance of the Gallium Anomaly. *Phys. Rev.*, C83:065504, 2011.

[168] Elena Giusarma, Eleonora Di Valentino, Massimiliano Lattanzi, Alessandro Melchiorri, and Olga Mena. Relic Neutrinos, thermal axions and cosmology in early 2014. *Phys. Rev.*, D90(4):043507, 2014.

[169] Jerome Gleyzes, David Langlois, Federico Piazza, and Filippo Vernizzi. Essential Building Blocks of Dark Energy. *JCAP*, 1308:025, 2013.

[170] Jrme Gleyzes, David Langlois, Federico Piazza, and Filippo Vernizzi. Healthy theories beyond Horndeski. *Phys. Rev. Lett.*, 114(21):211101, 2015.

[171] Jrme Gleyzes, David Langlois, and Filippo Vernizzi. A unifying description of dark energy. *Int. J. Mod. Phys.*, D23(13):1443010, 2015.

[172] V. Gluscevic, D. Hanson, M. Kamionkowski, and C. M. Hirata. First CMB constraints on direction-dependent cosmological birefringence from WMAP-7. *"PRD"*, 86(10):103529, November 2012.

[173] V. Gluscevic and M. Kamionkowski. Testing parity-violating mechanisms with cosmic microwave background experiments. *"PRD"*, 81(12):123529, June 2010.

[174] V. Gluscevic, M. Kamionkowski, and A. Cooray. Derotation of the cosmic microwave background polarization: Full-sky formalism. *PRD*, 80(2):023510, July 2009.

[175] Vera Gluscevic and Marc Kamionkowski. Testing Parity-Violating Mechanisms with Cosmic Microwave Background Experiments. *Phys. Rev.*, D81:123529, 2010.

[176] B. Gold, N. Odegard, J. L. Weiland, R. S. Hill, A. Kogut, C. L. Bennett, G. Hinshaw, X. Chen, J. Dunkley, M. Halpern, N. Jarosik, E. Komatsu, D. Larson, M. Limon, S. S. Meyer, M. R. Nolta, L. Page, K. M. Smith, D. N. Spergel, G. S. Tucker, E. Wollack, and E. L. Wright. Seven-year Wilkinson Microwave Anisotropy Probe (WMAP) Observations: Galactic Foreground Emission. *Ap. J. Suppl.* , 192:15, February 2011.

[177] Haim Goldberg and Lawrence J. Hall. A NEW CANDIDATE FOR DARK MATTER. *Phys. Lett.*, B174:151, 1986.

[178] A. B. Goncharov and Andrei D. Linde. Chaotic Inflation in Supergravity. *Phys. Lett.*, B139:27, 1984.

[179] B.-A. Gradwohl and J. A. Frieman. Dark matter, long-range forces, and large-scale structure. *Ap. J.* , 398:407–424, October 1992.

[180] Peter W. Graham, Igor G. Irastorza, Steven K. Lamoreaux, Axel Lindner, and Karl A. van Bibber. Experimental Searches for the Axion and Axion-Like Particles. *Ann. Rev. Nucl. Part. Sci.*, 65:485–514, 2015.

[181] Peter W. Graham, David E. Kaplan, and Surjeet Rajendran. Cosmological Relaxation of the Electroweak Scale. *Phys. Rev. Lett.*, 115(22):221801, 2015.

[182] Dario Grasso and Hector R. Rubinstein. Magnetic fields in the early universe. *Phys. Rept.*, 348:163–266, 2001.

[183] Anne M. Green, Stefan Hofmann, and Dominik J. Schwarz. The First wimpy halos. *JCAP*, 0508:003, 2005.

[184] E. Grohs, G. M. Fuller, C. T. Kishimoto, M. W. Paris, and A. Vlasenko. Neutrino energy transport in weak decoupling and big bang nucleosynthesis. 2015.

[185] Giulia Gubitosi, Federico Piazza, and Filippo Vernizzi. The Effective Field Theory of Dark Energy. *JCAP*, 1302:032, 2013. [JCAP1302,032(2013)].

[186] Alan H. Guth and Yasunori Nomura. What can the observation of nonzero curvature tell us? *Phys.Rev.*, D86:023534, 2012.

[187] D. Hanson, A. Challinor, G. Efstathiou, and P. Bielewicz. CMB temperature lensing power reconstruction. *Phys. Rev.* **D** , 83(4):043005, February 2011.

[188] D. L. Harrison, F. van Leeuwen, and M. A. J. Ashdown. A deconvolution map-making method for experiments with circular scanning strategies. *Astronomy and Astrophysics*, 532:A55, August 2011.

[189] M. Hasselfield, M. Hilton, T. A. Marriage, G. E. Addison, L. F. Barrientos, N. Battaglia, E. S. Battistelli, J. R. Bond, D. Crichton, S. Das, M. J. Devlin, S. R. Dicker, J. Dunkley, R. Dünner, J. W. Fowler, M. B. Gralla, A. Hajian, M. Halpern, A. D. Hincks, R. Hlozek, J. P. Hughes, L. Infante, K. D. Irwin, A. Kosowsky, D. Marsden, F. Menanteau, K. Moodley, M. D. Niemack, M. R. Nolta, L. A. Page, B. Partridge, E. D. Reese, B. L. Schmitt, N. Sehgal, B. D. Sherwin, J. Sievers, C. Sifón, D. N. Spergel, S. T. Staggs, D. S. Swetz, E. R. Switzer, R. Thornton, H. Trac, and E. J. Wollack. The Atacama Cosmology Telescope: Sunyaev-Zel'dovich selected galaxy clusters at 148 GHz from three seasons of data. *JCAP*, 7:8, July 2013.

[190] Arthur Hebecker, Jakob Moritz, Alexander Westphal, and Lukas T. Witkowski. Axion Monodromy Inflation with Warped KK-Modes. *Phys. Lett.*, B754:328–334, 2016.

[191] Ben Heidenreich, Matthew Reece, and Tom Rudelius. Sharpening the Weak Gravity Conjecture with Dimensional Reduction. 2015.

[192] Ben Heidenreich, Matthew Reece, and Tom Rudelius. Weak Gravity Strongly Constrains Large-Field Axion Inflation. *JHEP*, 12:108, 2015.

[193] M. B. Hindmarsh and T. W. B. Kibble. Cosmic strings. *Rept. Prog. Phys.*, 58:477–562, 1995.

[194] G. Hinshaw, M. R. Nolta, C. L. Bennett, R. Bean, O. Doré, M. R. Greason, M. Halpern, R. S. Hill, N. Jarosik, A. Kogut, E. Komatsu, M. Limon, N. Odegard, S. S. Meyer, L. Page, H. V. Peiris, D. N. Spergel, G. S. Tucker, L. Verde, J. L. Weiland, E. Wollack, and E. L. Wright. Three-Year Wilkinson Microwave Anisotropy Probe (WMAP) Observations: Temperature Analysis. *Ap. J. Suppl.* , 170:288–334, June 2007.

[195] Kurt Hinterbichler. Theoretical Aspects of Massive Gravity. *Rev. Mod. Phys.*, 84:671–710, 2012.

[196] C. M. Hirata and U. Seljak. Analyzing weak lensing of the cosmic microwave background using the likelihood function. *Phys. Rev.* **D** , 67(4):043001, February 2003.

[197] E. Hivon, K. M. Górski, C. B. Netterfield, B. P. Crill, S. Prunet, and F. Hansen. MASTER of the Cosmic Microwave Background Anisotropy Power Spectrum: A Fast Method for Statistical Analysis of Large and Complex Cosmic Microwave Background Data Sets. *Astrophys. J.*, 567:2–17, March 2002.

[198] Eric Hivon, Krzysztof M. Gorski, C. Barth Netterfield, Brendan P. Crill, Simon Prunet, and Frode Hansen. MASTER of the Cosmic Microwave Background Anisotropy Power Spectrum: A Fast Method for Statistical Analysis of Large and Complex Cosmic Microwave Background Data Sets. *The Astrophysical Journal*, 567(1):2–17, March 2002.

[199] R. Hlozek, D. Grin, D. J. E. Marsh, and P. G. Ferreira. A search for ultralight axions using precision cosmological data. *Phys. Rev.* **D** , 91(10):103512, May 2015.

[200] Dan Hooper, Farinaldo S. Queiroz, and Nickolay Y. Gnedin. Non-Thermal Dark Matter Mimicking An Additional Neutrino Species In The Early Universe. *Phys. Rev.*, D85:063513, 2012.

[201] Shaun Hotchkiss, Anupam Mazumdar, and Seshadri Nadathur. Observable gravitational waves from inflation with small field excursions. *JCAP*, 1202:008, 2012.

[202] Zhen Hou, Ryan Keisler, Lloyd Knox, Marius Millea, and Christian Reichardt. How Massless Neutrinos Affect the Cosmic Microwave Background Damping Tail. *Phys. Rev.*, D87:083008, 2013.

[203] W. Hu, R. Barkana, and A. Gruzinov. Fuzzy Cold Dark Matter: The Wave Properties of Ultralight Particles. *Physical Review Letters*, 85:1158–1161, August 2000.

[204] W. Hu and T. Okamoto. Mass Reconstruction with Cosmic Microwave Background Polarization. *Astrophys. J.*, 574:566–574, August 2002.

[205] Wayne Hu and Daniel J. Eisenstein. Small scale perturbations in a general MDM cosmology. *Astrophys.J.*, 498:497, 1998.

[206] Wayne Hu, Daniel J. Eisenstein, and Max Tegmark. Weighing neutrinos with galaxy surveys. *Phys.Rev.Lett.*, 80:5255–5258, 1998.

[207] Wayne Hu and Takemi Okamoto. Mass reconstruction with cmb polarization. *Astrophys.J.*, 574:566–574, 2002.

[208] Patrick Huber. On the determination of anti-neutrino spectra from nuclear reactors. *Phys. Rev.*, C84:024617, 2011. [Erratum: Phys. Rev.C85,029901(2012)].

[209] Rachel Jeannerot. A Supersymmetric SO(10) model with inflation and cosmic strings. *Phys. Rev.*, D53:5426–5436, 1996.

[210] Rachel Jeannerot, Jonathan Rocher, and Mairi Sakellariadou. How generic is cosmic string formation in SUSY GUTs. *Phys. Rev.*, D68:103514, 2003.

[211] Raul Jimenez, P. Talavera, and Licia Verde. An effective theory of accelerated expansion. *Int. J. Mod. Phys.*, A27:1250174, 2012.

[212] Nicholas T. Jones, Horace Stoica, and S. H. Henry Tye. The Production, spectrum and evolution of cosmic strings in brane inflation. *Phys. Lett.*, B563:6–14, 2003.

[213] Katherine Jones-Smith, Lawrence M. Krauss, and Harsh Mathur. A Nearly Scale Invariant Spectrum of Gravitational Radiation from Global Phase Transitions. *Phys. Rev. Lett.*, 100:131302, 2008.

[214] Shahab Joudaki, Kevork N. Abazajian, and Manoj Kaplinghat. Are Light Sterile Neutrinos Preferred or Disfavored by Cosmology? *Phys.Rev.*, D87:065003, 2013.

[215] Renata Kallosh and Andrei Linde. Universality Class in Conformal Inflation. *JCAP*, 1307:002, 2013.

[216] Nemanja Kaloper, Albion Lawrence, and Lorenzo Sorbo. An Ignoble Approach to Large Field Inflation. *JCAP*, 1103:023, 2011.

[217] Nemanja Kaloper and Lorenzo Sorbo. A Natural Framework for Chaotic Inflation. *Phys. Rev. Lett.*, 102:121301, 2009.

[218] M. Kamionkowski. How to Derotate the Cosmic Microwave Background Polarization. *Physical Review Letters*, 102(11):111302, March 2009.

[219] David E. Kaplan, Gordan Z. Krnjaic, Keith R. Rehermann, and Christopher M. Wells. Atomic Dark Matter. *jcap*, 1005:021, 2010.

[220] David E. Kaplan, Gordan Z. Krnjaic, Keith R. Rehermann, and Christopher M. Wells. Dark Atoms: Asymmetry and Direct Detection. *JCAP*, 1110:011, 2011.

[221] David E. Kaplan and Riccardo Rattazzi. A Clockwork Axion. 2015.

[222] N. Katayama and E. Komatsu. Simple Foreground Cleaning Algorithm for Detecting Primordial B-mode Polarization of the Cosmic Microwave Background. *ApJ*, 737:78, August 2011.

[223] E. Keihänen, R. Keskitalo, H. Kurki-Suonio, T. Poutanen, and A.-S. Sirviö. Making cosmic microwave background temperature and polarization maps with MADAM. *Astronomy and Astrophysics*, 510:A57, February 2010.

[224] E. Keihänen, H. Kurki-Suonio, T. Poutanen, D. Maino, and C. Burigana. A maximum likelihood approach to the destriping technique. *Astronomy and Astrophysics*, 428:287–298, December 2004.

[225] E. Keihänen and M. Reinecke. ArtDeco: a beam-deconvolution code for absolute cosmic microwave background measurements. *Astronomy and Astrophysics*, 548:A110, December 2012.

[226] R. Keisler, S. Hoover, N. Harrington, J. W. Henning, P. A. R. Ade, K. A. Aird, J. E. Austermann, J. A. Beall, A. N. Bender, B. A. Benson, L. E. Bleem, J. E. Carlstrom, C. L. Chang, H. C. Chiang, H-M. Cho, R. Citron, T. M. Crawford, A. T. Crites, T. de Haan, M. A. Dobbs, W. Everett, J. Gallicchio, J. Gao, E. M. George, A. Gilbert, N. W. Halverson, D. Hanson, G. C. Hilton, G. P. Holder, W. L. Holzapfel, Z. Hou, J. D. Hrubes, N. Huang, J. Hubmayr, K. D. Irwin, L. Knox, A. T. Lee, E. M. Leitch, D. Li, D. Luong-Van, D. P. Marrone, J. J. McMahon, J. Mehl, S. S. Meyer, L. Mocanu, T. Natoli, J. P. Nibarger, V. Novosad, S. Padin, C. Pryke, C. L. Reichardt, J. E. Ruhl, B. R. Saliwanchik, J. T. Sayre, K. K. Schaffer, E. Shirokoff, G. Smecher, A. A. Stark, K. T. Story, C. Tucker, K. Vanderlinde, J. D. Vieira, G. Wang, N. Whitehorn, V. Yefremenko, and O. Zahn. Measurements of sub-degree b-mode polarization in the cosmic microwave background from 100 square degrees of sptpol data. *Astrophys. J.*, 807(2):151, 2015.

[227] Justin Khoury, Burt A. Ovrut, Paul J. Steinhardt, and Neil Turok. The Ekpyrotic universe: Colliding branes and the origin of the hot big bang. *Phys. Rev.*, D64:123522, 2001.

[228] Jihn E. Kim, Hans Peter Nilles, and Marco Peloso. Completing natural inflation. *JCAP*, 0501:005, 2005.

[229] Matthew Kleban and Marjorie Schillo. Spatial Curvature Falsifies Eternal Inflation. *JCAP*, 1206:029, 2012.

[230] Anatoly Klypin, Igor Karachentsev, Dmitry Makarov, and Olga Nasonova. Abundance of Field Galaxies. *Mon. Not. Roy. Astron. Soc.*, 454(2):1798–1810, 2015.

[231] Anatoly A. Klypin, Andrey V. Kravtsov, Octavio Valenzuela, and Francisco Prada. Where are the missing Galactic satellites? *Astrophys. J.*, 522:82–92, 1999.

[232] Lev Kofman, Andrei D. Linde, and Alexei A. Starobinsky. Nonthermal phase transitions after inflation. *Phys. Rev. Lett.*, 76:1011–1014, 1996.

[233] Eiichiro Komatsu and David N. Spergel. Acoustic signatures in the primary microwave background bispectrum. *Phys. Rev.*, D63:063002, 2001.

[234] Karta Kooner, Susha Parameswaran, and Ivonne Zavala. Warping the Weak Gravity Conjecture. 2015.

[235] Joachim Kopp, Pedro A. N. Machado, Michele Maltoni, and Thomas Schwetz. Sterile Neutrino Oscillations: The Global Picture. *JHEP*, 05:050, 2013.

[236] Arthur Kosowsky and Suman Bhattacharya. A Future Test of Gravitation Using Galaxy Cluster Velocities. *Phys. Rev.*, D80:062003, 2009.

[237] Arthur Kosowsky, Tina Kahniashvili, George Lavrelashvili, and Bharat Ratra. Faraday rotation of the Cosmic Microwave Background polarization by a stochastic magnetic field. *Phys. Rev.*, D71:043006, 2005.

[238] Lawrence M. Krauss. Gravitational waves from global phase transitions. *Phys. Lett.*, B284:229–233, 1992.

[239] A. V. Kravtsov and S. Borgani. Formation of Galaxy Clusters. *Ann. Rev. Astron. Astroph.*, 50:353–409, September 2012.

[240] Kerstin E. Kunze and Eiichiro Komatsu. Constraints on primordial magnetic fields from the optical depth of the cosmic microwave background. *JCAP*, 1506(06):027, 2015.

[241] Paul D. Lasky et al. Gravitational-wave cosmology across 29 decades in frequency. 2015.

[242] Andrei Lazanu and Paul Shellard. Constraints on the Nambu-Goto cosmic string contribution to the CMB power spectrum in light of new temperature and polarisation data. *JCAP*, 1502(02):024, 2015.

[243] Jean-Luc Lehners and Sebastien Renaux-Petel. Multifield Cosmological Perturbations at Third Order and the Ekpyrotic Trispectrum. *Phys. Rev.*, D80:063503, 2009.

[244] Julien Lesgourgues, Gustavo Marques-Tavares, and Martin Schmaltz. Evidence for dark matter interactions in cosmological precision data? *JCAP*, 1602(02):037, 2016.

[245] Julien Lesgourgues and Sergio Pastor. Massive neutrinos and cosmology. *Phys.Rept.*, 429:307–379, 2006.

[246] A. Lewis and S. Bridle. Cosmological parameters from CMB and other data: A Monte Carlo approach. *Phys. Rev.* **D** , 66(10):103511–+, November 2002.

[247] A. Lewis, A. Challinor, and D. Hanson. The shape of the CMB lensing bispectrum. *JCAP*, 3:18, March 2011.

[248] Antony Lewis. CMB anisotropies from primordial inhomogeneous magnetic fields. *Phys. Rev.*, D70:043011, 2004.

[249] C. Li, T. L. Smith, and A. Cooray. Non-Gaussian covariance of CMB B modes of polarization and parameter degradation. *Phys. Rev.* **D** , 75(8):083501, April 2007.

[250] Andrei D. Linde. Chaotic Inflation. *Phys.Lett.*, B129:177–181, 1983.

[251] Andrei D. Linde. Particle physics and inflationary cosmology. *Contemp. Concepts Phys.*, 5:1–362, 1990.

[252] Joanes Lizarraga, Jon Urrestilla, David Daverio, Mark Hindmarsh, Martin Kunz, and Andrew R. Liddle. Constraining topological defects with temperature and polarization anisotropies. *Phys. Rev.*, D90(10):103504, 2014.

[253] Marilena LoVerde, Elliot Nelson, and Sarah Shandera. Non-Gaussian Mode Coupling and the Statistical Cosmological Principle. *JCAP*, 1306:024, 2013.

[254] A. Lue, L. Wang, and M. Kamionkowski. Cosmological Signature of New Parity-Violating Interactions. *Physical Review Letters*, 83:1506–1509, August 1999.

[255] Arthur Lue, Li-Min Wang, and Marc Kamionkowski. Cosmological signature of new parity violating interactions. *Phys. Rev. Lett.*, 83:1506–1509, 1999.

[256] David H. Lyth. What would we learn by detecting a gravitational wave signal in the cosmic microwave background anisotropy? *Phys.Rev.Lett.*, 78:1861–1863, 1997.

[257] David H. Lyth and David Wands. Generating the curvature perturbation without an inflaton. *Phys. Lett.*, B524:5–14, 2002.

[258] Chung-Pei Ma. Linear power spectra in cold + hot dark matter models: Analytical approximations and applications. *Astrophys. J.*, 471:13–23, 1996.

[259] M. E. Machacek. Growth of adiabatic perturbations in self-interacting dark matter. *Ap. J.* , 431:41–51, August 1994.

[260] Andrew Mack, Tina Kahniashvili, and Arthur Kosowsky. Microwave background signatures of a primordial stochastic magnetic field. *Phys. Rev.*, D65:123004, 2002.

[261] Mathew S. Madhavacheril, Neelima Sehgal, and Tracy R. Slatyer. Current Dark Matter Annihilation Constraints from CMB and Low-Redshift Data. *Phys. Rev.*, D89:103508, 2014.

[262] Juan M. Maldacena and Guilherme L. Pimentel. On graviton non-Gaussianities during inflation. *JHEP*, 09:045, 2011.

[263] Juan Martin Maldacena. Non-Gaussian features of primordial fluctuations in single field inflationary models. *JHEP*, 05:013, 2003.

[264] A. Maleknejad and M. M. Sheikh-Jabbari. Gauge-flation: Inflation From Non-Abelian Gauge Fields. *Phys. Lett.*, B723:224–228, 2013.

[265] Gianpiero Mangano, Alessandro Melchiorri, Paolo Serra, Asantha Cooray, and Marc Kamionkowski. Cosmological bounds on dark matter-neutrino interactions. *Phys. Rev. D*, 74:043517, 2006.

[266] Gianpiero Mangano, Gennaro Miele, Sergio Pastor, Teguayco Pinto, Ofelia Pisanti, et al. Relic neutrino decoupling including flavor oscillations. *Nucl.Phys.*, B729:221–234, 2005.

[267] A. Mantz, S. W. Allen, D. Rapetti, and H. Ebeling. The observed growth of massive galaxy clusters - I. Statistical methods and cosmological constraints. *Mon. Not. Roy. Astron. Soc.*, 406:1759–1772, August 2010.

[268] A. B. Mantz, S. W. Allen, R. G. Morris, D. A. Rapetti, D. E. Applegate, P. L. Kelly, A. von der Linden, and R. W. Schmidt. Cosmology and astrophysics from relaxed galaxy clusters - II. Cosmological constraints. *Mon. Not. Roy. Astron. Soc.*, 440:2077–2098, May 2014.

[269] A. B. Mantz, A. von der Linden, S. W. Allen, D. E. Applegate, P. L. Kelly, R. G. Morris, D. A. Rapetti, R. W. Schmidt, S. Adhikari, M. T. Allen, P. R. Burchat, D. L. Burke, M. Cataneo, D. Donovan, H. Ebeling, S. Shandera, and A. Wright. Weighing the giants - IV. Cosmology and neutrino mass. *Mon. Not. Roy. Astron. Soc.*, 446:2205–2225, January 2015.

[270] Fernando Marchesano, Gary Shiu, and Angel M. Uranga. F-term Axion Monodromy Inflation. *JHEP*, 09:184, 2014.

[271] D. J. E. Marsh and J. Silk. A model for halo formation with axion mixed dark matter. *Mon. Not. Roy. Astron. Soc.*, 437:2652–2663, January 2014.

[272] David J. E. Marsh. Axion Cosmology. 2015.

[273] E. Martínez-González, J. M. Diego, P. Vielva, and J. Silk. Cosmic microwave background power spectrum estimation and map reconstruction with the expectation-maximization algorithm. *Mon. Not. Roy. Astron. Soc.*, 345:1101–1109, November 2003.

[274] Liam McAllister, Eva Silverstein, and Alexander Westphal. Gravity Waves and Linear Inflation from Axion Monodromy. *Phys.Rev.*, D82:046003, 2010.

[275] Liam McAllister, Eva Silverstein, Alexander Westphal, and Timm Wrase. The Powers of Monodromy. *JHEP*, 09:123, 2014.

[276] Samuel D. McDermott, Hai-Bo Yu, and Kathryn M. Zurek. Turning off the Lights: How Dark is Dark Matter? *Phys. Rev. D*, 83:063509, 2011.

[277] P. Daniel Meerburg. Alleviating the tension at low ℓ through axion monodromy. *Phys. Rev.*, D90(6):063529, 2014.

[278] P. Daniel Meerburg, Rene Hloek, Boryana Hadzhiyska, and Joel Meyers. Multiwavelength constraints on the inflationary consistency relation. *Phys. Rev.*, D91(10):103505, 2015.

[279] P. Daniel Meerburg and Enrico Pajer. Observational Constraints on Gauge Field Production in Axion Inflation. *JCAP*, 1302:017, 2013.

[280] Justin L. Menestrina and Robert J. Scherrer. Dark Radiation from Particle Decays during Big Bang Nucleosynthesis. *Phys. Rev.*, D85:047301, 2012.

[281] G. Mention, M. Fechner, Th. Lasserre, Th. A. Mueller, D. Lhuillier, M. Cribier, and A. Letourneau. The Reactor Antineutrino Anomaly. *Phys. Rev.*, D83:073006, 2011.

[282] Marius Millea, Lloyd Knox, and Brian Fields. New Bounds for Axions and Axion-Like Particles with keV-GeV Masses. *Phys. Rev.*, D92(2):023010, 2015.

[283] Mehrdad Mirbabayi, Leonardo Senatore, Eva Silverstein, and Matias Zaldarriaga. Gravitational Waves and the Scale of Inflation. *Phys. Rev.*, D91:063518, 2015.

[284] Ben Moore, Sebastiano Ghigna, Fabio Governato, George Lake, Tom Quinn, Joachim Stadel, and Paolo Tozzi. Dark matter substructure in galactic halos. *Ap. J.* , 524:L19–L22, 1999.

[285] Adam Moss and Levon Pogosian. Did BICEP2 see vector modes? First B-mode constraints on cosmic defects. *Phys. Rev. Lett.*, 112:171302, 2014.

[286] Eva-Maria Mueller, Francesco de Bernardis, Rachel Bean, and Michael D. Niemack. Constraints on gravity and dark energy from the pairwise kinematic Sunyaev-Zeldovich effect. *Astrophys. J.*, 808(1):47, 2015.

[287] Eva-Maria Mueller, Francesco de Bernardis, Rachel Bean, and Michael D. Niemack. Constraints on massive neutrinos from the pairwise kinematic Sunyaev-Zeldovich effect. *Phys. Rev.*, D92(6):063501, 2015.

[288] Viatcheslav Mukhanov. Quantum Cosmological Perturbations: Predictions and Observations. *Eur. Phys. J.*, C73:2486, 2013.

[289] S. Naess, M. Hasselfield, J. McMahon, M. D. Niemack, G. E. Addison, P. A. R. Ade, R. Allison, M. Amiri, N. Battaglia, J. A. Beall, F. de Bernardis, J. R. Bond, J. Britton, E. Calabrese, H.-m. Cho, K. Coughlin, D. Crichton, S. Das, R. Datta, M. J. Devlin, S. R. Dicker, J. Dunkley, R. Dünner, J. W. Fowler, A. E. Fox, P. Gallardo, E. Grace, M. Gralla, A. Hajian, M. Halpern, S. Henderson, J. C. Hill, G. C. Hilton, M. Hilton, A. D. Hincks, R. Hlozek, P. Ho, J. Hubmayr, K. M. Huffenberger, J. P. Hughes, L. Infante, K. Irwin, R. Jackson, S. Muya Kasanda, J. Klein, B. Koopman, A. Kosowsky, D. Li, T. Louis, M. Lungu, M. Madhavacheril, T. A. Marriage, L. Maurin, F. Menanteau, K. Moodley, C. Munson, L. Newburgh, J. Nibarger, M. R. Nolta, L. A. Page, C. Pappas, B. Partridge, F. Rojas,

B. L. Schmitt, N. Sehgal, B. D. Sherwin, J. Sievers, S. Simon, D. N. Spergel, S. T. Staggs, E. R. Switzer, R. Thornton, H. Trac, C. Tucker, M. Uehara, A. Van Engelen, J. T. Ward, and E. J. Wollack. The Atacama Cosmology Telescope: CMB polarization at $200 < l < 9000$. *JCAP*, 10:7, October 2014.

[290] D. Nagai. The Impact of Galaxy Formation on the Sunyaev-Zel'dovich Effect of Galaxy Clusters. *Astrophys. J.*, 650:538–549, October 2006.

[291] D. Nagai, A. V. Kravtsov, and A. Vikhlinin. Effects of Galaxy Formation on Thermodynamics of the Intracluster Medium. *Astrophys. J.*, 668:1–14, October 2007.

[292] Ryo Namba, Emanuela Dimastrogiovanni, and Marco Peloso. Gauge-flation confronted with Planck. *JCAP*, 1311:045, 2013.

[293] Ryo Namba, Marco Peloso, Maresuke Shiraishi, Lorenzo Sorbo, and Caner Unal. Scale-dependent gravitational waves from a rolling axion. *JCAP*, 1601(01):041, 2016.

[294] T. Namikawa, D. Hanson, and R. Takahashi. Bias-hardened CMB lensing. *Mon. Not. Roy. Astron. Soc.*, 431:609–620, May 2013.

[295] Elliot Nelson and Sarah Shandera. Statistical Naturalness and non-Gaussianity in a Finite Universe. *Phys. Rev. Lett.*, 110(13):131301, 2013.

[296] Sami Nurmi, Christian T. Byrnes, and Gianmassimo Tasinato. A non-Gaussian landscape. *JCAP*, 1306:004, 2013.

[297] Se-Heon Oh, W. J. G. de Blok, Elias Brinks, Fabian Walter, and Robert C. Kennicutt, Jr. Dark and luminous matter in THINGS dwarf galaxies. *Astron. J.*, 141:193, 2011.

[298] T. Okamoto and W. Hu. Cosmic microwave background lensing reconstruction on the full sky. *Phys. Rev.* **D** , 67(8):083002–+, April 2003.

[299] K. A. Olive et al. Review of Particle Physics. *Chin. Phys.*, C38:090001, 2014.

[300] Kyle A. Oman et al. The unexpected diversity of dwarf galaxy rotation curves. *Mon. Not. Roy. Astron. Soc.*, 452(4):3650–3665, 2015.

[301] Nikhil Padmanabhan and Douglas P. Finkbeiner. Detecting dark matter annihilation with CMB polarization: Signatures and experimental prospects. *Phys. Rev.*, D72:023508, 2005.

[302] L. Page, G. Hinshaw, E. Komatsu, M. R. Nolta, D. N. Spergel, C. L. Bennett, C. Barnes, R. Bean, O. Doré, J. Dunkley, M. Halpern, R. S. Hill, N. Jarosik, A. Kogut, M. Limon, S. S. Meyer, N. Odegard, H. V. Peiris, G. S. Tucker, L. Verde, J. L. Weiland, E. Wollack, and E. L. Wright. Three-Year Wilkinson Microwave Anisotropy Probe (WMAP) Observations: Polarization Analysis. *Ap. J. Suppl.* , 170:335–376, June 2007.

[303] Eran Palti and Timo Weigand. Towards large r from [p, q]-inflation. *JHEP*, 04:155, 2014.

[304] Daniela Paoletti and Fabio Finelli. CMB Constraints on a Stochastic Background of Primordial Magnetic Fields. *Phys. Rev.*, D83:123533, 2011.

[305] Emmanouil Papastergis, Ann M. Martin, Riccardo Giovanelli, and Martha P. Haynes. The velocity width function of galaxies from the 40% ALFALFA survey: shedding light on the cold dark matter overabundance problem. *Astrophys. J.*, 739:38, 2011.

[306] Papastergis, E., Giovanelli, R., Haynes, M. P., and Shankar, F. Is there a "too big to fail" problem in the field? *A & A* , 574:A113, 2015.

[307] Minjoon Park, Kathryn M. Zurek, and Scott Watson. A Unified Approach to Cosmic Acceleration. *Phys. Rev.*, D81:124008, 2010.

[308] Marcel S. Pawlowski, Pavel Kroupa, and Helmut Jerjen. Dwarf galaxy planes: the discovery of symmetric structures in the local group. *Monthly Notices of the Royal Astronomical Society*, 435(3):1928–1957, 2013.

[309] R. D. Peccei and Helen R. Quinn. CP Conservation in the Presence of Instantons. *Phys. Rev. Lett.*, 38:1440–1443, 1977.

[310] Federico Piazza and Filippo Vernizzi. Effective Field Theory of Cosmological Perturbations. *Class. Quant. Grav.*, 30:214007, 2013.

[311] A. Pillepich, C. Porciani, and T. H. Reiprich. The X-ray cluster survey with eRosita: forecasts for cosmology, cluster physics and primordial non-Gaussianity. *Mon. Not. Roy. Astron. Soc.*, 422:44–69, May 2012.

[312] O. Pisanti, A. Cirillo, S. Esposito, F. Iocco, G. Mangano, G. Miele, and P. D. Serpico. PArthENoPE: Public Algorithm Evaluating the Nucleosynthesis of Primordial Elements. *Comput. Phys. Commun.*, 178:956–971, 2008.

[313] Planck Collaboration, R. Adam, P. A. R. Ade, N. Aghanim, M. Arnaud, M. Ashdown, J. Aumont, C. Baccigalupi, A. J. Banday, R. B. Barreiro, and et al. Planck 2015 results. IX. Diffuse component separation: CMB maps. *ArXiv e-prints*, February 2015.

[314] Planck Collaboration, R. Adam, P. A. R. Ade, N. Aghanim, and et al. Planck 2015 results. VIII. High Frequency Instrument data processing: Calibration and maps. *ArXiv e-prints*, February 2015.

[315] Planck Collaboration, P. A. R. Ade, N. Aghanim, C. Armitage-Caplan, M. Arnaud, M. Ashdown, F. Atrio-Barandela, J. Aumont, H. Aussel, C. Baccigalupi, and et al. Planck 2013 results. XXIX. The Planck catalogue of Sunyaev-Zeldovich sources. *A & A* , 571:A29, November 2014.

[316] Planck Collaboration, P. A. R. Ade, N. Aghanim, C. Armitage-Caplan, M. Arnaud, M. Ashdown, F. Atrio-Barandela, J. Aumont, H. Aussel, C. Baccigalupi, and et al. Planck 2013 results. XXXII. The updated Planck catalogue of Sunyaev-Zeldovich sources. *A & A* , 581:A14, September 2015.

[317] Planck Collaboration, P. A. R. Ade, N. Aghanim, C. Armitage-Caplan, M. Arnaud, M. Ashdown, F. Atrio-Barandela, J. Aumont, C. Baccigalupi, A. J. Banday, and et al. Planck 2013 results. XVII. Gravitational lensing by large-scale structure. *A & A* , 571:A17, November 2014.

[318] Planck Collaboration, P. A. R. Ade, N. Aghanim, C. Armitage-Caplan, M. Arnaud, M. Ashdown, F. Atrio-Barandela, J. Aumont, C. Baccigalupi, A. J. Banday, and et al. Planck 2013 results. XVIII. The gravitational lensing-infrared background correlation. *A & A* , 571:A18, November 2014.

[319] Planck Collaboration, P. A. R. Ade, N. Aghanim, M. Ashdown, J. Aumont, C. Baccigalupi, A. J. Banday, R. B. Barreiro, N. Bartolo, E. Battaner, K. Benabed, A. Benoît, A. Benoit-Lévy, J.-P. Bernard, M. Bersanelli, P. Bielewicz, A. Bonaldi, L. Bonavera, J. R. Bond, J. Borrill, F. R. Bouchet, M. Bucher, C. Burigana, R. C. Butler, E. Calabrese, J.-F. Cardoso, A. Catalano, A. Chamballu, R.-R. Chary, P. R. Christensen, S. Colombi, L. P. L. Colombo, B. P. Crill, A. Curto, F. Cuttaia, L. Danese, R. D. Davies, R. J. Davis, P. de Bernardis, A. de Rosa, G. de Zotti, J. Delabrouille, C. Dickinson, J. M. Diego, H. Dole, S. Donzelli, O. Doré, M. Douspis, A. Ducout, X. Dupac, G. Efstathiou, F. Elsner, T. A. Enßlin, H. K. Eriksen, J. Fergusson, F. Finelli, O. Forni, M. Frailis, E. Franceschi, A. Frejsel, S. Galeotta, S. Galli, K. Ganga, M. Giard, Y. Giraud-Héraud, E. Gjerløw, J. González-Nuevo, K. M.

Górski, S. Gratton, A. Gregorio, A. Gruppuso, F. K. Hansen, D. Hanson, D. L. Harrison, S. Henrot-Versillé, D. Herranz, S. R. Hildebrandt, E. Hivon, M. Hobson, W. A. Holmes, A. Hornstrup, W. Hovest, K. M. Huffenberger, G. Hurier, A. H. Jaffe, T. R. Jaffe, M. Juvela, E. Keihänen, R. Keskitalo, K. Kiiveri, T. S. Kisner, J. Knoche, M. Kunz, H. Kurki-Suonio, A. Lähteenmäki, J.-M. Lamarre, A. Lasenby, M. Lattanzi, C. R. Lawrence, J. P. Leahy, R. Leonardi, J. Lesgourgues, F. Levrier, M. Liguori, P. B. Lilje, M. Linden-Vørnle, V. Lindholm, M. López-Caniego, P. M. Lubin, J. F. Macías-Pérez, G. Maggio, D. Maino, N. Mandolesi, A. Mangilli, P. G. Martin, E. Martínez-González, S. Masi, S. Matarrese, P. Mazzotta, P. McGehee, P. R. Meinhold, A. Melchiorri, L. Mendes, A. Mennella, M. Migliaccio, S. Mitra, L. Montier, G. Morgante, D. Mortlock, A. Moss, D. Munshi, J. A. Murphy, P. Naselsky, F. Nati, P. Natoli, C. B. Netterfield, H. U. Nørgaard-Nielsen, D. Novikov, I. Novikov, F. Paci, L. Pagano, D. Paoletti, B. Partridge, F. Pasian, G. Patanchon, T. J. Pearson, O. Perdereau, L. Perotto, F. Perrotta, V. Pettorino, E. Pierpaoli, D. Pietrobon, E. Pointecouteau, G. Polenta, G. W. Pratt, G. Prézeau, S. Prunet, J.-L. Puget, J. P. Rachen, R. Rebolo, M. Reinecke, M. Remazeilles, A. Renzi, G. Rocha, C. Rosset, M. Rossetti, G. Roudier, J. A. Rubiño-Martín, B. Rusholme, M. Sandri, D. Santos, M. Savelainen, D. Scott, M. D. Seiffert, E. P. S. Shellard, L. D. Spencer, V. Stolyarov, R. Stompor, D. Sutton, A.-S. Suur-Uski, J.-F. Sygnet, J. A. Tauber, L. Terenzi, L. Toffolatti, M. Tomasi, M. Tristram, M. Tucci, J. Tuovinen, L. Valenziano, J. Valiviita, B. Van Tent, T. Vassallo, P. Vielva, F. Villa, L. A. Wade, B. D. Wandelt, R. Watson, I. K. Wehus, D. Yvon, A. Zacchei, and A. Zonca. Planck 2015 results. VI. LFI mapmaking. *ArXiv e-prints*, February 2015.

[320] Planck Collaboration, N. Aghanim, M. Arnaud, M. Ashdown, J. Aumont, C. Baccigalupi, A. J. Banday, R. B. Barreiro, J. G. Bartlett, N. Bartolo, and et al. Planck 2015 results. XI. CMB power spectra, likelihoods, and robustness of parameters. *ArXiv e-prints*, July 2015.

[321] Levon Pogosian, Amit P. S. Yadav, Yi-Fung Ng, and Tanmay Vachaspati. Primordial Magnetism in the CMB: Exact Treatment of Faraday Rotation and WMAP7 Bounds. *Phys. Rev.*, D84:043530, 2011. [Erratum: Phys. Rev.D84,089903(2011)].

[322] T. Poutanen, D. Maino, H. Kurki-Suonio, E. Keihänen, and E. Hivon. Cosmic microwave background power spectrum estimation with the destriping technique. *MNRAS*, 353:43–58, September 2004.

[323] Layne C. Price, Hiranya V. Peiris, Jonathan Frazer, and Richard Easther. Gravitational wave consistency relations for multifield inflation. *Phys. Rev. Lett.*, 114(3):031301, 2015.

[324] Stefano Profumo, Kris Sigurdson, and Marc Kamionkowski. What mass are the smallest protohalos? *Phys. Rev. Lett.*, 97:031301, 2006.

[325] Georg G. Raffelt. Neutrinos and the stars. *Proc. Int. Sch. Phys. Fermi*, 182:61–143, 2012.

[326] D. Rapetti, C. Blake, S. W. Allen, A. Mantz, D. Parkinson, and F. Beutler. A combined measurement of cosmic growth and expansion from clusters of galaxies, the CMB and galaxy clustering. *Mon. Not. Roy. Astron. Soc.*, 432:973–985, June 2013.

[327] Bharat Ratra. Cosmological 'seed' magnetic field from inflation. *Astrophys. J.*, 391:L1–L4, 1992.

[328] Marco Raveri, Bin Hu, Noemi Frusciante, and Alessandra Silvestri. Effective Field Theory of Cosmic Acceleration: constraining dark energy with CMB data. *Phys. Rev.*, D90(4):043513, 2014.

[329] C. L. Reichardt, B. Stalder, L. E. Bleem, T. E. Montroy, K. A. Aird, K. Andersson, R. Armstrong, M. L. N. Ashby, M. Bautz, M. Bayliss, G. Bazin, B. A. Benson, M. Brodwin, J. E. Carlstrom, C. L. Chang, H. M. Cho, A. Clocchiatti, T. M. Crawford, A. T. Crites, T. de Haan, S. Desai, M. A. Dobbs, J. P. Dudley, R. J. Foley, W. R. Forman, E. M. George, M. D. Gladders, A. H. Gonzalez, N. W. Halverson, N. L. Harrington, F. W. High, G. P. Holder, W. L. Holzapfel, S. Hoover, J. D. Hrubes,

C. Jones, M. Joy, R. Keisler, L. Knox, A. T. Lee, E. M. Leitch, J. Liu, M. Lueker, D. Luong-Van, A. Mantz, D. P. Marrone, M. McDonald, J. J. McMahon, J. Mehl, S. S. Meyer, L. Mocanu, J. J. Mohr, S. S. Murray, T. Natoli, S. Padin, T. Plagge, C. Pryke, A. Rest, J. Ruel, J. E. Ruhl, B. R. Saliwanchik, A. Saro, J. T. Sayre, K. K. Schaffer, L. Shaw, E. Shirokoff, J. Song, H. G. Spieler, Z. Staniszewski, A. A. Stark, K. Story, C. W. Stubbs, R. Šuhada, A. van Engelen, K. Vanderlinde, J. D. Vieira, A. Vikhlinin, R. Williamson, O. Zahn, and A. Zenteno. Galaxy Clusters Discovered via the Sunyaev-Zel'dovich Effect in the First 720 Square Degrees of the South Pole Telescope Survey. *Astrophys. J.*, 763:127, February 2013.

[330] Sebastien Renaux-Petel and Krzysztof Turzynski. On reaching the adiabatic limit in multi-field inflation. *JCAP*, 1506(06):010, 2015.

[331] Jonathan Rocher and Mairi Sakellariadou. D-term inflation, cosmic strings, and consistency with cosmic microwave background measurement. *Phys. Rev. Lett.*, 94:011303, 2005.

[332] Diederik Roest. Universality classes of inflation. *JCAP*, 1401:007, 2014.

[333] Tom Rudelius. Constraints on Axion Inflation from the Weak Gravity Conjecture. *JCAP*, 1509(09):020, 2015.

[334] Tom Rudelius. On the Possibility of Large Axion Moduli Spaces. *JCAP*, 1504(04):049, 2015.

[335] D.S. Salopek, J.R. Bond, and James M. Bardeen. Designing Density Fluctuation Spectra in Inflation. *Phys.Rev.*, D40:1753, 1989.

[336] Saswat Sarangi and S. H. Henry Tye. Cosmic string production towards the end of brane inflation. *Phys. Lett.*, B536:185–192, 2002.

[337] S. Schael et al. Precision electroweak measurements on the Z resonance. *Phys. Rept.*, 427:257–454, 2006.

[338] K. K. Schaffer, T. M. Crawford, K. A. Aird, B. A. Benson, L. E. Bleem, J. E. Carlstrom, C. L. Chang, H. M. Cho, A. T. Crites, T. de Haan, M. A. Dobbs, E. M. George, N. W. Halverson, G. P. Holder, W. L. Holzapfel, S. Hoover, J. D. Hrubes, M. Joy, R. Keisler, L. Knox, A. T. Lee, E. M. Leitch, M. Lueker, D. Luong-Van, J. J. McMahon, J. Mehl, S. S. Meyer, J. J. Mohr, T. E. Montroy, S. Padin, T. Plagge, C. Pryke, C. L. Reichardt, J. E. Ruhl, E. Shirokoff, H. G. Spieler, B. Stalder, Z. Staniszewski, A. A. Stark, K. Story, K. Vanderlinde, J. D. Vieira, and R. Williamson. The First Public Release of South Pole Telescope Data: Maps of a 95 deg^2 Field from 2008 Observations. *The Astrophysical Journal*, 743:90, December 2011.

[339] M. M. Schmittfull, A. Challinor, D. Hanson, and A. Lewis. Joint analysis of CMB temperature and lensing-reconstruction power spectra. *Phys. Rev.* **D** , 88(6):063012, September 2013.

[340] Uros Seljak and Anze Slosar. B polarization of cosmic microwave background as a tracer of strings. *Phys. Rev.*, D74:063523, 2006.

[341] Leonardo Senatore, Eva Silverstein, and Matias Zaldarriaga. New Sources of Gravitational Waves during Inflation. *JCAP*, 1408:016, 2014.

[342] Pasquale Dario Serpico, S. Esposito, F. Iocco, G. Mangano, G. Miele, and O. Pisanti. Nuclear reaction network for primordial nucleosynthesis: A Detailed analysis of rates, uncertainties and light nuclei yields. *JCAP*, 0412:010, 2004.

[343] Paolo Serra, Federico Zalamea, Asantha Cooray, Gianpiero Mangano, and Alessandro Melchiorri. Constraints on neutrino – dark matter interactions from cosmic microwave background and large scale structure data. *Phys. Rev. D*, 81:043507, 2010.

[344] J. Richard Shaw and Antony Lewis. Massive Neutrinos and Magnetic Fields in the Early Universe. *Phys. Rev.*, D81:043517, 2010.

[345] B. D. Sherwin and M. Schmittfull. Delensing the CMB with the cosmic infrared background. *Phys. Rev.* **D** , 92(4):043005, August 2015.

[346] Eva Silverstein and Alexander Westphal. Monodromy in the CMB: Gravity Waves and String Inflation. *Phys.Rev.*, D78:106003, 2008.

[347] G. Simard, D. Hanson, and G. Holder. Prospects for Delensing the Cosmic Microwave Background for Studying Inflation. *Ap. J.* , 807:166, July 2015.

[348] K. M. Smith. Pseudo-C_ℓ estimators which do not mix E and B modes. *Phys. Rev.* **D** , 74(8):083002–+, October 2006.

[349] K. M. Smith, D. Hanson, M. LoVerde, C. M. Hirata, and O. Zahn. Delensing CMB polarization with external datasets. *JCAP* , 6:014, June 2012.

[350] K. M. Smith, W. Hu, and M. Kaplinghat. Cosmological information from lensed CMB power spectra. *Phys. Rev.* **D** , 74(12):123002, December 2006.

[351] Lorenzo Sorbo. Parity violation in the Cosmic Microwave Background from a pseudoscalar inflaton. *JCAP*, 1106:003, 2011.

[352] Z. Staniszewski, P. A. R. Ade, K. A. Aird, B. A. Benson, L. E. Bleem, J. E. Carlstrom, C. L. Chang, H.-M. Cho, T. M. Crawford, A. T. Crites, T. de Haan, M. A. Dobbs, N. W. Halverson, G. P. Holder, W. L. Holzapfel, J. D. Hrubes, M. Joy, R. Keisler, T. M. Lanting, A. T. Lee, E. M. Leitch, A. Loehr, M. Lueker, J. J. McMahon, J. Mehl, S. S. Meyer, J. J. Mohr, T. E. Montroy, C.-C. Ngeow, S. Padin, T. Plagge, C. Pryke, C. L. Reichardt, J. E. Ruhl, K. K. Schaffer, L. Shaw, E. Shirokoff, H. G. Spieler, B. Stalder, A. A. Stark, K. Vanderlinde, J. D. Vieira, O. Zahn, and A. Zenteno. Galaxy Clusters Discovered with a Sunyaev-Zel'dovich Effect Survey. *Astrophys. J.*, 701:32–41, August 2009.

[353] Alexei A. Starobinsky. A New Type of Isotropic Cosmological Models Without Singularity. *Phys.Lett.*, B91:99–102, 1980.

[354] Gary Steigman. Equivalent Neutrinos, Light WIMPs, and the Chimera of Dark Radiation. *Phys. Rev.*, D87(10):103517, 2013.

[355] Andrew Stewart and Robert Brandenberger. Observational Constraints on Theories with a Blue Spectrum of Tensor Modes. *JCAP*, 0808:012, 2008.

[356] F. Stivoli, J. Grain, S. M. Leach, M. Tristram, C. Baccigalupi, and R. Stompor. Maximum likelihood, parametric component separation and CMB B-mode detection in suborbital experiments. *Mon. Not. Roy. Astron. Soc.*, 408:2319–2335, November 2010.

[357] Radek Stompor, Amedeo Balbi, Julian Borrill, Pedro Ferreira, Shaul Hanany, Andrew Jaffe, Adrian Lee, Sang Oh, Bahman Rabii, Paul Richards, George Smoot, Celeste Winant, and Jiun-Huei Wu. Making maps of the cosmic microwave background: The MAXIMA example. *Physical Review D*, 65(2):022003, December 2001.

[358] Alessandro Strumia and Francesco Vissani. Neutrino masses and mixings and... 2006.

[359] Kandaswamy Subramanian and John D. Barrow. Microwave background signals from tangled magnetic fields. *Phys. Rev. Lett.*, 81:3575–3578, 1998.

[360] R. A. Sunyaev and Y. B. Zel'dovich. The Observations of Relic Radiation as a Test of the Nature of X-Ray Radiation from the Clusters of Galaxies. *Comments on Astrophysics and Space Physics*, 4:173–+, November 1972.

[361] Tomohiro Takahashi and Jiro Soda. Chiral Primordial Gravitational Waves from a Lifshitz Point. *Phys. Rev. Lett.*, 102:231301, 2009.

[362] M. Tegmark. How to Make Maps from Cosmic Microwave Background Data without Losing Information. *The Astrophysical Journal Letters*, 480:L87–L90, May 1997.

[363] M. Tegmark et al. Cosmological parameters from sdss arecind wmap. *Phys. Rev.* **D** , page accepted, 2003. astro-ph/0310723.

[364] The POLARBEAR Collaboration, P. Ade, Y. Akiba, a. E. Anthony, K. Arnold, M. Atlas, D. Barron, D. Boettger, J. Borrill, S. Chapman, Y. Chinone, M. Dobbs, T. Elleflot, J. Errard, G. Fabbian, C. Feng, D. Flanigan, a. Gilbert, W. Grainger, N. W. Halverson, M. Hasegawa, K. Hattori, M. Hazumi, W. L. Holzapfel, Y. Hori, J. Howard, P. Hyland, Y. Inoue, G. C. Jaehnig, a. H. Jaffe, B. Keating, Z. Kermish, R. Keskitalo, T. Kisner, M. Le Jeune, a. T. Lee, E. M. Leitch, E. Linder, M. Lungu, F. Matsuda, T. Matsumura, X. Meng, N. J. Miller, H. Morii, S. Moyerman, M. J. Myers, M. Navaroli, H. Nishino, a. Orlando, H. Paar, J. Peloton, D. Poletti, E. Quealy, G. Rebeiz, C. L. Reichardt, P. L. Richards, C. Ross, I. Schanning, D. E. Schenck, B. D. Sherwin, a. Shimizu, C. Shimmin, M. Shimon, P. Siritanasak, G. Smecher, H. Spieler, N. Stebor, B. Steinbach, R. Stompor, a. Suzuki, S. Takakura, T. Tomaru, B. Wilson, a. Yadav, and O. Zahn. a Measurement of the Cosmic Microwave Background B -Mode Polarization Power Spectrum At Sub-Degree Scales With Polarbear. *The Astrophysical Journal*, 794(2):171, 2014.

[365] I. Tkachev, S. Khlebnikov, L. Kofman, and Andrei D. Linde. Cosmic strings from preheating. *Phys. Lett.*, B440:262–268, 1998.

[366] M. Tristram, C. Filliard, O. Perdereau, S. Plaszczynski, R. Stompor, and F. Touze. Iterative destriping and photometric calibration for Planck-HFI, polarized, multi-detector map-making. *Astronomy and Astrophysics*, 534:A88, October 2011.

[367] Michael S. Turner and Lawrence M. Widrow. Inflation Produced, Large Scale Magnetic Fields. *Phys. Rev.*, D37:2743, 1988.

[368] Jon Urrestilla, Neil Bevis, Mark Hindmarsh, Martin Kunz, and Andrew R. Liddle. Cosmic microwave anisotropies from BPS semilocal strings. *JCAP*, 0807:010, 2008.

[369] Jon Urrestilla, Pia Mukherjee, Andrew R. Liddle, Neil Bevis, Mark Hindmarsh, and Martin Kunz. Degeneracy between primordial tensor modes and cosmic strings in future CMB data from the Planck satellite. *Phys. Rev.*, D77:123005, 2008.

[370] T. Vachaspati. Magnetic fields from cosmological phase transitions. *Phys. Lett.*, B265:258–261, 1991.

[371] Tanmay Vachaspati. Estimate of the primordial magnetic field helicity. *Phys. Rev. Lett.*, 87:251302, 2001.

[372] Laura G. van den Aarssen, Torsten Bringmann, and Christoph Pfrommer. Is dark matter with long-range interactions a solution to all small-scale problems of Λ CDM cosmology? *Phys. Rev. Lett.*, 109:231301, 2012.

[373] K. Vanderlinde, T. M. Crawford, T. de Haan, J. P. Dudley, L. Shaw, P. A. R. Ade, K. A. Aird, B. A. Benson, L. E. Bleem, M. Brodwin, J. E. Carlstrom, C. L. Chang, A. T. Crites, S. Desai, M. A. Dobbs, R. J. Foley, E. M. George, M. D. Gladders, N. R. Hall, N. W. Halverson, F. W. High, G. P. Holder, W. L. Holzapfel, J. D. Hrubes, M. Joy, R. Keisler, L. Knox, A. T. Lee, E. M. Leitch, A. Loehr, M. Lueker, D. P. Marrone, J. J. McMahon, J. Mehl, S. S. Meyer, J. J. Mohr, T. E. Montroy, C.-C. Ngeow, S. Padin, T. Plagge, C. Pryke, C. L. Reichardt, A. Rest, J. Ruel, J. E. Ruhl, K. K. Schaffer, E. Shirokoff, J. Song, H. G. Spieler, B. Stalder, Z. Staniszewski, A. A. Stark, C. W. Stubbs, A. van Engelen, J. D. Vieira, R. Williamson, Y. Yang, O. Zahn, and A. Zenteno. Galaxy Clusters Selected with the Sunyaev-Zel'dovich Effect from 2008 South Pole Telescope Observations. *Astrophys. J.*, 722:1180–1196, October 2010.

[374] A. Vikhlinin, A. V. Kravtsov, R. A. Burenin, H. Ebeling, W. R. Forman, A. Hornstrup, C. Jones, S. S. Murray, D. Nagai, H. Quintana, and A. Voevodkin. Chandra Cluster Cosmology Project III: Cosmological Parameter Constraints. *Astrophys. J.*, 692:1060–1074, February 2009.

[375] A. Vilenkin. Cosmological Density Fluctuations Produced by Vacuum Strings. *Phys. Rev. Lett.*, 46:1169–1172, 1981. [Erratum: Phys. Rev. Lett.46,1496(1981)].

[376] M. Vogelsberger, J. Zavala, F.-Y. Cyr-Racine, C. Pfrommer, T. Bringmann, and K. Sigurdson. ETHOS - An Effective Theory of Structure Formation: Dark matter physics as a possible explanation of the small-scale CDM problems. *ArXiv e-prints*, December 2015.

[377] Robert V. Wagoner, William A. Fowler, and Fred Hoyle. On the Synthesis of elements at very high temperatures. *Astrophys. J.*, 148:3–49, 1967.

[378] Matthew G. Walker and Jorge Penarrubia. A Method for Measuring (Slopes of) the Mass Profiles of Dwarf Spheroidal Galaxies. *Astrophys. J.*, 742:20, 2011.

[379] D. H. Weinberg, M. J. Mortonson, D. J. Eisenstein, C. Hirata, A. G. Riess, and E. Rozo. Observational probes of cosmic acceleration. *Phys. Rept.*, 530:87–255, September 2013.

[380] Steven Weinberg. *Cosmology*. OUP Oxford, 2008.

[381] Steven Weinberg. Effective Field Theory for Inflation. *Phys.Rev.*, D77:123541, 2008.

[382] Steven Weinberg. Goldstone Bosons as Fractional Cosmic Neutrinos. *Phys.Rev.Lett.*, 110:241301, 2013.

[383] X. G. Wen and Edward Witten. World Sheet Instantons and the Peccei-Quinn Symmetry. *Phys. Lett.*, B166:397, 1986.

[384] S.D.M. White, J.F. Navarro, A.E. Evrard, and C.S. Frenk. The baryon content of galaxy clusters: A challenge to cosmological orthodoxy. *Nature*, 366:429, 1993.

[385] Ryan J. Wilkinson, Celine Boehm, and Julien Lesgourgues. Constraining Dark Matter-Neutrino Interactions using the CMB and Large-Scale Structure. *JCAP*, 1405:011, 2014.

[386] Ryan J. Wilkinson, Julien Lesgourgues, and Celine Boehm. Using the CMB angular power spectrum to study Dark Matter-photon interactions. *jcap*, 1404:026, 2014.

[387] E. L. Wright. Scanning and Mapping Strategies for CMB Experiments. *ArXiv Astrophysics e-prints*, November 1996.

[388] W. L. K. Wu, J. Errard, C. Dvorkin, C. L. Kuo, A. T. Lee, P. McDonald, A. Slosar, and O. Zahn. A Guide to Designing Future Ground-based Cosmic Microwave Background Experiments. *Astrophys. J.*, 788:138, 2014.

[389] Mark Wyman, Douglas H. Rudd, R. Ali Vanderveld, and Wayne Hu. Neutrinos Help Reconcile Planck Measurements with the Local Universe. *Phys. Rev. Lett.*, 112(5):051302, 2014.

[390] Matias Zaldarriaga. Non-Gaussianities in models with a varying inflaton decay rate. *Phys. Rev.*, D69:043508, 2004.

[391] Matias Zaldarriaga and Diego D. Harari. Analytic approach to the polarization of the cosmic microwave background in flat and open universes. *Phys. Rev.*, D52:3276–3287, 1995.

[392] J. Zavala, Y. P. Jing, A. Faltenbacher, G. Yepes, Y. Hoffman, S. Gottlober, and B. Catinella. The velocity function in the local environment from LCDM and LWDM constrained simulations. *Astrophys. J.*, 700:1779–1793, 2009.

[393] F. Zwicky. Die Rotverschiebung von extragalaktischen Nebeln. *Helvetica Physica Acta*, 6:110–127, 1933.

[394] Ogan zsoy, Kuver Sinha, and Scott Watson. How Well Can We Really Determine the Scale of Inflation? *Phys. Rev.*, D91(10):103509, 2015.